



HEINRICH HEINE
UNIVERSITÄT DÜSSELDORF

**Inhibiting protein-protein interactions in Hsp90
dimerization as a novel approach for targeting cancer**

Inaugural-Dissertation

zur Erlangung des Doktorgrades

der Mathematisch-Naturwissenschaftlichen Fakultät

der Heinrich-Heine-Universität Düsseldorf

vorgelegt von

Emanuele Ciglia

aus

Pescara

Düsseldorf, März 2015

Aus dem Institut für Pharmazeutische und Medizinische Chemie
der Heinrich-Heine-Universität Düsseldorf

Gedruckt mit der Genehmigung der
Mathematisch-Naturwissenschaftlichen Fakultät der
Heinrich-Heine-Universität Düsseldorf

Referent: Prof. Dr. Holger Gohlke

Korreferent: Prof. Dr. Georg Groth

Tag der mündlichen Prüfung:

Eidesstattliche Erklärung

Ich versichere an Eides Statt, dass die Dissertation von mir selbständig und ohne unzulässige fremde Hilfe unter Beachtung der „Grundsätze zur Sicherung guter wissenschaftlicher Praxis an der Heinrich-Heine-Universität Düsseldorf“ erstellt worden ist.

Diese Dissertation wurde in der vorgelegten oder einer ähnlichen Form noch bei keiner anderen Institution eingereicht, und es wurden bisher keine erfolglosen Promotionsversuche von mir unternommen.

Düsseldorf, den 31. März 2015

To my Family and Catherine

“Quis custodiet ipsos custodes?”

Juvenal, I century BC

TABLE OF CONTENTS

LIST OF PUBLICATIONS	viii
ABBREVIATIONS	ix
ABSTRACT	xi
ZUSAMMENFASSUNG	xii
1 INTRODUCTION.....	1
2 BACKGROUND	4
2.1 PPIs IN DRUG DISCOVERY – PUBLICATION I	4
2.1.1 PPIs: Functional and structural aspects.....	4
2.1.2 Druggability of PPIs	9
2.1.3 Methods for hot spot detection	12
2.1.4 Modulating PPIs for targeting cancer: success stories.....	15
2.1.5 Perspectives of modulating PPIs.....	22
2.2 HSP90 AS A NOVEL TARGET FOR CANCER THERAPY.....	26
2.2.1 Biology and pathophysiology of Hsp90	26
2.2.2 Structure of Hsp90	28
2.2.3 Mechanism of Hsp90’s function.....	29
2.2.4 Targeting Hsp90 for cancer therapy	31
3 SCOPE OF THE THESIS.....	35
4 RESOLVING HOT SPOTS IN THE C-TERMINAL DIMERIZATION DOMAIN THAT DETERMINE THE STABILITY OF THE MOLECULAR CHAPERONE HSP90 – PUBLICATION II.....	38
4.1 Background	38
4.2 Computational identification of hot spots in the hHsp90 CTD	39
4.3 Conclusions and significance	42
5 DESIGN AND BIOLOGICAL TESTING OF PEPTIDIC DIMERIZATION INHIBITORS OF HUMAN HSP90 THAT TARGET THE C-TERMINAL DOMAIN – PUBLICATION III	43
5.1 Background	43
5.2 Design and testing of peptidic hHsp90 inhibitors	43
5.3 Conclusions and significance	49
6 DESIGN, SYNTHESIS, AND CONFORMATIONAL ANALYSIS OF TRISPYRIMIDONAMIDES AS α-HELIX MIMETICS – PUBLICATION IV	50
6.1 Background	50
6.2 Conformational analysis of trispyrimidonamides.....	51

6.3	Conclusions and significance	54
7	SUMMARY AND PERSPECTIVES	56
8	ACKNOWLEDGEMENTS	57
9	REPRINT PERMISSIONS	58
10	PUBLICATION II.....	59
10.1	PUBLICATION II – Supporting Information.....	72
11	PUBLICATION III	86
12	PUBLICATION IV	114
12.1	PUBLICATION IV – Supporting Information	127
13	CURRICULUM VITAE	176
14	REFERENCES	179
15	APPENDIX – References of Figure 4	196

LIST OF PUBLICATIONS

This thesis is based on the following publications (contribution in parentheses):

- I. Alexander Metz[§], **Emanuele Ciglia[§] (37.5 %)**, and Holger Gohlke
Modulating Protein-Protein Interactions: From Structural Determinants of Binding to Druggability Prediction to Application
Current Pharmaceutical Design, **2012**; 18: 4630-4647
Impact factor reported for 2011: 3.870

- II. **Emanuele Ciglia[§] (30 %)**, Janina Vergin[§], Sven Reimann, Sander H.J. Smits, Lutz Schmitt, Georg Groth, and Holger Gohlke
Resolving Hot Spots in the C-terminal Dimerization Domain that Determine the Stability of the Molecular Chaperone Hsp90
PLOS ONE, **2014**; 9: e96031
Impact factor reported for 2012: 3.730

- III. Bertan Bopp[§], **Emanuele Ciglia[§] (30 %)**, Anissa Ouald-Chaib, Georg Groth, Holger Gohlke, and Joachim Jose
Design and Biological Testing of Peptidic Dimerization Inhibitors of Human Hsp90 that Target the C-terminal Domain
Submitted, **2015**

- IV. Lukas Spanier[§], **Emanuele Ciglia[§] (30 %)**, Finn K. Hansen, Krystina Kuna, Walter Frank, Holger Gohlke, and Thomas Kurz
Design, Synthesis, and Conformational Analysis of Trispyrimidonamides as α -Helix Mimetics
Journal of Organic Chemistry, **2014**; 79: 1582-1593
Impact factor reported for 2012: 4.564

[§] Both authors contributed equally to this work.

ABBREVIATIONS

$\Delta\Delta G$	difference in change in Gibbs free energy
ΔG	change in Gibbs free energy
ADME	absorption, distribution, metabolism, excretion
AML	acute myeloid leukemia
ATP	adenosine triphosphate
Bak	Bcl-2 homologous antagonist killer
Bcl-2	B-cell lymphoma 2
Bcl-xL	B-cell lymphoma-extra large
CTD	C-terminal domain
FDA	US Food and Drug Administration
FRET	fluorescence resonance energy transfer
GPCR	G-protein coupled receptor
GRP94	glucose-regulated protein 94
HSP(s)	heat shock protein(s)
hHsp90	human Hsp90
Hsp90	heat shock protein of 90 kDa
HTS	high throughput screening
HDM2	human double minute 2 protein
IC_{50}	half maximal inhibitory concentration
IL-2	interleukin-2
IL-2R α	interleukin-2 receptor subunit α
K_D	dissociation constant
$\log P$	logarithm of the octanol-water partition coefficient
M	middle domain
MD	molecular dynamics
MDM2	mouse double minute 2 protein
MM	molecular mechanics
MM-GB/SA	molecular mechanics generalized Born surface area
MM-PB/SA	molecular mechanics Poisson-Boltzmann surface area
MW	molecular weight
NHR2	nervy homology region 2
NME	new molecular entities
NMR	nuclear magnetic resonance
NTD	N-terminal domain
p53	tumor suppressor p53 protein

PDB	protein data bank
PPI(s)	protein-protein interaction(s)
PPIM(s)	protein-protein interaction modulator(s)
QSAR	quantitative structure-activity relationship
Ras	rat sarcoma guanosine-nucleotide-binding protein
RalGDS	ras-like guanine nucleotide dissociation stimulator
RMSD	root mean square deviation
RUNX1	runt-related transcription factor 1
RUNX1-ETO	RUNX1-ETO fusion protein
SAR	structure-activity relationship
SAXS	small angle X-ray scattering
SEM	standard error of the mean
TRAP-1	tumor necrosis factor receptor-associated protein-1

ABSTRACT

Protein-protein interactions (PPIs) are targets of outstanding interest in drug discovery, because of their ubiquitous involvement in virtually all biological processes, where they influence cellular signaling and regulation, both in physiological and pathophysiological mechanisms. Thus, modulating PPIs has become an appealing approach to target a number of diseases. The discovery of small molecule protein-protein interaction modulators (PPIMs) remains a big challenge, due to the dissimilarity of PPIs to classical drug targets, and to a still incomplete understanding of the mechanisms regulating the interactions between proteins. However, the intense research dedicated to PPIs in the last years led to the development of several PPIMs, some of which are being studied in advanced clinical trials, or are already marketed drugs.

Since the last decades, the *heat shock protein of 90 kDa (Hsp90)* emerged as a highly attractive target for cancer therapy, due to its involvement in a myriad of regulatory processes, and in the development and progression of several types of tumor. Several Hsp90 inhibitors have been developed that validated the chaperone as a druggable cancer target, and some of these are currently in advanced phases of clinical trials. However, most of the discovered inhibitors abolish Hsp90 activity by competing with ATP for binding in the N-terminal domain (NTD) binding site. Just a few inhibitors have been discovered that bind in the Hsp90's C-terminal domain (CTD), and none of those reported to date target the CTD dimerization interface.

The goal of this thesis is to investigate the human Hsp90 (hHsp90), with the ultimate objective of rationally identifying novel modulators that inhibit this chaperone by targeting the CTD dimerization, as an unprecedented approach to target hHsp90 for cancer therapy.

First, the salient structural and functional characteristics of PPIs are described, with a particular focus on their potential as drug targets, i.e. their *druggability*. Second, *hot spot* amino acids in the CTD interface that determine the stability of hHsp90 are predicted by computational means and experimentally validated. These findings are the essential starting point for what follows in the study, focused on the development of peptidic and non-peptidic molecules interfering with hHsp90 CTD dimerization. Accordingly, the hot spots information guides the design and experimental testing of peptidic inhibitors targeting the hHsp90 CTD. Finally, trispyrimidonamides are investigated as potential novel α -helix mimetics, and for their ability of mimicking the previously identified hHsp90 hot spots.

ZUSAMMENFASSUNG

Auf der Suche nach neuen Wirkstoffen sind *Protein-Protein-Interaktionen (PPIs)* Targets von größtem Interesse. Dies ist darauf zurückzuführen, dass sie nahezu in allen biologischen Prozessen involviert sind und hier einen großen Einfluss auf zelluläre Signaltransduktion und Regulation sowie in physiologischen und pathophysiologischen Mechanismen haben. Dies macht die Modulierung von PPIs zu einem interessanten Ansatz in der Therapie verschiedener Krankheitsbilder. Aufgrund des unterschiedlichen Charakters von PPIs zu klassischen Zielmolekülen und des unvollständigen Verständnisses der Mechanismen, die Interaktionen zwischen Proteinen regulieren, ist die Entdeckung neuer *niedermolekulare Modulatoren von Protein-Protein-Interaktionen (protein-protein-interaction-modulators, PPIMs)* eine große Herausforderung. Nichts desto trotz sind heutzutage, nach jahrelanger intensiver Forschung, PPIMs entwickelt worden, von denen sich einige in den letzten klinischen Phasen befinden und andere sogar schon auf dem Markt sind.

In den letzten Jahrzehnten kristallisierte sich das *heat shock protein 90 kDA (Hsp90)* als attraktives Target in der Krebstherapie heraus, was darauf zurückzuführen ist, dass es sowohl in unzähligen regulatorischen Prozessen, als auch in der Tumor-Entstehung und der Progression involviert ist. Bis zum heutigen Tage wurden mehrere Hsp90-Inhibitoren entwickelt, die dieses Chaperon als ein geeignetes Target in der Krebstherapie bestätigen konnten. Einige dieser Inhibitoren befinden sich schon in den späten Phasen der klinischen Studien. Die Mehrheit dieser Moleküle bindet in der N-terminalen Bindestelle und konkurriert dabei mit ATP. Bis jetzt wurden nur wenige Hsp90 Inhibitoren beschrieben, die an den C-Terminus (C-terminal domain, CTD) binden, und unter ihnen befindet sich keiner, der an der CTD Dimerisierungs-Interaktionsfläche angreift.

Das Ziel dieser Arbeit ist es, *humanes Hsp90 (hHsp90)* mit dem Bestreben einer rationalen Identifizierung neuer Modulatoren zu untersuchen, die die CTD-Dimerisierung blockieren, und somit, als neuartiger Ansatz in der Krebstherapie, das Chaperon in seiner natürlichen Funktion zu inhibieren.

Zunächst werden die strukturellen und funktionellen Charakteristiken von PPIs mit einem besonderen Fokus bezüglich ihres Potentials als pharmakologische Zielmoleküle (*druggability*) beschrieben. Im nächsten Schritt werden die *hot spot Aminosäuren* des CTD, die für die Stabilität des hHsp90 essentiell sind, durch computergestützte Berechnungsmethoden vorhergesagt und experimentell bestätigt. Diese Ergebnisse stellen den Ausgangspunkt der nachfolgenden Studien dar, die sich auf die Entwicklung von peptidischen

und nicht peptidischen Molekülen fokussieren, die mit der CTD Dimerisierung von hHsp90 interferieren. In einer ersten Untersuchung werden die Hot-Spot Information für die Entwicklung und die experimentelle Testung von peptidischen hHsp90 CTD Inhibitoren verwendet. Zum Schluss werden Trispyrimidonamide zum einen als potentielle, neue α -helix Mimetika und zum anderen auf ihre Fähigkeit, die zuvor identifizierten hHsp90 hot spots nachzustellen, untersucht.

1 INTRODUCTION

Drug discovery is an extremely complex and multifaceted process that requires enormous efforts and investments in terms of time and resources, and involves a number of players across academia and industry. Estimates from several independent studies converge on that the whole process of development of a new drug, from early stages to access into the market, requires an average time of 13 years and expenditures ranging from \$US 800 million up to 1.8 billion (1-3). Recently, many experts pointed out the critical circumstances the whole drug development machinery is undergoing (4,5), as evidenced particularly by a pronounced decrease in both pharmaceutical productivity and introduction of *new molecular entities (NME)* into the market (6). Surprisingly, the remarkable attrition in the number of drug candidates that eventually entered the market observed in the last years occurred in spite of the steadily increasing investments in drug development (5,7,8). The drastic reduction of the pharmaceutical industry's productivity is also in evident contrast with the unprecedented advances in the biomedical sciences achieved during the same period of time (7). On average, less than 5 % of all the compounds screened for a certain target eventually enter preclinical investigations, and just 2 % of these hits progress to clinical trials (8). The underlying causes of this phenomenon are a matter of intense debate, and a variety of solutions has been proposed to overcome the present alarming situation of "*drug drought*"(6). Since most drug candidates fail at later stages of clinical trials due to scarce efficacy or high toxicity, target identification and validation are among the most important factors conditioning the success of a drug discovery campaign. Accordingly, as also rationalized in an economic model of drug discovery developed by Paul *et al.* (6), intensifying research and investment efforts in the early "target to hit" stages is expected to lead to a substantial increase of the NME successfully becoming marketed drugs (8). As a consequence, since the last decade, several pharmaceutical companies are concentrating their efforts on the early stages of drug discovery (8). Unraveling the mechanisms that regulate disease-relevant biologic processes is the first step for the identification of new drug targets and therapeutic opportunities. The human genome contains approximately 22000 protein-encoding genes, and it is estimated that 2-7 % of the gene products (~600-1600 proteins) might have a direct association to human diseases, hence are potential targets for pharmacological intervention (9-12). Only ~100 of these proteins are current drug targets (9). Including also non-genes related targets, the total number thereof currently exploited by marketed drugs ranges from 200 to 400 (9,13,14). Clearly, there is a significant discrepancy between the number of potential drug targets and the ones

currently exploited in pharmacotherapy. This must be ascribed to an insufficient or partial characterization of most of the drug targets potentially available, as demonstrated by the fact that more than 50 % of the current drugs act on products of just four gene families: class-I G protein-coupled receptors (GPCRs), nuclear receptors, ligand-gated ion channels, and voltage-gated ion channels (Figure 1 A) (9). Furthermore, it has been evidenced that on average, ~78 % of the NME introduced into the market from 1983 to 2010 that act on targets encoded by the human genome address a previously drugged target, whereas just the remaining ~22 % address novel targets (Figure 1 B) (14).

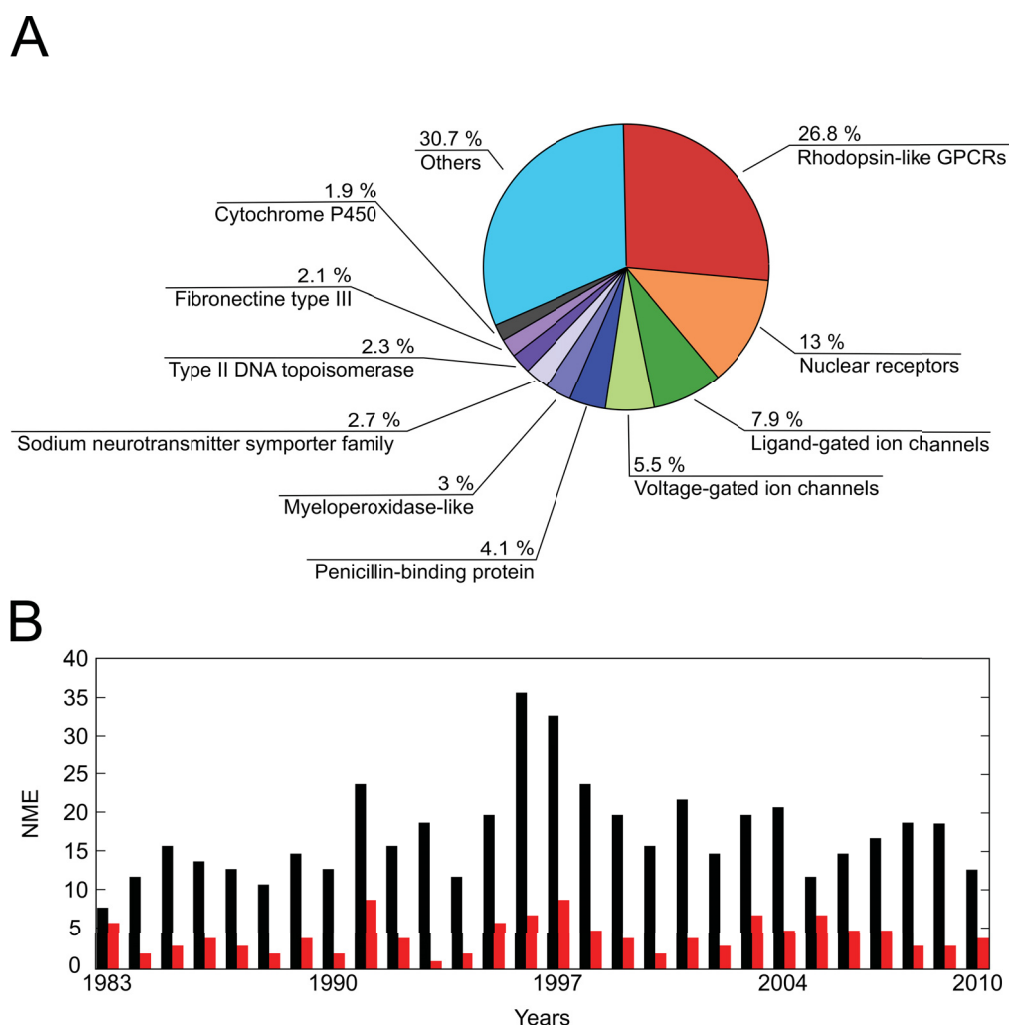


Figure 1. Targets of current drugs and drugs addressing novel targets. (A) Percentage of drugs currently approved from the FDA (US Food and Drug Administration) for each of the most drugged gene-families. The “Others” category includes further 120 domain families or singletons for which only a few drugs have been successfully launched (9). (B) Total number of new molecular entities (NME) acting on targets encoded in the human genome approved as drugs by the FDA from 1983 to 2010 (black), and those acting on novel targets (red) (14).

Altogether, these evidences suggest that discovering novel drug targets is a fundamental premise for obtaining significant advances in drug development. In this scenario, *protein-protein interactions (PPIs)* offer exceptional opportunities for targeting a number of diseases.

Approximately 100,000 to 650,000 PPIs are present in humans (15-17), where they represent control switches in signaling and regulation pathways and are involved in numerous physiological mechanisms. Additionally, PPIs are implicated in a number of diseases, such as cancer (18-20), neurodegenerative diseases (notably in Parkinson's and Alzheimer's diseases) (21), and many others (22,23). As such, modulating PPIs has emerged as a new paradigm for pharmacological intervention in a number of pathological conditions (22,24,25). However, pioneering drug discovery attempts toward these innovative targets have not been successful, and PPIs have been long classified as *undruggable* systems (11,26,27). The reasons for this initial defeat are to be ascribed to the novelty of PPI targets, and to their remarkable dissimilarity to "classic" drug targets. As a matter of fact, the conventional molecular recognition model where a rather large *receptor* (e.g. enzymes, ion channels) accommodates a relatively small *ligand* (*endogenous* or *xenobiotic*) in a pronounced and complementary cavity, explaining drug-receptor interactions, typically does not apply to PPIs. Hence, successfully exploiting PPIs' exceptional therapeutic potential requires gathering new knowledge, and the development of alternative methodologies. Although for certain aspects this field is still considered to be at its infancy, a number of success stories demonstrate that pharmaceutical intervention on PPIs is a feasible and very valuable approach for addressing several therapeutical needs (28-30).

In this thesis, the *heat shock protein of 90 kDa (Hsp90)* is investigated, with the aim of rationally identifying novel modulators that inhibit this chaperone by targeting the C-terminal dimerization domain (CTD). This study resulted in four publications.

First, in **Publication I** (31), the state of the art in the realm of PPIs is reviewed. Here, the salient structural and functional characteristics of these systems are described, with a particular focus on their potential as drug target, i.e. their *druggability*. Second, in **Publication II** (32), *hot spots* amino acids in the CTD that determine the stability of human Hsp90 (hHsp90) are predicted by computational means and experimentally validated. These findings are the foundation of the following investigations aimed at the development of peptidic and non-peptidic molecules interfering with hHsp90 dimerization. In **Publication III**, the hot spot information guides the design and experimental testing of peptidic inhibitors targeting the hHsp90 CTD. Finally, a novel trispyrimidonamide scaffold is investigated for its α -helix mimetic potential, and for its capability of mimicking the previously identified hHsp90 hot spots, as reported in **Publication IV** (33).

2 BACKGROUND

2.1 PPIs IN DRUG DISCOVERY – PUBLICATION I **

Recently, multiprotein complexes have become attractive targets for drug discovery (34,35) due to the essential role of non-covalent association of proteins in the communication of cell components (24). This is highlighted by the importance of these systems in signaling (36-39) and the regulation of, e.g., cellular growth (34) and apoptosis (40,41). It does not come as a surprise then that protein-protein interactions (PPIs) are involved in many diseases, such as cancer (18), neurodegenerative diseases (21), and viral and bacterial infections (23). For this reason, interfering with PPIs has a great therapeutic potential, providing attractive opportunities for pharmacological intervention (22-25,42). However, modulating PPIs is a daunting task. First, in contrast to “classical” targets such as enzymes or receptors, much less experience has been gained so far due to the novelty of many protein-protein targets. Second, the intrinsic complexity of PPIs requires innovative methodological approaches. Encouragingly, extensive investigations have proved the general feasibility of interfering with PPIs as a valuable approach for treating a number of diseases (22-25,42,43). Here, the most important goal is to identify small molecules protein-protein interaction modulators (PPIMs) that efficiently and selectively affect processes involving protein-protein binding. These successes have benefited from remarkable steps towards an understanding of PPI properties, the determinants of binding to protein-protein interfaces, as well as the implications of modulating PPIs for biological systems. This knowledge originates from an interdisciplinary approach, including the fields of structural biology, biochemistry, genomics, medicinal chemistry, and computational chemistry.

2.1.1 PPIs: Functional and structural aspects

“Classical” targets versus PPIs. In the case of protein-ligand binding, an enzyme or receptor (hereafter together referred to as “receptor”) interacts with a small molecule or a peptide within a relatively small and well-defined binding site located in a cavity on the receptor surface. When there are no conformational changes on the binding site of the receptor, this situation can be described by the simplistic “lock-and-key” model already suggested by Emil Fischer (44). According to this model, high affinity and specificity are achieved through shape and chemical complementarity, leading to a compact and tight fit between the binding

** **Section 2.1** is an adapted and re-elaborated version of **Publication I** (Metz, A., Ciglia, E., and Gohlke, H. Modulating Protein-Protein Interactions: From Structural Determinants of Binding to Druggability Prediction to Application. *Current Pharmaceutical Design*, **2012**; 18: 4630-4647).

partners (45). When trying to interfere with such a system, the most direct and obvious approach is to develop small molecules resembling the natural ligand, i.e., bearing chemical groups that can be accommodated by and form interactions with the binding site of the receptor. Especially for enzyme targets, it is possible to identify protein families that share the same biological function (42). Usually, members of the same protein family have common interaction mechanisms and binding pocket architectures. This allows exploiting information gained on one enzyme when trying to identify small-molecule ligands for other targets of the same family (46-50). As discussed in the following, PPI targets are intrinsically different from “classical” targets, such as enzymes and G protein-coupled receptors. This makes it difficult to target protein-protein interfaces by approaches established for classical targets.

Surface size and shape of PPIs. Structural characteristics provide the biggest challenge when aiming at modulating PPIs. First, on a global level, protein-protein interfaces are generally much larger than binding site regions of classical targets. In fact, ligand-receptor contact areas are typically about 300 to 1000 Å² in size (51-53), while protein-protein contact areas can range from ~1500 to 3000 Å² or even be larger (54,55). Second, protein-protein interfaces are often shallow and lack deep grooves or indentations, especially in the unbound conformation (Figure 2 A), that are usually present in classical targets (Figure 2 C). Third, interactions between protein binding partners often occur through several, not necessarily sequentially connected spots, thus leading to a discontinuous epitope. All of the above make identification of a spatially defined region within the interface that is responsible for binding a difficult task. Encouragingly, counterexamples have been presented that benefited from a deep knowledge of the respective protein-protein interface (23). Finally, proteins are usually promiscuous molecules (56,57) that are able to bind more than one binding partner, possibly even at the same site. While this allows proteins to take part in intricate interaction networks, it increases the level of difficulty for finding a small molecule that modulates a specific protein-protein interaction only.

Specificity and complementarity. Cells are crowded environments and, hence, potentially all molecules populating the same cellular compartment can contact each other (58,59). Accordingly, it is especially important for proteins that essential interactions maintain a high degree of specificity and occur only when needed, limiting the myriad of possible contacts (58,60). Thus, identifying the determinants of binding at protein-protein interfaces is an important goal in molecular biology with high relevance also in related fields, notably in pharmacology, genomics, and biological chemistry.

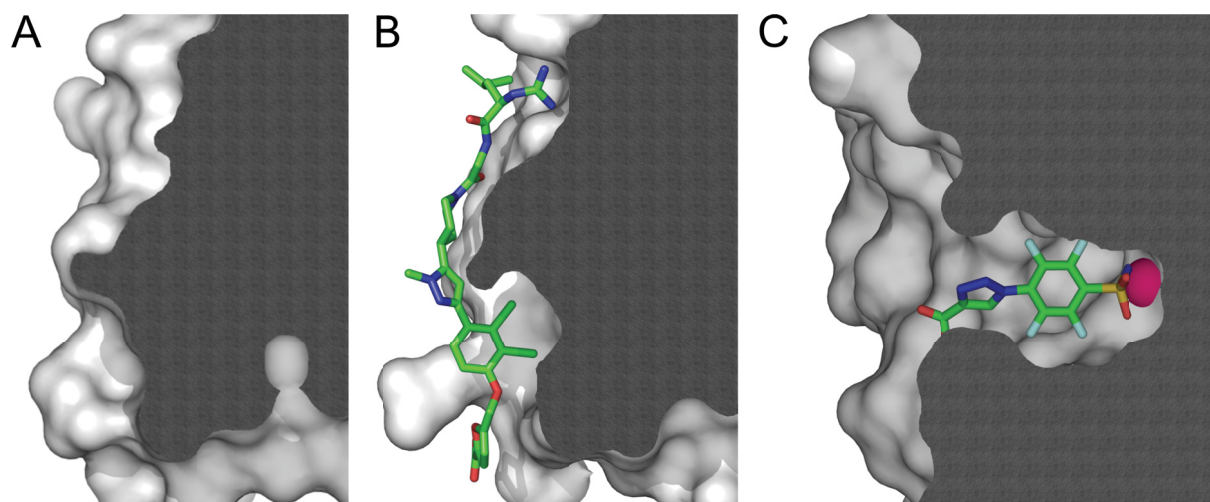


Figure 2. Classical vs PPIs binding sites. (A) Protein-protein interfaces usually lack deep pockets in the unbound state, as depicted for the unbound conformation of IL-2 (PDB code 1M47). (B) Surface flexibility can allow for the formation of druggable pockets, as depicted for a PPIM-bound conformation of IL-2 (PDB code 1PY2). (C) In contrast, classical targets present narrow and deep binding pockets, as depicted for carbonic anhydrase in complex with an inhibitor (PDB code: 3P25; Zn²⁺ ion highlighted in purple). Figure adapted from Publication I, Reference (31).

Although no common strategy can be devised to achieve binding affinity and specificity in PPIs, one can nevertheless identify some mechanisms that occur preferentially in PPIs. First, proteins are marginally stable molecules (61) forming an ensemble of conformational states, each of which could potentially interact with a binding partner (59). These conformational changes can result in the formation of cavities in the interfaces that could not be detected by visual inspection of the static representation of a crystal structure (62,63). That way, proteins can exhibit grooves that allow for molecular recognition and binding (64). Therefore, it is worth investigating conformational ensembles in solution by analyzing the dynamics of the protein of interest in detail. Several tools can assist in this task, among them NMR and scattering techniques (65,66) for determining protein structures in solution and molecular dynamics (MD) simulations for exploring the dynamic behavior of the system by computational means (62,67-73). The importance of accounting for receptor flexibility to identify adequate receptor conformations complementary to a PPIM is demonstrated in a study by Isvoran *et al.* (74) combining both experimental and computational approaches. Here, docking into multiple crystallographic and NMR receptor structures in connection with complex relaxation and rescoring identified binding poses of a terphenyl PPIM with calmodulin and human centrin 2 that are considerably closer to the native one than those from docking into individual, non-relaxed, and non-complementary structures.

Nussinov *et al.* pointed out that in protein-protein interfaces *unfilled pockets* and *complemented pockets* can be distinguished (75). Unfilled pockets are present both before and after protein-protein association. They are not crucial for complex formation, but are

important for the overall flexibility. In contrast, complemented pockets are detectable at the interface before binding, but disappear after association. These pockets are then filled by the binding partner, being responsible for tight and highly complementary binding of the proteins involved. The same authors also demonstrated that pre-existing pockets do not undergo significant rearrangement after binding. This means that complemented pockets offer a favorable setting for binding interactions. Interestingly, they also found that there is a weak correlation between the conservation of residues and their frequency of occurrence in complemented pockets (75). Such residues are often also hot spots because of their enlarged contact area and the exclusion from solvent (75,76). Conversely, this implies that it should be possible to identify hot spot and, hence, complemented pockets through the identification of conserved amino acids (77).

Hot spots. A fundamental characteristic of protein-protein interfaces is their energetic non-homogeneity (78). Evidence from alanine scanning experiments shows that the binding energy is not equally distributed among all amino acids participating in the interaction (79-82). Within the large surfaces involved in the interaction, generally some patches suffice for complex formation, the so-called *hot regions* (Figure 3 A and B) (83). These often have a conserved residue composition for binding similar proteins but can also differ in composition for promiscuous binding by the same interface (84). Furthermore, only some of the residues belonging to these regions account for most of the binding energy. These amino acids are called *hot spots* if, by definition, a mutation to alanine leads to a change in the binding free energy of $\geq 2 \text{ kcal mol}^{-1}$ (85). Hot spot amino acids on one face of the complex are usually located in correspondence to hot spots on the other face, forming interactions that lead to complex stabilization (Figure 3 B) (56). Within the hot regions, there is a very tight geometric and energetic complementarity between the binding partners. Thus, bulky side chains on one protein are accommodated in indentations on the other protein, hydrophobic groups on one protein form close contacts with hydrophobic groups on the other protein, and polar residues establish hydrogen bonds or salt bridges between the two proteins. Rajamani *et al.* showed that *anchor residues*, which are highly buried, preordered in the unbound state, (structurally) conserved, and often energetic hot spots of PPIs, are present in many protein-protein interfaces and can possibly be exploited as starting points for PPIM development (86). Similarly, Yogurteu *et al.* found that hot spots are more rigid than the surrounding interface in MD simulations (87). Hot spots within one hot region work together in a cooperative fashion, thereby stabilizing the protein complex (59,83,88). In contrast, energetic contributions from different patches are additive (89-91), suggesting that hot regions are independent from each

other. As a consequence, protein-protein interfaces appear to have a hierarchical and modular architecture being formed by separate patches, within which each hot spot amino acid strongly depends on the other close-by amino acids for an efficient interaction (59). Interestingly, hot spots are among the most conserved residues (75,76,92,93). This relation has also been proposed to be a way to distinguish between binding interfaces and otherwise exposed protein surfaces (76). This hypothesis is strengthened by the observation that no residue conservation was found within solvent exposed surfaces (76). Overall, this highlights the importance of hot spots for protein-protein complex formation, and explains why evolutionary changes rarely lead to a significant modification in hot spot composition (92).

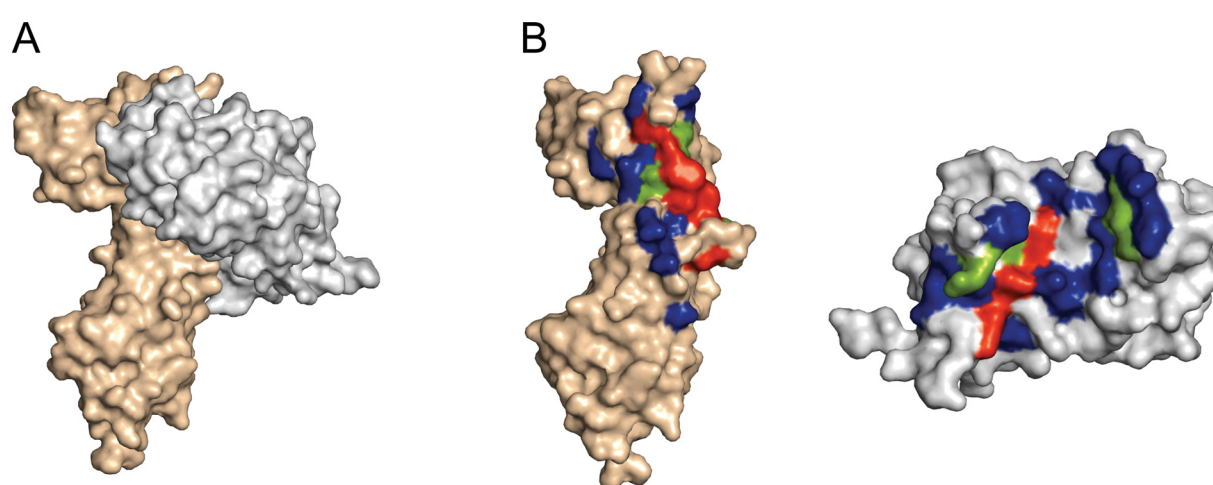


Figure 3 Hot spots in the human growth hormone-human growth hormone receptor PPI complex. (A) Surface representation of the crystal structure of the human growth hormone (grey) and its receptor (wheat) (PDB code 1AA2). (B) The interface between the two proteins reveals a functional epitope of complementary hot spots on each of the interaction partners. Amino acids are colored according to their energetic contribution to the binding energy, as calculated by experimental alanine scanning (blue: $< 1 \text{ kcal mol}^{-1}$, green: $1 < 2 \text{ kcal mol}^{-1}$, red $> 2 \text{ kcal mol}^{-1}$) (81,94).

Although the leading role in driving the interaction between protein binding partners relies on hot spots, the surrounding amino acids are also important. According to the *O-ring theory* (79), surrounding residues have the function to protect hot spots from solvent molecules, favoring hydrophilic or even hydrophobic interactions that would be otherwise disturbed by the presence of water. A high degree of complementarity between the binding partners is sometimes also achieved through water-mediated interactions (95-97). Such structural water molecules are particularly important in regulating hydrogen bond networks within the interface: I) By bridging interactions between the binding partners or II) by favoring the formation of a dry core in the interface that maximizes the interactions between hot spots surrounded by a rim of amino acids and water molecules (53).

Interaction types and amino acid composition. Given that protein-protein interfaces have considerable areas of hydrophobic residues, resembling cores of globular proteins (82), it has

been suggested that the hydrophobic effect is the driving force leading to protein-protein association (98-100). However, a careful analysis shows a situation similar to protein folding: the hydrophobic effect is a leading force but the proteins do not necessarily adopt a conformation with optimally buried non-polar surface area (101-104). This hints at further mechanisms being involved. In fact, even though hydrophobicity is important in this context, the role of electrostatic interactions cannot be neglected (105-108). Accordingly, the hydrophobicity of protein-protein interfaces is usually intermediate between the one found for a protein core and a solvent exposed protein surface. The amino acid composition in the hot spots, which has been shown to be non-random (109), reflects this situation. As a matter of fact, it has been observed that hot spots are enriched in tryptophan, tyrosine, arginine, and, to a lesser extent, isoleucine (78), whereas leucine, serine, threonine, and valine were found slightly depleted (76,79). One could argue that large side chains just contribute more, but functional considerations prevail. In particular, tyrosine and tryptophan allow establishing stacking and hydrophobic interactions owing to their aromatic, non-polar side chains, but at the same time offer the possibility to create hydrogen bonds due to the phenolic OH group and the indolic nitrogen. On the contrary, arginine, being a polar amino acid bearing a charged guanidinium group, is mostly involved in hydrogen bonds and salt bridges across the interface, although the electron delocalization of the guanidinium-system also confers a pseudo-aromatic character (79). This dual side chain behavior exemplifies the two-faced chemical nature of protein-protein interfaces. As a word of caution, even though the mentioned residues are the most frequent ones in PPIs, this knowledge should lead neither to neglecting the importance of other amino acids for binding nor to uncritically considering these residues hot spots just because of their occurrence in an interface.

2.1.2 Druggability of PPIs

PPIs are far from being widely exploited targets in drug development. Although there are some examples of marketed small-molecule drugs acting on PPIs (24,110-113) and some further molecules are in advanced clinical trials (Figure 4) (34,114-119), PPIs are usually considered high risk targets by pharmaceutical companies (26,35). This is for two reasons: First, initial attempts to identify PPIMs by high-throughput screening (HTS) were mostly unsuccessful, particularly when using chemical libraries designed for traditional targets (23). Second, the wideness of protein-protein interfaces, the lack of defined binding pockets, and the stability of PPIs led to PPIs being considered difficult to target if not *undruggable* (26,27). Also due to this overgeneralization, there is still a large gap between the knowledge gathered on these systems (22,24,25,34,42) and its actual use in the development of therapeutics. Yet,

some prominent counterexamples, such as the well-studied systems p53/MDM2 (23,42) (see **Paragraph 2.1.4**) and Bcl-xL/Bak (23), have contributed significantly to expose the myth depicting PPIs as undruggable systems (27,56,120) (Table 1).

A big challenge associated with PPIs is the high degree of diversity in terms of the molecular recognition properties encountered. Each interface is unique, bearing its own particular characteristics and, thus, requiring a specifically tailored approach. In fact, binding sites at protein-protein interfaces are often not well conserved, which is different from enzymes that bind the same type of substrate and, therefore, share many common features in the binding regions if they belong to the same family (42). Nevertheless, as the amount of structural data of bound PPIMs increases, approaches that exploit PPIM binding information from homologues (121) will become increasingly applicable. Furthermore, there are differences between protein-protein interfaces and the non-interacting surface of a protein that allow the sequence- and structure-based prediction of residues in the interface and an enrichment of hot spots, which often stand out in such analyses (122-127).

For establishing the suitability of a protein-protein interface as a target for drug discovery, first, one needs to define what is meant by “*druggability*” in this context. In the straightforward definition of Egner and Hillig, druggability can be considered as the likelihood of finding a selective, low molecular weight molecule that binds with high affinity to the target (128). But what are the characteristics of a PPI that allow targeting the interface? Due to the inherent complexity of the issue, it seems impossible to answer this question unambiguously. Aside from the particular characteristics of protein-protein interfaces, as presented earlier, it is important to consider that druggability is not an absolute property of a target molecule such as chemical class, molecular weight, or logP, but always refers to a specific application. Accordingly, authors have provided different concepts for assessing druggability both qualitatively and quantitatively (42,51,128-133). Utilizing computational techniques to assess a target’s druggability is appealing. An important reason for this is that it should permit to cut down research costs relating to experimental investigations that otherwise must be carried out in a more extensive fashion. However, despite large research efforts, initial progress is only emerging in this field (134,135).

Even though a unified approach for unambiguously establishing the druggability of a certain PPI is not available yet, there are some general considerations valid for all PPIs, which can be used for a preliminary assessment. An interesting approach to select protein-protein interfaces suitable for drug discovery is the decision tree proposed by Chene (42). The author showed that considerations on the physicochemical properties of an interface allow assessing whether

a PPI could be a suitable target for the design of modulators. A first point concerns the natural binding state of the protein of interest, i.e., whether it falls within the *obligate* or *non-obligate* class of protein-protein complexes. In the former class, the monomers involved do not exist in the non-associated form in the cell, while in the latter class the protein binding partners can be bound or dissociated at different times or conditions. Consequently, targeting a permanent PPI should be much harder than a transient one, though not impossible. Other important factors to be considered are the availability of structural information, the presence of cavities, the degree of interface hydrophobicity, and the size and complementarity of the interface. In an ideal case, there is a detailed characterization of the PPI by structural studies that clarifies the determinants of binding. Next, there should be cavities on the surface with appropriate sizes to accommodate PPIMs and to allow specific targeting. In addition, the overall hydrophobic character of the interface should be intermediate, permitting to develop molecules with an adequate trade-off between optimal binding and favorable pharmacokinetic properties. Another important factor influencing the druggability of PPIs is the presence of helices at the interface (29). With α -helices being the most frequently occurring type of secondary structure both in the protein core and in exposed regions (136,137), helices located on accessible surfaces are often responsible for molecular recognition. Along these lines, a survey on the Protein Data Bank (PDB) (138) by Arora *et al.* revealed that 62 % of the protein-protein complexes present in the database have helical interfaces (129,132). Furthermore, the authors divided these interfaces into three categories according to the helical character: I) receptors containing a cleft for helix binding, where a minimum of two close amino acids contribute importantly to the interaction (as in the p53/MDM2 complex (23,42,139)); II) extended interfaces where strong binding is achieved through multiple contacts between two- to five-turn helices and a higher number of residues; III) proteins featuring both of the described characteristics and showing quite weak interactions (132,136). From a drug discovery point of view, it appears obvious that complexes belonging to the first category offer better chances for developing PPIMs than complexes falling in the second and third categories. In addition, knowledge about how amino acids are arranged within interfacial helices can guide the design of α -helix mimetics with different chemical scaffolds (136). This may be a first step in the development of PPIMs.

Any analysis of a protein-protein interface should take these aspects into account in order to assess the druggability of the system. In addition, (computer-aided) binding pocket (here not described, see original **Publication I**: Ref. (31)) and hot spot detection have a great impact for characterizing the PPI and assessing the druggability of a protein-protein interface.

2.1.3 Methods for hot spot detection

Spatially clustered hot spots are crucial for the binding of small drug-like PPIMs in a large protein-protein interface (23,78). Thus, methods for the detection of hot spots (125) do not only provide a more detailed understanding of the energetic determinants of binding, but also yield information that complements the one derived from binding pocket detection. Initially, experimental methods for hot spot determination will be briefly introduced, followed by a more detailed discussion of two computational methods that are particularly relevant for the work presented in this thesis.

Experimental hot spot detection. Mutagenesis of interface amino acids is the most significant method to detect and validate hot spots. Mutating selected or, seldom, all such amino acids to alanine is called *alanine scanning*, and yields a fingerprint of the amino acids important for a PPI (81,140). A mutation to alanine is usually chosen because it has a small neutral side chain devoid of polar interactions and does not significantly influence the protein backbone as, e.g., glycine would do. Still, even a mutation to alanine can potentially introduce larger structural changes in the complex or influence the unbound state of a protein such that changes in relative binding free energies observed between wild type and mutant complex do not necessarily originate from interactions lost in the interface (140). In addition, even if alanine partially carries over interactions of the original amino acid, e.g., in terms of backbone interactions or because the original amino acid is similar to alanine, the change of affinity upon mutation will be less than the total contribution of the original amino acid. Furthermore, alanine scanning is very laborious because it requires protein purification and analysis. This bottleneck can be alleviated by combinatorial alanine scanning using phage display (141,142) or combinatorial solid-supported peptide libraries (143). Alternatively, methods of fragment-based drug design, including covalent tethering (144-147), co-crystallization (148), SAR by NMR (149,150), and SOS-NMR (151), can identify binding fragments of rather low affinity and, thereby, probe druggability (120,152). Also, solvent mapping by MSCS (153) and chemical shift perturbation (CSP) NMR experiments (154,155) are methods that suggest where organic molecules will preferably bind and so have been exploited in data-driven docking (134,156). All these methods can help identify a smaller, druggable, and hot spot-containing sub-region of the interface, even if there is no open binding pocket detectable in the unbound state of the receptor (157). Information about experimentally determined hot spots are available in several databases (85,158-162), although the coverage is low when compared to the number of PPIs considered to be interesting drug targets.

Computational hot spot detection. Since experimental methods for detecting hot spots are laborious, there is a high demand for computational prediction methods. Methods for performing *in silico* hot spot detection can be categorized into *in silico* alanine scanning, non-perturbing fully atomistic approaches, machine learning approaches, and approaches using nothing but unbound protein structures. A detailed description of all of these methods is beyond the scope of this thesis, and it was reviewed elsewhere by others and us (31,125,163). Here, I only focus on two methods that were critical to the characterization of the hHsp90 CTD dimerization described in the following (**Chapter 4, Publication II**) (32).

***In silico* alanine scanning.** Among the computational alternatives for hot spot detection that require experimentally determined or modeled structures of protein-protein complexes as input, *in silico* alanine scanning (78,140,164) is the most straightforward analogue of the above described experimental method. Here, a relative binding (free) energy (ΔG_{bind}) is calculated for a wild-type complex and one with alanine mutants in the interface. Afterwards, the change in relative binding free energy ($\Delta\Delta G_{\text{bind}}$) upon mutation of each amino acid to alanine is calculated, providing a quantification of the impact of each residue on the overall protein-protein binding. Usually, intermolecular energy and (de)solvation free energy terms are included in the calculations; sometimes, intramolecular energies and entropic contributions are also taken into account. Generally, *in silico* alanine scanning uses simple physical models or empirical (scoring) functions for assessing the energy change (78). Therefore, *in silico* alanine scanning is usually fast and computationally modest, allowing a rapid detection of binding determinants. As a downside, this method relies on approximations that often reduce its accuracy. Notably, many methods for hot spot prediction are applied to single experimental or modeled structures of a protein-protein complex. However, caution is needed because the hot spot detection outcome from a single complex structure may be less representative, especially if the proteins are flexible *in vivo*. Therefore, it is preferable to perform calculations on conformational ensembles of the proteins, e.g., obtained from MD or coarse-grained simulations. Krüger and Gohlke recently developed a webservice (<http://cpclab.uni-duesseldorf.de/dsppi>) for hot spot prediction in PPIs by *in silico* alanine scanning that uses the scoring function DrugScore^{PPI}. This method is founded on knowledge-based potentials derived according to the DrugScore formalism (165), adapted for use with PPIs by including information from experimental alanine scanning results. DrugScore^{PPI} consists of distance-dependent pair potentials derived from atom type-specific pair distribution functions from 851 experimental protein-protein complex structures. The weights of the pair potentials have been adapted by partial least squares regression on relative binding

affinities for the so far largest set of 309 alanine scanning results (166). The degree of buriedness of each interfacial amino acid is also included in the scoring function. The $\Delta\Delta G_{\text{bind}}$ is calculated according to Eq. 1 (see reference (166) for the equation of the DrugScore^{PPI} scoring function). DrugScore^{PPI} efficiently predicted affinity changes for an external set of 22 alanine mutants of the Ras/RalGDS complex showing higher correlation to experiment ($R = 0.66$) than FoldX ($R = 0.52$) (167), Robetta ($R = 0.43$) (168-170), and CC-PBSA ($R = 0.23$) (171).

$$\Delta\Delta G_{\text{bind}} = \text{DrugScore}^{\text{PPI}} (R = \text{Ala}) - \text{DrugScore}^{\text{PPI}} (R = \text{wildtype aa}) \quad (\text{Eq. 1})$$

MM-GB(PB)/SA calculations. As a complementary alternative to *in silico* alanine scanning, there are methods that calculate the contribution of individual amino acids to the binding free energy without mutating them, collectively referred to as *non-perturbing fully atomistic* approaches. Among them, the molecular mechanics-generalized Born surface area (MM-GB/SA) and the molecular mechanics-Poisson Boltzmann surface area (MM-PB/SA) methods predict the total binding free energy (ΔG_{bind}) by means of endpoint free energy calculations (172,173). These methods are advantageous as they provide accurate results at a relatively reduced computational cost, and have been widely applied to different systems for a variety of purposes, such as to evaluate docking poses, predict binding affinities, and identify hot spots. The MM-PBSA approach has been recently reviewed in detail, also with respect to its applications in PPI systems (174). The ΔG_{bind} is calculated as the difference of the free energy of the bound (G_{complex}) and unbound proteins (G_{receptor} , G_{ligand}) (Eq. 2), averaging the free energy of binding over an ensemble of statistically independent conformations extracted from MD simulations (indicated by the angle brackets in Eq. 2). This way, the conformational flexibility of the system is properly taken into account.

$$\Delta G_{\text{bind}} = \langle G_{\text{complex}} \rangle - \langle G_{\text{receptor}} \rangle - \langle G_{\text{ligand}} \rangle \quad (\text{Eq. 2})$$

The absolute free energy (G^{tot}) of complex, receptor, and ligand is calculated as the sum of gas-phase energy (E_{MM}), solvation free energy (G_{GB} and G_{SA}), and configurational entropy contribution ($-TS$) (Eq. 3). The gas-phase energy term includes bond, angle, dihedral, electrostatic, and van der Waals contributions from a molecular mechanics (MM) force field. The solvation free energy is computed as the sum of polar (based on the generalized Born (GB) or Poisson-Boltzmann (PB) continuum models) and non-polar (surface area-dependent, G_{SA}) contributions. Finally, a configurational entropy term can be included, calculated from normal mode or quasi harmonic analysis. However, the entropic term is often neglected, since

the resulting effective energy generally provides satisfactory predictions with the advantage of avoiding costly entropy calculations.

$$G^{\text{tot}} = E_{\text{MM}} + G_{\text{GB}} + G_{\text{SA}} - TS \quad (\text{Eq. 3})$$

If an effective energy is calculated, G^{tot} can be decomposed into contributions of individual residues, which allows identifying hot spots. Both MM-GB/SA and MM-PB/SA allow a per-residue decomposition of the binding free energy. It is also possible to further decompose the binding free energy into pairwise contributions, which highlights important interactions between pairs of amino acids. The method is usually used for post-processing ensembles from MD simulation trajectories. If the unbound proteins and the protein-protein complex are sampled individually, this leads to the conceptually rigorous *three-trajectory* approach (Eq. 2), which takes into account energetic differences caused by conformational changes upon complex formation, but is also computationally demanding. A widely used alternative is the *single-trajectory* approach (Eq. 4), in which the unbound structures are extracted from the trajectory of the complex without further relaxation.

$$\Delta G_{\text{bind}} = \langle G_{\text{complex}} - G_{\text{receptor}} - G_{\text{ligand}} \rangle \quad (\text{Eq. 4})$$

The latter approach, besides being faster, was shown to reproduce accurately experimental alanine scanning data. Indeed, the single-trajectory approach often proved to be superior to the three-trajectory alternative due to the cancellation of errors (63,80). However, it has to be mentioned that the MM-PB(GB)/SA energy function has also been applied for *in silico* alanine scanning on structural ensembles from MD simulation (164,175). In this context, Moreira *et al.* found improved predictions when using different dielectric constants to account for the varying extent of relaxation upon mutating charged, polar, and non-polar residues to alanine (176).

2.1.4 Modulating PPIs for targeting cancer: success stories

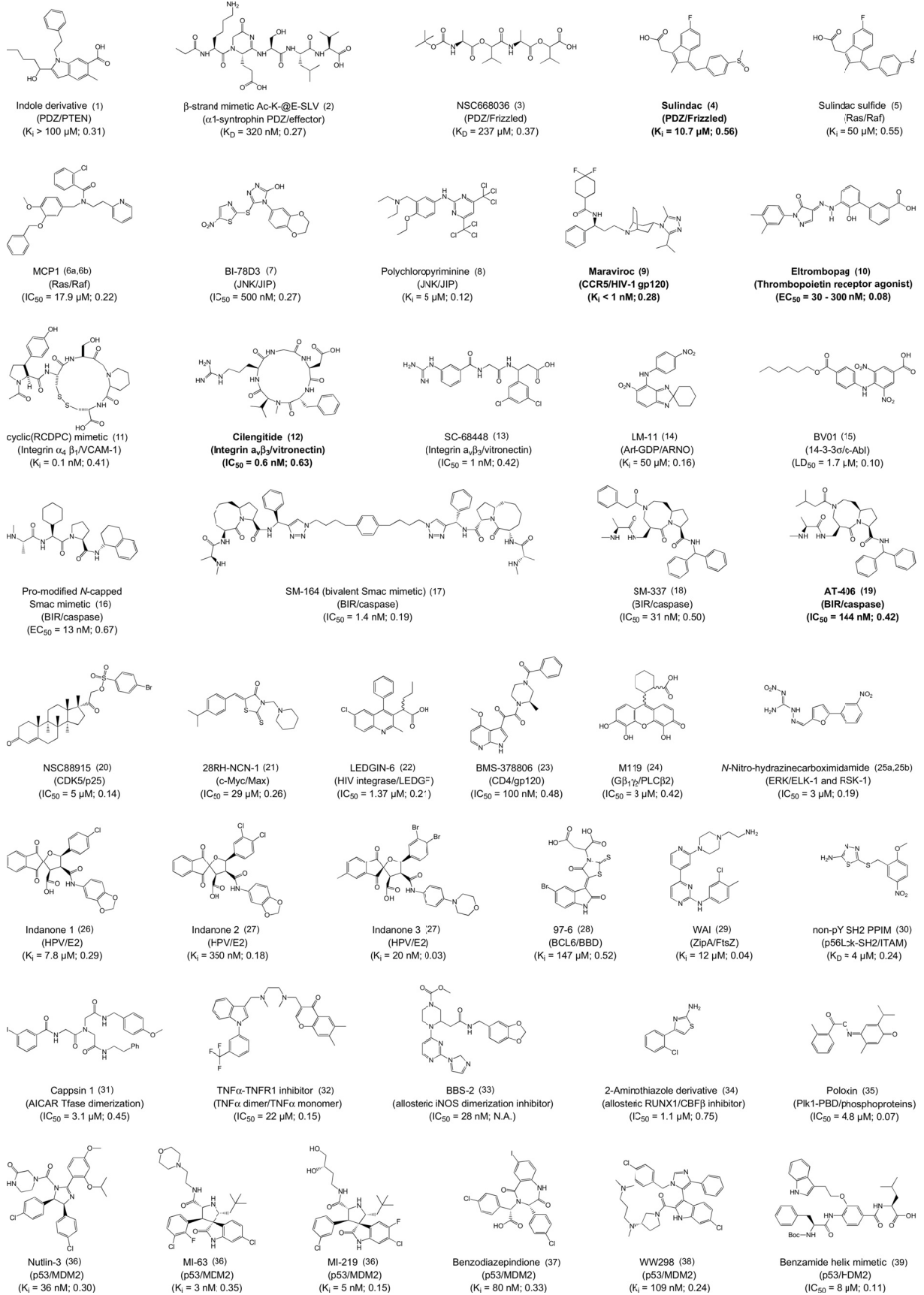
During the last two decades, many studies have investigated PPIs and identified PPIMs using both experimental and computational approaches. The available experimental data has been integrated into PPI-specific databases (38,177,178). Antibodies are currently the most successful class of drugs (179) inhibiting PPIs (180,181). As conveniently accessible high affinity PPIs, they can help reveal druggable epitopes, understand binding mechanisms (182), and may even inspire PPIM design (183) by complementing insights from non-antibody PPIs. As a drawback, antibodies are in some cases not cell permeable and lack oral bioavailability (184). Small-molecule PPIMs are an attractive alternative, as they should enable fast and efficient synthetic protocols, and provide better pharmacokinetic (ADME)

properties. The identification of small molecule PPIMs acting on several therapeutical targets has been the subject of intense research since the last two decades, and has been extensively reviewed (23,24,117,134,185-189). In Figure 4, a survey of the so far identified PPIMs is reported, with their potency and a druglikeness measure (Drug-Score) calculated by the OSIRIS druglikeness server (<http://www.organic-chemistry.org/prog/peo/>). The score highlights that not all of the so far discovered PPIMs are *drug-like*; this also includes those being marketed or tested in clinical trials for their potential pharmacological relevance. On the contrary, often the physico-chemical properties of PPIMs are significantly different from those of currently marketed drugs. This points out the need of revising our current understanding of what is meant by *drug-like* in the context of PPIs, extending the chemical space of conventional drugs to include the distinctive physico-chemical features of PPIMs (see **Paragraph 2.1.5**). Nevertheless, notable exceptions are present: although not frequently, some PPIMs are molecules presenting characteristics similar to conventional drugs, or are even marketed drugs for which an additional pharmacological activity on a PPI system has been demonstrated (Figure 4).

The modulation of PPIs has emerged as a particularly promising therapeutical approach for the treatment of cancer (Table 1). This is evidenced by: I) A thorough biological and structural characterization of a number of PPIs whose activity is linked to tumor development; II) the discovery of several small-molecule, potent PPIMs modulating cancer-related PPIs, some of which are currently being tested in clinical trials. In the following, three case studies that highlight the great potential of targeting PPIs for treating several types of cancer are presented. First, I describe PPIMs design for p53/HDM2, one of the most thoroughly investigated PPI systems. Then, I describe a retro- and a prospective study concerning interleukin-2 (IL-2) and nervy homology region 2 (NHR2) proteins.

HDM2

In many tumors, p53 acts as a tumor-suppressor protein (190-192). However, binding of the human double minute 2 (HDM2) protein (or the mouse analog MDM2), which is overexpressed in many tumors, blocks transactivation by p53 and increases p53's degradation. Thus, the p53/HDM2 interaction is an important pharmaceutical target for cancer treatment. Crystallographic structures revealed that the key interaction in the p53/MDM2 complex arises from the binding of a 15-residue α -helix of p53 into a hydrophobic cleft of MDM2 (Figure 5 A) (139). Furthermore, alanine scanning revealed three hot spots on the helix, F19, W23, L26 (Figure 5 A, Table 1) (193). Notably, this binding site suits most of the criteria in the decision tree proposed by Chene (42).



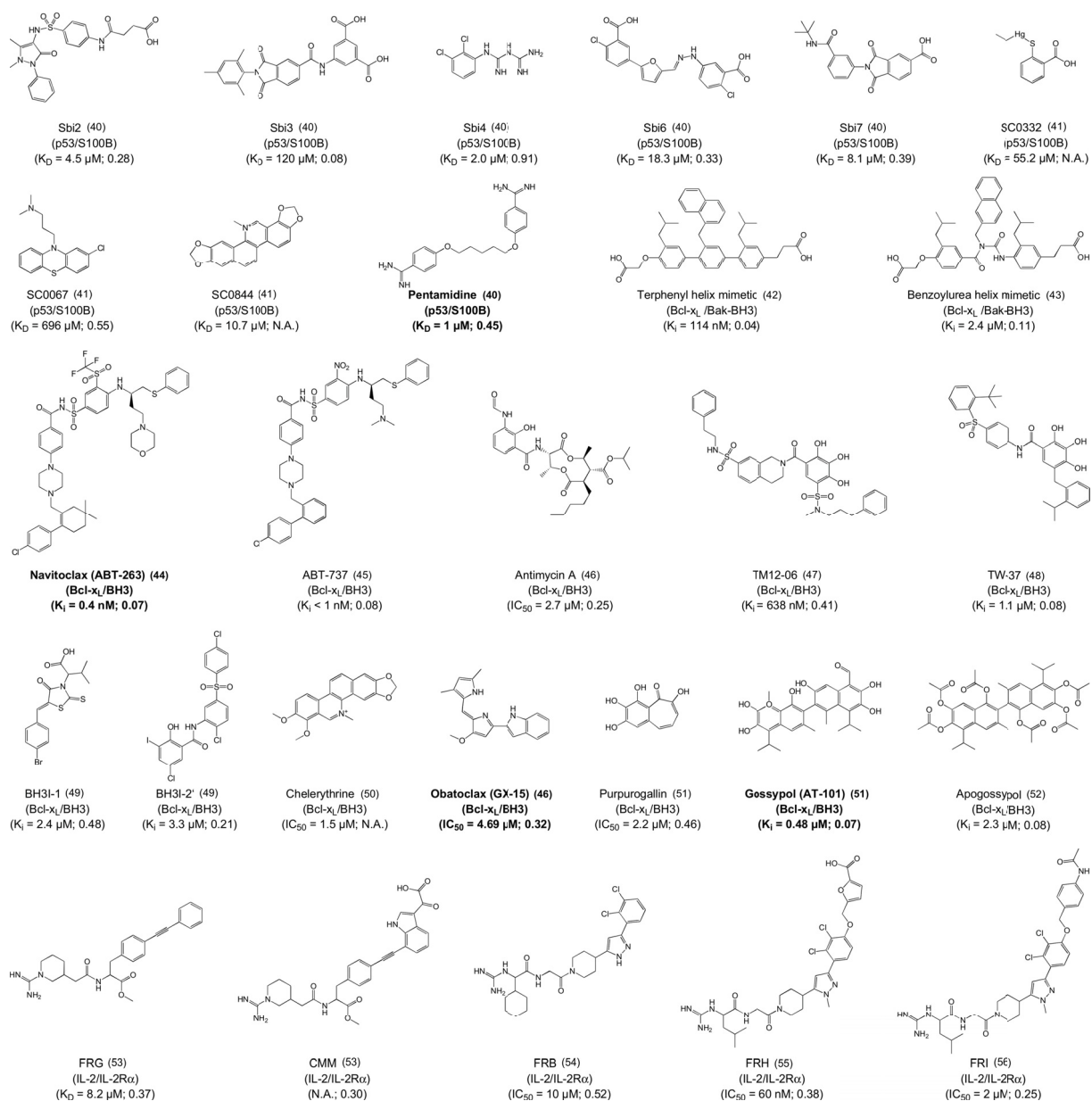


Figure 4. A survey of protein-protein interaction modulators. Labels contain the PPIM name followed by a reference detailing the potency. The references are reported in the **Appendix** (Page 196). Below, (PPI target/PPI competitor) and (potency; Drug-Score) are given in the first and second parentheses, respectively. Labels of marketed drugs or compounds that have been the subject of clinical trials are highlighted in bold. The Drug-Score was calculated by OSIRIS Property Explorer Drug-Score (<http://www.organic-chemistry.org/prog/peo/druglikeness.html>). Figure from Publication I, Reference (31).

Initially, PPIMs binding to HDM2, e.g., nutlins (Figure 5 B) (117,194), benzodiazepinediones (195), and others (Figure 4) (185,196-198), were identified via HTS. Structure-based design and molecular modeling were then used for ligand screening and optimization (199-203) leading to *in vitro* activities down to $IC_{50} = 3 \text{ nM}$ (201). Several computational techniques have helped designing and screening for ligands of HDM2 or MDM2. (I) MD simulations and computational alanine scanning could accurately predict the hot spots of the p53/MDM2 interaction already by efficiently post-processing wild-type trajectories (164). In the same study, also the change in binding affinity due to other covalent modifications, e.g.,

methylation of the hot spot tryptophan of p53, could be confirmed in good agreement with experimental data. Finally, the opening or widening of the binding pocket into a PPIM binding-competent conformation could be sampled by MD and detected computationally (62,70). (II) The molecular diversity of compound libraries (e.g., benzodiazepinediones) was maximized to optimize molecules for HTS and synthesis strategies (203,204). (III) Molecular docking (205,206), also in combination with *de novo* design (198,201,205), was applied to predict binding modes and optimize the design of PPIMs. (IV) Virtual Screening (202,207), QSAR (202), and receptor-based pharmacophore models using ensembles of receptor structures (208) were also applied. In general, these studies suggest that if there is no binding-competent pocket in the *apo* or protein-bound structure of a PPI target, such structures can potentially be found if multiple receptor conformations from NMR ensembles or crystallography are available (74). Alternatively, a conformational ensemble can be generated by molecular simulations, e.g., MD simulations, preferentially in solvent less polar than water (70), or constrained geometric simulation (63,70). Furthermore, post-processing schemes including complex relaxation and rescoring have been demonstrated to improve the ranking and identification of native like binding poses (74). In summary, many computational methods used in conventional computer-assisted drug design could be applied successfully to HDM2, also as a consequence of the deep binding cleft that is already preformed in the unbound HDM2 structure.

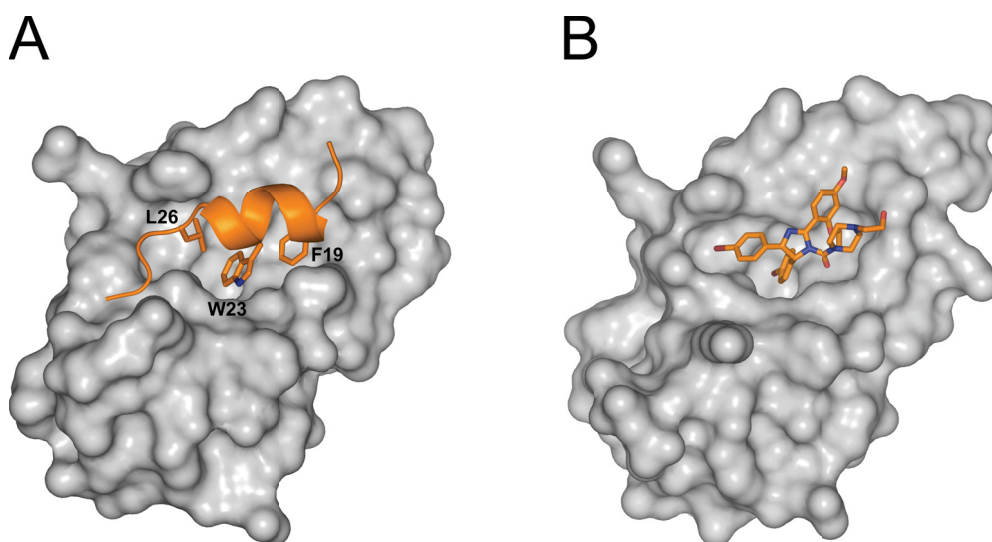


Figure 5 Crystal structures of p53- and Nutlin2-HDM2 complexes. (A) Native interaction of HDM2 (surface representation) with p53 (cartoon). The hot spot residues F19, W23, and L26 are shown as lines (PDB code 1YCR) (139). (B) PPIM Nutlin-2 interacts with HDM2 by binding in the same pocket as p53, mimicking the molecular interactions of the native ligand (PDB code 1RV1) (194).

INTERLEUKIN-2

IL-2 is a key cytokine involved in the regulation of the immune system with relevance for immunological diseases, transplant medicine, and cancer (209). Binding of the α -helical IL-2 to the trimeric IL-2 receptor is initiated by the association of IL-2 to the extracellular domain of the receptor's α subunit (IL-2R α). The IL-2/IL-2R α complex has been the subject of extensive studies that provided crystallographic structures and thermodynamic characterization of the protein-protein complex and five IL-2/PPIM complexes (Figure 4), rendering this system a perfect test case for structure-based computational methods on PPIM design. For the binding of a PPIM, a pocket in the flat but flexible interface of unbound (or receptor-bound) IL-2 has to open (Figure 2 B). The absence of such a pocket is a major obstacle for structure-based design if based solely on the unbound or receptor-bound structure of IL-2 (Figure 2 A). Additionally, it is difficult to decide which part of the large IL-2/IL-2R α interface ($\sim 2500 \text{ \AA}^2$) to address with a small molecule. Thus, it is not surprising that the first known PPIMs binding to IL-2 were not found by structure-based design but rather by HTS. Later, IL-2 PPIMs were designed using structural knowledge obtained by tethering experiments and/or fragment-based ligand design (144). This resulted in PPIMs with affinities down to the nanomolar range (210). Metz *et al.* were able to show that conformational sampling of the unbound IL-2 structure by a constrained geometric simulation method resulted in the opening of transient pockets, whereas MD simulations in explicit water failed in doing so, probably due to the hydrophobicity of these pockets (63). Using no knowledge about known IL-2 PPIMs, the same authors were then able to identify these pockets from the ensemble structures based on geometric criteria as provided by PocketAnalyzer^{PCA} (211). Notably, molecular docking into these pockets closely reproduced the bound state of the known IL-2 PPIMs, as could these PPIMs be successfully ranked by MM-PB(GB)/SA calculations and enriched in a large set of decoys. A narrow cluster of hot spots, forming a hot region, was predicted (63) by MM-PB(GB)/SA effective binding free energy decomposition (173) starting from the IL-2/IL-2R α complex (Table 1). Performing such decomposition for IL-2/PPIM complexes showed that essentially the same hot spots are also used for PPIM binding, pointing to a mimicry of the PPI by the small molecules. Being able to accurately predict transient pockets from an unbound structure, hot spot positions, and binding energetics from complex structures strongly suggests that the strategy and methods used here (Figure 6) will also be applicable in a prospective manner where nothing else than a protein-protein complex structure is known. Hence, this approach can provide a first step in any structure-based endeavor to identify PPIMs.

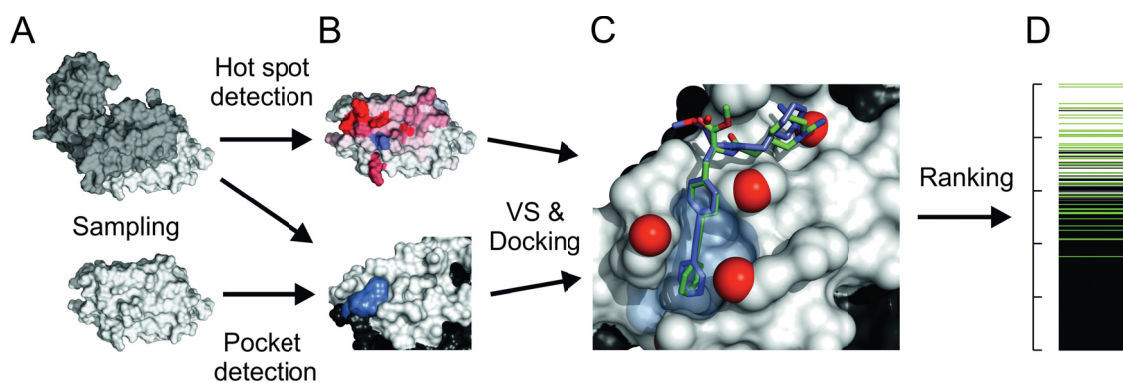


Figure 6 Strategy for PPIMs identification. (A) First, starting from a crystal structure (or homology model) of the target PPI, a conformational ensemble is generated by means of MD or geometric simulations. (B) Second, hot spots and pockets detection is performed. Surface coloring of hot spots (red) are shown on a linear color scale, as calculated by per-residue free energy decomposition; pocket volume depicted as blue surface. (C) Third, the hot spots information is transferred to a pharmacophore model used for virtual screening (VS) and subsequent docking of the identified hits. (D) Finally, the identified small molecules are ranked with respect to their predicted ability of mimicking the molecular interactions of the hot spots in the native PPI. Figure adapted from Publication I, Reference (31).

NHR2

NHR2 (nervy homology region 2) is the α -helical oligomerization domain of the RUNX1-ETO fusion protein present in approximately 12 % of all acute myeloid leukemia (AML) (212). The formation of NHR2 homotetramers from dimers has been shown to be essential for the leukemogenic activity of RUNX1-ETO (213). In a prospective study, spatially clustered hot spots in the tetramer interface were predicted by MM-GB/SA free energy decomposition (Figure 7 A, Table 1), and were subsequently validated by *in vitro* and *in vivo* experiments (213). These results reveal that alanine mutants of the hot spots prevent tetramerization of NHR2 and abolish AML formation in a mouse transplant model, thereby validating NHR2 as a promising cancer therapy target. A shallow, elongated cavity was detected next to the hot spots (Figure 7 B), suggesting that it could be a potentially druggable site in this PPI. The anti-parallel orientation of helices C1 and C2 in the NHR2 dimer places D533, E536, and W540 (Figure 7 C) in close proximity to residues W498 and W502 (Figure 7 D), which results in a spatially compact arrangement of the hot spot residues. Furthermore, these residues are not located in the center of the interface, which is rather flat, but at its edges. Starting from these findings, Metz *et al.* developed a 18mer peptide derived from the wild-type NHR2 sequence as an initial tetramerization inhibitor. Interestingly, this peptide showed *in vitro* inhibitory activity on NHR2 tetramerization, with an $IC_{50} \sim 390 \mu\text{M}$ measured in an ELISA assay (214). Based on this proof-of-principle, a virtual screening for small molecules was performed on the ZINC database (215), exploiting the knowledge about the predicted and validated hot spots. Convincingly, some of the top-ranking small molecules from this screening exhibited *in vitro* PPIM activity in NHR2 tetramerization assays. Additionally, a

fingerprint similarity search for structural analogs of the most promising compound deriving from the virtual screening allowed to identify the first small molecule inhibitor of NHR2 tetramerization, active in cells at micromolar concentration ($EC_{50} < 10 \mu\text{M}$) (214).

In summary, it was possible to (I) identify hot spots of the tetramerization of NHR2 that could be confirmed experimentally. These hot spots were (II) transferred to a peptide that is currently further optimized. After identifying a potent peptidic PPI modulator (III) virtual screening for molecules exhibiting an arrangement of pharmacophoric groups as found in the peptide was carried out. These results demonstrate that the mutual integration of experimental and computational techniques is a promising approach to cope with the challenges of protein-protein interfaces in PPIM identification and design.

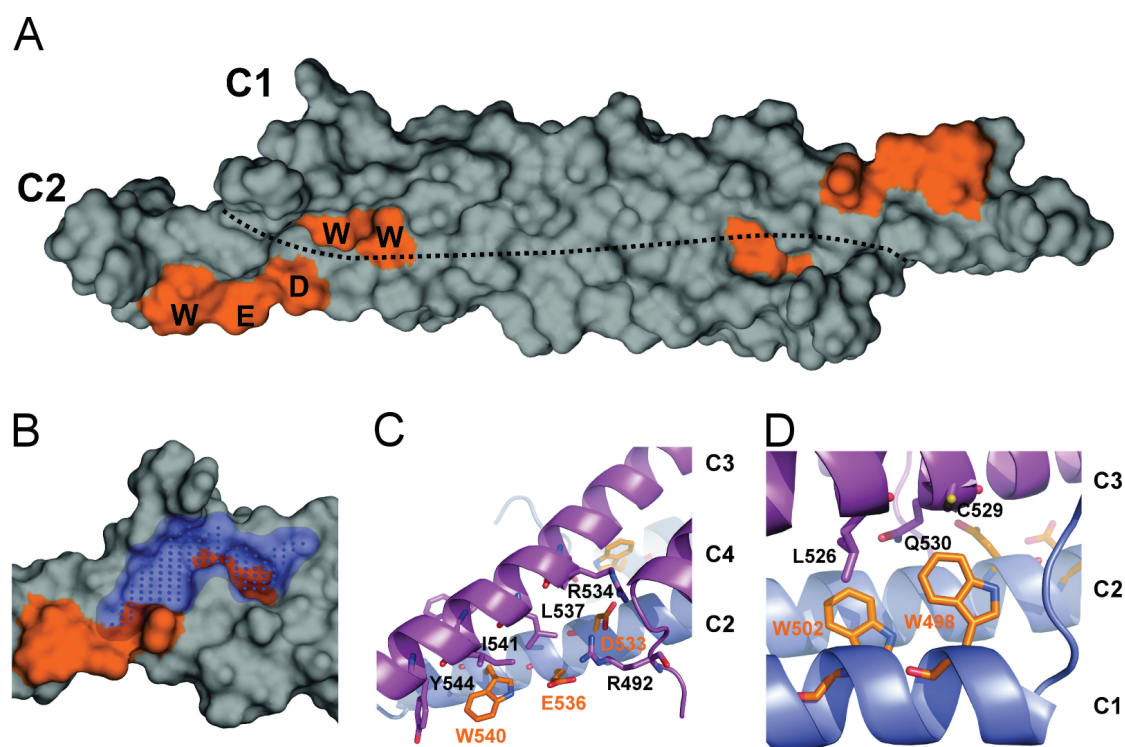


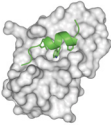
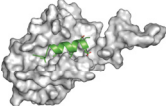
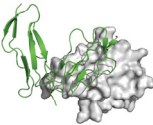
Figure 7 NHR2: structure and determinants of binding. (A) Hot spots (W498, W502, D533, E536, and W540) in the dimer/dimer interface of NHR2 (PDB code: 1WQ6) calculated by per-residue MM-PBSA free energy decomposition. The dotted line represents the border between the two antiparallel-helices C1 and C2. (B) Potentially druggable pocket in the dimer/dimer interface of NHR2. The blue dots mark the location of the largest indentation in the binding epitope. Intermolecular contacts involving (C) hot spots D533, E536, and W540 on helix C2 as well as (D) hot spots W498 and W502 on helix C1. Figure adapted from Publication I, Reference (31).

2.1.5 Perspectives of modulating PPIs

Targeting protein-protein interfaces is currently a topic of outstanding interest in drug discovery. Since these targets offer great opportunities to interfere with PPI networks, and consequently for the development of new therapeutics, considerable effort has been undertaken for the discovery of PPIMs. As a result, the detailed characterization of many PPIs

brought us remarkably closer towards an understanding of PPIs and their druggability (27). While many PPIMs have been discovered by HTS, the structural insight into PPIs from experimentally determined protein-protein complexes, and the experimental and computational methods for the identification of clustered hot spots and binding pockets has accelerated the rational design of PPIMs. Indeed, there are already a few examples of marketed small-molecule drugs acting on PPIs (24,110-113,181,216). However, PPIs are different from classical targets in that binding pockets are often less pronounced, and hot spots are not in all cases arranged in a manner that they can easily be addressed by a small molecule. As pointed out by Morelli *et al.* along with the observation that there is not yet a unified approach for PPIM discovery, it appears that any such attempt has to be tailored for a specific PPI (217). Nevertheless, the wealth of reported PPIMs shows that many PPIs are at least *ligandable* (27) (Figure 4). With respect to the druggability of PPIs, it has to be mentioned that many of the so far developed PPIMs address PPIs that are predisposed by having preformed pockets and clustered hot spots and, accordingly, are more druggable than other PPIs (Table 1). Additionally, it has to be mentioned that many of the reported PPIMs are not *drug-like* in the sense of Lipinski's rules, leaving considerable space for improvement and optimization to achieve the desired specificity and ADME properties. With the increasing number of known PPIMs, it is becoming clear that their chemical space is not identical to that of the majority of marketed drugs (218,219). In fact, many of the PPIMs with pharmacological and clinical relevance do not exhibit the characteristics classically considered to be preferable for a drug-like molecule. Rather, PPIMs are generally larger and more hydrophobic molecules (28,220-222), often violating Lipinski's rule of five (223), although notable exceptions have been reported (Figure 4). Sperandio *et al.* performed a statistical analysis on 66 PPIMs and 557 regular drugs, in order to identify molecular descriptors able to discriminate between the two classes of ligands. These authors reported an average MW of 421 Da for PPIMs versus 341 Da for regular drugs, and an average AlogP of 3.58 versus 2.61, respectively. Furthermore, they evidenced that the number of rings and aromatic moieties are higher in PPIMs than in conventional drugs (188). The same authors performed a similar analysis on a larger database (115 PPIMs and 1730 enzyme inhibitors) and confirmed this trend (218). Consequently, it is evident that most currently available screening compounds libraries are predominantly comprised of molecules with characteristics appropriate for classical targets, and therefore are not ideal for the identification of PPIMs. Accordingly, the development of methods for tailoring libraries that are specifically suitable for PPIM identification is highly needed (224).

Table 1. Examples of druggable PPIs involved in cancer.

PPI complex	Type of cancer	Affinity ^a	Hot spots ^b	Pocket volume ^c	Inhibitors ^d	PDB ^e
 MDM2/p53	Soft tissue sarcoma, osteosarcoma, breast cancer, prostate cancer	600	F19, W23, L26	351	36, 37, 38, 39	1YCR
 Bcl-xL/Bak	Prostate cancer, small-cell lung cancer, non-Hodgkin's lymphomas	340	V74, L78, I81, D83, D84	97	42, 43	1BXL
 IL-2/IL-2R	Melanoma, renal cell cancer, leukemia, breast cancer	10	K35, R38, F42, E62, L72	146	53, 54, 55, 56	1Z92
 NHR2	Acute myeloid leukemia	1*	W498, W502, D533, E536, W540	269	225	1WQ6

[a] Affinity of the PPI complex, in nM (177).

[b] Hot spots residues revealed from experimental alanine scanning/computational methods.

[c] Volume of the binding pocket, in Å³ (177,214).

[d] References of the most important known inhibitors for the respective PPI, as reported in Figure 4 and in the Appendix, page 196. For NHR2, this refers to the case study reported in Chapter 2.1.4 (214,225).

[e] Crystal structure of the PPI complex available in the PDB.

* Estimated K_D in nM, as described in Reference (225).

Note, however, that the trend in recently approved NME shows that the traditional criteria for drug-like properties, though desirable, are not a strict criterion for exclusion (219). In addition, there are several examples for the optimization of non-drug-like molecules (226) and novel drug-delivery approaches (227) with which some of the barriers for non-drug-like PPIMs may be overcome.

Any attempt to identify or optimize PPIMs can greatly benefit from integrating computational and experimental methods of pocket and hot spot detection, screening, and rational design (228). However, even though the success of several such attempts has been reported, it is hard to decide which computational methods will work best for a specific PPI because many of these methods have only been applied to one or a few targets. Furthermore, the performance of general strategies for the prediction of pockets and hot spots is hardly comparable, for two reasons. First, the datasets used to validate many methods vary considerably, often as a consequence of the prerequisites each individual method has. Second, the definition of pockets and hot spots often varies, thus complicating a statistical comparison of the prediction performance. To overcome this situation there is a high demand for common benchmarking

datasets and a comparative database with experimental data, as well as predictions from various methods for enabling a comparison amongst subsets of known targets and to extrapolate to new ones. Furthermore, adapting the content of (virtual) screening libraries in order to cover the chemical space of PPIMs (217,224), e.g., by including large but pre-organized scaffolds containing hydrophobic/aromatic groups as often found in PPIMs and privileged scaffolds such as peptidomimetics, will facilitate the identification of new PPIMs. In fact, the amount of available data on PPIs is still very low in comparison to classical targets. However, with the expected progress in experimentally determined PPI structures, targets, and affinity data thereof and of PPIMs it will eventually be possible to compare PPI targets, transfer successful strategies, and exploit the potential of modulating PPIs to its full extent.

2.2 HSP90 AS A NOVEL TARGET FOR CANCER THERAPY

In the intricate cellular environment, abnormal protein folding and aggregation may occur because of constitutive *macromolecular crowding* or upon stress events, resulting in protein malfunction and eventually pathological conditions (229). For this reason, *molecular chaperones* and other proteins are committed to help newly synthesized polypeptides to adopt their functional conformation, assemble macromolecular complexes, and prevent misfolding and aggregation. Among them, the *heat shock proteins* (HSPs) are a large family of evolutionary conserved chaperones present in most organisms from bacteria to mammals that are particularly activated upon exposure to elevated temperatures.

2.2.1 Biology and pathophysiology of Hsp90

The *heat shock protein of 90 kDa* (*Hsp90*) is a prominent member of the HSPs family, being a highly conserved and ubiquitously expressed molecular chaperone. In humans and eukaryotic organisms, the protein is essential for cell's viability, and it constitutes 1-2 % of the total cellular protein content (229). Hsp90 plays an essential role in maintaining protein homeostasis in the cell, being involved in (re)folding, stabilization, maturation, intracellular transport of its substrates (or *clients*) (230-232), not to mention post-translational signal transduction, epigenetic regulation, chromatin remodeling, and proteasomal degradation (230). In physiological conditions, Hsp90 is characterized by a high basal expression, which ensures the correct *de novo* protein folding and prevents misfolding and aggregation (233,234). Conversely, its expression and activity are increased in response to environmental stress events (e.g. heat, hypoxia, acidosis, exposure to heavy metals, etc.), exerting a protective effect for the exposed cells (235). However, the importance of the chaperone goes beyond the response to environmental stress, influencing a number of pathways and processes (Figure 8) (229,236), and an estimated 10-30 % of the proteome (237,238). Hsp90 is in fact a protagonist of a very complex protein network, as evidenced by an interactome consisting of hundreds of putative clients including kinases, transcription factors, and a large range of structurally unrelated proteins (236,239,240). Typical Hsp90's substrates are signal transducer proteins that are central to growth control, cell survival, and developmental processes (241). In contrast to enzymes such as kinases, which covalently modify their substrates upon interaction, Hsp90 (and chaperones in general) interacts with its clients forming transient complexes in a cyclical manner. These recognition and binding processes are driven by ATP binding and hydrolysis, and involve considerable conformational rearrangements (235) (see

Paragraph 2.2.3). In its active form, Hsp90 builds up large macromolecular complexes by association with clients and a wide variety of auxiliary proteins (*co-chaperones*) (Figure 8).

Four Hsp90 family members have been reported in humans, which differ in the cellular localization: two cytosolic isoforms (α and β), and the homologues glucose-regulated protein 94 (GRP94) and tumor necrosis factor receptor-associated protein-1 (TRAP-1), found in the endoplasmic reticulum and mitochondrion, respectively (242). The β isoform is constitutively expressed, whereas the α isoform is inducible, “cytoprotective”, and overexpressed in stress conditions. However, a well-defined functional distinction between the two cytosolic isoforms has not been elucidated yet (243,244).

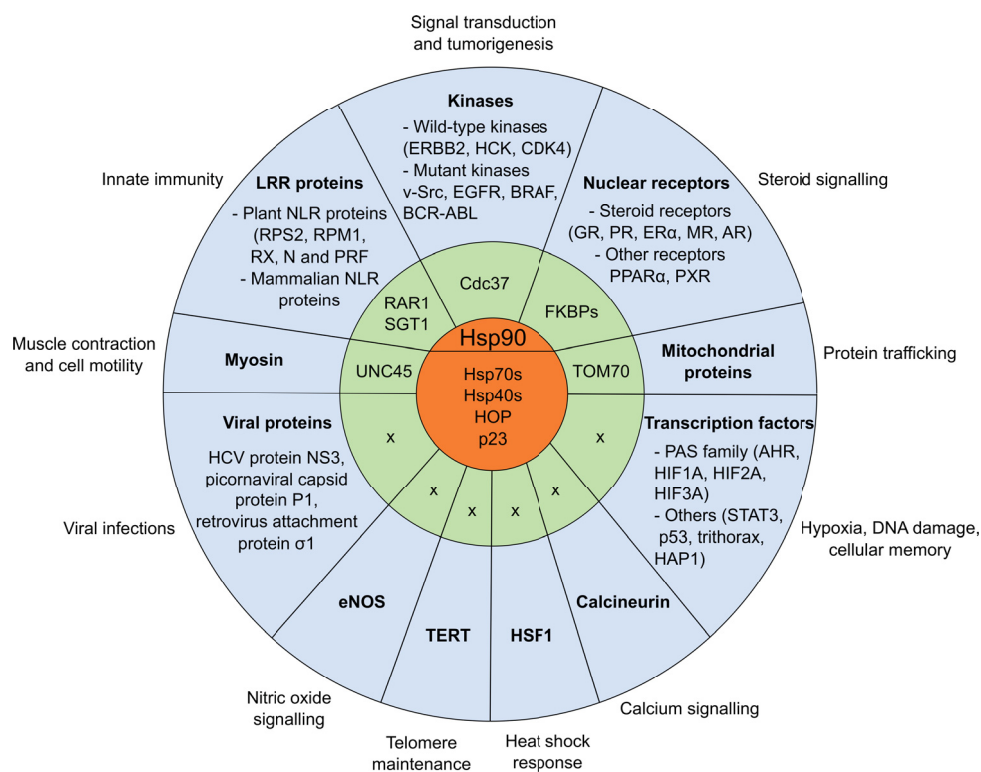


Figure 8. Hsp90's network of client proteins, co-chaperones and corresponding cellular processes controlled. Hsp90 interacts with the essential co-chaperone p23, HOP and the Hsp70-Hsp40 chaperone systems (orange). The interaction with client proteins (blue) elicits a cellular response, and it is often mediated by adaptor co-chaperones (green). Interactions mediated by an unknown adaptor are indicated by an x. Abbreviations used: AHR, aryl hydrocarbon receptor; AR, androgen receptor; CDK4, cyclin-dependent kinase 4; EGFR, epidermal growth factor receptor; eNOS, endothelial nitric oxide synthase; ER α , estrogen receptor- α ; FKBP, FK506-binding protein; GR, glucocorticoid receptor; HAP1, haeme activator protein 1; HCK, haematopoietic cell kinase; HCV, hepatitis C virus; HIF, hypoxia-inducible factor; HSF1, heat shock factor 1; LRR, Leu-rich repeat; MR, mineralocorticoid receptor; N, nucleoprotein; NALP, NACHT, LRR and PYD domains-containing protein; NLR, nucleotide-binding LRR; NOD1, nucleotide-binding oligomerization domain-containing protein 1; PPAR α , peroxisome proliferator-activated receptor- α ; PR, progesterone receptor; PRF, *Pseudomonas* resistance and fenthion sensitivity; PXR, pregnane X receptor; RPS2, resistance to *Pseudomonas syringae* 2; STAT3, signal transducer and activator of transcription 3; TERT, telomerase reverse transcriptase; TOM70, translocase of outer membrane 70 kDa. Figure adapted from Reference (229).

Along its multiple physiological functions, Hsp90 has an essential role in favoring cancer. The chaperone is found overexpressed in tumors, where it helps the survival of malignant

cells by maintaining their homeostasis and tolerating mutations in crucial signaling molecules that would normally lead to apoptosis (235). This way, Hsp90 contributes to promoting oncogenesis and metastasis in several types of cancer (e.g. leukemia, melanoma, multiple myeloma, breast cancer, non-small-cell lung carcinoma), and it is associated with higher invasive potential and poor prognosis (235,245,246). On a molecular basis, this is due to the fact that several oncoproteins are among Hsp90's clients. The chaperone-mediated stabilization of substrates such as kinases, steroid hormone receptors, telomerase, AKT, hypoxia-inducible factor 1- α (HIF1 α), and matrix metalloproteinase-2 (MMP2) favors in malignant cells uncontrolled proliferation, immortalization, impaired apoptosis, angiogenesis and metastasis (235). Furthermore, Hsp90 can be secreted into the extracellular matrix enclosing cancer cells, this way contributing to tumor invasiveness (247). For these reasons, cancer cells are highly dependent on Hsp90 for sustaining and propagating the malignant characteristics typical of a tumor (246). Consequently, in the last two decades, big efforts have been dedicated to the development of modulators of Hsp90 activity as drug candidates for the treatment of cancer (see below **Paragraph 2.2.4**).

2.2.2 Structure of Hsp90

Hsp90 is a large and flexible protein that exists principally as a homodimer. Although several authors showed that Hsp90 can also form higher oligomeric complexes, both in physiological and in stress conditions (248-251), the functional form of the protein is the homodimeric one. Each monomer consists of three major functional domains: amino terminal domain (NTD), middle domain (M), and carboxy terminal domain (CTD) (233,252,253) (Figure 9 A). The NTD encloses an adenine-nucleotide-binding pocket, and it is responsible for the hydrolysis of ATP, which is essential in the chaperone's activity cycle (see below **Paragraph 2.2.3**, Figure 10) (254,255). This domain is very well characterized at the molecular level, with several X-ray structures available in the Protein Data Bank (PDB). Most of the Hsp90 inhibitors reported up to date bind in the NTD ATP pocket (see below **Paragraph 2.2.4** and Figure 11) (256-258). In eukaryotes, a charged region (CR) serves as flexible linker between NTD and M domain. The M domain constitutes the main interaction site for client proteins, and modulates ATP hydrolysis by direct interaction with the γ -phosphate of ATP bound to the NTD (Figure 9 A) (233,235,255). The CTD is the protein's principal dimerization site, and it is involved in the regulation of the ATPase activity (234,259), likely through a second putative nucleotide-binding site (235,260,261). The CTD is also the site of action of few Hsp90 inhibitors (260,262,263), which bind in a region peripheral to the dimerization interface (Figure 9 A and B, Figure 11 D) (264). The CTD dimerization occurs through the

interaction of two pairs of helices (from each monomer) forming a characteristic four-helix bundle (Figure 9 B) (233,265). Helices H4 and H5 form most of the dimerization interface, which consist principally of hydrophobic contacts (Figure 9 B and C). The corresponding amino acids are considerably buried upon dimerization, with a buried surface area of $\sim 1267 \text{ \AA}^2$ per monomer in the human Hsp90 (251,265). Finally, the C-terminal end of the CTD carries a highly flexible, charged 35-amino acids tail that seems to be involved in the recruitment of co-chaperones through a conserved MEEVD motif (235).

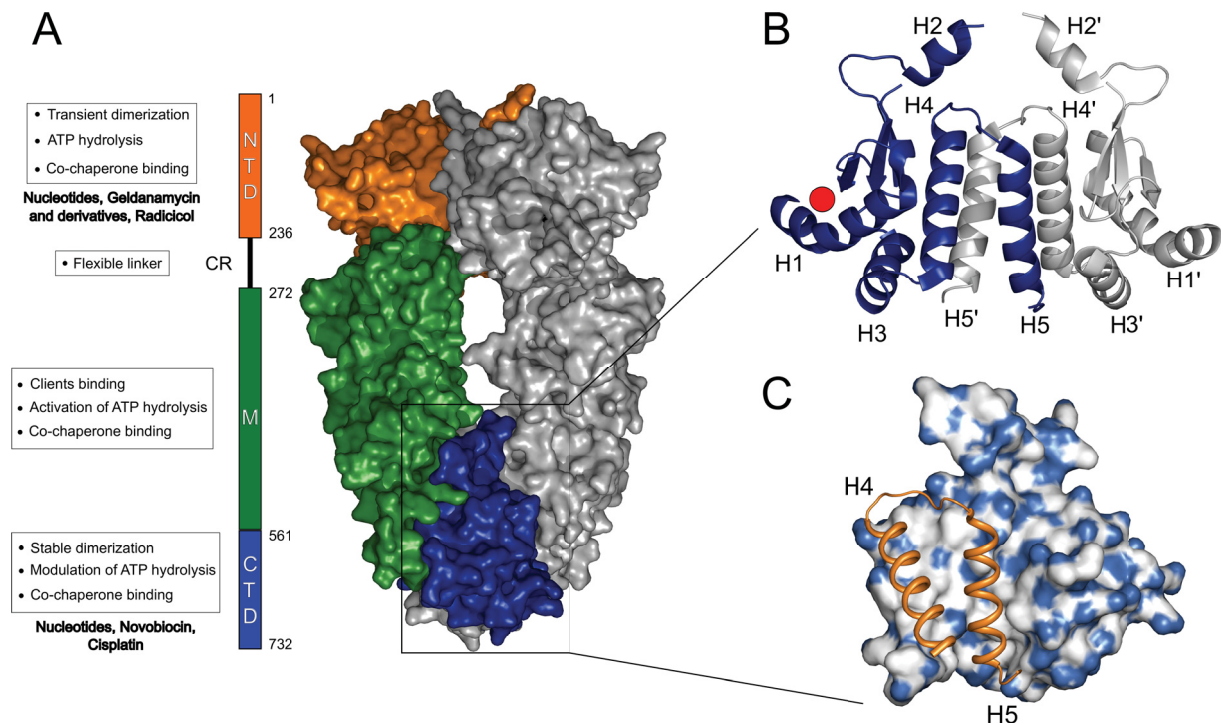


Figure 9 Domain organization of Hsp90. (A) Surface representation of the full-length *S. cerevisiae* Hsp90 (PDB code 2CG9). The three protein domains are shown in the structure and in the adjacent schematic representation: N-terminal domain: orange, middle domain: green, C-terminal domain: blue, charged region (CR): black. In the boxes, the main biological functions of each domain are given. In bold, Hsp90 inhibitors binding in the respective protein domains are mentioned. (B) Cartoon representation of the hHsp90 CTD crystal structure (PDB code 3Q6M), showing how the monomers (blue and grey) interact and form the characteristic four-helix bundle. The red circle indicates the putative binding region of Novobiocin (264). (C) Representation of the same domain highlighting the shape complementarity between the two monomers, and the groove at the interface (surface) that accommodates helices H4 and H5 (cartoon). The surface representation underlines the high hydrophobicity of the dimer interface (white: hydrophobic; blue: polar).

2.2.3 Mechanism of Hsp90's function

Hsp90 is an intrinsically highly flexible protein, whose chaperone function is dependent on ATP binding and hydrolysis, and accompanied by complex conformational rearrangements. This conformationally coupled ATPase cycle is conserved among Hsp90 homologs, and a number of structural and biochemical studies on full-length and isolated Hsp90 domains from human and other organisms (e.g. *E. coli* and *S. cerevisiae*) contributed to assemble an extensive picture of the mechanism regulating Hsp90's function (233,251,266-268). ATP

binds in the NTD, in a highly conserved pocket that is delimited by two α -helices, and extends from the surface to the buried face of a twisted antiparallel β -sheet (Figure 11 A) (233,252). Early studies led to the observation that ATP binding and consequent Hsp90 activity are coupled with the transition from an open, hydrophobic state, to a closed one (233,269). Accordingly, in the apo state, Hsp90 adopts an open, V-shaped conformation, where the protein is dimerized via the CTD, and the NTDs are apart from each other (Figure 10 A and E) (230,267). Through a complex series of events, binding of a molecule of ATP in the NTD of each monomer triggers significant structural rearrangements that eventually lead to the association of the NTDs, allowing the hydrolysis of the substrate and, consequently, activation of the chaperone (Figure 10 B).

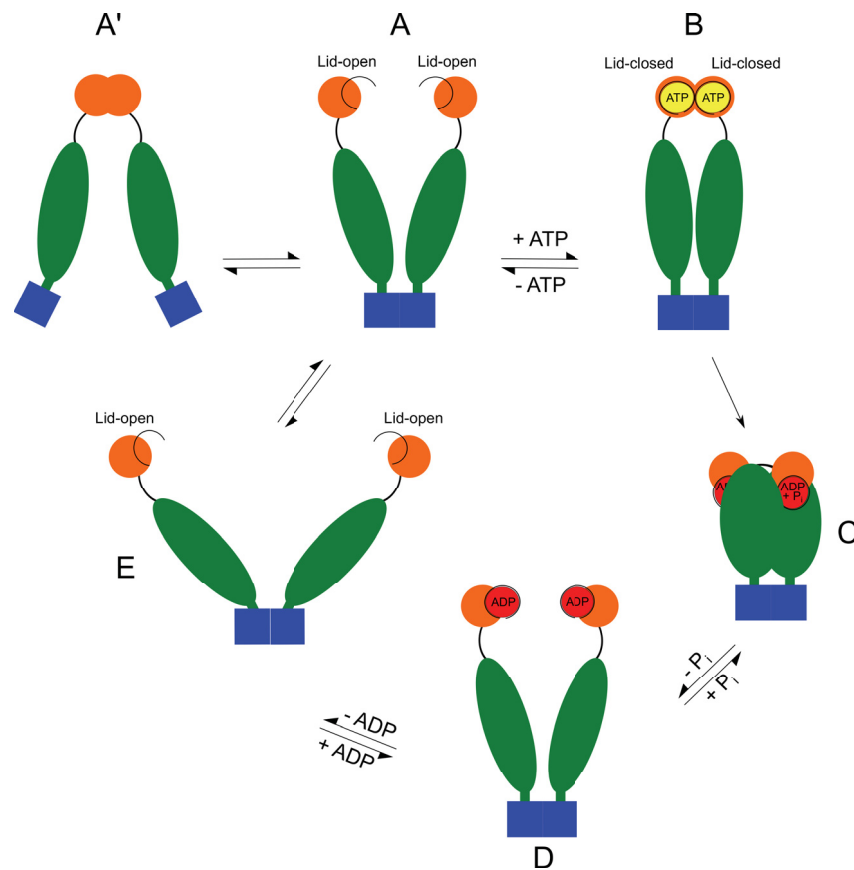


Figure 10 Hsp90's ATPase/conformational cycle. (A) Hsp90 apo conformation, where the protein is associated via the CTD. The lid region (black circles) is open, allowing the binding of ATP. This conformation is physiologically in equilibrium with a CTD-open conformation (A') (270). (B) Upon ATP binding, Hsp90 adopts a closed conformation, where both NTD and CTD are associated. The lid region is closed over the binding pocket. (C) ATP hydrolysis yields a compact conformation, where the NTDs are projected towards the M domain. The release of phosphate (D), and subsequently ADP (E), leads the protein back to an open conformation, ready for another hydrolytic cycle. Hsp90's domains are indicated in the scheme as: N-terminal domain: orange, middle domain: green, C-terminal domain: blue.

During this process, at first the binding of ATP initiates the motion of two α -helices in the NTD, the so-called *lid region* (residues 100-125), which close over the nucleotide binding site, promoting ATP hydrolysis and association of the two NTDs via strand exchange (Figure

10 A and B) (266). Interestingly, ATP binds in the NTD in a kinked conformation that allowed the design of very specific inhibitors mimicking this characteristic orientation (Figure 11 A and B). Afterwards, residues from a flexible loop of the M domain contact the NTD, leading to a twisted, closed conformation, and favoring ATP hydrolysis. Small angle X-ray scattering (SAXS) and electron microscopy experiments revealed that before ADP release, Hsp90 transiently adopts a very compact conformation where the NTDs are projected toward the M domains, in the inner part of the complex (Figure 10 C) (267,271-273). This conformation is thought to favor the maturation and release of the clients. Finally, the lid opens again, the chaperone returns to an open conformation, and ADP and client(s) are released (Figure 10 D and E). The rate-limiting step of the whole process is the large conformational rearrangements leading to the NTD dimerization (266). Initially when the mechanism behind Hsp90's function was first elucidated, it was assumed that the CTD is permanently dimerized, and the motions associated with the transition between open and closed conformations can be compared to the opening and closing of a clamp. This early hypothesis was supported by a variety of experiments, among which were biochemical and electron microscopy evidences (233). The very stable Hsp90 dimerization ($K_D = 60$ nM and 24 nM for *S. cerevisiae* and *E. coli* Hsp90, respectively (265,274)) did not easily allow to investigate NTD and CTD dimerization equilibria separately. However, Ratzke *et al.* recently showed with single-molecule fluorescence resonance energy transfer (smFRET) experiments that the CTD can open and close with fast kinetics (270) (Figure 10 A'). Interestingly, these authors showed that CTD and NTD dimerization are anti-correlated, suggesting the existence of long-range communication between these domains, and are strongly influenced by the presence of ATP and ADP (270). Signal propagation mechanisms and long-range communication pathways between CTD and NTD have been also described at a molecular level in a comprehensive computational study by Morra *et al.* (275). These recent findings evidence novel mechanistic aspects of Hsp90 activity, and the elucidation of the CTD opening suggests that inhibiting the CTD dimerization is a feasible strategy to modulate Hsp90's activity.

2.2.4 Targeting Hsp90 for cancer therapy

Since its role in favoring malignant transformation and progression was recognized, already in the early 1990's, Hsp90 has been proposed as a promising target for cancer therapy (244). Considering the large variety of mechanisms controlled by the chaperone in cancer cells, Hsp90 inhibition is expected to provide a simultaneous alteration of multiple oncogenic pathways. Although addressing a single target was proven extremely successful in the case of

some current chemotherapy agents (276,277), interfering with large parts of molecular pathways is emerging as a novel attractive concept for developing drugs (13,278). As such, interfering with Hsp90 activity should yield a broader efficacy, and provide an interesting alternative to the classic “single-drug, single-target” approach (235,269). Accordingly, the initial skepticism toward the notion of targeting a regulatory protein involved in a myriad of cellular processes was largely overcome, also due to the development of several NME, some of which showed clinical activity as Hsp90 modulators (Figure 11 C and D, Table 2) (244).

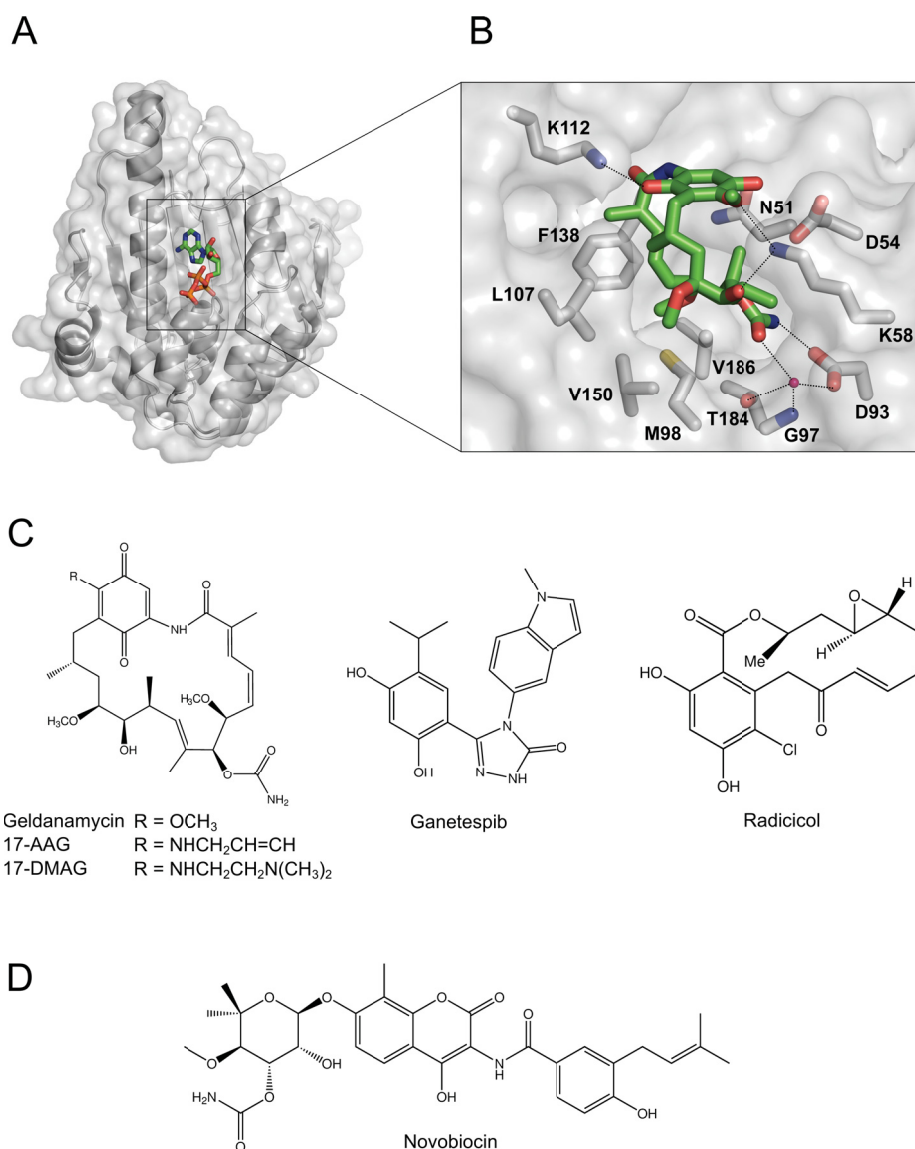


Figure 11 Small-molecule Hsp90 inhibitors. (A) Crystal structure of the hHsp90 NTD, showing the binding pocket with the native ligand, ATP (PDB code 3T0Z) (279) (B) Blow-up of the NTD ATP binding pocket with the inhibitor Geldanamycin bound. The residues of Hsp90 involved in important interactions with the ligand are represented as sticks; hydrogen bonds as dashed lines; a water molecule forming a salt bridge as pink sphere (PDB code 1YET) (280) (C) Chemical structures of some extensively investigated Hsp90 NTD inhibitors, and (D) of a CTD inhibitor.

The latter was a fundamental milestone that validated Hsp90 as pharmacological target for the treatment of different types of tumors (230,235,281-284). Currently, the druggability of this

chaperone is no longer questioned, and Hsp90 is in fact one of the most intensively investigated cancer drug targets from academia and industry (244,285). On a cellular level, inhibition of Hsp90 activity causes an increased degradation of oncogenic clients and depletion of their cytosolic levels. Consequently, Hsp90 inhibition antagonizes uncontrolled replication, insensitivity to growth suppression signals, avoidance of apoptosis mechanisms, increased angiogenesis, invasion, and metastasis, which are typical characteristics of malignant cells (246).

Table 2. Representative members of various classes of Hsp90 inhibitors subjected to clinical trials (286-288).

Drug	Type of cancer	Phase of clinical studies	Route
Geldanamycin analogues			
Tanespimycin (17-AAG)	HER2-positive breast cancer, myeloma, melanoma, ovarian, prostate, renal cell cancer	1-2	IV
Alvespimycin (17-DMAG)	HER2-positive breast cancer, AML, melanoma, prostate cancer, ovarian cancer	1	IV, oral
Retaspimycin	HER2-positive breast cancer, GIST, NSCLC	1-3	IV
Resorcinol derivatives			
Ganetespib (STA-9090)	Rectal cancer, melanoma, AML, CML, NSCLC	1-3	IV
NVP-AUY922 (VER52296)	HER2-positive breast cancer, NSCLC	1-2	IV
AT-13387	GIST	1-2	IV, oral
Purine analogues			
BIIB021 (CNF 2024)	CLL, HER2-positive breast cancer	1-2	Oral

Abbreviations: AML = acute myeloid leukemia; CML = chronic myeloid leukemia. CLL = chronic lymphocytic leukemia; GIST = gastrointestinal stromal tumor; IV = intravenous; NSCLC = non-small-cell lung cancer

Interestingly, it has been observed that in cancer cells the affinity of Hsp90 for its inhibitors is ~100-fold higher than in normal cells (235,289). This selectivity relies on three principal factors: I) Cancer cells are “addicted” to the uncontrolled activity of oncogenic proteins that promote malignancy. Consequently, pharmacological antagonism of oncogenic processes has a higher influence on tumor cells. II) In cancer cells, many oncoproteins are mutated, and consequently more labile and more dependent on Hsp90 for their stability and activity. III) Cancer cells depend on Hsp90 (and other chaperones) to establish and maintain the non-physiological microenvironment typical of tumors (hypoxia, acidosis and nutrient

deprivation) (269). The high selectivity of Hsp90 inhibitors should be advantageous particularly with respect to the toxicity profile of the potential drugs developed. Several Hsp90 inhibitors drug candidates are currently in clinical trials for the treatment of leukemia, melanoma, multiple myeloma, breast cancer, non-small-cell lung carcinoma, and other types of tumor (Table 2) (236,242,256,286-288). In particular, as of February 2015, Hsp90 inhibitors were reported to be in different stages of a total of 104 clinical studies worldwide (<https://clinicaltrials.gov>) (244). Most of the reported inhibitors act by targeting Hsp90's NTD ATP binding pocket, and this approach led to the development of several interesting drug candidates (Table 2) (244,256-258). Only few Hsp90 inhibitors have been reported acting at the CTD (e.g., Novobiocin and related coumarin antibiotics) (Figure 11 D) (260,263). While the investigation on the latter class of compounds is still at a preclinical phase, Hsp90 CTD inhibition is considered an attractive alternative approach to interfere with the chaperone for cancer therapy. As such, Hsp90 CTD inhibition has been shown to trigger a significantly lower activation of the heat shock transcription factor 1 (HSF1), a typical cellular adaptive response to NTD inhibitors that limits their activity (244). To the best of my knowledge, none of the CTD inhibitors reported until now target the chaperone's dimerization interface. This provided me with the incentive to pursue a novel approach for interfering with Hsp90 activity aimed at rationally developing Hsp90 inhibitors targeting the CTD dimerization interface. In the following, an overview of the strategy and the outcome of this study is reported.

3 SCOPE OF THE THESIS

During the last decades, a growing number of studies evidenced the enormous importance of PPIs in controlling many biological functions, and remarkable steps have been made toward the understanding of these novel systems. Today, several success stories demonstrate the feasibility of targeting PPIs for pharmacological intervention in a number of pathological conditions (**Section 2.1, Publication I**). The Hsp90 chaperone is a PPI whose function is essential in numerous critical cellular physiological functions, but also implicated in the development and malignant propagation of cancer. For this reason, Hsp90 is an attractive target for cancer therapy, and intensive research efforts from academia and industry led to the discovery of several Hsp90 inhibitors, most of which target an ATP binding site located in the NTD of the protein. Although a limited number of CTD inhibitors have been identified, to date no Hsp90 inhibitors have been reported that act by targeting the Hsp90 CTD dimerization interface (**Section 2.2**).

In the present work, I first described the structural and functional characteristics of PPIs, and strategies that allow to advantageously exploit some of these features for the rational design of PPIMs. Additionally, I presented three case studies of PPIs that are involved in the development of human tumors, and for which a thorough structural and biological characterization, combined with computational investigations, permitted to successfully develop PPIMs (**Section 2.1, Publication I** (31)). Second, I investigated the hHsp90 molecular chaperone, with the aim of rationally identifying novel modulators that inhibit this PPI by targeting the CTD dimerization, following a strategy previously devised by Metz *et al.* (63,225). As a first step to address this objective, I computationally predicted *hot spot* amino acids in the CTD that determine the stability of hHsp90, by performing a per-residue decomposition of the effective dimerization energy with the MM-GB/SA approach (173), and *in silico* alanine scanning with the software DrugScore^{PPI} (166). These calculations revealed a hydrophobic functional epitope in the CTD interface composed by four hot spots that account for most of the dimerization energy. A subset of the hot spot amino acids was mutated to alanine, and size exclusion chromatography, differential scanning fluorimetry, and multi-angle light scattering experiments[†] revealed a significant loss in stability, and a reduced

[†] The experiments were performed in the laboratories of Prof. Dr. G. Groth and Prof. Dr. L. Schmitt at the Heinrich Heine University, Düsseldorf. In particular, mutagenesis, differential scanning fluorimetry, and size exclusion chromatography were performed by Janina Vergin in the Institute for Biochemical Plant Physiology. Multi-angle light scattering experiments were performed by Sven Reimann and Dr. Sander H. J. Smits in the Institute for Biochemistry.

stoichiometry of the of mutants versus wild type CTD, which could be clearly linked to a transition from a dimeric to a monomeric state (**Chapter 4 and 10, Publication II (32)**).

Once hot spot amino acids in the CTD interface have been identified and experimentally validated, I used this information as a starting point to design peptides as potential hHsp90 inhibitors targeting the CTD dimerization. To this aim, I investigated the secondary structure propensity of three peptides derived from the hHsp90 CTD interface by performing MD simulations, starting from the assumption that the magnitude of the α -helical content of the unbound peptides in solution will affect their binding affinity to the dimerization interface of the CTD. The MD simulations were found in agreement with CD experiments. The designed peptides were subsequently experimentally tested in a newly established dimerization assay, and two of them showed *in vitro* inhibition of hHsp90 dimerization. Furthermore, microscale thermophoresis experiments revealed an *in vitro* affinity of one of the peptides toward the hHsp90 CTD in the low micromolar range ($K_D = 3.35 \mu\text{M}$)[‡]. The results suggest that this peptide acts very likely as a competitive dimerization inhibitor by binding at the CTD interface. To the best of my knowledge, this results in the first reported hHsp90 inhibitor targeting the CTD dimerization (**Chapter 5 and 11, Publication III**).

Finally, I investigated trispyrimidonamides as a potential, novel α -helix mimetic scaffold, and for their capability of mimicking the previously identified hHsp90 hot spots. MD simulations suggested that the conformational preferences of trispyrimidonamides are strongly dependent on the solvent, and two alternative conformations prevail in apolar or polar solvents, respectively. Importantly, the MD simulations are in excellent agreement with 2D NMR and crystallographic experiments[§]. This study revealed that in polar solvents trispyrimidonamides can adopt a conformation that allows to address the spatial and angular arrangement of amino acid side chains at positions i , $i + 4$, $i + 8$, and, with a lower propensity, i , $i + 4$, $i + 7$ of an α -helix. This suggests that trispyrimidonamides may be able to mimic hHsp90 hot spots, and hence inhibit the CTD dimerization (**Chapter 6 and 12, Publication IV (33)**).

[‡] The experiments were performed in the laboratories of Prof. Dr. G. Groth and Prof. Dr. J. Jose at the Heinrich Heine University, Düsseldorf and Westphalian Wilhelms-University, Münster, respectively. In particular, expression and purification of the hHsp90 CTD were carried out by Anissa Ouald-Chaib in the Institute for Biochemical Plant Physiology. Autodisplay assay, microscale thermophoresis and CD spectroscopy measurements were performed by Bertan Bopp in the Institute for Pharmaceutical and Medicinal Chemistry.

[§] The experiments were performed in the laboratories of Prof. Dr. T. Kurz and Prof. Dr. W. Frank at the Heinrich Heine University, Düsseldorf. In particular, synthesis and NMR studies were performed by Lukas Spanier and Dr. F. K. Hansen in the Institute for Pharmaceutical and Medicinal Chemistry. Crystallographic studies were performed by Prof. Dr. W. Frank in the Institute for Inorganic Chemistry and Structural Chemistry.

Experimental testing of trispyrimidonamides substituted with side chains analogues of hHsp90 hot spots, aimed at evaluating their ability of inhibiting hHsp90's CTD dimerization, is currently in progress.

4 RESOLVING HOT SPOTS IN THE C-TERMINAL DIMERIZATION DOMAIN THAT DETERMINE THE STABILITY OF THE MOLECULAR CHAPERONE HSP90 – PUBLICATION II

Ciglia, E.[§] (30 %), Vergin, J.[§], Reimann, S., Smits, S.H.J., Schmitt, L., Groth, G., Gohlke, H.

PLOS ONE (2014) 9(4): e96031

Original publication, see page 59

[§] Both authors contributed equally to this work.

4.1 Background

Since the fundamental role of PPIs in the control of a vast array of biological processes and diseases has been recognized, targeting protein-protein complexes has emerged as a new paradigm in drug discovery. After discouraging early drug discovery attempts, multiple success stories demonstrate that PPIs can be suitable drug targets, opening a new avenue for the treatment of a broad range of pathological conditions (22-25,42,43,214). A distinct trait of PPIs of particular significance from a drug design standpoint is their energetic non-homogeneity. Accordingly, PPIs often feature large interaction surfaces, but only few hot spot residues account for most of the binding affinity (79,81,173). Identifying such amino acids offers a very valuable way to develop PPIMs targeting the functional epitope containing the hot spots (29,63,214,290,291) (see **Paragraphs 2.1.2, 2.1.4**).

Hsp90 is an evolutionary conserved and widespread molecular chaperone essential in numerous cellular functions, particularly protein (re) folding, cytosolic transport, prevention of aggregation, proteasomal degradation and many others (230,237). Hsp90 is found over-expressed and activated in many human tumors where, through interaction with oncogenic proteins, it favors malignant transformation, tumor progression, and metastasis (see **Paragraph 2.2.1**). Targeting Hsp90 is a validated approach for cancer therapy and has been the focus of several drug discovery campaigns in the last decades. Several Hsp90 inhibitors have been developed, some of which are currently in advanced phases of clinical trials. Most of these inhibitors modulate the chaperone activity competing for ATP at its NTD binding site, whereas just a few molecules bind at the protein's CTD (Figure 12 A). None of the CTD inhibitors reported to date target the protein-protein dimerization interface (see **Paragraph 2.2.4**).

Here, we set out to identify hot spot residues in the CTD that are crucial for the dimerization of hHsp90. This will provide insights into the energetics of this PPI, uncovering the functional epitope in the CTD that account for most the dimerization energy. Furthermore, it will be a crucial starting point for the following structure-based rational identification of novel hHsp90 inhibitors targeting the CTD dimerization.

4.2 Computational identification of hot spots in the hHsp90 CTD

First, I generated a structural model of the hHsp90 CTD, since a crystal structure of the full-length protein or of its CTD were initially not available. Crystal structures of hHsp90 homologues from *S. cerevisiae* and *E. coli* available in the PDB with sufficient sequence similarity (74 % and 43 %, respectively) allowed me to generate a homology model with the software MODELLER (292). The homology model provided a good starting structure for the following calculations, as assessed, first, with the PROCHECK software (293) (Supporting Information, page 72), and, second, by comparison with a crystal structure of a M-CTD construct of the hHsp90 reported later by Lee *et al.* (PDB code 3Q6M) (251). A very good agreement between the two structures is evidenced overlaying the homology model with the crystal structure, with a root mean square deviation (RMSD) calculated for all C α atoms (for C α atoms located in the four-helix bundle: helices H4, H4' and H5, H5') of ~ 0.8 Å (~ 0.7 Å) (Figure 12 B and C). The homology model and the crystal structure were subjected to molecular dynamics (MD) simulations of 100 ns length in explicit water with the AMBER 11 software and standard procedures (TIP3P water, PBC, PME, SHAKE, time step of 2 fs) (294).

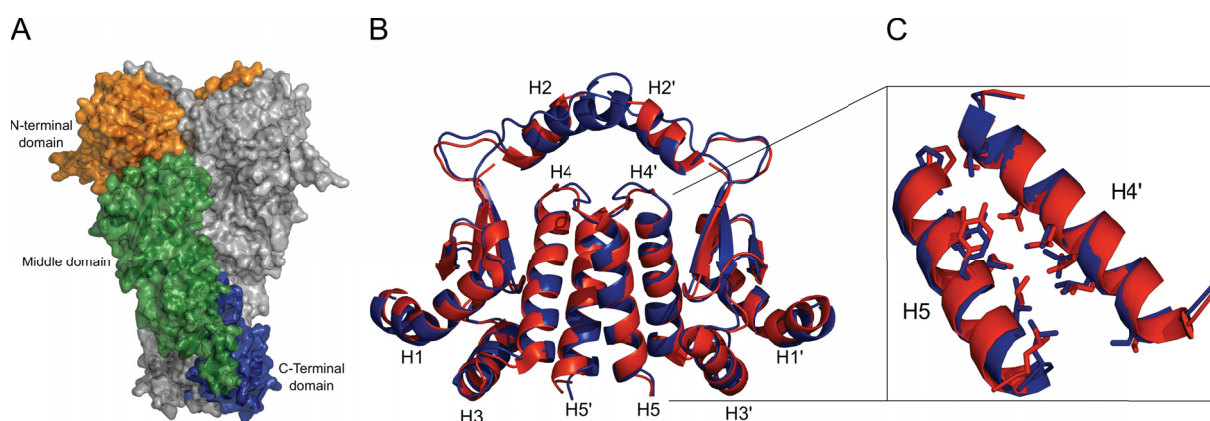


Figure 12 Homology model. (A) Surface representation of the full-length *S. cerevisiae* Hsp90 (PDB code 2CG9), showing the three different protein domains (N-terminal domain: orange, middle domain: green, C-terminal domain: blue). (B) Homology model of hHsp90 C-terminal domain (blue) overlaid with a crystal structure (PDB code 3Q6M) of the same domain (red). (C) Blow-up of the overlay highlighting the side chain orientation of residues located at the interface of helices H5 and H4'. Figure from Publication II, page 59.

This way, I generated a conformational ensemble for the following hot spot prediction, which was performed using two independent methods: a per-residue decomposition of the effective

dimerization energy calculated by the MM-GB/SA approach (173), and *in silico* alanine scanning carried out with the webserver DrugScore^{PPI} developed in our group (166,295) (Methods described in **Paragraph 2.1.3**). Amino acids contributing to the effective dimerization energy with $\Delta G < -2$ kcal mol⁻¹ are considered hot spots (79). Calculations with both methods, and regardless if performed starting from the homology model or from the CTD crystal structure, revealed two principal clusters of hot spots located in the interior of the CTD dimerization interface, on helices H4 and H5, and a single hot spot on H3 (Figure 13 A). The most relevant cluster is located on H5 and is formed by residues I688, Y689, I692, and L696 (Figure 13 A-C).

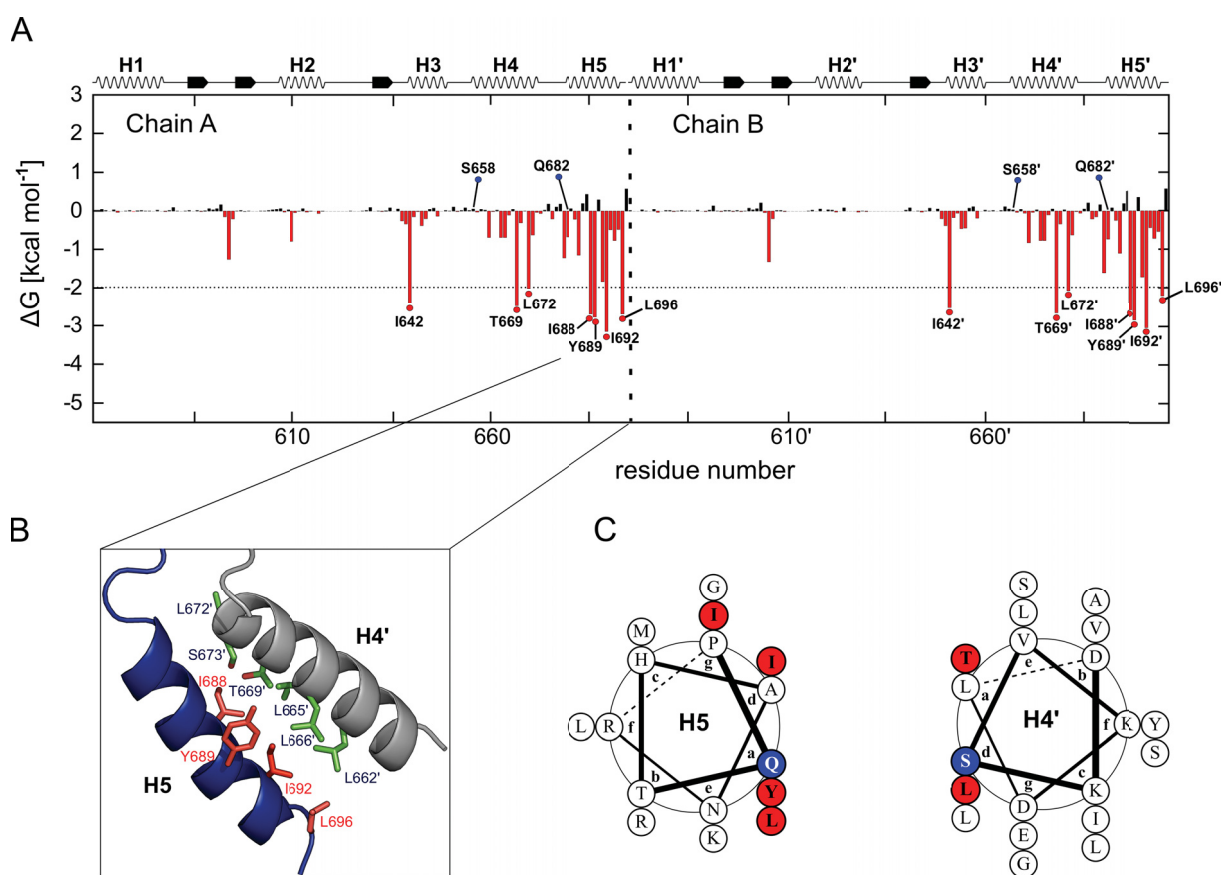


Figure 13 Hot spot and cold spot prediction. (A) Contribution to the dimer stabilization of each amino acid within the hHsp90 CTD. ΔG values are calculated by the MM-GB/SA approach (174,296) starting from the homology model, employing a structural decomposition of the effective energy (173). The standard error in the mean is < 0.1 kcal mol⁻¹ in all cases. Amino acids contributing to the dimerization with $\Delta G < -2$ kcal mol⁻¹ are considered hot spots and are indicated in the graphic by red dots. In addition, two “cold spots” mentioned in the text are marked with blue dots. In the upper part of the panel, the secondary structure of the CTD is shown. The amino acids are numbered according to the full-length hHsp90 α isoform (UniProt code: P07900). (B) Hot spot residues localized on H5 (red) and interacting residues on H4 (green). (C) Helical wheel representation showing the position of hot spots (red) and cold spots (blue) on helices H5 and H4. Figure from Publication II, page 59.

These aliphatic and aromatic residues constitute a rather hydrophobic epitope, and establish hydrophobic and stacking interactions with non-polar residues located on H4' (Figure 13 B). In addition, Y689 is flexible and can engage in hydrogen bonding with several residues

located on H4' and H3, depending on the orientation of its side chain (Figure 13 B). Hot spots simultaneously able to establish stacking and polar interaction (tryptophan, tyrosine and arginine) are recurrent in PPIs (see **Paragraph 2.1.1**) (78). This dual behavior is favorable when designing inhibitors mimicking such hot spots, because it allows a good balance between hydrophobic contacts and polar interactions conferring specificity of binding (217,297). Interestingly, Y689 is accommodated by an indentation in the binding epitope of H4'. The predicted hot spots are spatially clustered, and feature $i, i + 4, i + 7$ and $i, i + 4, i + 8$ patterns. This appears advantageous in the perspective of using them as pharmacophoric models in the development of α -helix mimetics or small-molecule hHsp90 inhibitors. Additionally, the calculations suggested that some residues, although located at the CTD interface on helices H4 and H5 adjacent to the hot spot clusters, should not contribute significantly to the dimerization energy. Among them, I selected residues S658 and Q682 as “cold spots” as a negative control for the following experimental validation (Figure 13 A and C). Finally, I observed that the hot spots are considerably buried in the protein complex, and therefore I assessed if a simpler calculation would have provided similar results in terms of identified hot spots. Interestingly, considering only the residue-wise relative change in the solvent-accessible surface area upon complex formation suggests that almost all residues at the CTD interface would be hot spots (Supporting Information, page 72). This demonstrates that a better specificity in the prediction is achieved by our energy-based approach, rather than taking into account geometric criteria only.

The hot spot prediction was validated with three independent experimental techniques: differential scanning fluorimetry (Thermofluor assay) (298), size exclusion chromatography (SEC), and multi-angle light scattering (MALS).*** To this end, hot spot alanine triple mutants CTD^{Y689A/I692A/L696A}, CTD^{I688A/Y689A/I692A}, single mutants CTD^{I688A}, CTD^{Y689A}, CTD^{I692A}, CTD^{L696A}, and a cold spot mutant CTD^{S658A/Q682A} were generated. The Thermofluor assay showed that upon mutation of the hot spots to alanine (both in single and triple mutants), the melting temperature (T_m) of the hHsp90 CTD decreases drastically. The pronounced shift in the melting temperature observed ($\Delta T_m \geq 13^\circ\text{C}$) indicates a significant loss in protein stability. Conversely, the cold spot mutant showed a melting temperature almost identical to the wild type protein, revealing that substitution of cold spots to alanine

*** The experimental validation was carried out by our cooperation partners in the laboratories of Prof. Dr. G. Groth and Prof. Dr. L. Schmitt at the Heinrich Heine University, Düsseldorf. In particular, mutagenesis, Thermofluor assay, and SEC experiments were performed by Janina Vergin in the Institute for Biochemical Plant Physiology. MALS experiments were performed by Sven Reimann and Dr. Sander H. J. Smits in the Institute for Biochemistry.

does not markedly affect the stability of the CTD. Similar results were obtained when analyzing the CTD wild type and mutants by SEC. With this technique, we could establish that the decrease in stability upon mutation of the hot spots relates to a change in the relative molecular mass and thus, in the stoichiometry of the complex. However, it was not possible to distinguish unarguably if the change observed is due to a shift from a tetramer to a dimer, or from a dimer to a monomer. This information was provided from MALS experiments, which clearly demonstrated that the wild type CTD exists predominantly as a dimer (~100 %), whereas mutating the hot spots to alanine triggers a substantial shift towards a monomeric form (77 % and 69 % for the triple mutants CTD^{Y689A/I692A/L696A} and CTD^{I688A/Y689A/I692A}, respectively).

4.3 Conclusions and significance

In this study, I predicted hot spot amino acids at the hHsp90 CTD dimerization interface by two independent computational approaches. The predictions have been tested and validated with three experimental techniques. The experiments allowed me to confirm the importance of the identified hot spots on the stability and stoichiometry of the protein-protein complex. This analysis revealed the presence of a rather hydrophobic functional epitope in the hHsp90 protein-protein interface, which has advantageous characteristics with respect to being used as a starting point for developing novel inhibitors targeting the CTD dimerization.

The principal results of this study are:

- Hot spot residues at the hHsp90 CTD interface were predicted by MM-GB/SA calculations and *in silico* alanine scanning.
- The hot spot prediction was validated by three independent experimental approaches, which revealed that mutating these residues to alanine disrupts the CTD dimerization.
- The identified hot spots are spatially clustered, and have favorable properties with respect to exploiting them as pharmacophoric template for identifying and designing small-molecule inhibitors of hHsp90 dimerization.

In the following of this work, I will make use of these findings to guide the design of peptidic inhibitors of the hHsp90 dimerization (**Chapter 5, Publication III**), and to evaluate the potential of trispyrimidonamides as α -helix mimetic scaffolds targeting the hHsp90 CTD hot spots (**Chapter 6, Publication IV**).

5 DESIGN AND BIOLOGICAL TESTING OF PEPTIDIC DIMERIZATION INHIBITORS OF HUMAN HSP90 THAT TARGET THE C-TERMINAL DOMAIN – PUBLICATION III

Bopp, B.[§], Ciglia, E.[§] (30 %), Ouald-Chaib, A., Groth, G., Gohlke, H., Jose, J.

Submitted, (2015)

Manuscript, see page 86

[§] Both authors contributed equally to this work.

5.1 Background

In the previous study, we identified a functional epitope of spatially clustered hot spot amino acids in the CTD interface that determine the stability of the hHsp90 chaperone (**Chapter 4, Publication II**). Earlier, several authors showed that the knowledge of the essential molecular interactions of a PPI given from the hot spots can be successfully exploited to design PPIMs (214,299,300). Furthermore, the design of peptides that mimic the hot spots of a PPI as proof-of-concept, intermediate probe molecules is a viable approach prior to pursuing the design of small molecule PPIMs with improved pharmacokinetic properties (139,301-304). Following this strategy, we make use of the hot spots information gained in the previous publication (**Chapter 4, Publication II**) to design and experimentally test peptidic inhibitors of hHsp90 dimerization.

5.2 Design and testing of peptidic hHsp90 inhibitors

Our previous results showed that the stability of hHsp90 is critically influenced by two hot spots clusters located in the four-helix bundle, at the dimerization interface of the CTD: I688, Y689, I692, and L696 on helix H5, and T669 and L672 on helix H4 (Figure 14 A and B, and Figure 13 A-C in **Chapter 4, Publication II**). I assumed that peptides enclosing the hot spots that account for most of the dimerization energy should act as competitive inhibitors by binding to the CTD dimerization interface. Consequently, I proposed three peptides as potential hHsp90 dimerization inhibitors: H5, a 16mer containing the residues of the first hot spots cluster; H4, a 20mer containing the residues of the smaller hot spot cluster; H6, which combines H5 and H4 together with residues of the loop connecting the two (Figure 14 C). I decided to include in the peptides all of the amino acids of the respective native α -helices (Figure 14 B and C) in order to improve their secondary structure stability, as I expected that

they should bind in a helical form to the dimerization interface. Accordingly, I set out to investigate the secondary structure propensity of the three peptides by means of MD simulations, as I assumed that this will be crucial for their binding affinity to the CTD monomer. H5, H4, and H6 were each simulated in explicit water in the unbound form, and in complex with the corresponding hHsp90 CTD monomer, for 1 μ s and 500 ns, respectively (Figure 14 C).

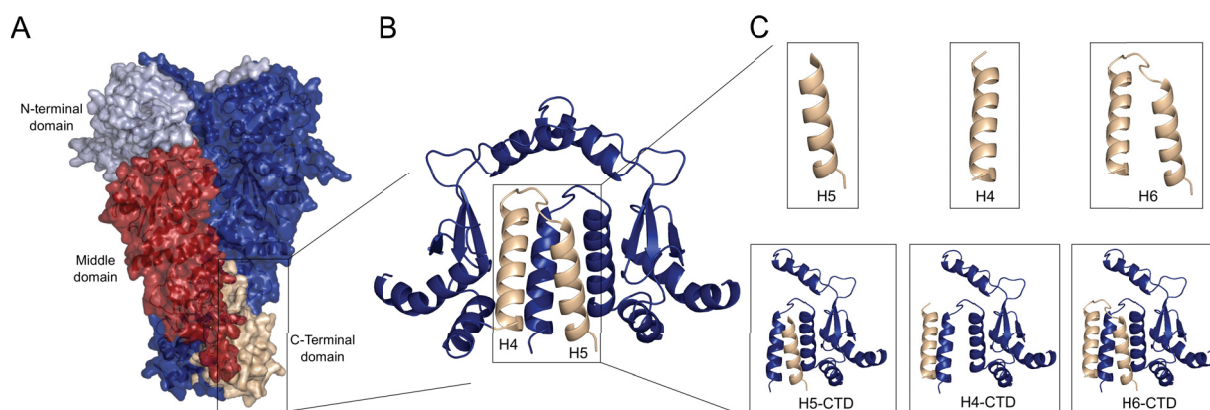


Figure 14. Peptides derived from the dimerization interface of the hHsp90 CTD (A) Surface representation of the full-length *S. cerevisiae* Hsp90 (PDB code 2CG9) showing the three protein domains (N-terminal domain: light blue, middle domain: red, C-terminal domain: wheat). (B) Homology model of the hHsp90 CTD dimer (blue), generated as described in (32). The pair of helices from which the interface peptides investigated by MD simulations, CD spectroscopy, and FACS assay were derived are colored in wheat in the box. (C) Blow-up of the starting structures for the MD simulations: single peptides (H5, H4 and H6, upper panel) and peptides in complex with the Hsp90 CTD monomer (H5-CTD, H4-CTD, and H6-CTD, lower panel). Figure from Publication III, page 86.

The length of the MD simulations performed is 5-fold longer than the experimentally determined time required for α -helix formation (305-307), and this is expected to provide a satisfactory conformational sampling to predict the secondary structure propensities of the peptides, as shown in earlier studies (308). Furthermore, three independent simulations of each peptide and peptide-CTD complex were performed, in order to evaluate the statistical significance of the results, and whether convergence was achieved with respect to the calculated secondary structure content. This was confirmed by the standard error of the mean (SEM) calculated for the residues' average α -helical content (Figure 15, Figure 16, and Figure 17, A and B). Additionally, in the course of the MD simulations, pronounced and repeated changes in the per-residue secondary structure could be observed for most of the residues, showing that a thorough sampling of the conformational space was achieved. In the MD simulations, H5 has a very low average residue-wise α -helical content ($\sim 7.0 \pm 1.2\%$ (SEM), Table 1 in the original publication, page 86), and does not show any other dominating secondary structure element (Figure 15 A). This peptide appears to be largely unstructured in the unbound state: it quickly unfolds and loses its initial α -helical secondary structure, which is partially replaced by 3_{10} helical stretches later in the simulations (Figure 15 A). In contrast,

H5 in complex with the CTD has a significantly higher average α -helical content ($\sim 54.7 \pm 10.2\%$ (SEM)), and almost all of the amino acids retain their α -helical character during the complete simulation (Figure 15 B). Conversely, MD simulations of H4 and H6 reveal very different secondary structure propensities for these peptides, which are predicted to have a significantly higher α -helical content both in the bound and unbound states.

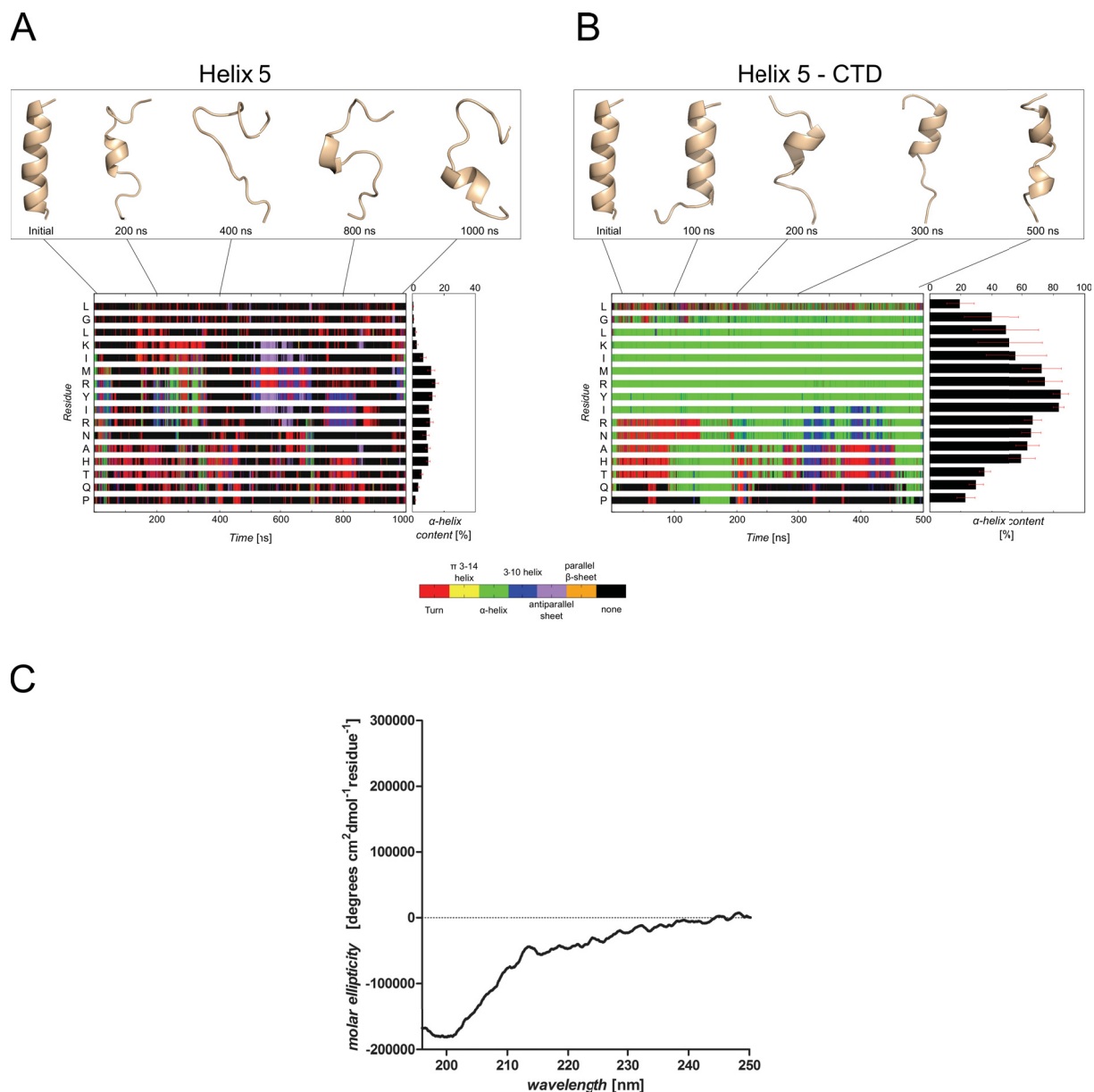


Figure 15. Secondary structure of H5 in MD simulations and CD spectroscopy. In the upper panels, representative conformations of the peptide simulated by itself (A) or extracted from the peptide-CTD complex (B) are shown at different times during the MD simulations. In the lower panel, the secondary structure of each peptide residue (as indicated by the color scale below) is given as a function of the simulation time. The histograms on the right show the α -helix content of each peptide residue averaged over the three independent MD simulations; the standard error of the mean (SEM) is indicated by the red bars (see Experimental Procedures in the original publication, page 86). (C) CD spectrum of the peptide in aqueous solution in the range 180-250 nm. Figure from Publication III, page 86.

The calculated average α -helical content of the unbound H4 and H6 is $\sim 21.1 \pm 5.6\%$ (SEM) and $\sim 34.6 \pm 6.0\%$ (SEM), respectively (Table 1 in the original publication, page 86), and when the peptides are bound to the CTD $\sim 31.6 \pm 9.1\%$ (SEM) and $\sim 69.2 \pm 2.7\%$ (SEM), respectively (Figure 16 and Figure 17 A and B). Additionally, amino acids located in the central region of peptides H4 and H6 can show a very high (up to 100%) α -helical content (Figure 16 and Figure 17 A and B), whereas no α -helical content is observed in the loop region of H6, as expected.

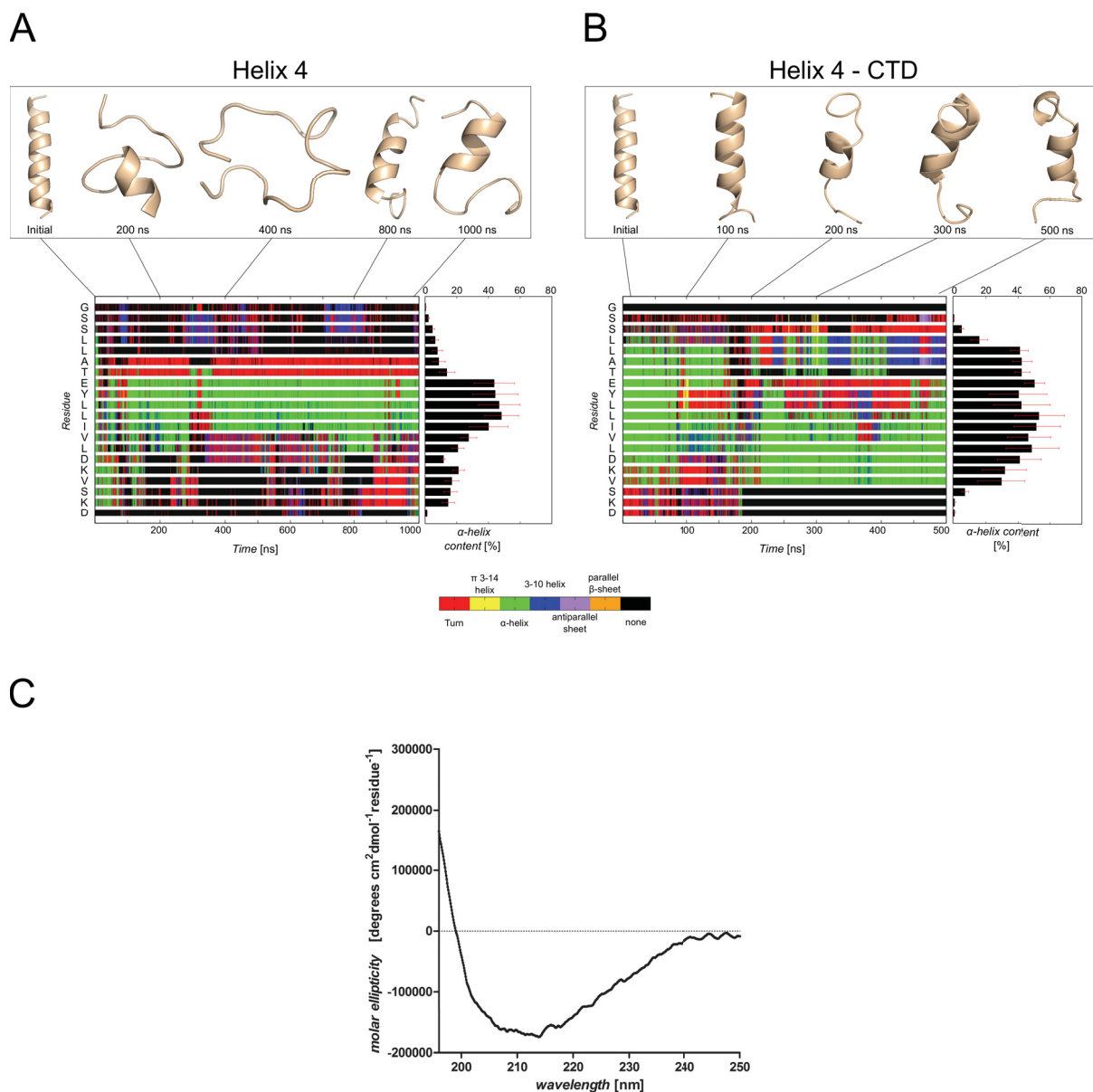


Figure 16. Secondary structure of H4 in MD simulations and CD spectroscopy. For further details, see Figure 15. Figure from Publication III, page 86.

These findings are in good agreement with CD spectroscopy measurements of the unbound peptides in aqueous solution, which did not reveal any secondary structure content for H5 (Figure 15 C), whereas H4 and H6 showed minima at ~ 208 nm and ~ 220 nm that indicate a

predominantly α -helical secondary structure (Figure 16 and Figure 17 C) (Table 1 in the original publication, page 86).

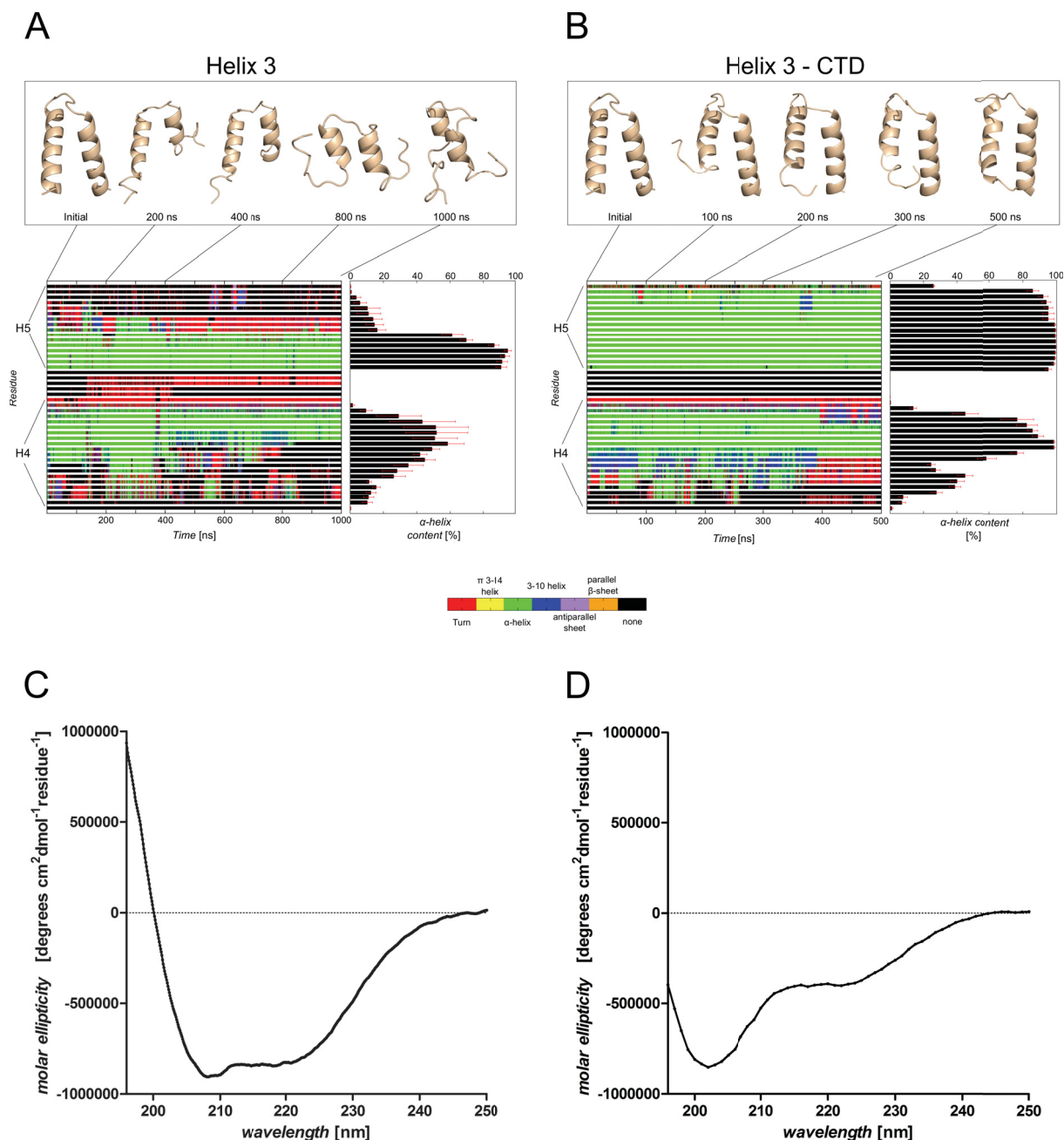


Figure 17. Secondary structure of H6 in MD simulations and CD spectroscopy. For further details, see Figure 15. Figure from Publication III, page 86.

In order to test whether the designed peptides are able to inhibit hHsp90 dimerization, a novel flow cytometry-based Autodisplay competition assay was developed. Testing the peptides in this assay revealed that H4 and H6 are both able to inhibit hHsp90 dimerization, and analyzing the dose-dependency of the inhibition produced by H6 revealed an IC_{50} value of 8.96 μ M. Additionally, in order to resolve whether the peptides inhibit hHsp90 by binding at the CTD, as expected, microscale thermophoresis experiments were performed with H6 and

the purified CTD.^{††} These experiments demonstrated that H6 binds to the CTD of hHsp90, with a K_D value of 3.35 μ M. Interestingly, Gavenonis *et al.* synthesized and tested analogues of a peptide derived from the CTD dimerization interface that differs from H5 only by having two additional residues, one Asp in the N-terminus, and one Gly in the C-terminus (299). Although the authors showed that these peptides inhibit hHsp90's chaperone activity, and they could exclude a NTD-mediated mode of action, they did not provide evidence that the peptides inhibit hHsp90 dimerization by binding at the CTD. Thus, to the best of my knowledge, H6 is the first peptidic hHsp90 inhibitor reported that targets the CTD dimerization. Testing H5 in the flow cytometry-based Autodisplay competition assay revealed no inhibitory activity for this peptide. This appeared initially surprising, since H5 contains the bigger cluster of hot spots. However, this could be explained by the very low α -helical content of the unbound peptide in aqueous solution, as predicted by MD simulations and confirmed by CD spectroscopy measurements (Figure 15 A and C, Table 1 in the original publication, page 86). Accordingly, I argue that the high energy cost needed for the unbound H5 to adopt an α -helix conformation prevents its binding to the hHsp90 CTD, and consequently its inhibitory activity. Conversely, since unbound H4 and H6 present a more stable secondary structure, they can more easily establish native-like molecular interactions with the CTD and, hence, inhibit hHsp90 dimerization. Finally, we aimed at investigating the inhibitory activity of a peptide H6mut, in which the amino acids of the main cluster of hot spots are mutated to alanine. However, we observed a strong tendency of H6mut to form aggregates, which may result from an unstructured peptide in solution. This is also supported by CD spectroscopy measurements, which did not reveal any secondary structure content for H6mut (Figure 17 D). For this reason, it was not possible to further investigate H6mut in our experimental setting.

^{††} The experiments were performed by our cooperation partners in the laboratories of Prof. Dr. G. Groth and Prof. Dr. J. Jose at the Heinrich Heine University, Düsseldorf and Westphalian Wilhelms-University, Münster, respectively. In particular, expression and purification of the hHsp90 CTD were carried out by Anissa Ouald-Chaib in the Institute for Biochemical Plant Physiology. Autodisplay assay, microscale thermophoresis, and CD spectroscopy measurements were performed by Bertan Bopp in the Institute for Pharmaceutical and Medicinal Chemistry.

5.3 Conclusions and significance

In this study, the design and experimental testing of peptidic inhibitors of hHsp90 dimerization was presented, based on the hot spots information gained in the previous publication (**Chapter 4, Publication II**).

The principal results of this study are:

- Three peptides derived from the CTD interface have been proposed as hHsp90 dimerization inhibitors, and their conformational preferences were investigated by MD simulations and CD spectroscopy.
- Two of the peptides inhibited hHsp90 dimerization in a new flow-cytometry-based Autodisplay assay. Furthermore, one peptide was shown to bind the hHsp90 CTD with a low micromolar affinity.
- This study resulted in the first peptidic hHsp90 dimerization inhibitor targeting the CTD, very likely by competitively binding at the CTD interface.

These results validated our previous study, and importantly, provided a proof-of-concept of the feasibility of inhibiting hHsp90 CTD dimerization by molecules that mimic the native molecular interactions of the hot spots. Accordingly, the designed peptides can be used as a starting point to design new small molecules that inhibit the CTD dimerization of hHsp90, which could open a new route for cancer therapy.

6 DESIGN, SYNTHESIS, AND CONFORMATIONAL ANALYSIS OF TRISPYRIMIDONAMIDES AS α -HELIX MIMETICS – PUBLICATION IV

Spanier, L.[§], Ciglia, E.[§] (30 %), Hansen, F.K., Kuna, K., Frank, W., Gohlke, H., Kurz, T.

J. Org Chem. (2014), 79, 1582-1593.

Original publication, see page 114

[§] Both authors contributed equally to this work.

6.1 Background

Despite the large interfaces involved, often PPIs are mediated by small secondary structure domains, which project hot spot amino acid side chains into the complementary surface of an interacting protein (309). As a consequence, the design of peptidomimetics, i.e. molecules able to act as structural and functional mimics of protein secondary structure elements, has been the subject of extensive investigation in medicinal chemistry during the last decade. In particular, since α -helices are the prevailing recognition motifs in protein-protein interfaces (129), a large variety of scaffolds that target this type of secondary structure (i.e., α -helix mimetics) have been designed and studied, following the pioneering work of Horwell and Hamilton (309-312) (Figure 18). This resulted in the development of a number of α -helix mimetic classes, which have proven valuable as biophysical probes or modulators of PPIs (23,313-316). Additionally, they provide an attractive alternative to peptides, which often suffer from poor pharmacokinetics properties. However, the synthesis of several α -helix mimetics still presents limitations with respect to amino acid patterns targeted, side chains that can be included, and physicochemical properties. In this study, we report the design and synthesis of trispyrimidonamides as a novel class of α -helix mimetics (Figure 18, III). First, we extensively analyze the conformational properties of this scaffold by molecular modeling, 2D NMR, and X-ray crystallography. Additionally, we describe the characteristics that make this unprecedented α -helix mimetic scaffold potentially suitable for targeting PPIs, and for mimicking the hot spots in the dimerization interface of the hHsp90 CTD previously described (see **Chapter 4, Publication II**).

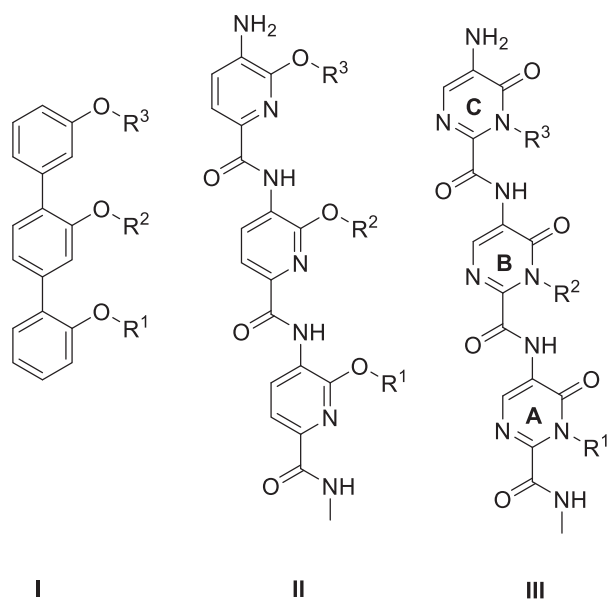


Figure 18. (I) Terphenyl, (II) trispyridylamide, and (III) trispyrimidonamide. Scaffold rings of III are labeled A, B, C. Figure from Publication IV, page 114.

6.2 Conformational analysis of trispyrimidonamides

First, using a dimethyl-substituted bispyrimidonamide as model molecule (Figure S4 A in the Supporting Information of the original publication, page 127), I parameterized based on *ab initio* calculations the torsion angles ϕ and ψ , expected to be decisive for the inter-ring orientation, and for the projection of substituents R^1 , R^2 , and R^3 in the space (Figure 18, III). The energy minima of the calculated potentials are in good agreement with ϕ and ψ values found in the crystal structure of a tri-substituted trispyrimidonamide (Figure S4 B in the Supporting Information of the original publication, page 127). Afterwards, I subjected a trimethyl-substituted trispyrimidonamide (**IV**, Figure 19 A) to MD simulations of 1.5 μ s length, in explicit chloroform and methanol, and generated relative free energy maps of **IV** as a function of the orientation of the methyl substituents of ring A and B (torsion angle Ω_1), and B and C (torsion angle Ω_2) (Figure 19 A and B). The frequent rotations around the ϕ and ψ angles observed in the MD simulations, as well as the symmetry of the relative free energy maps strongly suggest that equilibrium was reached with respect to the sampled conformations. The relative free energy maps reveal that, in chloroform, **IV** predominantly adopts a conformation **C**₁, where R^1 and R^3 are oriented on the same side, whereas R^2 points in the opposite direction ($\Omega_1 \sim \pm 165^\circ$; $\Omega_2 \sim \pm 155^\circ$, Figure 19 B and C). In contrast, an alternative conformation **C**₂, which presents all side chains on one side ($\Omega_1 \sim \pm 55^\circ$; $\Omega_2 \sim \pm 55^\circ$, Figure 19 B and D) is energetically disfavored by a $\Delta G \sim 2.5$ kcal mol⁻¹. In the conformational ensemble at 300 K from the MD simulations, conformers **C**₁ and **C**₂ are populated with a ratio of 98.5/1.5. The MD simulations of **IV** in methanol reveal a reversed

situation: C_2 is now the energetically favored conformer, and C_1 is disfavored by a $\Delta G \sim 1$ kcal mol⁻¹ (Figure 19 B). Here, the ratio of the populations of C_1 versus C_2 in the conformational ensemble at 300 K from MD simulations is 19/81.

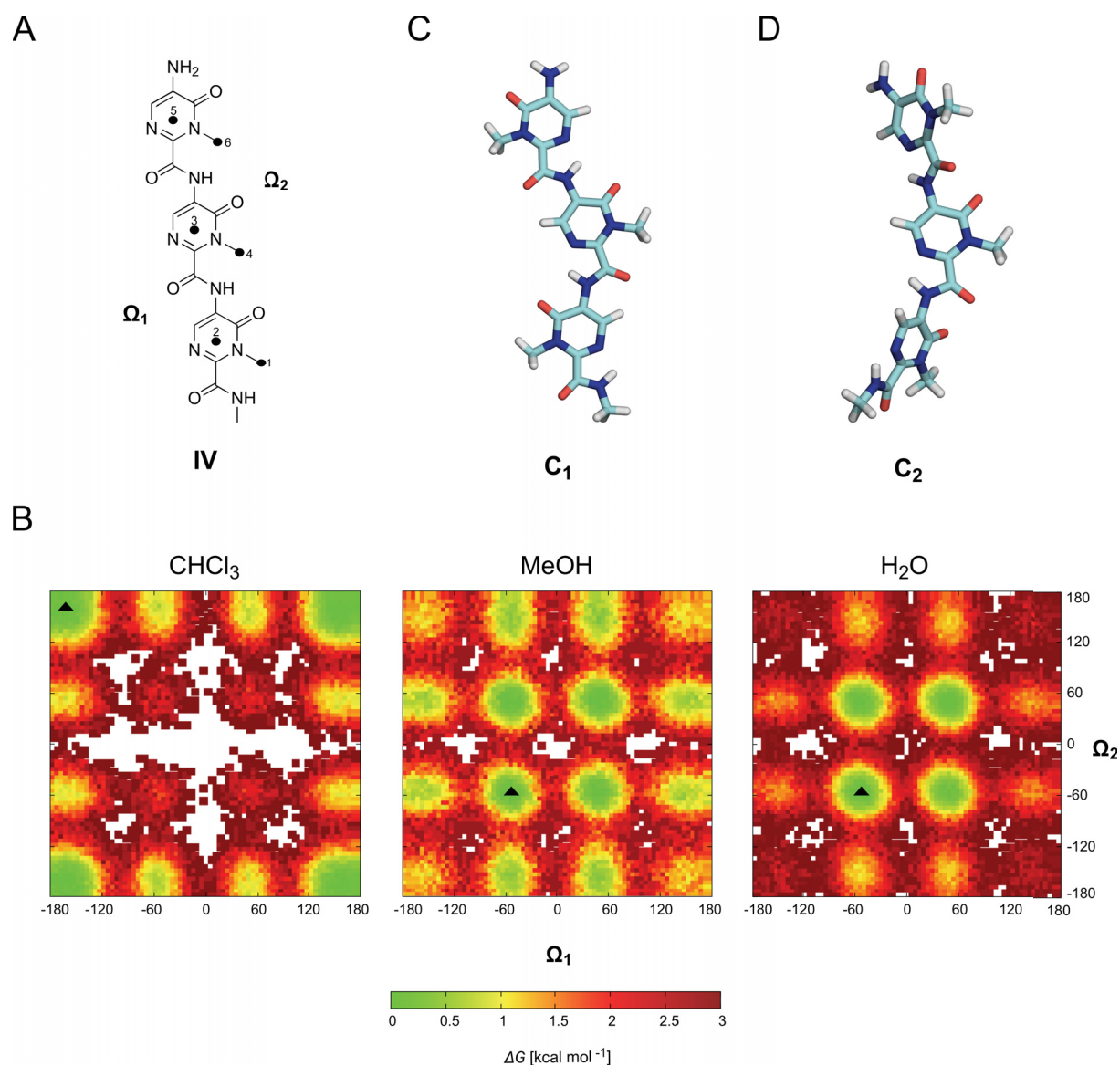


Figure 19. Relative free energy of trispyrimidonamide IV as a function of the orientation of the methyl substituents of rings A and B, or B and C, with respect to each other. (Ω_1 and Ω_2 torsion angles as defined by the point quadruples (1, 2, 3, 4) and (4, 3, 5, 6) in the structure shown in panel A). The relative free energy of each conformation is calculated from the frequency of the conformation's occurrence during a MD simulation of 1.5 μ s length in explicit chloroform, explicit methanol, and explicit water (see respective plots in panel B) via $\Delta G = -RT \ln P_x/P_{\text{ref}}$ (where R is the gas constant, $T = 300$ K, P_x is the frequency of occurrence of conformation x , and P_{ref} is the frequency of occurrence of the most frequently represented conformation). The white spots indicate Ω_1 and Ω_2 angle combinations not found in the MD simulations. Energetically favorable conformations of IV in the different solvents are shown in panel C (chloroform; C_1) and D (methanol and water; C_2); their locations on the relative free energy maps are marked by triangles. Figure from Publication IV, page 114.

Remarkably, these results are in excellent agreement with 2D NMR experiments performed in chloroform and methanol, which showed the same conformational preferences for two differently substituted trispyrimidonamides (see original publication, page 114). Furthermore,

the almost coplanar orientation of the pyrimidone rings of **C**₁ in the MD simulations is reminiscent of the ring orientation found in the crystal structure of a trisubstituted trispyrimidonamide (see Figure 1 A in the original publication, page 114). These results validated the setup of MD simulations and force field parameters used, and allowed me to extend the study to investigate the conformational preferences of trispyrimidonamides in water, for which it was not possible to obtain experimental data. MD simulations of 1.5 μ s length of **IV** in explicit water revealed that, in aqueous solution, **C**₂ becomes even more favored over **C**₁. The latter is energetically disfavored by $\Delta G \sim 3 \text{ kcal mol}^{-1}$, which relates to a ratio of $<1/99$ for the populations of **C**₁ versus **C**₂ in the MD conformational ensemble at 300 K. Once the conformational preferences of trispyrimidonamides in polar solvents were resolved, I set out to evaluate the potential of this scaffold to project substituents in a way that mimics the orientation of amino acid side chains of a α -helix.

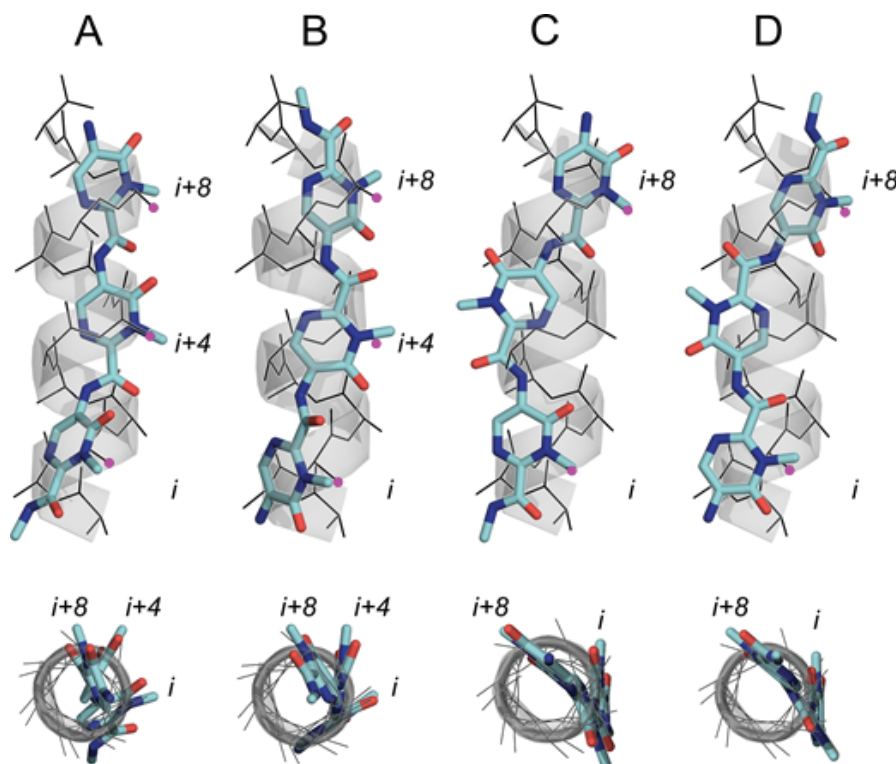


Figure 20. Overlay of C_{β} atoms of a canonical α -helix onto corresponding methyl groups of **IV**. In conformation **C**₂ (A), this results in an $i, i + 4, i + 8$ pattern, whereas in conformation **C**₁ (C), in an $i, i + 8$ pattern. Ring C is oriented towards the C-terminus of the helix. (B), (D): Equivalent superimpositions when **IV** is reversed with respect to the helix axis. The magenta dots highlight the C_{β} atoms addressed by the trispyrimidonamide's R groups. In the lower panel the overlays are rotated by 90° , with the peptide C-terminus oriented in the direction of the viewer. Figure from Publication IV, page 114.

Trispyrimidonamides are found to closely mimic the spatial arrangement of amino acid side chains at positions $i, i + 4, i + 8$, as evidenced by superimposing the methyl groups of **IV** in the conformation **C**₂ with the C_{β} atoms of a canonical α -helix (Figure 20 A and B). When ring C is oriented toward the helix's C-terminus, the RMSD of the coordinates of the respective

atom pairs is 0.69 Å, and the average angle deviation between the bond vectors is $\sim 20^\circ$ (Figure 20 A); these values increase to 0.73 Å and $\sim 30^\circ$, respectively, when **IV** is reversed with respect to the helix axis (Figure 20 B). In the case of conformation **C**₁, two methyl groups can address C _{β} atoms of a canonical α -helix at positions i and $i + 8$. The RMSD and average angle deviation between bond vectors are 0.2 Å (0.55 Å) and $\sim 10^\circ$ ($\sim 38^\circ$), respectively, when ring C is oriented towards the C(N)-terminus of the helix (Figure 20 C and D). To the best of my knowledge, the side chain pattern $i, i + 4, i + 8$ is currently addressed just by another class of α -helix mimetics (317). These results suggest trispyrimidonamides as an interesting novel scaffold when aiming at mimicking side chains of a PPI located on the same side of an α -helix, but more distant than in the classical case of $i, i + 4, i + 7$ (136). However, although with a lower propensity, trispyrimidonamides can address also an $i, i + 4, i + 7$ pattern. In this case, for conformer **C**₂ the RMSD and the average angle deviations between bond vectors are 1.1 Å (1.5 Å) and 22° (39°), respectively, when ring C is oriented towards the C(N)-terminus of the helix. For conformer **C**₁, these values deteriorate to RMSD = 1.2 Å (1.7 Å) and average angle deviations between bond vectors = 54° (70°) when ring C is oriented towards the C(N)-terminus of the helix (Figure S6 in the Supporting information, page 127).^{‡‡}

6.3 Conclusions and significance

In this study, I investigated the conformational preferences of trispyrimidonamides in different solvents, and their potential as α -helix mimetics for addressing different amino acid side chain patterns. Trispyrimidonamides preferentially adopt conformations that can lead to $i, i + 4, i + 8$ and $i, i + 8$ patterns of side chain orientation. As a consequence, I expect that trispyrimidonamides may be able to mimic hHsp90 hot spots I688, I692 and L696, and Y689, I692 and L696, and hence to inhibit the CTD dimerization.

The principal results of this study are:

- The conformational preferences of trispyrimidonamides in chloroform and methanol have been computationally predicted by means of MD simulations, and showed an excellent agreement with 2D NMR and X-ray crystallography experiments.

^{‡‡} Synthesis, NMR, and crystallographic studies were performed by our cooperation partners in the laboratories of Prof. Dr. T. Kurz and Prof. Dr. W. Frank at the Heinrich Heine University, Düsseldorf. In particular, synthesis and NMR studies were performed by Lukas Spanier and Dr. F. K. Hansen in the Institute for Pharmaceutical and Medicinal Chemistry; crystallographic studies were performed by Prof. Dr. W. Frank in the Institute for Inorganic Chemistry and Structural Chemistry.

- The same computational setup has been used to investigate the conformational preferences of trispyrimidonamides in water, for which experimental data could not be obtained.
- In polar solvents, trispyrimidonamides preferentially adopt conformations that make them suitable scaffolds to mimic the spatial arrangement of amino acid side chains at positions $i, i + 4, i + 8$ or $i, i + 8$. Targeting a $i, i + 4, i + 7$ pattern appears to be less likely, although it cannot be excluded.

This study presents trispyrimidonamides as novel α -helix mimetics, which extend the arsenal of scaffolds currently available to modulate PPIs. Low energy conformations of trispyrimidonamides can address the spatial and angular orientation of hot spots located at the CTD dimerization interface of hHsp90. Trispyrimidonamides substituted with hHsp90's hot spots are currently being tested for their *in vitro* ability of disrupting the chaperone dimerization, and consequently inhibiting its activity (*unpublished results*).

7 SUMMARY AND PERSPECTIVES

In this thesis, I investigated the hHsp90 chaperone, aiming at rationally identifying novel inhibitors targeting the CTD dimerization interface, as an alternative, unprecedented approach for targeting this PPI for cancer therapy.

Following a strategy previously devised by Metz *et al.* (63,225), I first aimed at resolving the determinants of binding of hHsp90, and computationally predicted seven hot spot amino acids at the CTD interface that critically influence the stability of the protein, and whose mutation to alanine disrupts the native dimeric state. A comprehensive validation by independent experimental techniques confirmed the predictions, providing insights into the energetics of Hsp90 CTD dimerization, and the basis for the following rational design of hHsp90 dimerization inhibitors (**Chapter 4, Publication II**).

In a first effort toward this goal, I designed three peptides derived from the CTD interface as potential hHsp90 inhibitors, and computationally investigated their secondary structure propensities. Experimental testing showed that two of these peptides inhibit hHsp90 dimerization in the low micromolar range, and one of them was shown to bind in the hHsp90 CTD, likely at the dimerization interface, with a $K_D = 3.35 \mu\text{M}$. This led to the first peptidic hHsp90 dimerization inhibitor targeting the CTD, and provided the important proof-of-concept that inhibition of hHsp90 can be achieved by molecules that target the chaperone's CTD dimerization and mimic the hot spots (**Chapter 5, Publication III**).

Finally, I investigated trispyrimidonamides as potential novel class of α -helix mimetics. An extensive computational and experimental study provided insights into the conformational preferences of this scaffold in different solvents, showing that trispyrimidonamides can address an amino acid side chains pattern suitable to mimic hHsp90's hot spots. Trispyrimidonamides substituted with hHsp90's hot spots are currently undergoing experimental testing aimed at investigating their *in vitro* ability of inhibiting hHsp90's activity (**Chapter 6, Publication III**).

In all, the results presented in this thesis evidence that integrating computational and experimental methods for hot spot detection, rational design, and screening provides a successful strategy for the identification of PPIMs. Furthermore, this study significantly validates the concept of inhibiting hHsp90 by disrupting the CTD dimerization, providing the basis for future investigations aimed at the identification of small molecules PPIMs targeting hHsp90 as a new route for targeting the chaperone in cancer therapy.

8 ACKNOWLEDGEMENTS

Few years ago, moving to Düsseldorf, I started a journey that ended up being dense of happenings, stimulating, and exciting, though in certain moments also very tough. I want to express my gratitude to some of the people who contributed making this time unique.

Thanks to Prof. Dr. Holger Gohlke, for giving me the possibility of doing a PhD at the Heinrich Heine University, and for his continuous enthusiastic and knowledgeable support, teaching, and strategic guidance throughout these years.

Thanks to all of my colleagues and friends of the CPC lab. In particular, I would like to thank: Dr. Christopher Pflieger and Christian Hanke, for their constant, invaluable and patient help in calculations, scripting, reading this thesis, and much more; Dr. Alexander Metz for constantly and capably advising me during these years, and for our shared successes.

Thanks to Prof. Dr. Georg Groth, Janina Vergin, Prof. Dr. Thomas Kurz, Dr. Lukas Spanier, Dr. Finn Hansen, Prof. Dr. Joachim Jose, Bertan Bopp, Anissa Ouald-Chaib, Prof. Dr. Matthias Kassack, and Ana Rodrigues-Moita, for the collaboration that brought our joint efforts to a success in the Hsp90 project. Thanks to Dr. Alexandra Hamacher for the supervision and the good atmosphere in the AMA practical course.

Thanks to Dr. Mariangela Agamennone, to whom I will always be grateful for initiating me earlier into this field.

Furthermore, I would like to thank (in alphabetic order): Alexander Metz, Andreas Marmann, Anissa Ouald-Chaib, Catalina Pérez-Hemphill, Christian Hanke, Christopher Pflieger, Dhana Thomy, Giulia Pagani, Heike Goldbach-Gecke, Ido Ben Shalom, Jagmohan Saini, Kirsten Famulla, Lena Hammerschmidt, Patrizia, Cem and Deniz Kandemir, Stephan Schwed, and Tobias Kröger, for the numerous experiences shared, and the unforgettable time spent together.

A big thanks to my parents and my brothers Andrea and Matteo, for their constant and unconditional presence, love and support in any moment of my life.

A special thanks to Catherine: you are the most precious gift of these years in Düsseldorf, whose greatest memories are indissolubly bound to you. The conclusion of this period is just the start of a new life adventure for us together.

9 REPRINT PERMISSIONS

Publication I

Reprinted and adapted with permission from:

“Modulating Protein-Protein Interactions: From Structural Determinants of Binding to Druggability Prediction to Application”

Alexander Metz, Emanuele Ciglia and Holger Gohlke

Current Pharmaceutical Design, **2012**; 18, 4630-4647

Copyright (2012) Bentham Science Publishers Ltd.

Publication II

Reprinted from:

“Resolving Hot Spots in the C-terminal Dimerization Domain that Determine the Stability of the Molecular Chaperone Hsp90”

Emanuele Ciglia, Janina Vergin, Sven Reimann, Sander H.J. Smits, Lutz Schmitt, Georg Groth and Holger Gohlke

PLOS ONE, **2014**; 9(4): e96031

Copyright (2014) Ciglia et al. This is an open-access article distributed under the terms of the Creative Commons Attribution License, which permits unrestricted use, distribution, and reproduction in any medium, provided the original author and source are credited.

Publication IV

Reprinted with permission from:

“Design, Synthesis, and Conformational Analysis of Trispyrimidonamides as α -helix Mimetics”

Lukas Spanier, Emanuele Ciglia, Finn K. Hansen, Krystina Kuna, Walter Frank, Holger Gohlke and Thomas Kurz

Journal of Organic Chemistry, **2014**; 79, 1582-1593

Copyright (2014) American Chemical Society

10 PUBLICATION II

Resolving Hot Spots in the C-Terminal Dimerization Domain that Determine the Stability of the Molecular Chaperone Hsp90

Emanuele Ciglia [§], Janina Vergin [§], Sven Reimann, Sander H.J. Smits, Lutz Schmitt, Georg Groth, Holger Gohlke

PLOS ONE, 2014; 9(4): e96031

[§] Both authors contributed equally to this work



Resolving Hot Spots in the C-Terminal Dimerization Domain that Determine the Stability of the Molecular Chaperone Hsp90

Emanuele Ciglia¹*, Janina Vergin²*, Sven Reimann³, Sander H. J. Smits³, Lutz Schmitt³, Georg Groth², Holger Gohlke¹*

1 Institute for Pharmaceutical and Medicinal Chemistry, Heinrich-Heine-University, Düsseldorf, Germany, **2** Institute for Biochemical Plant Physiology, Heinrich-Heine-University, Düsseldorf, Germany, **3** Institute of Biochemistry, Heinrich-Heine-University, Düsseldorf, Germany

Abstract

Human heat shock protein of 90 kDa (hHsp90) is a homodimer that has an essential role in facilitating malignant transformation at the molecular level. Inhibiting hHsp90 function is a validated approach for treating different types of tumors. Inhibiting the dimerization of hHsp90 via its C-terminal domain (CTD) should provide a novel way to therapeutically interfere with hHsp90 function. Here, we predicted hot spot residues that cluster in the CTD dimerization interface by a structural decomposition of the effective energy of binding computed by the MM-GBSA approach and confirmed these predictions using *in silico* alanine scanning with DrugScore^{PPi}. Mutation of these residues to alanine caused a significant decrease in the melting temperature according to differential scanning fluorimetry experiments, indicating a reduced stability of the mutant hHsp90 complexes. Size exclusion chromatography and multi-angle light scattering studies demonstrate that the reduced stability of the mutant hHsp90 correlates with a lower complex stoichiometry due to the disruption of the dimerization interface. These results suggest that the identified hot spot residues can be used as a pharmacophoric template for identifying and designing small-molecule inhibitors of hHsp90 dimerization.

Citation: Ciglia E, Vergin J, Reimann S, Smits SHJ, Schmitt L, et al. (2014) Resolving Hot Spots in the C-Terminal Dimerization Domain that Determine the Stability of the Molecular Chaperone Hsp90. PLoS ONE 9(4): e96031. doi:10.1371/journal.pone.0096031

Editor: Suzannah Rutherford, Fred Hutchinson Cancer Research Center, United States of America

Received: August 13, 2013; **Accepted:** April 2, 2014; **Published:** April 23, 2014

Copyright: © 2014 Ciglia et al. This is an open-access article distributed under the terms of the Creative Commons Attribution License, which permits unrestricted use, distribution, and reproduction in any medium, provided the original author and source are credited.

Funding: This work was supported by funds from the Strategischer Forschungsfonds of the Heinrich-Heine-University, Düsseldorf. The funders had no role in study design, data collection and analysis, decision to publish, or preparation of the manuscript.

Competing Interests: The authors have declared that no competing interests exist.

* E-mail: gohlke@uni-duesseldorf.de

☯ These authors contributed equally to this work.

Introduction

Protein-protein complexes have gained increasing attention in structural biology and drug discovery due to their ubiquitous participation in fundamental cellular processes. As such, protein-protein interactions (PPIs) are involved in a variety of physiological regulatory mechanisms, e.g., signaling, cellular growth, and apoptosis [1,2]. PPIs also play an important role in pathophysiology [3,4] such that modulating PPIs is considered a valuable approach for treating diseases [2,3,5–7]. Targeting PPIs is considered difficult, however, because of the size, lack of deep binding pockets, and stability of PPIs. Yet, protein-protein interfaces have been shown to be energetically non-homogeneous in that only a few “hot spot” residues account for most of the binding affinity [8–10]. Accordingly, PPI modulators often target only the functional epitope that contains these hot spots [11–13]. Thus, identifying such hot spots provides important insights into the energetics of PPIs, which can be exploited for the identification of PPI modulators [12].

Here, we aim at resolving hot spots in the C-terminal dimerization domain of the human heat shock protein of 90 kDa (hHsp90). Hsp90 is a molecular chaperone that belongs to a highly conserved family of proteins that are central to a number of cellular functions, including protein (re) folding,

stabilization, and quality control [14–16]. Despite its high basal expression in eukaryotes and prokaryotes [17,18], Hsp90 remains mostly in a latent state under physiological conditions. In response to environmental stress, the cellular activity of Hsp90 (along with other heat shock proteins) is increased in order to protect the exposed cell [16,19]. Recent data has also demonstrated essential roles for chaperones in facilitating malignant transformation at the molecular level: the chaperone allows tumor cells to tolerate mutations in multiple critical signaling molecules that would otherwise be lethal [20,21]. Accordingly, many studies have validated Hsp90 inhibition as an approach for treating different types of tumors [14,22–26].

Regarding its structure, Hsp90 is a flexible homodimeric protein; each monomer consists of three major domains: an amino terminal domain (NTD), a middle domain (M), and a carboxy terminal domain (CTD) [17,27] (Figure 1, A). The NTD contains a nucleotide binding pocket, responsible for Hsp90's ATPase activity, which is coupled to the chaperone activity [28,29]. This pocket is the binding site of most of the known Hsp90 inhibitors [30,31]. The M domain is the major interaction site for Hsp90 clients, and bridges NTD and CTD [28]. In addition to being involved in regulating ATPase activity and co-chaperone recruitment, the CTD is responsible for Hsp90 dimerization [18,32]. The dimerization interface is formed by

two pairs of helices creating a characteristic four helix bundle [17,33]. Recent results showed that the C-terminal dimer opens and closes with fast kinetics [34] in contrast to previous assumptions that the C-terminal interface is permanently dimerized [17]. These findings led us to hypothesize that inhibiting the C-terminal dimerization will be a viable way to interfere with Hsp90 activity. Although some Hsp90 inhibitors have been described that act on the CTD [35,36] to the best of our knowledge none of these targets the dimerization interface.

In order to identify hot spots as a first step to define the functional epitope in the dimerization interface, we conducted a combined computational and experimental study. First, we predicted potential hot spot candidates by two independent computational approaches, MM-GB/SA [37] and DrugScore^{PPI} [38,39], using a homology model of the human C-terminal Hsp90 domain. A subset of these was mutated to alanine, and the stability of wild type and mutant proteins was evaluated by a ThermoFluor assay [40], size exclusion chromatography (SEC), and multi-angle light scattering (MALS). Our findings provide insights into the energetics of CTD dimerization in Hsp90, which are valuable for pursuing a novel approach that aims at therapeutically interfering with Hsp90 activity.

Results

Homology modeling and molecular dynamics simulations

When starting this study, neither a crystal structure of the human full length Hsp90 (hHsp90) nor of its CTD was available, which would be required for any later structure-based endeavor to identify PPI modulators. Thus, we set out to generate a model of the hHsp90 CTD by comparative modeling with MODELLER [41] using crystal structures from *S. cerevisiae* and *E. coli* as templates. The sequence identity (similarity) between the target sequence and the template sequences is sufficiently high (*S. cerevisiae*: 54% (74%); *E. coli*: 25% (43%); (Figure S1 in File S1). The obtained model is of good structural quality as assessed with the PROCHECK software [42] (Figure S2 in File S1). Recently, a crystal structure of an M-CTD construct of hHsp90 has been reported (PDB code: 3Q6M) [43]. Our model and the crystal structure show very good structural agreement as demonstrated by

a root mean square deviation (RMSD) of all C_α atoms of ~0.8 Å (Figure 1, B). This value decreases to ~0.7 Å when the C_α atoms of only the amino acids located in the four helix bundle (helices H4, H4' and H5, H5') are taken into account (Figure 1, C). The orientation of the side chains in the dimerization interface agrees almost perfectly between the model and the crystal structure (Figure 1, C) such that the results of the hot spot prediction (see below) should not depend on whether the prediction is based on one or the other structure.

The homology model was subjected to molecular dynamics simulations (MD) of 100 ns length in explicit water to generate a conformational ensemble for the subsequent hot spots detection. The CTD dimer remains stable during the simulation time: the RMSD of the single domains is ~6.5 Å, and the dimer shows structural deviations of ~8 Å (Figure S3, A in File S1). Relevant conformational changes are only observed in the region of helices H2 and H2' (Figure 1, B) and account for most of the structural deviations observed. As such, not taking into account H2 and H2', the RMSD of the single domains and the dimer drops to ~3 Å (Figure S3, B in File S1). This is in agreement with previous experimental and computational findings according to which the mobility of H2 and H2' is required for forming interactions between the CTD and substrates and, hence, Hsp90 function [33,44].

Hot spot prediction

In order to identify amino acids at the CTD interface that are crucial for dimer stability, we performed MM-GB/SA calculations combined with a decomposition of the effective energy (i.e., the sum of gas phase and solvation free energy) of dimerization on a per residue level. The approach mimics computational alanine scanning and has been applied successfully by us in retro- and prospective studies on the determinants of protein-protein interactions [10–12,45]. The results reveal a distinctive interaction profile, which is almost identical for the two monomers (Figure 2, A). Residues are identified as hot spots if their contribution to the effective energy of dimerization $\Delta G < -2$ kcal mol⁻¹ [46].

The hot spots are spatially clustered and are located on H4 and H5, except for a single hot spot on H3. The main cluster is formed by residues I688, Y689, I692, and L696 located on H5 at the inner side of the four helix bundle (Figure 2, B). I692 and L696 form

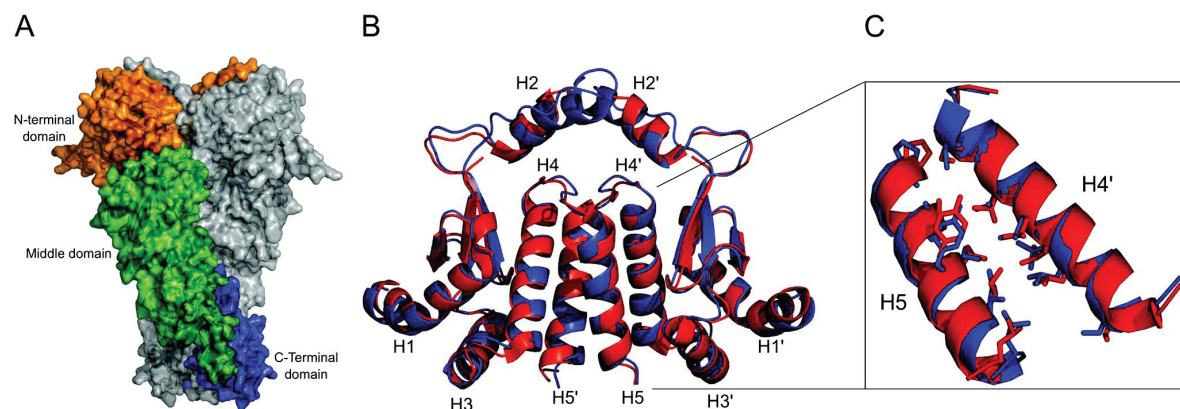


Figure 1. Homology model. (A) Surface representation of the full length *S. cerevisiae* Hsp90 (PDB code 2CG9), showing the three different protein domains (N-terminal domain: orange, middle domain: green, C-terminal domain: blue). (B) Homology model of hHsp90 C-terminal domain (blue) overlaid with a crystal structure (PDB code 3Q6M) of the same domain (red) (C) Blow-up of the overlay highlighting the side chain orientation of residues located at the interface of helices H5 and H4'.

doi:10.1371/journal.pone.0096031.g001

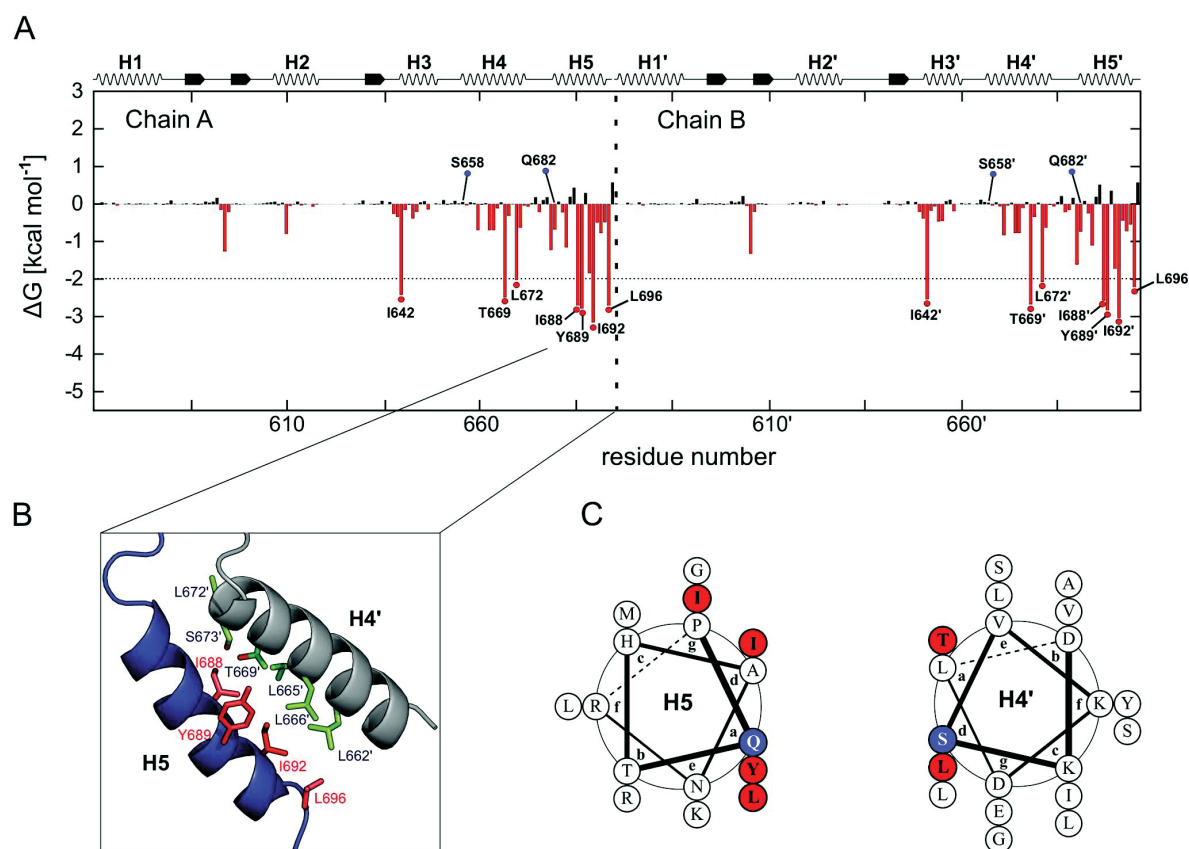


Figure 2. Hot spot and cold spot prediction. (A) Contribution to the dimer stabilization of each amino acid within the hHsp90 CTD. ΔG values are calculated by the MM-GB/SA approach [37,83] starting from the homology model, employing a structural decomposition of the effective energy [10]. The standard error in the mean is <0.1 kcal mol⁻¹ in all cases. Amino acids contributing to the dimerization with $\Delta G < -2$ kcal mol⁻¹ are considered hot spots and are indicated in the graphic by red dots. In addition two “cold spots” mentioned in the text are marked with blue dots. In the upper part of the panel, the secondary structure of the CTD is shown. The amino acids are numbered according to the full length hHsp90 α isoform (UniProt code: P07900). (B) Hot spot residues localized on H5 (red) and interacting residues on H4' (green). (C) Helical wheel representation showing the position of hot spots (red) and cold spots (blue) on helices H5 and H4'. doi:10.1371/journal.pone.0096031.g002

hydrophobic contacts with L662', L665', and L666' located on H4'; Y689 establishes hydrophobic interactions with L665' and L666' (Figure 2, B) but also forms hydrogen bonds with S673' and T669' on H4' and H640' on the loop located above the N-terminal end of H3. The multiple hydrogen bond formation is possible because the side chain of Y689 adopts two conformations during the MD simulations, one where the aromatic ring points in the direction of H3' and one where it points to H4', i.e., the interior of the interface. In the latter case, an indentation in the binding epitope of H4' accommodates the side chain. L672 and T669 form a second, smaller cluster on H4. The latter residue is involved in interactions with Y689' (see above); L672 interacts with P681 on H5'. Finally, I642 on H3 is located in a peripheral position with respect to the interface but forms hydrophobic contacts with the C-terminal end of H5, that way apparently contributing to the stabilization of this secondary structure element.

As the crystal structure of an M-CTD construct of hHsp90 became available only recently (PDB code: 3Q6M) [43], we repeated the hot spot prediction for a CTD dimer of that structure, using the same settings for these computations and the

prior MD simulations as in the case of the homology model. The resulting interaction profile (Figure S4 in File S1) is in very good agreement with the one of the homology model (Figure 2, A) such that all of the above mentioned hot spots are identified again. While this may have been expected from the high structural similarity between our model and the crystal structure (see above), these findings validate, in an indirect manner, the quality of our homology model and demonstrate the robustness of our MM-GB/SA-based hot spot predictions. In order to independently confirm the MM-GB/SA calculations, we performed *in silico* alanine scanning on the homology model with the DrugScore^{PPI} web server developed by us [38,39]. The interaction profile obtained is in good agreement with the above findings, pointing to essentially the same hot spots that are crucial for hHsp90 CTD dimerization (Table S1 in File S1). We also tested if the above hot spots could have been identified by a simpler computational approach given that these hot spots are largely buried upon complex formation. For this, we computed the residue-wise relative change in the solvent-accessible surface area upon complex formation (using the SA values of the MM-GB/SA calculations starting from the CTD dimer of the crystal structure; Figure S5 in File S1). This suggests

essentially all residues in the dimer interface as hot spots, indicating a pronounced loss of specificity in the predictions compared to when additional energy contributions are considered. In turn, L696, which is more peripheral to the dimer interface, is not found among the top candidates anymore when using the surface area-based approach. In our view, these findings demonstrate the predictive value of the energy-based methods.

Finally, we selected residues S658 and Q682 as “cold spots” ($\Delta G = 0.06$ and -0.67 kcal mol⁻¹, respectively, as calculated with the MM-GB/SA approach starting from the homology model; Figure 2, A and C), which will serve as negative controls in the subsequent experiments. These amino acids are located at the CTD interface between H5 and H4', but they are predicted to be only marginally important for the dimerization (Figure 2, A and C). Consequently, mutating these “cold spots” to alanine should not impact the CTD stability.

Analysis of hHsp90 stability by Thermofluor assay

The stability of the CTD of hHsp90 wild type, cold spot and hot spot alanine mutants was analyzed by differential scanning fluorimetry (Table 1, Table 2) [40]. In this assay thermally-induced protein unfolding is monitored by the binding of the fluorescent dye SYPRO orange [47] to the hydrophobic core of the protein that becomes exposed upon unfolding, and the related increase in fluorescence emission. The temperature at the midpoint of the unfolding transition is defined as melting temperature (T_m) of the protein [48]. A shift in T_m of a protein in its native state, or in site-specific or chemically modified forms, indicates a change in the stability of the protein [49]. In order to identify conditions under which the native state is most stable we analyzed the thermal unfolding of the purified wild type hHsp90 CTD in the pH range from 3–10. These studies (Figure 3, A) showed that the CTD of hHsp90 is most stable at mild neutral conditions (pH 7.5). Thus, screening of all hot spot and cold spot variants of hHsp90 was done at this pH condition.

The wild type form of hHsp90 is characterized by a melting temperature of 73°C (Figure 3, B). In contrast, hot spot substitution mutants carrying alanines at positions 689, 692 and 696 (CTD^{Y689A/I692A/L696A}, Figure 3, D) or at positions 688, 689 and 692 (CTD^{I688A/Y689A/I692A}, Figure 3, E) show a significant decrease ($\Delta T_m \geq 13^\circ\text{C}$) in their melting temperatures indicating a substantial loss in the stability due to the substitution of the native hHsp90 residues in these positions by the small, non-polar alanine. These triple mutations were chosen, respectively, out of the four hot spots of the main cluster because they result in patterns of sequence localization that could be mimicked by non-peptidic α -helix mimetics (see Discussion for further details).

Additionally, alanine single mutants were analyzed at the same conditions to reveal the potential contribution of individual positions at the dimerization interface on the stability of the CTD dimer. To this end we substituted the predicted hot spots at positions I688, Y689, I692 and L696 individually to alanines (Table S2, Table S3 in File S1) and determined the melting temperature and protein stability of the single mutants. Compared to the alanine triple mutants, all of the single mutants showed a much lower reduction ($\Delta T_m < 8^\circ\text{C}$) in their melting temperature with respect to the wild type of hHsp90 (Figure S6, Table S4 in File S1). Alanine substitutions at positions S658 and Q682 identified as cold spots (Figure 2, A–C) had no effect on the stability of the protein. The related mutant (Figure 3, C) showed a melting temperature corresponding to the hHsp90 wild type.

Analysis of hHsp90 multimer stability by size exclusion chromatography

The effect of alanine substitutions in predicted hot and cold spots positions of hHsp90 with respect to disrupting the oligomerization state of the protein was analyzed by SEC. In order to relate the elution volume on the gel filtration column to the molecular mass of the purified wild type and alanine mutants of hHsp90 (Table 1), a number of protein standards (Lysozyme 14.000 Da, Carbonic Anhydrase 29.000 Da, BSA 66.000 Da, Alcohol Dehydrogenase 150.000 Da, β -Amylase 200.000 Da, Apoferritin 443.000 Da) were applied to the gel filtration column. Based on the calibration proteins the main peak of the elution profile (at a buffer volume of ~ 14 mL) of the wild type CTD corresponds to a molecular mass (M_w) of 80–90 kDa. Assuming that the overall fold of the recombinant CTD resembles the globular form of the protein standards, the M_w calculated from the SEC experiments implies that the wild type CTD exists as tetramer in solution (Figure 4, A). However, if the protein analyzed by SEC is asymmetrical or elongated - a condition met with the CTD of hHsp90 - the protein can easily elute at a position twice the M_w of a globular protein [50]. Thus, the apparent M_w calculated from the SEC experiments and the complex stoichiometry deduced from this should not be taken as absolute numbers in the case of the hHsp90 CTD but rather as relative measures to indicate whether mutations at the dimerization interface affect the stability of the complex. At a lower elution volume of ~ 13 mL, a small shoulder is visible in the elution profile that, based on the calibration, corresponds to $M_w = 160$ – 190 kDa, i.e., an apparent octamer. Figure 4, C–D shows the elution profile for the hot spot mutants CTD^{Y689A/I692A/L696A} and CTD^{I688A/Y689A/I692A}. Compared to the wild type the main fractions of both hHsp90 mutants elute at higher buffer volumes (~ 15.5 mL) from the column. This clearly shows that these variants predominantly possess a lower molecular mass than the wild type and form complexes of lower subunit stoichiometry. Based on the calibration with the globular protein standards each of the alanine substitution mutants has a molecular mass of 58 kDa, which would indicate an apparent trimeric or dimeric state. In addition, a smaller peak is visible in the elution profile at a buffer volume similar to that found for the wild type, indicating a low population of apparent tetramers. In contrast, the elution profile of the cold spot mutant was virtually identical to that of the CTD of wild type hHsp90 (Figure 4, B): The main fraction of the mutant eluted at a buffer volume comparable to that of the main peak of hHsp90 wild type, with a small shoulder visible again at a lower buffer volume. This indicates that the molecular masses of both variants are comparable. Taking together the information of the different gel filtrations, we conclude that the organizational state of the CTD of hHsp90 is larger in the wild type and the cold spot variants, whereas the hot spot variants predominantly form complexes of lower stoichiometry. The data clearly indicate that the hot spot mutations substantially affect the apparent M_w and the complex stoichiometry.

Multi-angle light scattering

In order to resolve whether the effects of the hot spot mutations on the apparent M_w correspond to a shift from a tetramer to a loosely associated dimer or from an elongated dimer to a monomer, we performed MALS experiments on wild type CTD and the two hot spot mutants. MALS allows determining the absolute molar mass of particles in solution. For the wild type, the experiments revealed a predominant species of 45.4 ± 0.1 kDa (Table 3; Figure 5, A), in almost perfect agreement with the expected M_w of 43 kDa of the dimer CTD (Table 1). Additionally,

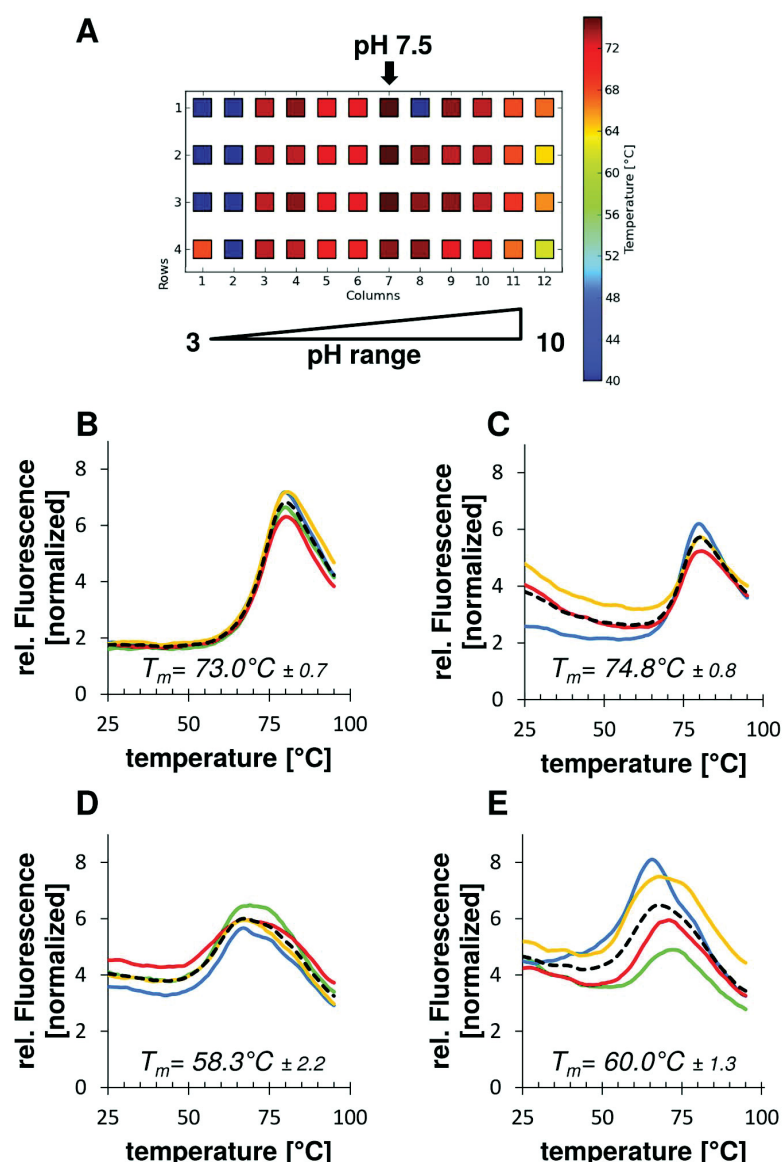


Figure 3. Thermofluor assay for investigating the stability of wild type and mutant hHsp90 CTD. Protein stability was analyzed in 12 different pH buffers in four independent measurements. (A) Heatmap for wild type hHsp90 CTD. Melting curves of measurements at pH 7.5 with the average T_m and standard deviation are shown below for wild type hHsp90 CTD (B), hHsp90 CTD with cold spot mutants as negative control (C), as well as hot spot alanine mutants CTD^{Y689A/I692A/L696A} (D) and CTD^{I688A/Y689A/I692A} (E). The mean value (dotted black line) was calculated from four independent measurements (yellow, red, blue, green lines) in reaction buffer with 100 mM Tris. doi:10.1371/journal.pone.0096031.g003

higher oligomeric species are present eluting earlier from the column (Figure 5, A). Although we could not clearly assign a specific mass for this peak and thereby the exact oligomeric state due to a low population and an insufficient separation from the dimer signal, this species might represent a tetramer. For both hot spot mutants CTD^{Y689A/I692A/L696A} and CTD^{I688A/Y689A/I692A}, the predominant species detected had $M_w = 23.5 \pm 0.2$ and 23.2 ± 0.2 kDa, respectively (Table 3; Figure 5, B and C), corresponding to monomeric CTDs (Table 1). In addition, with a population of ~23% and ~31%, respectively, species with

$M_w = 48.7 \pm 0.5$ kDa and $M_w = 50.1 \pm 0.5$ kDa were detected, corresponding to residual dimeric CTDs. With a much lower population, higher oligomeric species were detected again (Figure 5, B and C). Taken together, the MALS experiments reveal that hot spot mutations substantially influence the stability of the CTD complex in that the predominant form of the wild type CTD is a dimer whereas the predominant forms of the hot spot mutants are monomers.

Table 1. Variants of the CTD of hHsp90 investigated in this study.

Variant	Abbreviation	MW ^[a]	Extinction coefficient
Wild type	wt	21469.3	13075
Cold spot mutant	CTD ^{S658A/Q682A}	21396.2	13075
Hot spot mutant I	CTD ^{Y689A/I692A/L696A}	21293.0	11585
Hot spot mutant II	CTD ^{I688A/Y689A/I692A}	21293.0	11585

^[a]Computed molecular weight in Da.
doi:10.1371/journal.pone.0096031.t001

Circular dichroism spectroscopy

To demonstrate that the predicted hot spots have no impact on the overall protein folding, circular dichroism (CD) spectroscopy measurements were performed. We observed similar spectra for wild type, hot spot, and cold spot mutants (Figure S7 in File S1) with minima at 207 nm and 225 nm that indicate a predominately α -helical secondary structure of hHsp90 CTD, which agrees well with the secondary structure content derived from the CTD of the crystal structure (data not shown). Similar to the hot spot and cold spot mutants do the alanine single mutants show a high α -helical secondary structure (Figure S7 in File S1). Taken together, the CD measurements underline that the selected substitutions in the hot spot, cold spot, and single mutants do not perturb the overall folding of the hHsp90 CTD.

Discussion

Identifying hot spots in protein-protein interfaces yields insights into the energetics of PPIs that can be exploited for the identification of PPI modulators [10–12,45,51]. Here, we aimed at identifying hot spot residues that determine the stability of the hHsp90 CTD dimer following the idea that inhibiting CTD dimerization should provide a novel way to therapeutically interfere with Hsp90 activity. Performing MM-GB/SA calculations together with a structural decomposition of the effective binding energy [10], we identified a main cluster of four hot spot residues (I688, Y689, I692 and L696) located on H5 in the dimer interface. The importance of these residues for dimerization was also confirmed by *in silico* alanine scanning [38,39]. A smaller cluster of two residues (I669 and I672) and a single hot spot (I642) were predicted by these methods, too. The residues in the main cluster have a mainly hydrophobic character, leading to multiple hydrophobic contacts of these residues with residues on H4'. In addition, Y689 forms hydrogen bond interactions with several residues on H4'. Residues that are able to form hydrophobic and stacking interactions and at the same time engage in polar interactions such as tyrosine, arginine, and tryptophan are frequently found as hot spots in protein-protein interfaces [52]. The influence of the hot spot residues in the main cluster on the stability of the hHsp90 CTD was experimentally confirmed by SEC, MALS, and differential scanning fluorimetry. In contrast to the wild type, for which the CTD dimer is the predominant form in solution, monomeric forms are the predominant species of the CTD^{I688A/Y689A/I692A} and CTD^{Y689A/I692A/L696A} mutants; in addition, a pronounced decrease of the melting temperature by more than 13°C was found for these mutants compared to the wild type. The reduced subunit stoichiometry and the loss of stability indicate that the interaction between individual monomers in the complex is disrupted by substituting the hot spot clusters Y689/I692/L696 or I688/Y689/I692 with small, nonpolar alanine

Table 2. T_m of hHsp90 CTD wild type and alanine mutants.

	CTD wt	CTD ^{S658A/Q682A}	CTD ^{Y689A/I692A/L696A}	CTD ^{I688A/Y689A/I692A}
T_m ^[a]	73.0±0.7	74.8±0.8	58.3±2.2	60.0±1.3
ΔT_m ^[b]	0.0	1.8	-14.8	-13.0

^[a]The detected fluorescence signal corresponds to the denaturation state of hHsp90. The melting temperature T_m of hHsp90 CTD wild type, cold spot, and alanine mutants was determined from the derivative of the fluorescence data by the implemented software (qPCRsoft V2.0.37.0, Analytik Jena AG, Germany). The mean value and standard deviation were calculated from four independent measurements in reaction buffer with 100 mM Tris at pH 7.5 in °C.
^[b]Difference in the T_m with respect to the wild type in °C.
doi:10.1371/journal.pone.0096031.t002

residues. Data on all four single alanine mutants demonstrate that each substitution at a single position destabilizes the CTD dimer, too, albeit to only half of the extent observed for the triple mutants. This suggests that the destabilizing effects of single mutations at

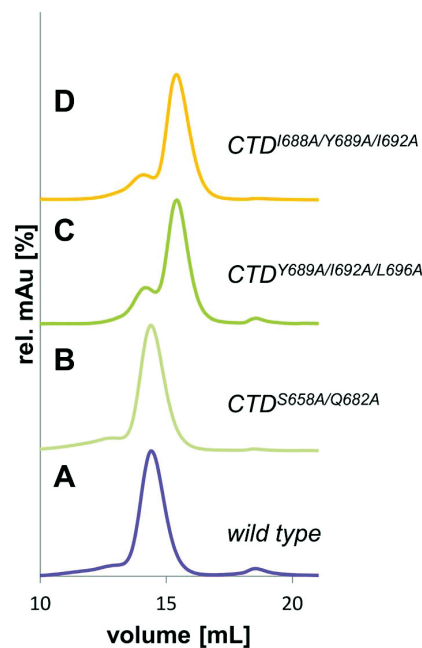


Figure 4. Elution profiles of hHsp90 CTD variants using size exclusion chromatography. Chromatograms for wild type hHsp90 CTD (A), cold spot (B), and hot spot alanine mutants (C and D). Experiments were performed in triplicates on a Superdex SD200 10/300 column in HPLC-buffer (10 mM MES/KOH, 200 mM KCl, 1 mM EDTA, 1% Glycerol) at pH 6 with 110 μ L of purified hHsp90 CTD. The molecular weight of hHsp90 CTD variants was calculated based on the slope of the calibration curve obtained with standard proteins. The elution peak of the wild type corresponds to a molecular weight of 88±0.5 kDa, indicating an apparent tetrameric complex. The cold spot mutant shows the same elution profile as the wild type protein corresponding to a molecular weight of 88±0.3 kDa. Alanine mutants CTD^{Y689A/I692A/L696A} and CTD^{I688A/Y689A/I692A} show a shift to lower molecular weights of 57–58 kDa (57±0.2 kDa for CTD^{Y689A/I692A/L696A} and 57±0.4 kDa for CTD^{I688A/Y689A/I692A}). This indicates a smaller protein complex suggesting a weakly associated dimer or closely associated trimer configuration.
doi:10.1371/journal.pone.0096031.g004

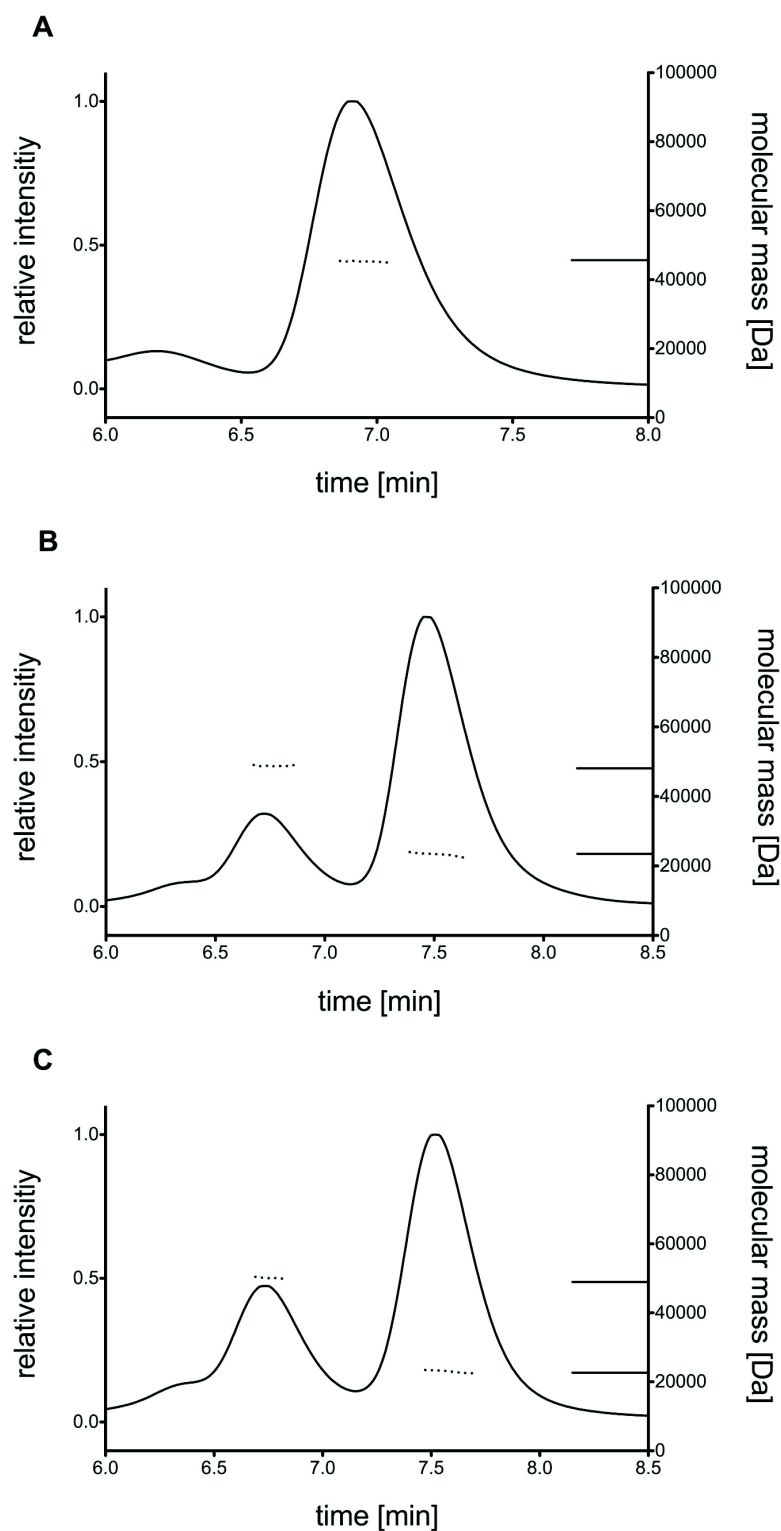


Figure 5. Differential refractive index and molecular mass of hHsp90 variants using multi-angle light-scattering. (A) For wild type hHsp90 CTD a species with molar mass of 45.4 ± 0.1 kDa was determined. Molar masses of higher oligomeric species could not be specified due to

insufficient separation. (B, C) Hot spot mutants of hHsp90 CTD, CTD^{Y689A/I692A/L696A} (B) and CTD^{I688A/Y689A/I692A} (C), revealed species with molar masses of 23.5 ± 0.2 kDa and 23.2 ± 0.2 kDa, respectively, and additional species with molar masses of 48.7 ± 0.5 kDa and 50.1 ± 0.5 kDa, respectively. Furthermore, also higher oligomeric species were detectable but could not be analyzed with respect to molar masses. doi:10.1371/journal.pone.0096031.g005

the predicted hot spot positions are additive.

In previous studies, a dimer was identified as the basic functional unit of hHsp90 [33,53]. In this work, analysis of the Mw of the CTD by SEC and calibration with protein standards suggests that the isolated hHsp90 CTD exists as an apparent tetramer under physiological conditions, although a dimer might better describe the stoichiometry of the complex in solution when the asymmetrical, elongated form of the CTD is kept in mind. Our MALS experiments demonstrate that the predominant form of wild type CTD is a dimer. Our SEC experiments furthermore show that complex formation in the CTD significantly depends on a few hot spot positions at the dimerization interface of the four-helix bundle (I688, Y689, I692 and L696): Substitution of these residues results in a decomposition of the complex into monomers, as shown by our MALS experiments. Other residues at the same interface play a less pivotal role in the stabilization of the CTD dimer: Substitution of these positions to alanine has no effect on the stoichiometry of the hHsp90 CTD complex as shown for the S658A/Q682A cold spot mutant, which resulted in an elution profile in our SEC studies essentially undistinguishable from that of the wild type CTD.

In both the SEC and MALS experiments low populations of higher oligomeric species of wild type CTD were observed, with the SEC experiments suggesting a species with twice the Mw as the predominant dimeric form. The ability of Hsp90 to self-oligomerize has been described before [54,55], and tetrameric and higher even-numbered species have been found [55]. Structural information on a hexameric assembly has been obtained for the isolated hHsp90 M-CTD (aa 293–732) in recent crystallization studies [43]; these crystals revealed that M provides the essential contacts for the hexameric arrangement in this construct. Hence, while electrophoretic studies of deletion mutants of Hsp90 also demonstrated that the C-terminal 200 amino acids are able to form oligomers [54], it is still not clear which residues form the interface mediating the potential tetrameric assembly in our isolated CTD.

The information on the complex stability of the wild type, the hot spot, and cold spot mutants obtained from our SEC and MALS studies is confirmed by differential scanning fluorimetry. Although the ThermoFluor assay does not directly detect dissociation and stoichiometry of the CTD complex in the different hHsp90 variants, the decreased melting temperatures observed for the CTD hot spot mutants correlate well with their expected role in stabilizing the interaction at the four-helix bundle interface and, thereby, the interaction of the entire complex. As the melting temperature reflects the transition of a protein from its native to the denatured state, a reduction of the melting

temperature as observed for the hot spot mutants is indicative of a less stable protein or protein assembly. Analysis of protein stability by ThermoFluor assay has been already successfully applied in previous studies to resolve different thermostabilities of wild type and mutant proteins [56,57]. As for the hHsp90, hot spot mutants reduced melting temperatures were observed for the mutants of the MMACHC protein [58]. However, the high melting temperature of 73°C observed in our study for the hHsp90 wild type is rather untypical for proteins studied by ThermoFluor analysis, which usually show much lower melting temperatures. Hence, the high melting temperature observed with the hHsp90 CTD in our study probably reflects the molecular function of Hsp90 to serve as thermo-tolerant molecular chaperone [59]. Similar to the unusual melting temperature itself, hHsp90 CTD wild type and hot spot mutants showed a large difference in their melting temperature ($\Delta T_m \geq 13^\circ\text{C}$). ThermoFluor studies on other proteins showed a less pronounced effect ($\Delta T_m < 5^\circ\text{C}$) of mutations on the melting temperatures [58,60]. Hence, the large differences observed for wild type and hot spot mutants of hHsp90 are clearly indicative that the positions at the dimerization interface identified by our computational approach have a substantial effect on the stability of the protein complex. Such an influence of interface interactions has been described previously for a variety of protein systems [45,61–64].

Cimpmperman *et al.* [65] showed that the melting temperature of a protein is also controlled by ligand binding. As the C-terminal domain of Hsp90 was proposed to have an ATP binding site, too, in addition to the one in the N-terminal domain [35,66] we have studied the effect of the ligands Mg and ATP on the stability of the hHsp90 CTD by ThermoFluor analysis. We observed an increase in the melting temperature by 2°C when one of the ligands was present (Table S5 and Figure S8 in File S1). When compared to the high difference obtained with the hot spot mutants this quantity again underlines the large influence of the selected point mutations at the dimerization interface on the stability of the protein complex.

Mimicking localized interactions in hot spot regions by small molecules has been found as a viable way to interfere with PPIs [4,11,12,67–69]. Regarding the physicochemical properties of our hot spots, the predominantly hydrophobic character is in line with the rule of four [70], a characterization of the chemical space of PPI inhibitors, which suggests that inhibitors should have $\log P > 4$. At the same time, inhibitors should be able to form polar interactions, which confer specificity of binding [71]; this would be given when mimicking Y689. The latter is also of interest because Y689 is accommodated by an indentation in the binding epitope of H4'. In this context, PPI inhibitors have been found to be

Table 3. Molecular weights and mass distributions measured by MALS.

	Mass species 1 ^[a]	Mass species 2 ^[a]	Distribution species 1/species 2
CTD wt	-	45.4 ± 0.1	0/1
CTD ^{Y689A/I692A/L696A}	23.5 ± 0.2	48.7 ± 0.5	0.77/0.23
CTD ^{I688A/Y689A/I692A}	23.2 ± 0.2	50.1 ± 0.5	0.69/0.31

^[a]In kDa.

doi:10.1371/journal.pone.0096031.t003

particularly effective when they bind to well-defined clefts or grooves in the protein-protein interface [7,72]. Finally, the hot spots in the main cluster show an $i, i+4, i+8$ pattern with respect to sequence localization when starting with I688, which could be mimicked by a novel class of non-peptidic α -helix mimetics recently described [73]. In reverse order, an $i, i+4, i+7$ pattern emerges, for which several scaffolds for α -helix mimetics have been described [74,75]. Thus, it seems promising to use the hot spots of the main cluster as a pharmacophoric template [12] for searching and designing inhibitors that interfere with the dimerization of hHsp90.

In summary, our computational results reveal the presence of spatially clustered hot spot residues in the hHsp90 CTD interface, which form a functional epitope and account for most of the protein dimerization energy. The influence of these residues on the stability and the oligomeric state of the CTD has been demonstrated by experiments. These hot spots have favorable properties with respect to using them as a pharmacophoric template for identifying and designing small-molecule inhibitors of hHsp90 dimerization. This opens up a new avenue for interfering with hHsp90 function for treating cancer.

Materials and Methods

Materials

Chemicals and reagents were purchased from AppliChem, Sigma-Aldrich, Carl Roth, VWR, Merck and Fluka at analytical grade. Plasmids were derived from pET vectors from Merck/Novagen (Darmstadt, Germany). SYPRO Orange was obtained from Sigma-Aldrich (Steinheim, Germany).

Multiple sequence alignment and homology model

Sequences of the Hsp90 CTD from *S. cerevisiae* and *E. coli* were retrieved from the Protein Data Bank (PDB). Two sequences from *S. cerevisiae* were used, corresponding to the PDB entries 2CG9 and 2CGE (UniProt code P02829, amino acids 540–677). One sequence from *E. coli* was considered, corresponding to the PDB entry 1SF8 (UniProt code P0A6Z3, amino acids 510–624). The sequence of the hHsp90 α isoform CTD was retrieved from the UniProt database (UniProt code P07900, amino acids 561–697). A multiple sequence alignment was generated by means of CLUSTALW [76,77].

Five homology models for the hHsp90 CTD were developed using the “automodel” procedure and default parameters in MODELLER 9.8 [41]. As templates, crystal structures from *S. cerevisiae* (PDB codes 2CG9 and 2CGE) and *E. coli* (PDB code 1SF8) were used. The best model as evaluated from the MODELLER objective function was chosen for the subsequent work. The quality of this homology model was assessed by means of PROCHECK [42] using default parameters.

Molecular dynamics simulations

All the procedures described in the following were performed with the Amber 11 software package [78], using the ff99SB force field [79]. The homology model and a CTD dimer of a crystal structure of an M-CTD construct of hHsp90 (PDB code: 3Q6M) were initially placed in an octahedral periodical box of TIP3P water molecules [80], where the distance between the edges of the box and the closest atom of the solute is at least 11 Å. Long-range electrostatic interactions were treated using the Particle Mesh Ewald (PME) method [81], and the SHAKE algorithm [82] was employed to constrain bond lengths of heavy atoms to hydrogen atoms. The time step for all MD simulations was set to 2 fs, with a non-bonded cutoff of 8 Å. The homology model and the CTD

dimer of the crystal structure, first, were geometry-optimized by 10 rounds of energy minimization; in each round 50 steps of steepest descent minimization were followed by 450 steps of conjugate gradient minimization, applying decreasing harmonic restraints on the solute atoms (the force constant was 25 kcal mol⁻¹ Å⁻² in the first five rounds, and reduced to 5 kcal mol⁻¹ Å⁻² in the remaining). The systems were heated from 100 K to 300 K during an MD simulation of 50 ps length performed in the canonical (NVT) ensemble, applying harmonic restraints with force constants of 5 kcal mol⁻¹ Å⁻² to all solute atoms. Afterwards, MD simulations of 250 ps length in the isothermal-isobaric ensemble (NPT) were performed applying the same harmonic restraints as in the previous step, in order to adjust the solvent density. Finally, MD simulations of 100 ps length in the NVT ensemble were performed, gradually reducing the force constants of the harmonic restraints on the solute atoms to zero. Additional 100 ns of MD simulations at 300 K were performed, and the coordinates were stored every 20 ps. These were used to extract 5000 snapshots for calculating the effective energy of dimerization and the structural decomposition.

MM-GB/SA calculations, free energy decomposition and in silico alanine scanning

MM-GB/SA calculations were performed employing the “single trajectory approach” [83]. All counterions and water molecules were stripped. For each snapshot, the gas-phase energy (i.e., the sum of the internal energies plus electrostatic and van der Waals energies) was calculated based on the ff99SB force field [79] without applying a non-bonded cutoff. Polar contributions to the solvation free energy were calculated using the “OBC” generalized Born model [84] together with mbondi2 radii, with a dielectric constant of 1 for the solute and 80 for the solvent. The polar contributions were computed at 100 mM ionic strength. Nonpolar contributions to the solvation free energies were calculated by a solvent-accessible surface area (SASA)-dependent term using a surface tension of $\gamma = 0.0072$ kcal mol⁻¹ Å⁻². Changes in the configurational entropy upon dimerization were not considered. The contributions on a per-residue basis to the overall effective energy (i.e., sum of gas-phase plus solvation free energy) of dimerization were calculated employing the decomposition scheme implemented in Amber 11 [78]. The same snapshots were used to perform *in silico* alanine scanning using the DrugScore^{PPI} web server [38,39].

Cloning, expression and purification

Synthetic codon optimized DNA (GeneScript, Piscataway, NJ) corresponding to the coding region of residues 563–732 of hHsp90 was cloned into expression vector pTEV21-a in *E. coli* BL21 (DE3) (Agilent Technologies). Cultures were grown at 37°C in LB media (5 g l⁻¹ sodium chloride, 5 g l⁻¹ yeast extract and 10 g l⁻¹ peptone) with ampicillin to OD₆₀₀ 0.8–1.2. The production of recombinant protein was induced by adding 1 mM isopropyl-1-thio- β -D-galactopyranoside, and cells were grown for another 4 h at 28°C. Cells were harvested by centrifugation, suspended in binding buffer (40 mM HEPES, 20 mM KCl, 1 mM DTT, 1 mM EDTA, 0.002% PMSF, pH 7.5) [85] and disrupted by sonification. Recombinant proteins were purified via a C-terminal His₆-tag by immobilized metal ion affinity chromatography to homogeneity (Figure S9 in File S1).

Alanine mutants and cold spot creation

Alanines at positions 689, 692, and 696 as well as at positions 688, 689, and 692 for the hot spot mutants and at positions 658

and 682 for the cold spot mutant were introduced into the constructs as described in the QuikChange Site-Directed Mutagenesis Kit (Stratagene) using *Pvu* polymerase and designed mutagenesis primers (Table 4). Additionally, alanine single mutants were constructed with alanines at positions 688, 689, 692, and 696, respectively (Table S3 in File S1).

Stability assay by Fluorescence Thermal Shift Assay (ThermoFluor)

Stability assay was performed in the real-time thermo-cycler qTOWER 2.0 (Analytik Jena AG, Germany) with 0.15 mg/mL protein and the fluorescent dye SYPRO Orange (1:1000) in 96 well PCR plates. The fluorescence signal of the SYPRO Orange dye was measured at an initial start temperature of 25°C. Up to 12 different conditions were tested (Table 5) [86] with increasing the temperature stepwise up to 95°C. When hydrophobic residues of the protein become more accessible, this leads to binding of SYPRO Orange. Fluorescence changes in the wells of the plate were monitored simultaneously with Channel Photo Multiplier (CPM). The wavelengths for excitation and emission were 490 nm and 580 nm, respectively. The detected fluorescent signal corresponds to the denaturation state of hHsp90. Melting points were determined by the implemented software (qPCRsoft V2.0.37.0, Analytik Jena AG, Germany) from the derivative of the fluorescence data.

Size exclusion chromatography

Size exclusion chromatography analyses were accomplished in triplicates on a Superdex SD200 10/300 column on an ÄKTAprius plus chromatography system (GE lifescience). The experiments were performed at 4°C in HPLC buffer (10 mM MES, 200 mM KCl, 1 mM EDTA, 1% Glycerol) with a flow rate of 0.5 mL/min at pH 6. Samples were centrifuged before for 15 min at 14.000xg, and 110 µL of the purified CTD of hHsp90 was loaded on the column. Data were analyzed using the software PrimeView Evaluation 5.0 (UNICORN, GE), and the maximal absorbance was determined by peak integration.

Table 5. pH values of screening buffers [86] for ThermoFluor assay.

No.	Buffer [100 mM]	pH
1	Glycine	3.0
2	Citric acid	4.0
3	Sodium citrate	5.5
4	Sodium/potassium phosphate	6.0
5	MES	6.2
6	Bis-tris propane	6.5
7	Sodium/potassium phosphate	7.0
8	Tris	7.5
9	EPPS	8.0
10	Tris	8.5
11	CHES	9.0
12	CHAPS	10.0

doi:10.1371/journal.pone.0096031.t005

Multi-angle light scattering

A size exclusion chromatography (SEC) column (Bio SEC-5, 150 Å, Agilent Technologies) was equilibrated with the above HPLC buffer without glycerol using a HPLC system (Agilent Technologies) connected with a multi-angle light-scattering detector (miniDAWN TREOS, Wyatt Technologies) and a differential refractive-index detector (Optilab T-rEX, Wyatt Technologies). Samples with concentrations of 2.4 mg/ml were centrifuged at 74.000xg for 30 minutes at 4°C and loaded onto the equilibrated SEC column and data were analyzed with the ASTRA software (Wyatt Technologies).

CD spectroscopy

CD measurements for wild type hHsp90 CTD as well as for all mutants generated (CTD^{I688A/Y689A/I692A}, CTD^{Y689A/I692A/L696A}, CTD^{S658A/Q682A}, CTD^{I688A}, CTD^{Y689A}, CTD^{I692A}, and

Table 4. Mutagenesis primers^[a].

Cold spot mutant: CTD ^{S658A/Q682A}
Primer 1: TCG (Ser) → GCA (Ala): 45 nt (5'-3')
Forw.: CAGAAGCTGATAAAAACGACAAAG C AGTGAAAGATCTGGTTATCC
Rev.: GGATAACCAGATCTTTC A CT G CTTTGTCGTTTTATCAGCTTCTG
Primer 2: CAG (Gln) → GCA (Ala): 34 nt (5'-3')
Forw.: AGCCTGGAAGACCC G CAACGCATGCCAACCGTA
Rev.: TACGGTTGGCATGCGTT G CCGGGTCTTCCAGGCT
Hot spot mutant I: CTD ^{Y689A/I692A/L696A}
TAC (Tyr) → GCA (Ala); ATC (Ile) → GCA (Ala); CTG (Leu) → GCA (Ala): 44 nt (5'-3')
Forw.: CAACCGTATT G CACGCAT G GCAAACTGGGG C AGGTATTGATG
Rev.: CATCAATACCT G CGCCAGTTT G CCATGCGT G CAATACGGTTG
Hot spot mutant I: CTD ^{I688A/Y689A/I692A}
ATT (Ile) → GCA (Ala); TAC (Tyr) → GCA (Ala); ATC (Ile) → GCA (Ala): 37 nt (5'-3')
Forw.: GCATGCCAACCGT G CAGCAGCAT G GCAAACTGGGCC
Rev.: GGCCAGTTT G CCATGCGT G CT G CACGGTTGGCATGC

^[a]The primers were obtained by Sigma-Aldrich Chemie GmbH Steinheim, Germany. Bold nucleotides indicate the newly introduced alanines.
doi:10.1371/journal.pone.0096031.t004

CTD^{L696A}) were performed on a Jasco J-715 spectrometer, using 0.2 mg/ml protein solutions in 50 mM potassium phosphate buffer, pH 7.6 and a cuvette with a path length of 1 mm. The spectra were obtained by averaging five measurements for each protein sample and correcting the signal by subtracting the buffer signal. Data points were collected every 0.2 nm in the range from 195 to 260 nm.

Supporting Information

File S1 The file contains additional information to the manuscript explaining results in further details. It consists of 14 pages, 5 tables and 9 figures. (PDF)

References

- Zinzalla G, Thurston DE (2009) Targeting protein-protein interactions for therapeutic intervention: a challenge for the future. *Future Med Chem* 1: 65–93.
- Fischer PM (2005) Protein-protein Interactions in Drug Discovery. *Drug Des Rev—Online* 2: 179–207.
- Wells JA, McClendon CL (2007) Reaching for high-hanging fruit in drug discovery at protein-protein interfaces. *Nature* 450: 1001–1009.
- Blazer LL, Neubig RR (2009) Small molecule protein-protein interaction inhibitors as CNS therapeutic agents: current progress and future hurdles. *Neuropsychopharmacology* 34: 126–141.
- Ryan DP, Matthews JM (2005) Protein-protein interactions in human disease. *Curr Opin Struct Biol* 15: 441–446.
- Gerrard JA, Hutton CA, Perugini MA (2007) Inhibiting protein-protein interactions as an emerging paradigm for drug discovery. *Mini Rev Med Chem* 7: 151–157.
- Chene P (2006) Drugs targeting protein-protein interactions. *ChemMedChem* 1: 400–411.
- Clackson T, Wells JA (1995) A hot spot of binding energy in a hormone-receptor interface. *Science* 267: 383–386.
- Bogan AA, Thorn KS (1998) Anatomy of hot spots in protein interfaces. *J Mol Biol* 280: 1–9.
- Gohlke H, Kiel C, Case DA (2003) Insights into protein-protein binding by binding free energy calculation and free energy decomposition for the Ras-Raf and Ras-RalGDS complexes. *J Mol Biol* 330: 891–913.
- Metz A, Pfeiffer C, Kopitz H, Pfeiffer-Marek S, Baringhaus KH, et al. (2012) Hot spots and transient pockets: predicting the determinants of small-molecule binding to a protein-protein interface. *J Chem Inf Model* 52: 120–133.
- Metz A, Schanda J, Grez M, Wichmann C, Gohlke H (2013) From determinants of RUNX1/ETO tetramerization to small-molecule protein-protein interaction inhibitors targeting acute myeloid leukemia. *J Chem Inf Model* 53: 2197–2202.
- Zerbe BS, Hall DR, Vajda S, Whitty A, Kozakov D (2012) Relationship between hot spot residues and ligand binding hot spots in protein-protein interfaces. *J Chem Inf Model* 52: 2236–2244.
- Mayer MP, Prodromou C, Frydman J (2009) The Hsp90 mosaic: a picture emerges. *Nat Struct Mol Biol* 16: 2–6.
- Wiech H, Buchner J, Zimmermann R, Jakob U (1992) Hsp90 chaperones protein folding in vitro. *Nature* 358: 169–170.
- Young JC, Agashe VR, Siegers K, Hartl FU (2004) Pathways of chaperone-mediated protein folding in the cytosol. *Nat Rev Mol Cell Biol* 5: 781–791.
- Pearl LH, Prodromou C (2006) Structure and mechanism of the Hsp90 molecular chaperone machinery. *Annu Rev Biochem* 75: 271–294.
- Wandinger SK, Richter K, Buchner J (2008) The Hsp90 chaperone machinery. *J Biol Chem* 283: 18473–18477.
- Nathan DF, Vos MH, Lindquist S (1997) In vivo functions of the Saccharomyces cerevisiae Hsp90 chaperone. *Proc Natl Acad Sci U S A* 94: 12949–12956.
- Bagatell R, Whitesell L (2004) Altered Hsp90 function in cancer: a unique therapeutic opportunity. *Mol Cancer Ther* 3: 1021–1030.
- Whitesell L, Lindquist SL (2005) HSP90 and the chaperoning of cancer. *Nat Rev Cancer* 5: 761–772.
- Young JC, Moarefi I, Hartl FU (2001) Hsp90: a specialized but essential protein-folding tool. *J Cell Biol* 154: 267–273.
- Pearl LH, Prodromou C (2000) Structure and in vivo function of Hsp90. *Curr Opin Struct Biol* 10: 46–51.
- Whitesell L, Mimnaugh EG, De Costa B, Myers CE, Neckers LM (1994) Inhibition of heat shock protein HSP90-pp60v-src heteroprotein complex formation by benzoquinone ansamycins: essential role for stress proteins in oncogenic transformation. *Proc Natl Acad Sci U S A* 91: 8324–8328.
- Sharma SV, Agatsuma T, Nakano H (1998) Targeting of the protein chaperone, HSP90, by the transformation suppressing agent, radicicol. *Oncogene* 16: 2639–2645.
- Mahalingam D, Swords R, Carew JS, Nawrocki ST, Bhalla K, et al. (2009) Targeting HSP90 for cancer therapy. *Br J Cancer* 100: 1523–1529.

Acknowledgments

H.G. is grateful to the “Zentrum für Informations- und Medientechnologie” of the Heinrich-Heine-University (HHU), Düsseldorf, for computational support. We thank the Institute of Physical Biology at HHU for providing us access to the CD spectrometer, Alexander Minges (Institute of Biochemical Plant Physiology, HHU) for providing the ThermoFluor Analysis Software PyDSF, and Daniel Schlieper (Institute of Biochemical Plant Physiology, HHU) for critical reading of the manuscript.

Author Contributions

Conceived and designed the experiments: LS GG HG. Performed the experiments: EC JV SR SHJS. Analyzed the data: EC JV SR SHJS GG HG. Wrote the paper: EC JV SR SHJS LS GG HG.

- Prodromou C, Roe SM, O'Brien R, Ladbury JE, Piper PW, et al. (1997) Identification and structural characterization of the ATP/ADP-binding site in the Hsp90 molecular chaperone. *Cell* 90: 65–75.
- Obermann WM, Sondermann H, Russo AA, Pavletich NP, Hartl FU (1998) In vivo function of Hsp90 is dependent on ATP binding and ATP hydrolysis. *J Cell Biol* 143: 901–910.
- Panaretou B, Prodromou C, Roe SM, O'Brien R, Ladbury JE, et al. (1998) ATP binding and hydrolysis are essential to the function of the Hsp90 molecular chaperone in vivo. *EMBO J* 17: 4829–4836.
- Powers MV, Workman P (2007) Inhibitors of the heat shock response: biology and pharmacology. *FEBS Lett* 581: 3758–3769.
- Sharp S, Workman P (2006) Inhibitors of the HSP90 molecular chaperone: current status. *Adv Cancer Res* 95: 323–348.
- Minami Y, Kimura Y, Kawasaki H, Suzuki K, Yahara I (1994) The carboxy-terminal region of mammalian HSP90 is required for its dimerization and function in vivo. *Mol Cell Biol* 14: 1459–1464.
- Harris SF, Shiau AK, Agard DA (2004) The crystal structure of the carboxy-terminal dimerization domain of htpG, the Escherichia coli Hsp90, reveals a potential substrate binding site. *Structure* 12: 1087–1097.
- Ratzke C, Mickler M, Hellenkamp B, Buchner J, Hugel T (2010) Dynamics of heat shock protein 90 C-terminal dimerization is an important part of its conformational cycle. *Proc Natl Acad Sci U S A* 107: 16101–16106.
- Marcu MG, Chadli A, Bouhouche I, Catelli M, Neckers LM (2000) The heat shock protein 90 antagonist novobiocin interacts with a previously unrecognized ATP-binding domain in the carboxyl terminus of the chaperone. *J Biol Chem* 275: 37181–37186.
- Yun BG, Huang W, Leach N, Hartson SD, Malters RL (2004) Novobiocin induces a distinct conformation of Hsp90 and alters Hsp90-cochaperone-client interactions. *Biochemistry* 43: 8217–8229.
- Massova I, Kollman PA (2000) Combined molecular mechanical and continuum solvent approach (MM-PBSA/GBSA) to predict ligand binding. *Perspect Drug Discovery Des* 18: 113–135.
- Krüger DM, Gohlke H (2010) DrugScore(PPI) webserver: fast and accurate in silico alanine scanning for scoring protein-protein interactions. *Nucleic Acids Res* 38: W480–W486.
- Krüger DM, Gohlke H (2011) Protein-protein interactions, web-based analysis. *Nachr Chem* 59: 44–45.
- Pantoliano MW, Petrella EC, Kwasnoski JD, Lobanov VS, Myslik J, et al. (2001) High-density miniaturized thermal shift assays as a general strategy for drug discovery. *J Biomol Screening* 6: 429–440.
- Sali A, Blundell TL (1993) Comparative protein modelling by satisfaction of spatial restraints. *J Mol Biol* 234: 779–815.
- Laskowski RA, MacArthur MW, Moss DS, Thornton JM (1993) Procheck - a Program to Check the Stereochemical Quality of Protein Structures. *J Appl Crystallogr* 26: 283–291.
- Lee CC, Lin TW, Ko TP, Wang AH (2011) The hexameric structures of human heat shock protein 90. *PLoS One* 6: e19961.
- Sgobba M, Degliesposti G, Ferrari AM, Rastelli G (2008) Structural models and binding site prediction of the C-terminal domain of human Hsp90: a new target for anticancer drugs. *Chem Biol Drug Des* 71: 420–433.
- Wichmann C, Becker Y, Chen-Wichmann L, Vogel V, Vojtkova A, et al. (2010) Dimer-tetramer transition controls RUNX1/ETO leukemogenic activity. *Blood* 116: 603–613.
- Thorn KS, Bogan AA (2001) ASEdb: a database of alanine mutations and their effects on the free energy of binding in protein interactions. *Bioinformatics* 17: 284–285.
- Niesen FH, Berglund H, Vedadi M (2007) The use of differential scanning fluorimetry to detect ligand interactions that promote protein stability. *Nat Protoc* 2: 2212–2221.
- Matulis D, Kranz JK, Salem FR, Todd MJ (2005) Thermodynamic stability of carbonic anhydrase: measurements of binding affinity and stoichiometry using ThermoFluor. *Biochemistry* 44: 5258–5266.

Hot Spots in the C-Terminal Domain of Human Hsp90

49. Bullock AN, Henckel J, DeDecker BS, Johnson CM, Nikolova PV, et al. (1997) Thermodynamic stability of wild-type and mutant p53 core domain. *Proc Natl Acad Sci U S A* 94: 14338–14342.
50. Erickson HP (2009) Size and shape of protein molecules at the nanometer level determined by sedimentation, gel filtration, and electron microscopy. *Biol Proced Online* 11: 32–51.
51. Archontis G, Simonson T, Karplus M (2001) Binding free energies and free energy components from molecular dynamics and Poisson-Boltzmann calculations. Application to amino acid recognition by aspartyl-tRNA synthetase. *J Mol Biol* 306: 307–327.
52. Moreira IS, Fernandes PA, Ramos MJ (2007) Hot spots—a review of the protein-protein interface determinant amino-acid residues. *Proteins* 68: 803–812.
53. Retzlaff M, Stahl M, Eberl HC, Lagleder S, Beck J, et al. (2009) Hsp90 is regulated by a switch point in the C-terminal domain. *EMBO Rep* 10: 1147–1153.
54. Nemoto T, Sato N (1998) Oligomeric forms of the 90-kDa heat shock protein. *Biochemical Journal* 330 (Pt 2): 989–995.
55. Moullintraffort L, Bruneaux M, Nazabal A, Allegro D, Giudice E, et al. (2010) Biochemical and biophysical characterization of the Mg²⁺-induced 90-kDa heat shock protein oligomers. *J Biol Chem* 285: 15100–15110.
56. Lavinder JJ, Hari SB, Sullivan BJ, Magliery TJ (2009) High-throughput thermal scanning: a general, rapid dye-binding thermal shift screen for protein engineering. *J Am Chem Soc* 131: 3794–3795.
57. Mulepati S, Bailey S (2011) Structural and Biochemical Analysis of Nuclease Domain of Clustered Regularly Interspaced Short Palindromic Repeat (CRISPR)-associated Protein 3 (Cas3). *Journal of Biological Chemistry* 286: 31896–31903.
58. Froese DS, Healy S, McDonald M, Kochan G, Oppermann U, et al. (2010) Thermolability of mutant MMACHC protein in the vitamin B12-responsive cblC disorder. *Mol Genet Metab* 100: 29–36.
59. Whitley D, Goldberg SP, Jordan WD (1999) Heat shock proteins: a review of the molecular chaperones. *J Vasc Surg* 29: 748–751.
60. Kervinen J, Ma H, Bayoumy S, Schubert C, Milligan C, et al. (2006) Effect of construct design on MAPKAP kinase-2 activity, thermodynamic stability and ligand-binding affinity. *Arch Biochem Biophys* 449: 47–56.
61. Bjork A, Mantzilas D, Sirevag R, Eijsink VG (2003) Electrostatic interactions across the dimer-dimer interface contribute to the pH-dependent stability of a tetrameric malate dehydrogenase. *FEBS Lett* 553: 423–426.
62. Baden EM, Owen BA, Peterson FC, Volkman BF, Ramirez-Alvarado M, et al. (2008) Altered dimer interface decreases stability in an amyloidogenic protein. *J Biol Chem* 283: 15853–15860.
63. Mandelman D, Schwarz FP, Li H, Poulos TL (1998) The role of quaternary interactions on the stability and activity of ascorbate peroxidase. *Protein Sci* 7: 2089–2098.
64. Mateu MG, Fersht AR (1998) Nine hydrophobic side chains are key determinants of the thermodynamic stability and oligomerization status of tumour suppressor p53 tetramerization domain. *EMBO J* 17: 2748–2758.
65. Gimperman P, Baranaukiene L, Jachimoviciute S, Jachno J, Torresan J, et al. (2008) A quantitative model of thermal stabilization and destabilization of proteins by ligands. *Biophys J* 95: 3222–3231.
66. Garnier C, Lafitte D, Tsvetkov PO, Barbier P, Leclerc-Devin J, et al. (2002) Binding of ATP to heat shock protein 90: evidence for an ATP-binding site in the C-terminal domain. *J Biol Chem* 277: 12208–12214.
67. Thanos CD, DeLano WL, Wells JA (2006) Hot-spot mimicry of a cytokine receptor by a small molecule. *Proc Natl Acad Sci U S A* 103: 15422–15427.
68. Azzarito V, Long K, Murphy NS, Wilson AJ (2013) Inhibition of alpha-helix-mediated protein-protein interactions using designed molecules. *Nat Chem* 5: 161–173.
69. Golden MS, Cote SM, Sayeg M, Zerbe BS, Villar EA, et al. (2013) Comprehensive experimental and computational analysis of binding energy hot spots at the NF-kappaB essential modulator/IKKbeta protein-protein interface. *J Am Chem Soc* 135: 6242–6256.
70. Morelli X, Bourgeois R, Roche P (2011) Chemical and structural lessons from recent successes in protein-protein interaction inhibition (2P2I). *Curr Opin Chem Biol* 15: 475–481.
71. Gohlke H, Klebe G (2002) Approaches to the description and prediction of the binding affinity of small-molecule ligands to macromolecular receptors. *Angew Chem Int Ed Engl* 41: 2644–2676.
72. Metz A, Ciglia E, Gohlke H (2012) Modulating protein-protein interactions: from structural determinants of binding to druggability prediction to application. *Curr Pharm Des* 18: 4630–4647.
73. Spanier L, Ciglia E, Hansen FK, Kuna K, Frank W, et al. (2014) Design, synthesis, and conformational analysis of trispyrimidonamides as α -helix mimetics. *J Org Chem* DOI: 10.1021/jo402353z.
74. Cummings CG, Hamilton AD (2010) Disrupting protein-protein interactions with non-peptidic, small molecule alpha-helix mimetics. *Curr Opin Chem Biol* 14: 341–346.
75. Davis JM, Tsou LK, Hamilton AD (2007) Synthetic non-peptide mimetics of alpha-helices. *Chem Soc Rev* 36: 326–334.
76. Larkin MA, Blackshields G, Brown NP, Chenna R, McGettigan PA, et al. (2007) Clustal W and Clustal X version 2.0. *Bioinformatics* 23: 2947–2948.
77. Goujon M, McWilliam H, Li W, Valentin F, Squizzato S, et al. (2010) A new bioinformatics analysis tools framework at EMBL-EBI. *Nucleic Acids Res* 38: W695–699.
78. Case DA, Darden TA, Cheatham TEI, Simmerling CL, Wang J, et al. (2010) AMBER 11. University of California, San Francisco.
79. Hornak V, Abel R, Okur A, Strockbine B, Roitberg A, et al. (2006) Comparison of multiple Amber force fields and development of improved protein backbone parameters. *Proteins* 65: 712–725.
80. Jorgensen WL, Chandrasekhar J, Madura JD, Impey RW, Klein ML (1983) Comparison of Simple Potential Functions for Simulating Liquid Water. *J Chem Phys* 79: 926–935.
81. Darden T, York D, Pedersen L (1993) Particle Mesh Ewald - an NLog(N) Method for Ewald Sums in Large Systems. *J Chem Phys* 98: 10089–10092.
82. Ryckaert JP, Ciccotti G, Berendsen HJC (1997) Numerical-Integration of Cartesian Equations of Motion of a System with Constraints - Molecular-Dynamics of N-Alkanes. *J Comput Phys* 23: 327–341.
83. Homeyer N, Gohlke H (2012) Free Energy Calculations by the Molecular Mechanics Poisson-Boltzmann Surface Area Method. *Mol Inf* 31: 114–122.
84. Onufriev A, Bashford D, Case DA (2004) Exploring protein native states and large-scale conformational changes with a modified generalized born model. *Proteins* 55: 383–394.
85. Richter K, Soroka J, Skalniak L, Leskova A, Hessling M, et al. (2008) Conserved conformational changes in the ATPase cycle of human Hsp90. *J Biol Chem* 283: 17757–17765.
86. Jancarik J, Pufan R, Hong C, Kim SH, Kim R (2004) Optimum solubility (OS) screening: an efficient method to optimize buffer conditions for homogeneity and crystallization of proteins. *Acta Crystallogr Sect D Biol Crystallogr* 60: 1670–1673.

10.1 PUBLICATION II – Supporting Information

Supporting Information

Resolving Hot Spots in the C-Terminal Dimerization Domain that Determine the Stability of the Molecular Chaperone Hsp90

Emanuele Ciglia^{1§}, Janina Vergin^{2§}, Sven Reimann³, Sander H.J. Smits³, Lutz Schmitt³,
Georg Groth², and Holger Gohlke*¹

¹Institute for Pharmaceutical and Medicinal Chemistry, Heinrich-Heine-University,
Düsseldorf, Germany

²Institute for Biochemical Plant Physiology, Heinrich-Heine-University, Düsseldorf,
Germany

³Institute of Biochemistry, Heinrich-Heine-University, Düsseldorf, Germany

[§]These authors contributed equally to this work.

*To whom correspondence should be addressed: Universitätsstr. 1, 40225 Düsseldorf,
Germany, Phone: +49-211-81-13662, Fax: +49-211-81-13847, Email: gohlke@uni-
duesseldorf.de

Supplemental Tables

*Comparison of hot spot predictions with MM-GB/SA and DrugScore^{PPI}*Table S1: Predicted hot spot residues of the hHsp90 CTD.^[a]

Residue	MM-GBSA	DrugScore ^{PPI}
	$\Delta G^{[b]}$	$\Delta\Delta G^{[c]}$
I642	-2.52	-1.85
T669	-2.66	-0.41
L672	-2.04	-0.92
I688	-2.63	-1.23
Y689	-2.80	-1.52
I692	-3.20	-1.57
L696	-2.50	-0.81

[a] In kcal mol⁻¹.

[b] Mean values of effective energy contributions to the dimerization of hHsp90 CTD as computed with MM-GB/SA calculations starting from the homology model [1]. The standard error in the mean is < 0.1 kcal mol⁻¹.

[c] *In silico* alanine scanning results with DrugScore^{PPI} [2].

hHsp90 CTD single alanine mutants

Table S2: Single alanine mutants of the CTD of hHsp90 investigated in this study.

Variant	Abbreviation	MW ^[a]	Extinction coefficient
Alanine mutant I	CTD ^{I688A}	21427.2	13075
Alanine mutant II	CTD ^{Y689A}	21377.3	11585
Alanine mutant III	CTD ^{I682A}	21427.2	13075
Alanine mutant IV	CTD ^{L696A}	21427.2	13075

[a] Computed molecular weight in Da.

Table S3: Mutagenesis primers for single alanine mutants.^[a]

<p>I688A: ATT (Ile) → GCA (Ala): 30 nt (5'-3') <i>Forw.:</i> CATGCCAACCGTGCATACCGCATGATCAAA <i>Rev.:</i> TTTGATCATGCGGTATGCACGGTTGGCATG</p>
<p>Y689A: TAC (Tyr) → GCG (Ala): 31 nt (5'-3') <i>Forw.:</i> ATGCCAACCGTATTGCGCGCATGATCAAACCT <i>Rev.:</i> AGTTTGATCATGCGCGCAATACGGTTGGCAT</p>
<p>I692A: ATC (Ile) → GCG (Ala): 30 nt (5'-3') <i>Forw.:</i> ATTTACCGCATGGCGAAACTGGGCCTGGGT <i>Rev.:</i> ACCCAGGCCAGTTTCGCCATGCGGTAAT</p>
<p>L696A: CTG (Leu) → GCG (Ala): 31 nt (5'-3') <i>Forw.:</i> ATCAAACCTGGGCGCGGGTATTGATGAAGATG <i>Rev.:</i> CATCTTCATCAATACCCCGCGCCAGTTTGAT</p>

[a] The primers were obtained by Sigma-Aldrich Chemie GmbH Steinheim, Germany. Bold nucleotides indicate the newly introduced alanines.

Table S4: T_m of hHsp90 CTD wild type and single alanine mutants.

	CTD wt	CTD ^{I688A}	CTD ^{Y689A}	CTD ^{I692A}	CTD ^{L696A}
T_m ^[a]	73.0 ± 0.7	66.7 ± 1.8	65.4 ± 0.9	66.1 ± 1.3	65.1 ± 0.7
ΔT_m ^[b]	0.0	-6.3	-7.6	-6.9	-7.9

[a] The detected fluorescence signal corresponds to the denaturation state of hHsp90. The melting temperature T_m of hHsp90 CTD single alanine mutants was determined from the derivative of the fluorescence data by the implemented software (qPCRsoft V2.0.37.0, Analytik Jena AG, Germany). The mean value and standard deviation were calculated from at least three independent measurements in reaction buffer with 100 mM Tris at pH 7.5 in °C.

[b] Difference in the T_m with respect to the wild type in °C.

Thermofluor analysis of hHsp90 CTD with ligands

Table S5: T_m of hHsp90 wild type in the presence of ATP or MgCl₂.

	pH 7	pH 7.5	pH 8	pH 8.5
wt T_m ^[a]	73.5 ± 0.5	73.0 ± 0.7	71.5 ± 1.1	71.8 ± 0.4
ATP T_m ^[a]	75.5 ± 0.9	74.8 ± 0.4	73.8 ± 0.4	73.5 ± 1.1
ΔT_m ATP ^[b]	+2.0	+1.3	+1.5	+2.3
MgCl ₂ T_m ^[a]	75.0 ± 0.0	75.0 ± 0.7	74.5 ± 0.5	73.8 ± 0.8
ΔT_m MgCl ₂ ^[b]	+1.5	+1.5	+2.3	+2.3

[a] The detected fluorescence signal corresponds to the denaturation state of hHsp90. The melting temperature T_m of hHsp90 CTD wild type in the presence of ATP or MgCl₂ was determined from the derivative of the fluorescence data by the implemented software (qPCRsoft V2.0.37.0, Analytik Jena AG, Germany). The mean value and standard deviation were calculated from four independent measurements in reaction buffer with 100 mM Tris at pH 7, 7.5 8 and 8.5 in °C.

[b] Difference in the T_m with respect to the wild type in °C.

Supplemental Figures

Sequence alignment

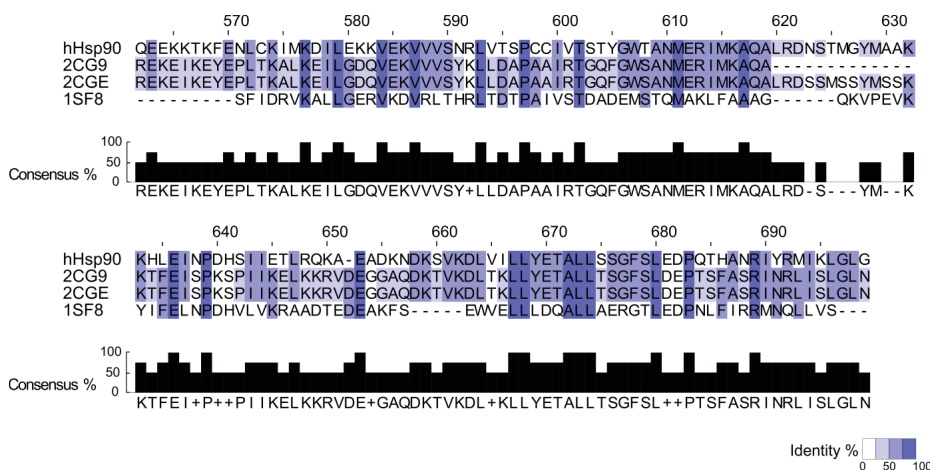


Figure S1: Multiple sequence alignment of Hsp90 CTD from *S. cerevisiae* (2CG9 and 2CGE), *E. coli* (1SF8), and *H. sapiens*. The sequence identity is represented with color on the sequences, ranging from blue (100%) to white (0%). The histograms located below the alignment show the overall consensus between the four sequences.

Validation of the homology model

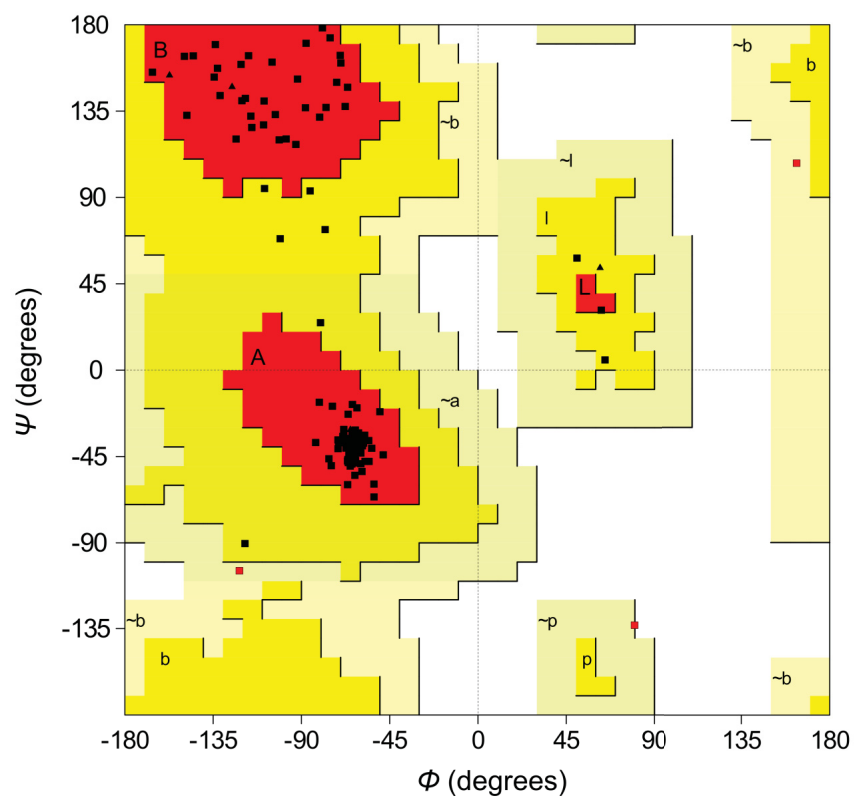


Figure S2: Ramachandran plot showing the ϕ/ψ torsion angles for all residues of the homology model. 91.4% of the residues are located in the most favorable regions of the plot (A, B, L), 6.2% of the residues are located in additionally allowed regions (a, b, l, p), and 2.3% in generously allowed regions ($\sim a$, $\sim b$, $\sim l$, $\sim p$) [3].

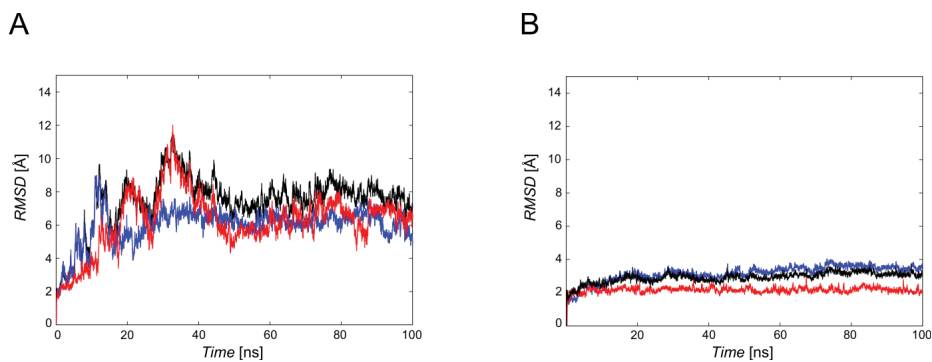
Structural deviations during MD simulations

Figure S3: Root mean square deviations (RMSD) of backbone atoms during MD simulations of 100 ns length of hHSP90 CTD. (A) RMSD of the dimer (black) and single domains (Chain A, blue; Chain B, red). (B) RMSD of backbone atoms of dimer, chain A, and chain B (black, blue, red, respectively) calculated excluding helices H2 and H2'.

Predicted hot spots for a CTD dimer of the crystal structure of an M-CTD construct of hHsp90

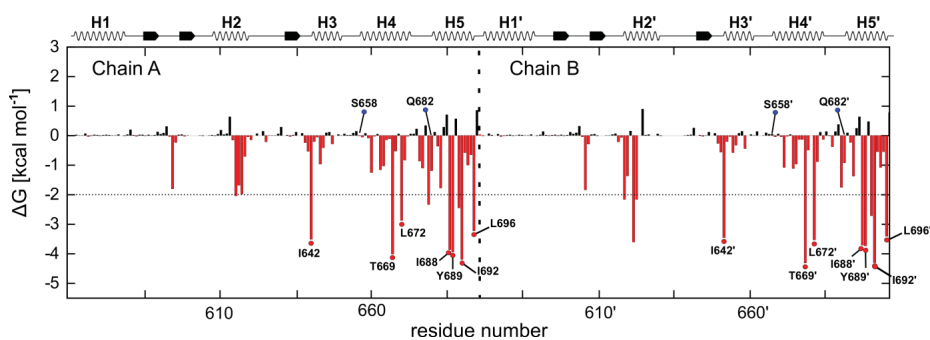


Figure S4: Contribution to the dimer stabilization of each amino acid within the hHsp90 CTD crystal structure (3Q6M). ΔG values are calculated by the MM-GB/SA approach [1,4] starting from the CTD dimer of the crystal structure of an M-CTD construct of hHsp90 (PDB code: 3Q6M) [5] and employing a structural decomposition of the effective energy [6]. The standard error in the mean is $< 0.1 \text{ kcal mol}^{-1}$ in all cases. Amino acids contributing to the dimerization with $\Delta G < -2 \text{ kcal mol}^{-1}$ are considered hot spots and are indicated in the graphic by red dots. The “cold spots” are marked with blue dots.

Hot spot prediction based on buried surface area

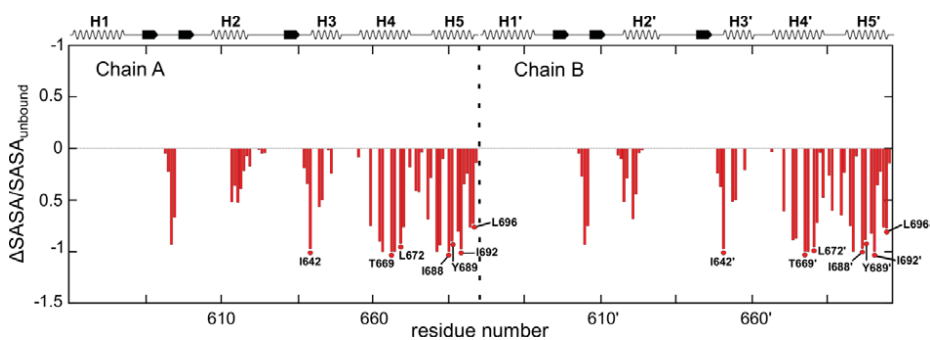


Figure S5: Residue-wise relative change in the buried surface area upon formation of the hHsp90 CTD dimer. For the calculations, the surface area values of the MM-GB/SA calculations starting from the CTD dimer of the crystal structure were used.

Thermofluor analysis of single alanine mutants of hHsp90 CTD

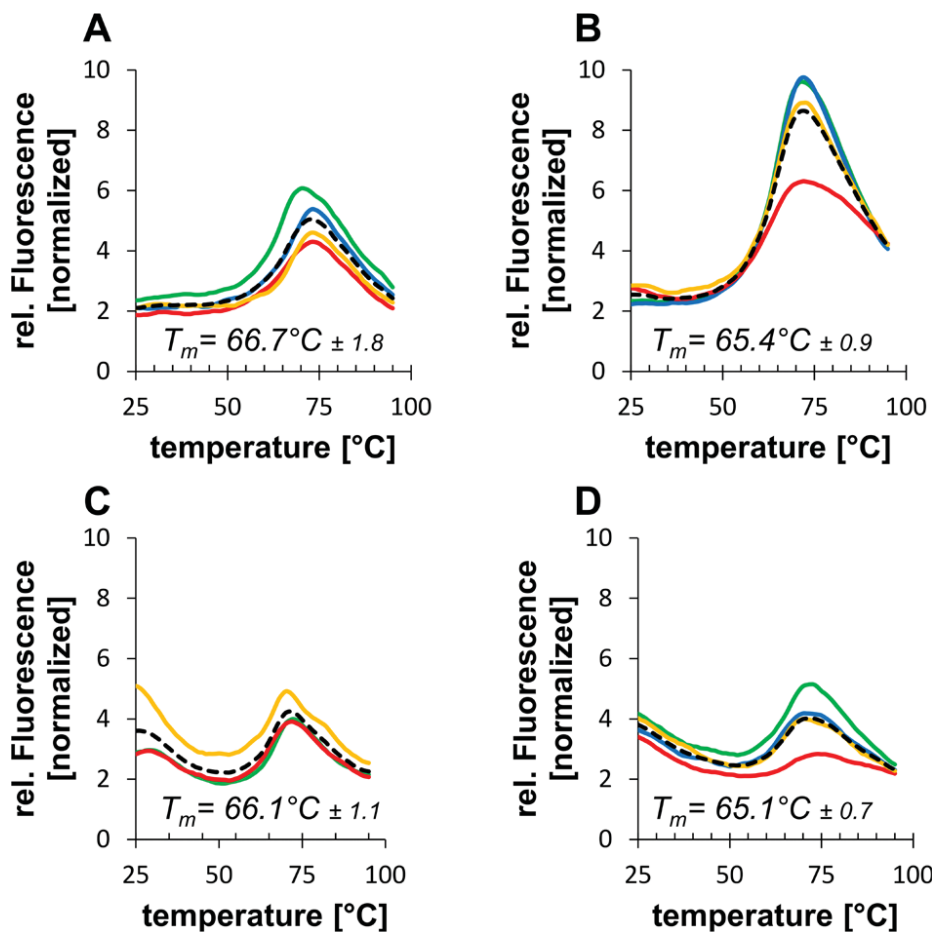


Figure S6: Thermofluor assay for investigating the stability of single alanine hHsp90 CTD mutants: Melting curves of measurements at pH 7.5 with the average $T_m \pm$ standard deviation are shown below the curves for the alanine single mutants I688A (A), Y689A (B), I692A (C), and L696A (D). The mean value (dotted black line) was calculated from three to four independent measurements (yellow, red, blue, green lines) in reaction buffer with 100 mM Tris.

CD spectroscopy measurements

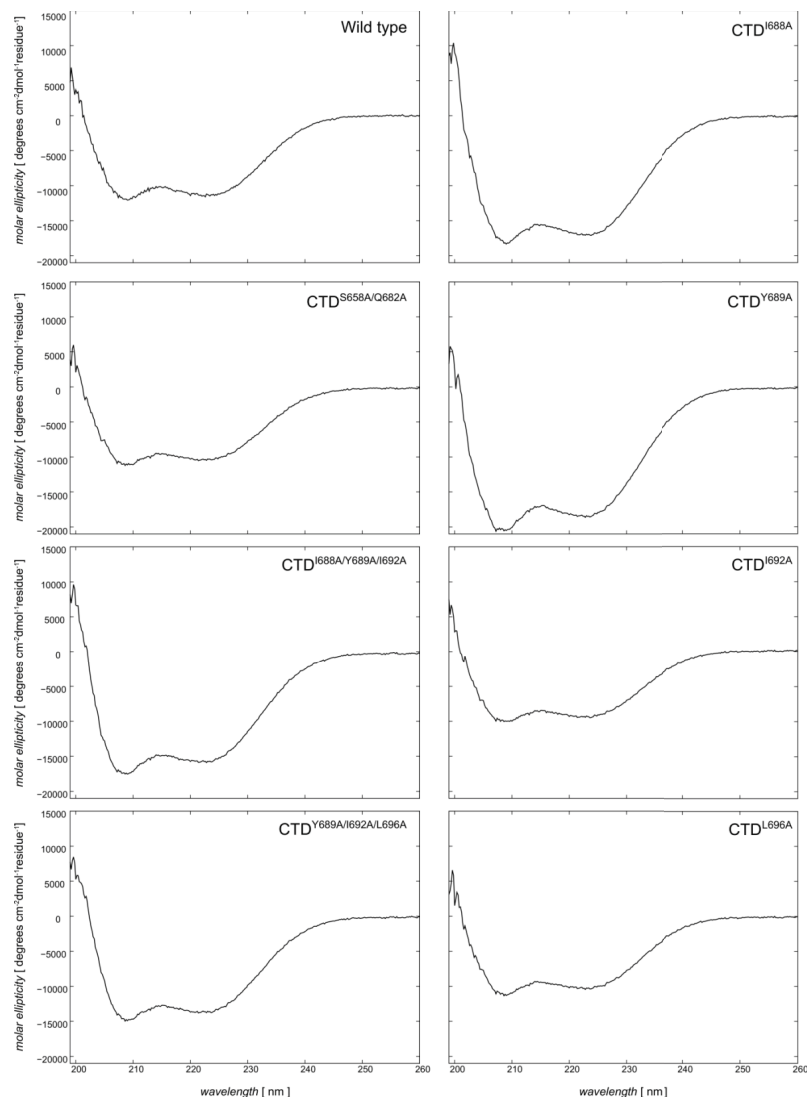


Figure S7: CD spectra of the hHsp90 CTD wild type and hHsp90 CTD mutants in the range 198-260 nm. The two pronounced peaks at about 207 and 225 nm reveal in all the cases the existence of a well-defined and mostly α -helical secondary structure.

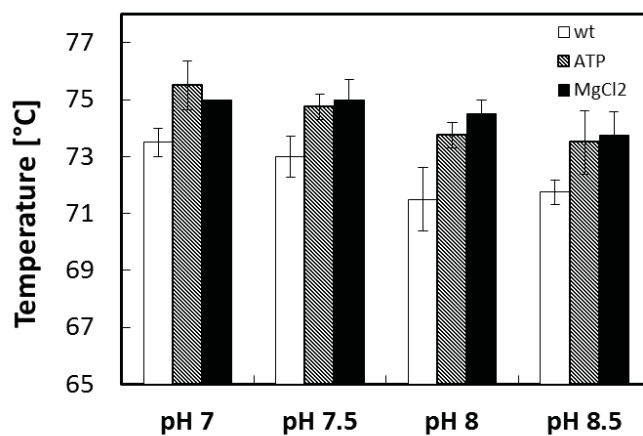
Thermofluor analysis of hHsp90 CTD with ligands

Figure S8: ATP and MgCl₂ effect on wild type hHsp90 CTD: Addition of 5 mM ATP (hatched) or 10 mM MgCl₂ (black) compared to the CTD of hHsp90 wild type (white). The mean value and standard deviation were calculated from four independent measurements in reaction buffer with 100 mM Tris at pH 7, 7.5 8 and 8.5 in °C.

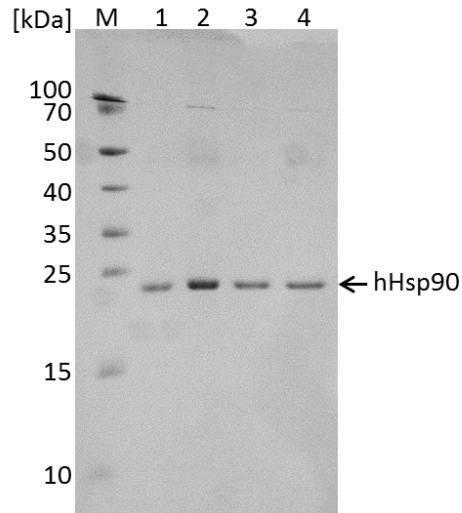
Purification of CTD of hHsp90 variants

Figure S9: SDS-PAGE of Ni^{2+} -NTA purified CTD of hHsp90 variants: After expression and purification 1000 ng of wild type (1), CTD^{Y689A/I692A/L696A} (2), CTD^{I688A/Y689A/I692A} (3), and CTD^{S658A/Q682A} (4) were solved in 5x LAP buffer [7]. Protein variants were analyzed on a 18% polyacrylamide gel with 2 μL of a protein standard (PageRuler™ Prestained Protein Ladder; Thermo Scientific) and stained with colloidal Coomassie Blue [8]. Appearing protein bands (arrow) correspond to the molecular weight of 21.5 kDa (Table 1) for the CTD of hHsp90 variants indicating a pure protein solution.

Supplemental References

1. Massova I, Kollman PA (2000) Combined molecular mechanical and continuum solvent approach (MM-PBSA/GBSA) to predict ligand binding. *Perspect Drug Discovery Des* 18: 113-135.
2. Krüger DM, Gohlke H (2010) DrugScore(PPI) webserver: fast and accurate in silico alanine scanning for scoring protein-protein interactions. *Nucleic Acids Res* 38: W480-W486.
3. Laskowski RA, Macarthur MW, Moss DS, Thornton JM (1993) Procheck - a Program to Check the Stereochemical Quality of Protein Structures. *J Appl Crystallogr* 26: 283-291.
4. Homeyer N, Gohlke H (2012) Free Energy Calculations by the Molecular Mechanics Poisson-Boltzmann Surface Area Method. *Molecular Informatics* 31: 114-122.
5. Lee CC, Lin TW, Ko TP, Wang AH (2011) The hexameric structures of human heat shock protein 90. *PLoS One* 6: e19961.
6. Gohlke H, Kiel C, Case DA (2003) Insights into protein-protein binding by binding free energy calculation and free energy decomposition for the Ras-Raf and Ras-RalGDS complexes. *J Mol Biol* 330: 891-913.
7. Laemmli UK (1970) Cleavage of structural proteins during the assembly of the head of bacteriophage T4. *Nature* 227: 680-685.
8. Kang DH, Gho YS, Suh MK, Kang CH (2002) Highly sensitive and fast protein detection with coomassie brilliant blue in sodium dodecyl sulfate-polyacrylamide gel electrophoresis. *Bull Korean Chem Soc* 23: 1511-1512.

11 PUBLICATION III

Design and Biological Testing of Peptidic Dimerization Inhibitors of Human Hsp90 that Target the C-Terminal Domain

Bertan Bopp [§], Emanuele Ciglia [§], Anissa Ouald-Chaib, Georg Groth, Holger Gohlke,
Joachim Jose

Submitted, 2015

[§] Both authors contributed equally to this work.

Design and Biological Testing of Peptidic Dimerization Inhibitors of Human Hsp90 that Target the C-terminal Domain

Bertan Bopp^{‡1}, Emanuele Ciglia^{§1}, Anissa Ouald-Chaib[§], Georg Groth[†], Holger Gohlke^{§2,3} and Joachim Jose^{‡2,3}

[‡]Institute for Pharmaceutical and Medicinal Chemistry, PharmaCampus, Westphalian Wilhelms-University, Münster, Germany

[§]Institute for Pharmaceutical and Medicinal Chemistry, Heinrich-Heine-University, Düsseldorf, Germany

[†]Institute for Biochemical Plant Physiology, Heinrich-Heine-University, Düsseldorf, Germany

*Running title: *Peptidic inhibitors of Hsp90 dimerization*

To whom correspondence should be addressed: joachim.jose@uni-muenster.de, gohlke@uni-duesseldorf.de

Keywords: Heat shock protein 90 (Hsp90); Protein-protein interactions (PPIs); Molecular dynamics simulations (MD); Fluorescence-activated cell sorting (FACS); Autodisplay

Background: The homodimeric chaperone Hsp90 is a validated target for cancer therapy.

Results: Hsp90 dimerization is blocked by peptides identified with computational analysis, tested with a novel autodisplay-based dimerization assay.

Conclusion: The peptidic inhibitors identified here provide a valuable starting point for the design of small molecule Hsp90 inhibitors.

Significance: Blocking the dimerization of Hsp90 opens a new route for cancer therapy.

ABSTRACT

The homodimeric human Hsp90 (Hsp90) is a ubiquitous molecular chaperone, essential for the maturation of numerous proteins. Some of these proteins are involved in tumor formation and growth, which makes Hsp90 an interesting drug target for cancer treatment. To date, many Hsp90 inhibitors are known that target the ATP-binding pocket in the N-terminal domain, and some inhibitors targeting the C-terminal domain (CTD) have also been reported, but none of them has been shown to bind at the C-terminal dimerization interface. We previously identified hot spot amino acids important for the C-terminal dimerization of Hsp90. Based on this information, three

peptides were designed, with the aim of inhibiting Hsp90 C-terminal dimerization. Computational and biophysical methods indicated an α -helical structure for two of the three peptides. A novel dimerization assay was developed based on the Autodisplay technology, and in this assay these two peptides were shown to inhibit Hsp90 dimer formation. For peptide H3, an IC_{50} value of 8.96 μ M was determined. Dimer formation of the C-terminal dimerization domain (CTD) was analyzed by microscale thermophoresis (MST) and a K_D of 1.29 nM was determined. Furthermore, MST studies demonstrated a high affinity binding of H3 to the CTD with a K_D of 1.46 μ M. H3 is the first inhibitor of C-terminal Hsp90 dimerization shown to bind to the CTD with a low micromolar affinity. These results can be used to design and screen for small molecules that inhibit the CTD dimerization of Hsp90, which could open a new route for cancer therapy.

The heat shock protein of 90 kDa (Hsp90) is a chaperone that influences critical cellular processes in eukaryotic organisms, such as signal transduction, vesicular transport, immune response, steroid signaling, viral infections, and cancer development (1-3). It does so by interacting

with a broad range of client proteins involved in these processes (3,4), thereby directing their folding, stabilization, and maturation. Here, dimerization of Hsp90 is essential for the interaction with client proteins (5,6).

Hsp90 is overexpressed in cancer cells, and is essential for the malignant transformation and progression of several tumor types (3,7,8). Accordingly, inhibiting Hsp90 activity is an attractive strategy for cancer therapy. The recent discovery of several small molecule Hsp90 inhibitors, some of which are currently in clinical trials, provided an important validation of this concept (9-16).

Hsp90 is a large and flexible homodimer; each monomer is organized in three major functional domains: amino terminal domain (NTD), middle domain (M), and carboxy terminal domain (CTD) (Figure 1, A) (17). Hsp90's activity is coupled with binding and hydrolysis of ATP, which takes place at the NTD. The M domain is involved in the recognition of clients and co-chaperons, and connects the NTD to the CTD. The latter mediates Hsp90 dimerization; the dimerization interface is formed by one pair of α -helices from each monomer creating a characteristic four helix bundle (Figure 1, B) (17,18). Thus, inhibiting the dimerization of Hsp90 will open up a new avenue for interfering with Hsp90 function for treating cancer.

Targeting protein-protein interactions (PPIs) is considered difficult, due to the size, hydrophobicity, and lack of deep binding pockets at the interfaces. Yet, a number of success stories demonstrate that these hurdles can be overcome (19-22). One strategy to identify small molecule mimetics of the molecular interactions essential for protein-protein binding starts from identifying hot spot amino acids at the interface (19,22-27), makes use of this information to design peptidic inhibitors as an intermediate proof-of-principle, and finally utilizes the gained knowledge for the rational discovery of small molecules with the same mode of action but improved pharmacokinetic properties (22,28).

Following this strategy, we recently resolved hot spots in the dimerization interface of the Hsp90 CTD by a combined computational and experimental approach (29). Our results were subsequently confirmed by an independent computational study (30). Additionally, Gavenonis *et al.* identified peptides derived from the

dimerization interface that inhibit Hsp90 activity (31); however, the authors did not provide evidence that the peptides target the CTD. More generally, to the best of our knowledge, none of the so far reported Hsp90 inhibitors (32) was shown to target the CTD dimerization interface.

Here, peptidic inhibitors of Hsp90 dimerization were designed and experimentally tested, making use of the identified amino acids in the CTD of Hsp90 (29) with a maximum contribution to the dimer formation. First, the conformational preferences of the designed peptides were analyzed by molecular dynamics (MD) simulations and circular dichroism (CD) experiments. Then, a novel flow cytometric Hsp90 dimerization assay based on the Autodisplay technology (33,34) was developed, which revealed *in vitro* inhibitory activity of two of the designed peptides. Additionally, it was demonstrated by means of MST that the best inhibitor peptide H3 binds to the Hsp90 CTD with micromolar affinity.

EXPERIMENTAL PROCEDURES

Molecular dynamics simulations – Peptides derived from the hHsp90 CTD interface, containing the previously identified hot spot amino acids that crucially influence the Hsp90 dimerization (29), were subjected to MD simulations. The starting structures were extracted from a homology model of the Hsp90 CTD (29). The amino acid sequences of the peptides (corresponding to the Hsp90 α isoform, UniProt code P07900) were: H1: ACE-PQTHANRIYRMIKLGL-NME; H2: ACE-DKSVKDLVILLYETALLSSG-NME; H3: ACE-DKSVKDLVILLYETALLSSGFSLEDPQTHANRIYRMIKLGL-NME. ACE and NME denote acetyl and *N*-methylamino capping groups at the N and C-terminus, respectively. In addition, structures of the peptides in complex with a monomeric CTD (denoted H1-CTD, H2-CTD, and H3-CTD) were generated from the homology model of the Hsp90 CTD dimer (29). All MD simulations were performed with the Amber 11 software package (35), using the GPU-version of pmemd (36) and the ff99SB force field (37). H1, H2, H3 and H1-CTD, H2-CTD, H3-CTD were placed in an octahedral periodic box of TIP3P water molecules (38) where the smallest distance between the edges of the box and the closest solute atom is 11 Å. The SHAKE algorithm (39) was applied to constrain

Peptidic inhibitors of Hsp90 dimerization

bond lengths of hydrogen atoms to heavy atoms, and long-range electrostatic interactions were taken into account using the Particle Mesh Ewald (PME) method (40). The time step was set to 2 fs with a non-bonded cutoff of 8 Å. The starting structures were geometry-optimized by 10 rounds of energy minimization, where each round consisted of 50 steps of steepest descent minimization followed by 450 steps of conjugate gradient minimization. During the minimization, the solute atoms were restrained applying decreasing harmonic potentials, with a force constant of 25 kcal mol⁻¹ Å⁻² in the first five rounds, reduced to 5 kcal mol⁻¹ Å⁻² in the remaining. The systems were heated from respectively 100 K, 105 K, and 110 K to 300 K during three independent MD simulations of 50 ps length performed in the canonical (NVT) ensemble, applying harmonic restraints with force constants of 5 kcal mol⁻¹ Å⁻² to all solute atoms. Afterwards, MD simulations of 250 ps length, using the isothermal-isobaric ensemble (NPT) to accommodate the solvent density were performed, applying harmonic restraints with a force constant of 5 kcal mol⁻¹ Å⁻². Last, the force constants of the harmonic restraints on the solute atoms were constantly reduced to zero in MD simulations of 100 ps length in the NVT ensemble. Finally, MD simulations of 1 μs length for H1, H2, H3 and 500 ns length for H1-CTD, H2-CTD, H3-CTD were performed. For each system, three independent MD simulations were performed (following the independent heating steps), and the coordinates were stored every 20 ps. The distribution of secondary structure and the average α -helix content of the peptides were analyzed with the Amber module ptraj (41).

Circular dichroism spectroscopy - Hsp90 CTD derived peptides H1, H2 and H3 were synthesized by JPT Peptide Technologies GmbH (Berlin, Germany). In addition, the control peptide H3mut, which differs from H3 by replacing four of the amino acids identified as hot spots (29) by alanine (see Results section) (ACE-DKSVKDLVILLYETALLSSGFSLEDPQTHANR **AARM****A****K****L****G****A****G**-NME) was also synthesized. The peptides were solubilized in H₂O at a final concentration of 0.1 mol/l. Circular dichroism (CD) measurements were taken at RT with the J-815 Spectropolarimeter from JASCO Corp. (Hachioji City, Japan). The response time was set

to 1 s and the data pitch to 0.1 nm, while the scanning speed was at 100 nm/min. Each peptide was measured 5 times, and the average was taken as result. The control measurement (H₂O only) was subtracted from the average result.

Bacterial strains and culture conditions - *E. coli* strain BL21 (DE3) [B, F⁻, *dcm*, *ompT*, *lon*, *hsdS* (rB⁻ mB⁻), *gal*, λ (DE3)] was used for the expression of the fusion proteins needed for autodisplay. *E. coli* JM110 *rpsL*, (Str^r), *thr*, *leu*, *thi-1*, *lacY*, *galK*, *galT*, *ara*, *tonA*, *tsx*, *dam*, *dcm*, *supE44*, Δ (*lac*-proAB), [F['], *traD36*, *proAB*, *lacIqZAM15*] was used for preparative restriction of the plasmid pETSH-3 (42).

Recombinant bacteria were routinely grown at 37 °C in lysogeny broth (LB) containing carbenicillin (100 μg/ml).

Recombinant DNA techniques - The coding sequence for Hsp90AA1 was obtained (catalog# GC-Z2581-10, GeneCopoeia, Rockville, Maryland, USA), amplified via PCR using the primers BB010 (5'-AAA TCT AGA CAG ACC CAA GAC CAA CCG) and BB011 (5'-AAA AGA TCT GTC TAC TTC CAT GCG TG) to add restrictions sites for 3'-BglIII and 5'-XbaI laterally and to delete the start-codon. The insertion of the PCR fragment into pETSH-3 cleaved with the same restriction enzymes resulted in plasmid pETSH-3 Hsp90 encoding a fusion protein consisting of a Sec-dependent CtxB signal peptide, Hsp90, and the AIDA-I autotransporter. Plasmid pETSH-3 SDH08 encoding CtxB signal peptide, AIDA-I autotransporter and sorbitol dehydrogenase, which was used as control, has been described earlier (43). Preparation of plasmid DNA, ligation, restriction digestion, and DNA electrophoresis were performed according to standard protocols.

Membrane protein preparation - *E. coli* BL21 (DE3) pETSH-3 Hsp90 or *E. coli* BL21 (DE3) pETSH-3 SDH08 cells were grown overnight, and 1 ml was used to inoculate a fresh 40 ml culture. Cells were cultivated at 37 °C with vigorous shaking (200 rpm) until an OD₆₀₀ of 0.5 was reached. Protein expression was induced by adding IPTG at a final concentration of 1 mM. Cultures then were incubated at 30 °C with shaking (200 rpm) for 1 h, and the induction was stopped by harvesting the cells and washing them with

Peptidic inhibitors of Hsp90 dimerization

buffer (0.2 M Tris-HCl, pH 8). Prior to membrane protein isolation by differential cell fractionation as described in detail elsewhere (44), cells were incubated at RT for 1 h with or without addition of proteinase K (25 mg/ml). The membrane proteins were washed, suspended in H₂O, and prepared for SDS-PAGE.

SDS-PAGE and Western blot analysis - Membrane preparations were diluted 1:2 with sample buffer (100 mM Tris/HCl pH 6.8 containing 4 % SDS, 0.2 % bromophenol blue, 20 % glycerol with or without 200 mM dithiothreitol), boiled for 5 minutes and separated on 12.5 % polyacrylamide gels. The gels were analyzed using the Gel iX Imager (Intas, Göttingen, Germany). The pictures of the gels were further analyzed to evaluate the density of the protein bands using the software ImageJ (ImageJ, U. S. National Institutes of Health, Bethesda, Maryland, USA, <http://imagej.nih.gov/ij/>).

For Western blot analysis, proteins were transferred on a nitrocellulose membrane, and the membrane was subsequently blocked with TBS containing dried-milk powder (5 %) for 1 h at RT. The membrane was then incubated with mouse-derived anti-Hsp90 monoclonal antibody, diluted 1:2000 in TBS containing 0.05 % Tween-20 (TBS-T), overnight at 4 °C.

The membrane was washed three times with TBS-T and incubated with the secondary antibody, a goat anti-mouse conjugate with horseradish peroxidase, diluted 1:5000 in TBS-T, for 1.5 hours at RT. Antigen-antibody conjugates were visualized by adding a solution consisting of 4-chloro-1-naphthol and H₂O₂ in TBS.

Expression and purification of p53 - *E. coli* BL21 (DE3) cells were transformed with pET19b-p53wt encoding for human p53 (45). A single cell clone was incubated overnight in 40 ml LB-medium at 37 °C. 2 l of LB-medium were inoculated with 20 ml of the overnight culture, grown to mid-log phase, and then protein expression was induced with 1 mM IPTG (final concentration) for 6 h at 30 °C. Cells were harvested and suspended in 20 ml of 20 mM Tris-HCl, 0.1 M KCl, 5 mM MgCl₂, 0.1 % Tween-20, pH 8.0 (TMK) with addition of 1 mg/ml Lysozyme, 1 mM benzamidine and 1 mM phenylmethylsulfonylfluoride (PMSF) (final concentrations), incubated for 20 min on ice and

subsequently sonicated. The lysate was cleared by centrifugation and loaded onto a pre-equilibrated Ni²⁺-chelate agarose column. The column was washed with 10 volumes of TMK-buffer, followed by 10 volumes of TMK-buffer containing 50 mM imidazole and 5 volumes of TMK-buffer containing 100 mM imidazole. p53 was eluted by TMK-buffer containing 500 mM imidazole and subsequently dialyzed overnight against PBS, pH 7.5. The purification yielded a concentration of 3.75 mg/ml in a total volume of 6 ml verified by SDS-PAGE and Bradford quantification according to standard protocols.

Fluorescein-5-isothiocyanate (FITC) labeling of p53 was performed using a kit from Calbiochem (Merck, USA) according to manufacturer's protocol.

Autodisplay dimerization assay - *E. coli* BL21 (DE3) cells displaying Hsp90 were grown to the mid log phase (OD₆₀₀ = 0.5), harvested and suspended in identical volume of PBS. Protein expression was induced by adding 1 mM IPTG (final concentration) for 16 h at 30 °C. Subsequently, cells were washed three times and suspended in PBS to an OD₆₀₀ = 0.35 in a final volume of 100 µl. Cells were incubated for 15 minutes either with or without peptide. Cells were washed three times with PBS to avoid unspecific binding and FITC labeled p53 was added subsequently to the cells in a final concentration of 1 µM with or without addition of ATP or the non-hydrolysable ATP analogue Adenosine 5'-(β-γ-imido) triphosphate (AMP-PNP) in a final concentration of 10 mM. Cells were incubated for 1 h in the dark and again washed three times with filter sterilized PBS containing 0.1 % Tween-20. Cellular fluorescence was measured with a FACS Aria III (BD, Heidelberg, Germany), using 488 nm as excitation wavelength, 530 nm for detection, and filter-sterilized PBS as sheath fluid as described before (33). Solely intact cells were analyzed after background noise elimination. For each sample, at least 50,000 events were counted using a flow rate of 1000 events per s.

Microscale Thermophoresis (MST) - The Hsp90 CTD was purified as described before (29) and labeled with the Monolith NTTM Protein Labeling Kit RED-NHS (Amine reactive) of NanoTemper (NanoTemper Technologies GmbH, München,

Peptidic inhibitors of Hsp90 dimerization

Germany) according to the manufacturer's protocol. This resulted in coupling of the fluorescent dye NT-647. For determination of the K_{dim} value of the Hsp90 CTD dimer, 10 μ l of 10 nM labeled Hsp90 CTD in PBS including 0.5 % BSA and 0.1 % Tween-20 were mixed with 10 μ l unlabeled Hsp90 CTD in different concentrations ranging from 76.3 pM to 2.5 μ M. These mixtures were incubated for 15 min at RT in the dark. Subsequently, thermophoresis of each concentration was measured at 1475 nm \pm 15 nm using the Monolith NT.115 (NanoTemper Technologies GmbH, München, Germany) (46). Each measurement was performed at 25 °C for 20 s at 95 % LED power and 80 % infrared laser power. The measurement was repeated 3 times independently for each sample. For determining the apparent K_D of Hsp90 CTD and H3, 200 nM labeled Hsp90 CTD in PBS including 0.5 % BSA and 0.1 % Tween-20 were mixed with 10 μ l peptide H3 in different concentrations ranging from 1.95 nM to 8 μ M. The mixtures were incubated for 15 min at RT in the dark and thermophoresis was measured as described above. Each measurement was performed at 25 °C for 20 s at 20 % LED power and 30 % infrared laser power. For each sample, the measurement was repeated 10 times independently. The fluorescence of each measurement was normalized and plotted against the different concentrations of the titrant. The K_D Fit formula $Y = E + (A - E) / (2 * (T + x + K_D - \sqrt{(T + x + K_D)^2 - 4 * T * x}))$ was used to calculate the K_D value using the GraphPad Prism software (GraphPad Software, Inc. La Jolla, USA). T, the concentration value for the labeled protein CTD, was set to 5 nM for determining the K_D of the Hsp90 CTD dimer, and 200 nM for determining the K_D of Hsp90 CTD and H3.

RESULTS

Design of inhibitory peptides and determination of their secondary structure content

Recently, hot spots amino acids were identified in the CTD of Hsp90 that contribute markedly to the stability of the dimer (29). Based on these hot spots, three peptides were proposed as competitive dimerization inhibitors of hHsp90: H1, a 16mer formed by residues of helix α 13 of the CTD, which contains the hot spot cluster I688, Y689,

I692 and L696; H2, a 20mer from helix α 12, which contains the smaller hot spot cluster L672 and T669; and H3, which combines H1 and H2 together with residues of the loop connecting the two (Figure 1, C). Since these peptides enclose the hot spot residues accounting for most of the dimerization energy, it was expected that they should act as competitive inhibitors by binding to the dimerization interface. As a structural instability of the peptides in the unbound form would have an adverse effect on their binding affinity (47), the secondary structure propensity of these peptides was investigated by means of MD simulations and CD spectroscopy. In the MD simulations, each peptide was simulated in explicit water by itself and in complex with the corresponding Hsp90 CTD monomer, for 1 μ s and 500 ns, respectively (Figure 1, C). Three independent simulations were performed (see Experimental Procedures) for evaluating the statistical significance of the results. In the course of the MD simulations, H1 rapidly unfolds and loses its α -helical secondary structure, which in part reappears as 3_{10} helical stretches in later stages of the simulations (Figure 2, A). With an average residue-wise α -helical content of $\sim 7.0 \pm 1.2\%$ (SEM) and the absence of any other dominating secondary structure element (Figure 2, A), the MD simulations suggest that H1 is largely unstructured if it is unbound. In contrast, H1 in complex with the CTD retains almost completely its α -helical secondary structure in the MD simulations (Figure 2, B): The average α -helical content is $\sim 54.7 \pm 10.2\%$ (SEM), and almost all amino acids are in an α -helical conformation over the complete simulation time (Figure 2, B). CD measurements of unbound H1 in aqueous solution did not reveal any secondary structure content (Figure 2, C), as proposed by the MD simulations.

In contrast to H1, both peptides H2 and H3 revealed a higher α -helical content in the MD simulations, regardless if unbound or bound to the Hsp90 CTD: the average α -helical content of the unbound peptides was $\sim 21.1 \pm 5.6\%$ (SEM) and $\sim 34.6 \pm 6.0\%$ (SEM), and $\sim 31.6 \pm 9.1\%$ (SEM) and $\sim 69.2 \pm 2.7\%$ (SEM) when bound to the CTD (Figure 3 and Figure 4, A, B). Especially in the core regions of the peptides, the α -helical content can reach between 50 and 100% (Figure 3 and Figure 4, A, B), whereas no α -helical content was observed in the loop region of H3, as expected. Note that the peptides showed pronounced and

Peptidic inhibitors of Hsp90 dimerization

repeated changes in the per-residue secondary structure for most of the residues over the time of the MD simulations, demonstrating a thorough sampling of the conformational space. The results of the independent simulations were in good agreement, as demonstrated by the standard error of the mean (SEM) calculated for the residues' average α -helical content (Figure 2, Figure 3 and Figure 4, A and B), suggesting convergence in the predicted secondary structure content. To verify the predicted α -helical content of peptides H2 and H3, CD measurements were performed. CD spectra of unbound H2 and H3 exhibited minima at ~ 208 nm and ~ 220 nm that indicate a predominantly α -helical secondary structure (Figure 3 and Figure 4, C).

Finally, the secondary structure content of the control peptide H3mut, which differs from H3 by the replacement of hot spot residues I688, Y689, I692, and L696 of the larger cluster by Ala, was analyzed. The CD spectrum of free H3mut in solution exhibited only a minimum at 202 nm, and hence, no secondary structure element (Figure 4, D).

Autodisplay of Hsp90 on the surface of E. coli

In order to display Hsp90 on the surface of *E. coli* BL21 (DE3), cells were transformed with pETSH-3 Hsp90 via heat-shock transformation (48), and expression of the protein (see Experimental Procedures) was verified by SDS-PAGE and Western-blot analysis of the outer membrane protein fractions (Figure 5). Samples lacking the plasmid and samples containing the plasmid, but without induction of protein expression, served as controls. An expected band at 137 kDa indicated the correct expression of the Hsp90 monomeric fusion protein (Figure 5, A). A protein of similar size was not detectable in control cells without plasmid (Figure 5, A and B, lane 5). In non-induced *E. coli* cells containing the plasmid, a slight protein band of similar size was detectable. This band may arise from the known leakiness of the *lac* promoter used for these experiments, leading to a slight background protein expression without the addition of inducer.

For verification of Hsp90 expression, Western-blot analysis with the identical outer membrane preparations was performed. Interestingly, a second band at approximately 300 kDa appeared, when the proteins were prepared in sample buffer

without reducing agent DTT (Figure 5, B, lane 1). In contrast, no such band is detectable when DTT is used in the sample buffer. These results gave a first hint that Hsp90 monomers displayed at the cell surface might also form dimers, as an Hsp90-specific antibody was used for immunodetection. Dimer formation is probably facilitated due to the motility of the anchoring domain of Hsp90 in the plane of the outer membrane, as previously observed in the Autodisplay for other proteins (49,50). It is a special characteristic of the surface display of this system, that monomers of proteins forming dimers or multimers in the native state show a passenger-driven dimerization or multimerization. As Hsp90 has been reported to form a dimer, this result was not unexpected (Figure 6). The amount of surface displayed Hsp90 was determined by densitometric analysis of the protein band corresponding to Hsp90 in comparison to the OmpA band in the Coomassie stained SDS-gel. The Hsp90 protein band showed a 1.94 times higher density than the OmpA protein band in the same lane (Figure 5, A, lane 1). OmpA is known to have a constant number of 1×10^5 copies per single cell (51). In order to calculate the number of Hsp90 molecules from this number, the different molecular weights of the two proteins have to be taken into account, as it is well known that the density of the Coomassie stained protein bands correlates with the entire amount of protein. The Hsp90 fusion protein has a calculated molecular weight of 137 kDa, whereas OmpA is reported to have a molecular weight of 37 kDa. Taking into account these data, the calculated number of Hsp90 molecules are about half of the OmpA molecules in the cell, resulting in an approximate number of 5.2×10^4 molecules of Hsp90 displayed at the cell surface of *E. coli*.

Functionality of displayed Hsp90 and Autodisplay based dimerization assay

The transcription factor p53 is a natural client protein of Hsp90, with a binding affinity (K_D) to the Hsp90 dimer reported to be $1 \mu\text{M}$ (52). p53 was labeled with FITC, and the labeled client protein was added in a final concentration of $1 \mu\text{M}$ to *E. coli* BL21 (DE3) cells displaying Hsp90 at an $\text{OD}_{600} = 0.35$ in a final volume of $100 \mu\text{l}$. This corresponded to 1×10^7 cells with an estimated number of 5.2×10^{11} protein molecules on the surface. The cells incubated with FITC labeled p53

Peptidic inhibitors of Hsp90 dimerization

were subjected to flow cytometer analysis. This led to an increase in cellular fluorescence (median value of fluorescence, $mF = 754$) in comparison to control cells displaying sorbitol dehydrogenase, a protein of similar size, which were also incubated with FITC labeled p53 ($mF = 3.28$) (Figure 7 A). The experiments were also performed in the presence of ATP and in the presence of the non-hydrolysable ATP analog AMP-PNP. Both controls showed no effect on the cellular fluorescence, and hence on the apparent affinity of p53 to Hsp90 in the assay (data not shown). Thus, all subsequent assays were performed without ATP. As another control, cells displaying Hsp90 were incubated with apolipoprotein E (ApoE), which is not a client protein of Hsp90. For this purpose, ApoE was labeled with the amine reactive Promofluor633 (PF633). As illustrated in Figure 7 B, incubation of cells displaying Hsp90 with PF633 labeled ApoE did not result in a notable increase in fluorescence intensity ($mF = 1.79$) in comparison to control cells displaying SDH ($mF = 2.64$). Taken together, the increase of cellular fluorescence as shown in Figure 7 A suggested the specific binding of FITC labeled p53 to surface displayed Hsp90 on *E. coli* and indicated an active and hence correctly folded dimeric Hsp90.

In the next step, *E. coli* cells displaying Hsp90 were incubated separately with the peptides H1, H2, H3, or H3mut before FITC labeled p53 was added. The ability of these peptides to compete with the monomer in the CTD would result in blocking the dimerization, which in turn should lead to a reduction of p53 binding. As a consequence, this would result in a lower cellular fluorescence in the flow cytometer analysis. For the preincubation, each peptide was added separately in a concentration of 100 μ M. Preincubation with peptide H1 and subsequent addition of FITC labeled p53 did not result in a reduction of cellular fluorescence in comparison to control cells, indicating no effect of H1 on the dimerization of Hsp90 (Figure 7, C). Preincubation of *E. coli* cells displaying Hsp90 with H2 or H3 led to a significantly reduced cellular fluorescence (Figure 7, D and E; $mF = 4.77$, $mF = 5.01$), in comparison to control cells ($mF = 32$). This indicated for both peptides a reduced binding affinity of FITC labeled p53 and in consequence a reduced amount of functional Hsp90 on the cell surface, due to inhibition of dimerization. As

expected, no reduction in cellular fluorescence was obtained when *E. coli* cells displaying Hsp90 were incubated with H3mut before FITC labeled p53 was added (data not shown).

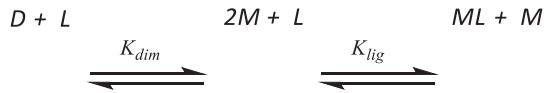
To investigate whether the inhibitory effect of H3 on dimerization was dose-dependent, different concentrations of H3 ranging from 1 μ M to 50 μ M were incubated with the same amount of *E. coli* cells displaying Hsp90. Subsequently, FITC labeled p53 was added as described above, and the resulting cellular fluorescence was determined by flow cytometry. *E. coli* cells displaying sorbitol dehydrogenase served as controls and were treated identically. As shown in Figure 8 A, increasing concentrations of H3 resulted in decreasing cellular fluorescence, indicating that H3 inhibited Hsp90 dimerization in a dose dependent manner. The fluorescence of cells displaying Hsp90 incubated with FITC labeled p53 alone was set as 100 % dimerization. The values of cellular fluorescence obtained with the different H3 concentration were set into relation in order to obtain relative inhibition of dimerization. From these data, an IC_{50} of 8.96 μ M for H3 was approximated by linear regression analysis for dimerization inhibition of surface displayed Hsp90 (Figure 8, B).

Peptide H3 binds to the C-terminal domain (CTD) of Hsp90

The Autodisplay based assay showed that the H3 peptide, which was designed based on the hot spot interactions in the Hsp90 CTD, inhibits the dimerization of Hsp90. The similarity of H3 with the CTD suggests that it binds to the CTD interface, and thereby interferes with Hsp90 dimerization. To validate this hypothesis, MST measurements were performed with the purified recombinant CTD of Hsp90 labeled with NT-647. H3 was applied in 13 different concentrations ranging from 1.95 nM to 8 μ M, and mixed with a constant concentration of 200 nM of the labeled Hsp90 CTD. MST was recorded for each sample, and a nonlinear regression curve was fit with the K_D Fit formula (see Experimental Procedures). The inflection point of the curve revealed an apparent K_D value of 1.46 μ M (Figure 8, D), indicating binding of H3 to the CTD of Hsp90. The apparent K_D value obtained by this strategy is a composite of the dissociation constant of the Hsp90 CTD dimer and the association constant of an Hsp90

Peptidic inhibitors of Hsp90 dimerization

CTD monomer and H3: As the dimeric Hsp90 CTD (D) is in equilibrium with its monomer (M), the peptide H3 (L) is only able to bind to the monomer (M) after dissociation of (D) according to the following scheme:



The equilibrium constants are defined as dissociation constants: $K_{dim} = [M]^2/[D]$, and $K_{lig} = [M] \cdot [L]/[ML]$. It was not possible to determine K_{lig} directly, as the thermophoresis signal showed a high variation at the low ligand concentrations L required for this determination. Instead, K_{lig} was determined as a function of IC_{50} and K_{dim} according to the following equations (53).

The equilibrium of D and M is described by K_{dim} (Eq. 1):

$$K_{dim} = \frac{[M]^2}{[D]} \quad (\text{Eq. 1})$$

In the absence of an inhibitor L, the concentration of unbound Hsp90 monomer M is $[M]_0$, and the concentration of the Hsp90 dimer is $[D]_0$. The total concentration of Hsp90 monomer is thus $[M]$ (Eq. 2):

$$[M] = 2[D]_0 + [M]_0 \quad (\text{Eq. 2})$$

Substituting Eq. 2 into Eq. 1 and solving the obtained quadratic equation with respect to $[M]_0$ leads to Eq. 3:

$$[M]_0 = -\frac{K_{dim}}{4} + \sqrt{\left(\frac{K_{dim}}{4}\right)^2 + \frac{K_{dim}[M]}{2}} \quad (\text{Eq. 3})$$

Substituting Eq. 3 into Eq. 2, the concentration of dimeric Hsp90 CTD $[D]_0$ is given as a function of K_{dim} and $[M]$ and can be calculated with the resulting equation Eq. 4,

$$[D]_0 = \frac{[M] + \frac{K_{dim}}{4} - \sqrt{\left(\frac{K_{dim}}{4}\right)^2 + \frac{K_{dim}[M]}{2}}}{2}$$

$$(\text{Eq. 4})$$

where K_{dim} is constant and $[M]$ is the summed concentration of all Hsp90 monomers.

$[L]_{tot}$ is defined as the total concentration of H3 present at the measured IC_{50} value, so $[L]_{tot} = IC_{50}$. In this case $[M]$ is defined by equation Eq. 5,

$$[M] = 2[D]_{50} + [M]_{50} + [ML]_{50} \quad (\text{Eq. 5})$$

where $[D]_{50}$, $[M]_{50}$, and $[ML]_{50}$ are the concentrations of the respective species in the presence of $[L]_{tot}$. In this case, $[D]_{50}$ is half of the maximal dimer concentration $[D]_0$ at $[L] = 0$ (Eq. 6):

$$[D]_{50} = \frac{[D]_0}{2} \quad (\text{Eq. 6})$$

The unbound Hsp90 CTD monomer $[M]_{50}$ is obtained by substituting Eq. 6 into Eq. 1 (Eq. 7):

$$[M]_{50} = \sqrt{\frac{K_{dim}[D]_0}{2}} \quad (\text{Eq. 7})$$

To determine K_{lig} , the law of mass action can be used to form the following equation, with the assumption that binding of the ligand depends on the predissociation of the Hsp90 CTD dimer D,

$$K_{lig} = \frac{[M]_{50}[L]_{50}}{[ML]_{50}} \quad (\text{Eq. 8})$$

in which $[L]_{50}$ is defined as unbound ligand H3 at the measured IC_{50} . $[L]_{50}$ has to be calculated in order to solve the equation for K_{lig} . As $[L]_{tot}$ is defined as the total concentration of H3 at the IC_{50} , it is composed of the concentrations $[L]_{50}$ and $[ML]_{50}$ according to equation Eq. 9:

$$[L]_{tot} = IC_{50} = [L]_{50} + [ML]_{50} \quad (\text{Eq. 9})$$

As a consequence, we determined K_{dim} of the Hsp90 CTD dimer via MST (Figure 8, C). For this purpose, 10 μl of 10 nM purified and NT-647 labeled Hsp90 CTD were mixed with 10 μl unlabeled Hsp90 CTD in different concentrations ranging from 76.3 pM to 2.5 μM . MST was recorded as described above and the nonlinear regression curve was fit with the K_{D} Fit formula. The inflection point of the curve revealed a K_{dim} of 1.29 nM.

The concentration of the total number of monomeric Hsp90 [M] present in the Autodisplay competition assay was estimated via SDS-PAGE of the membrane preparation (Figure 5) to be 5.2×10^4 . The number of *E. coli* cells per 100 μl was 1×10^7 and hence a total amount of 5.2×10^{11} Hsp90 monomers were applied in our reaction settings. Making use of the Avogadro constant, the concentration of surface displayed Hsp90 in the Autodisplay assay could be determined as 8.63 nM.

Using the equations as described above, a total concentration [M] = 8.63 nM and a measured $K_{\text{dim}} = 1.29$ nM and $\text{IC}_{50} = 8.96$ μM leads to a $K_{\text{lig}} = 3.35$ μM .

DISCUSSION

Hsp90 is an anti-cancer target with a high potential due to its involvement in many cellular regulatory processes (11,32,54). Although only few molecules targeting the Hsp90 CTD have been reported to date, these are promising alternatives to the more extensively studied NTD inhibitors (32,55,56). None of the CTD inhibitors has been shown to target the CTD dimerization interface (32). Previously, we identified a functional epitope of spatially clustered hot spots in the Hsp90 CTD dimerization interface (29). Exploiting this knowledge in the present study, we designed peptidic inhibitors derived from the dimerization interface, showed by means of a novel dimerization assay based on the Autodisplay technology that these peptides inhibit Hsp90 dimer formation, and demonstrated an *in vitro* affinity in the low micromolar range of one of the peptides towards the Hsp90 CTD by microscale thermophoresis.

Designing peptides as intermediate probes that mimic the molecular interactions required for a PPI is a validated approach on the way to small

molecule protein-protein interaction modulators (PPIMs) (22,57-61). In our previous study (22) and studies of others (31,62) it has been shown that information on hot spots located at the protein interface can be successfully exploited in such a design. Using such hot spot information for the Hsp90 CTD (29), we predicted three peptides as potential Hsp90 dimerization inhibitors: H1, a 16mer that encloses amino acids I688, Y689, I692 and L696 of the main hot spots cluster located on helix $\alpha 13$ of the CTD; H2, a 20mer containing the smaller hot spot cluster L672 and T669 from helix $\alpha 12$; and H3, which includes H1 and H2 together with the loop connecting them (Figure 1, C). H1, H2, and H3 include all residues of the respective α -helices in the native four-helix bundle (Figure 1, B and C); this design was chosen based on the assumption that it would provide improved secondary structure stability of the peptides.

In order to test the inhibitory activity of the designed peptides, we developed an assay based on the fact that p53 is a client protein of and is activated by Hsp90. CTD dimer formation of Hsp90 is essential for chaperone activity, which requires binding of Hsp90 to its client proteins (63,64). Accordingly, Hsp90 displayed on the surface of *E. coli* with Autodisplay will lead to an increased cellular fluorescence indicating functional dimerization of Hsp90 when FITC-labeled p53 is added. Conversely, inhibitors of Hsp90 dimerization will result in a dose-dependent reduction of p53-mediated cellular fluorescence. It has been reported before that proteins can dimerize on the surface of *E. coli* when displayed with Autodisplay (42,43). This is a consequence of autodisplayed proteins being anchored in the outer membrane of *E. coli* by an amphiphilic β -barrel. The β -barrel can move within the plane of the membrane such that a self-driven dimerization or even multimerization of the autodisplayed protein is possible (65-67). In the present study, we used this feature of autodisplay for the first time to investigate potential inhibitors of a PPI. The novel assay provides a valuable addition to the still limited arsenal of *ex vivo* assays to investigate the inhibition of PPIs.

The assay was validated by several control experiments. First, expression of Hsp90 on the surface of *E. coli* was analyzed by SDS-PAGE and Western-Blot. This yielded a protein band of the expected size of a monomer of Hsp90 and, in addition, a protein band with a molecular weight

Peptidic inhibitors of Hsp90 dimerization

approximately twice as large (Figure 5, A, lane 1, and Figure 5, B, lane 1). This result already indicates that Hsp90 dimerization can occur on the cell surface. Second, FITC-labeled p53 was used to confirm correct folding and dimerization of Hsp90. Cells displaying Hsp90 were incubated with FITC-labeled p53, and the cellular fluorescence was determined by flow cytometry. This resulted in a large increase of the median fluorescence ($mF = 754$) in comparison to control cells treated identically ($mF = 3.28$) (Figure 7, A). Finally, in order to exclude that the fluorescence increase results from non-specific binding, ApoE, a protein known to be no client of Hsp90, was labeled with PF633 and used in an identical setting. There, no marked increase in cellular fluorescence in comparison to control cells was observed. This finding provides a strong indication for the specific binding of FITC-labeled p53 to surface-displayed Hsp90.

Next, we used the developed assay to test the inhibitory activity of peptides H1, H2, and H3 on Hsp90 dimerization. When testing H2 in this flow cytometer based Autodisplay competition assay, a significant loss in cellular fluorescence was observed after addition of FITC labeled p53, in comparison to control cells treated identically (Figure 7, D). Likewise, a significant loss in fluorescence intensity was observed with H3 (Figure 7, E). A dose-dependent analysis of the loss of fluorescence intensity in the presence of H3 resulted in an IC_{50} value of $8.96 \mu\text{M}$ for the inhibition of Hsp90 dimerization (Figure 8). In contrast, when testing H1, no change in the fluorescence intensity was observed compared to control cells, indicating no inhibition of Hsp90 dimerization (Figure 7, A).

The lack of inhibitory activity of H1 was unexpected, because this peptide contains the main hot spots that contribute most to the dimerization energy (29). However, assuming that the peptides act as competitive inhibitors, the conformational preference of the unbound peptides in solution will also affect their binding affinity to the respective area in the dimerization interface of the CTD (68). To probe this conformational preference, we employed MD simulations of $1 \mu\text{s}$ length, which are 5-fold longer than the time required for α -helix formation as determined from experiments (69-71); such simulation times have been demonstrated to provide adequate conformational sampling for successfully predicting secondary structure

propensity of peptides (72). The simulations showed that H1 is essentially unfolded when unbound (Figure 2, A), whereas unbound H2 and H3 revealed residue-wise α -helix propensities of up to 95 % for the core residues of the peptides (Figure 3 and Figure 4, A). The results were confirmed by two additional, independent MD simulations for each peptide, strongly suggesting that convergence was achieved in the MD simulations, as well as by CD spectroscopy (Figure 2, Figure 3, and Figure 4, C). MD simulations of 500 ns length each of the peptides bound to the CTD revealed an α -helical conformation for all three peptides for almost all of the simulation times (Figure 2, Figure 3, and Figure 4, B). These results were again confirmed by two additional, independent MD simulations for each peptide-CTD complex. In all, these findings suggest that binding, and hence inhibitory activity, of H1 is hampered by the cost of conformational free energy required for α -helix formation of the peptide upon binding.

In contrast, the stable secondary structure of unbound H2 and H3 does not incur such a cost such that these peptides could more easily engage in native-like molecular interactions with the CTD and, hence, inhibit Hsp90 dimerization. Microscale thermophoresis experiments performed with purified Hsp90 CTD and H3 revealed an apparent K_D value of $1.46 \mu\text{M}$ (Figure 8, D). This result provided evidence that H3 binds to the C-terminal domain of Hsp90. Nevertheless, the apparent K_D value describes only the composite of the dissociation constant of the Hsp90 CTD dimer (K_{dim}) and the association constant of Hsp90 CTD and H3 (K_{lig}^{-1}), as in our system dimerized Hsp90 must first dissociate in order to bind H3. Hence, to determine the dissociation constant of monomeric Hsp90 CTD and H3, we first measured the K_{dim} of dimeric Hsp90 via MST (Figure 8, C). Thermophoresis measurement revealed a K_{dim} of 1.29 nM . We did not succeed in obtaining K_{lig} of monomeric Hsp90 and H3 in a direct manner, because the thermophoresis signal showed a high variation at low H3 concentrations. Hence, we calculated K_{lig} according to Eqs. 1-9 through the measured IC_{50} , the K_{dim} , and the concentration of the total number of monomeric Hsp90. This calculation revealed a K_{lig} of $3.35 \mu\text{M}$.

Finally, we intended to probe if mutating the amino acids of the main cluster of hot spots of H3 to alanine would cause a loss of inhibitory activity

Peptidic inhibitors of Hsp90 dimerization

of the resulting peptide H3mut. However, flow cytometric analysis revealed a strong tendency of H3mut to form aggregates. This tendency may result from an unstructured peptide in solution, as CD spectroscopy did not reveal a secondary structure content for H3mut (Figure 4, D). Moreover, these aggregates were binding to FITC-labeled p53 and revealed a fluorescence signal that was not distinguishable from fluorescent cell signal. In this case, the flow cytometer results obtained with cells displaying Hsp90 in the presence of H3mut and FITC labeled p53 were not valid.

In a previous study, Gavenonis *et al.* synthesized and tested several analogues of a peptide derived from the Hsp90 CTD interface that differs from H1 in terms of two additional residues, namely one Asp in the N-terminus, and one Gly in the C-terminus (31). By functional studies, the authors showed that these peptides inhibit Hsp90's chaperone activity but did not show that the peptides inhibit Hsp90 dimerization. Furthermore, while they excluded that the peptides act via NTD binding, they did not provide experimental evidence that the peptides act by binding to the CTD.

In summary, we report the design and experimental validation of peptidic inhibitors of Hsp90 dimerization. For the experimental validation, we developed a novel dimerization assay based on the Autodisplay technology. One of the designed peptides was demonstrated to bind to the Hsp90 CTD with a low micromolar affinity. This peptide is the first inhibitor of Hsp90 C-terminal dimerization shown to bind to the CTD. As the peptide is derived from the CTD dimerization interface, we presume that it acts as a competitive dimerization inhibitor by binding there. These results can be used to design and screen for small molecules that inhibit the CTD dimerization of Hsp90, which could open a new route for cancer therapy.

REFERENCES

1. Taipale, M., Jarosz, D. F., and Lindquist, S. (2010) HSP90 at the hub of protein homeostasis: emerging mechanistic insights. *Nat. Rev. Mol. Cell. Biol.* **11**, 515-528
2. Makhnevych, T., and Houry, W. A. (2012) The role of Hsp90 in protein complex assembly. *Biochim. Biophys. Acta* **1823**, 674-682
3. Rohl, A., Rohrberg, J., and Buchner, J. (2013) The chaperone Hsp90: changing partners for demanding clients. *Trends Biochem. Sci.* **38**, 253-262
4. Taipale, M., Krykbaeva, I., Koeva, M., Kayatekin, C., Westover, K. D., Karras, G. I., and Lindquist, S. (2012) Quantitative analysis of HSP90-client interactions reveals principles of substrate recognition. *Cell* **150**, 987-1001
5. Weikl, T., Muschler, P., Richter, K., Veit, T., Reinstein, J., and Buchner, J. (2000) C-terminal regions of Hsp90 are important for trapping the nucleotide during the ATPase cycle. *J. Mol. Biol.* **303**, 583-592
6. Prodromou, C., Panaretou, B., Chohan, S., Siligardi, G., O'Brien, R., Ladbury, J. E., Roe, S. M., Piper, P. W., and Pearl, L. H. (2000) The ATPase cycle of Hsp90 drives a molecular 'clamp' via transient dimerization of the N-terminal domains. *EMBO J.* **19**, 4383-4392
7. Bagatell, R., and Whitesell, L. (2004) Altered Hsp90 function in cancer: a unique therapeutic opportunity. *Mol. Cancer Ther.* **3**, 1021-1030
8. Whitesell, L., and Lindquist, S. L. (2005) HSP90 and the chaperoning of cancer. *Nat. Rev. Cancer* **5**, 761-772
9. Powers, M. V., and Workman, P. (2007) Inhibitors of the heat shock response: biology and pharmacology. *FEBS Lett.* **581**, 3758-3769
10. Sharp, S., and Workman, P. (2006) Inhibitors of the HSP90 molecular chaperone: current status. *Adv. Cancer Res.* **95**, 323-348
11. Mahalingam, D., Swords, R., Carew, J. S., Nawrocki, S. T., Bhalla, K., and Giles, F. J. (2009) Targeting HSP90 for cancer therapy. *Br. J. Cancer* **100**, 1523-1529
12. Mayer, M. P., Prodromou, C., and Frydman, J. (2009) The Hsp90 mosaic: a picture emerges. *Nat. Struct. Mol. Biol.* **16**, 2-6
13. Pearl, L. H., and Prodromou, C. (2000) Structure and in vivo function of Hsp90. *Curr. Opin. Struct. Biol.* **10**, 46-51
14. Sharma, S. V., Agatsuma, T., and Nakano, H. (1998) Targeting of the protein chaperone, HSP90, by the transformation suppressing agent, radicicol. *Oncogene* **16**, 2639-2645
15. Whitesell, L., Mimnaugh, E. G., De Costa, B., Myers, C. E., and Neckers, L. M. (1994) Inhibition of heat shock protein HSP90-pp60v-src heteroprotein complex formation by benzoquinone ansamycins: essential role for stress proteins in oncogenic transformation. *Proc. Natl. Acad. Sci. USA* **91**, 8324-8328
16. Young, J. C., Moarefi, I., and Hartl, F. U. (2001) Hsp90: a specialized but essential protein-folding tool. *J. Cell Biol.* **154**, 267-273
17. Pearl, L. H., and Prodromou, C. (2006) Structure and mechanism of the Hsp90 molecular chaperone machinery. *Annu. Rev. Biochem.* **75**, 271-294
18. Harris, S. F., Shiau, A. K., and Agard, D. A. (2004) The crystal structure of the carboxy-terminal dimerization domain of htpG, the Escherichia coli Hsp90, reveals a potential substrate binding site. *Structure* **12**, 1087-1097
19. Metz, A., Ciglia, E., and Gohlke, H. (2012) Modulating protein-protein interactions: from structural determinants of binding to druggability prediction to application. *Curr. Pharm. Des.* **18**, 4630-4647
20. Zinzalla, G., and Thurston, D. E. (2009) Targeting protein-protein interactions for therapeutic intervention: a challenge for the future. *Future Med. Chem.* **1**, 65-93
21. Chene, P. (2006) Drugs targeting protein-protein interactions. *Chemmedchem.* **1**, 400-411
22. Metz, A., Schanda, J., Grez, M., Wichmann, C., and Gohlke, H. (2013) From determinants of RUNX1/ETO tetramerization to small-molecule protein-protein interaction inhibitors targeting

- acute myeloid leukemia. *J. Chem. Inf. Model* **53**, 2197-2202
23. Blazer, L. L., and Neubig, R. R. (2009) Small molecule protein-protein interaction inhibitors as CNS therapeutic agents: current progress and future hurdles. *Neuropsychopharmacol.* **34**, 126-141
 24. Metz, A., Pflieger, C., Kopitz, H., Pfeiffer-Marek, S., Baringhaus, K. H., and Gohlke, H. (2012) Hot Spots and Transient Pockets: Predicting the Determinants of Small-Molecule Binding to a Protein-Protein Interface. *J. Chem. Inf. Model* **52**, 120-133
 25. Azzarito, V., Long, K., Murphy, N. S., and Wilson, A. J. (2013) Inhibition of alpha-helix-mediated protein-protein interactions using designed molecules. *Nat. Chem.* **5**, 161-173
 26. Gohlke, H., Kiel, C., and Case, D. A. (2003) Insights into protein-protein binding by binding free energy calculation and free energy decomposition for the Ras-Raf and Ras-RalGDS complexes. *J. Mol. Biol.* **330**, 891-913
 27. Wichmann, C., Becker, Y., Chen-Wichmann, L., Vogel, V., Vojtkova, A., Herglotz, J., Moore, S., Koch, J., Lausen, J., Mantele, W., Gohlke, H., and Grez, M. (2010) Dimer-tetramer transition controls RUNX1/ETO leukemogenic activity. *Blood* **116**, 603-613
 28. Bonache, M. A., Balsera, B., Lopez-Mendez, B., Millet, O., Brancaccio, D., Gomez-Monterrey, I., Carotenuto, A., Pavone, L. M., Reille-Seroussi, M., Gagey-Eilstein, N., Vidal, M., de la Torre-Martinez, R., Fernandez-Carvajal, A., Ferrer-Montiel, A., Garcia-Lopez, M. T., Martin-Martinez, M., de Vega, M. J., and Gonzalez-Muniz, R. (2014) De Novo Designed Library of Linear Helical Peptides: An Exploratory Tool in the Discovery of Protein-Protein Interaction Modulators. *ACS Comb. Sci.*
 29. Ciglia, E., Vergin, J., Reimann, S., Smits, S. H., Schmitt, L., Groth, G., and Gohlke, H. (2014) Resolving hot spots in the C-terminal dimerization domain that determine the stability of the molecular chaperone Hsp90. *PLoS One* **9**, e96031
 30. Rastelli, G. (2014) Dimerization hot spots in the structure of human Hsp90. *Medchemcomm.* **5**, 797-801
 31. Gavenonis, J., Jonas, N. E., and Kritzer, J. A. (2014) Potential C-terminal-domain inhibitors of heat shock protein 90 derived from a C-terminal peptide helix. *Bioorg Med Chem* **22**, 3989-3993
 32. Neckers, L., and Workman, P. (2012) Hsp90 molecular chaperone inhibitors: are we there yet? *Clin. Cancer Res.* **18**, 64-76
 33. Raaf, J., Guerra, B., Neundorf, I., Bopp, B., Issinger, O.-G., Jose, J., Pietsch, M., and Niefind, K. (2013) First Structure of Protein Kinase CK2 Catalytic Subunit with an Effective CK2 β -Competitive Ligand. *ACS Chem. Biol.* **8**, 901-907
 34. Jose, J., and Meyer, T. F. (2007) The autodisplay story, from discovery to biotechnical and biomedical applications. *Microbiol. Mol. Biol. R.* **71**, 600-619
 35. Case, D. A., Darden, T. A., Cheatham, T. E. I., Simmerling, C. L., Wang, J., Duke, R. E., Luo, R., Walker, R. C., Zhang, W., Merz, K. M., Roberts, B., Wang, B., Hayik, S., Roitberg, A., Seabra, G., Kolossváry, I., Wong, K. F., Paesani, F., Vanicek, J., Liu, J., Wu, X., Brozell, S. R., Steinbrecher, T., Gohlke, H., Cai, Q., Ye, X., Wang, J., Hsieh, M.-J., Cui, G., Roe, D. R., Mathews, D. H., Seetin, M. G., Sagui, C., Babin, V., Luchko, T., Gusarov, S., Kovalenko, A., and Kollman, P. A. (2010) AMBER 11. *University of California, San Francisco*
 36. Salomon-Ferrer, R., Gotz, A. W., Poole, D., Le Grand, S., and Walker, R. C. (2013) Routine Microsecond Molecular Dynamics Simulations with AMBER on GPUs. 2. Explicit Solvent Particle Mesh Ewald. *J. Chem. Theory Comput.* **9**, 3878-3888
 37. Hornak, V., Abel, R., Okur, A., Strockbine, B., Roitberg, A., and Simmerling, C. (2006) Comparison of multiple Amber force fields and development of improved protein backbone parameters. *Proteins* **65**, 712-725
 38. Jorgensen, W. L., Chandrasekhar, J., Madura, J. D., Impey, R. W., and Klein, M. L. (1983) Comparison of Simple Potential Functions for Simulating Liquid Water. *J. Chem. Phys.* **79**, 926-935
 39. Ryckaert, J. P., Ciccotti, G., and Berendsen, H. J. C. (1977) Numerical-Integration of Cartesian Equations of Motion of a System with Constraints - Molecular-Dynamics of N-Alkanes. *J. Comput. Phys.* **23**, 327-341

40. Darden, T., York, D., and Pedersen, L. (1993) Particle Mesh Ewald - an N.Log(N) Method for Ewald Sums in Large Systems. *J. Chem. Phys.* **98**, 10089-10092
41. Case, D. A., Cheatham, T. E., 3rd, Darden, T., Gohlke, H., Luo, R., Merz, K. M., Jr., Onufriev, A., Simmerling, C., Wang, B., and Woods, R. J. (2005) The Amber biomolecular simulation programs. *J. Comput. Chem.* **26**, 1668-1688
42. Jose, J., and Handel, S. (2003) Monitoring the cellular surface display of recombinant proteins by cysteine labeling and flow cytometry. *Chembiochem.* **4**, 396-405
43. Jose, J., and von Schwichow, S. (2004) "Cysteine tagging" for labeling and detection of recombinant protein expression. *Anal. Biochem.* **331**, 267-274
44. Park, M., Yoo, G., Bong, J. H., Jose, J., Kang, M. J., and Pyun, J. C. (2015) Isolation and characterization of the outer membrane of Escherichia coli with autodisplayed Z-domains. *Biochim. Biophys. Acta* **1848**, 842-847
45. Schuster, N., Gotz, C., Faust, M., Schneider, E., Prowald, A., Jungbluth, A., and Montenarh, M. (2001) Wild-type p53 inhibits protein kinase CK2 activity. *J. Cell. Biochem.* **81**, 172-183
46. Seidel, S. A., Dijkman, P. M., Lea, W. A., van den Bogaart, G., Jerabek-Willemsen, M., Lazic, A., Joseph, J. S., Srinivasan, P., Baaske, P., Simeonov, A., Katritch, I., Melo, F. A., Ladbury, J. E., Schreiber, G., Watts, A., Braun, D., and Duhr, S. (2013) Microscale thermophoresis quantifies biomolecular interactions under previously challenging conditions. *Methods* **59**, 301-315
47. Tirado-Rives, J., and Jorgensen, W. L. (2006) Contribution of conformer focusing to the uncertainty in predicting free energies for protein-ligand binding. *J. Med. Chem.* **49**, 5880-5884
48. Hanahan, D. (1983) Studies on Transformation of Escherichia coli with Plasmids. *J. Mol. Biol.* **166**, 557-580
49. Jose, J., and von Schwichow, S. (2004) Autodisplay of active sorbitol dehydrogenase (SDH) yields a whole cell biocatalyst for the synthesis of rare sugars. *Chembiochem.* **5**, 491-499
50. Jose, J., Bernhardt, R., and Hannemann, F. (2001) Functional display of active bovine adrenodoxin on the surface of E. coli by chemical incorporation of the [2Fe-2S] cluster. *Chembiochem.* **2**, 695-701
51. Koebnik, R., Locher, K. P., and Van Gelder, P. (2000) Structure and function of bacterial outer membrane proteins: barrels in a nutshell. *Mol. Microbiol.* **37**, 239-253
52. Muller, L., Schaupp, A., Walerych, D., Wegele, H., and Buchner, J. (2004) Hsp90 regulates the activity of wild type p53 under physiological and elevated temperatures. *J. Biol. Chem.* **279**, 48846-48854
53. Metz, A. (2014) Predicting and Exploiting the Determinants of Protein/Protein Interactions to Identify Low-Molecular Inhibitors of RUNX1-ETO Tetramerization. *PhD thesis, Heinrich-Heine-University, Düsseldorf*
54. Kim, Y. S., Alarcon, S. V., Lee, S., Lee, M. J., Giaccone, G., Neckers, L., and Trepel, J. B. (2009) Update on Hsp90 inhibitors in clinical trial. *Curr. Top. Med. Chem.* **9**, 1479-1492
55. Donnelly, A., and Blagg, B. S. (2008) Novobiocin and additional inhibitors of the Hsp90 C-terminal nucleotide-binding pocket. *Curr. Med. Chem.* **15**, 2702-2717
56. Donnelly, A. C., Mays, J. R., Burlison, J. A., Nelson, J. T., Vielhauer, G., Holzbeierlein, J., and Blagg, B. S. (2008) The design, synthesis, and evaluation of coumarin ring derivatives of the novobiocin scaffold that exhibit antiproliferative activity. *J. Org. Chem.* **73**, 8901-8920
57. Milroy, L. G., and Brunsveld, L. (2013) Pharmaceutical implications of helix length control in helix-mediated protein-protein interactions. *Future Med. Chem.* **5**, 2175-2183
58. Mukherjee, P., Desai, P., Zhou, Y. D., and Avery, M. (2010) Targeting the BH3 domain mediated protein-protein interaction of Bcl-xL through virtual screening. *J. Chem. Inf. Model* **50**, 906-923
59. Cardinale, D., Guaitoli, G., Tondi, D., Luciani, R., Henrich, S., Salo-Ahen, O. M., Ferrari, S., Marverti, G., Guerrieri, D., Ligabue, A., Frassinetti, C., Pozzi, C., Mangani, S., Fessas, D., Guerrini, R., Ponterini, G., Wade, R. C., and Costi, M. P. (2011) Protein-protein interface-binding peptides inhibit the cancer therapy target human thymidylate synthase. *Proc. Natl. Acad. Sci. USA* **108**, E542-549
60. London, N., Raveh, B., Movshovitz-Attias, D., and Schueler-Furman, O. (2010) Can self-

- inhibitory peptides be derived from the interfaces of globular protein-protein interactions? *Proteins* **78**, 3140-3149
61. Kussie, P. H., Gorina, S., Marechal, V., Elenbaas, B., Moreau, J., Levine, A. J., and Pavletich, N. P. (1996) Structure of the MDM2 oncoprotein bound to the p53 tumor suppressor transactivation domain. *Science* **274**, 948-953
 62. Li, Y., Liu, X., Dong, X., Zhang, L., and Sun, Y. (2014) Biomimetic design of affinity peptide ligand for capsomere of virus-like particle. *Langmuir* **30**, 8500-8508
 63. Wang, C., and Chen, J. (2003) Phosphorylation and hsp90 binding mediate heat shock stabilization of p53. *J. Biol. Chem.* **278**, 2066-2071
 64. Wayne, N., and Bolon, D. N. (2007) Dimerization of Hsp90 is required for in vivo function. Design and analysis of monomers and dimers. *J. Biol. Chem.* **282**, 35386-35395
 65. Engelman, D. M. (2005) Membranes are more mosaic than fluid. *Nature* **438**, 578-580
 66. Jose, J., Bernhardt, R., and Hannemann, F. (2002) Cellular surface display of dimeric Adx and whole cell P450-mediated steroid synthesis on *E. coli*. *J. Biotechnol.* **95**, 257-268
 67. Detzel, C., Maas, R., and Jose, J. (2011) Autodisplay of nitrilase from *Alcaligenes faecalis* in *E. coli* yields a whole cell biocatalyst for the synthesis of enantiomerically pure R -mandelic acid. *ChemCatChem* **3**, 719-725
 68. Gohlke, H., and Klebe, G. (2002) Approaches to the description and prediction of the binding affinity of small-molecule ligands to macromolecular receptors. *Angew. Chem. Int. Ed. Engl.* **41**, 2644-2676
 69. Lin, M. M., Mohammed, O. F., Jas, G. S., and Zewail, A. H. (2011) Speed limit of protein folding evidenced in secondary structure dynamics. *Proc. Natl. Acad. Sci. USA* **108**, 16622-16627
 70. Gnanakaran, S., Nymeyer, H., Portman, J., Sanbonmatsu, K. Y., and Garcia, A. E. (2003) Peptide folding simulations. *Curr. Opin. Struct. Biol.* **13**, 168-174
 71. De Sancho, D., and Best, R. B. (2011) What is the time scale for alpha-helix nucleation? *J. Am. Chem. Soc.* **133**, 6809-6816
 72. Spomer, L., Gertzen, C. G., Schmitz, B., Haussinger, D., Gohlke, H., and Keitel, V. (2014) A membrane-proximal, C-terminal alpha-helix is required for plasma membrane localization and function of the G Protein-coupled receptor (GPCR) TGR5. *J. Biol. Chem.* **289**, 3689-3702
 73. Gawarzewski I., D. F., Winterer E., Tschapek B., Sander H.J.S., Jose J., Schmitt L. (2014) Crystal structure of the transport unit of the autotransporter adhesin involved in diffuse adherence from *Escherichia coli*. *J. Struct. Biol.* **187**, 20-29

Acknowledgments—H.G. is grateful to the “Zentrum für Informations- und Medientechnologie” of the Heinrich-Heine-University (HHU), Düsseldorf, for computational support. We are grateful to T.J. Schmidt and A. Schnieders (Institute for Pharmaceutical Biology and Phytochemistry, Westphalian Wilhelms-University, Münster) for performing the CD spectroscopy. We thank C. Götz (Institute for Medicinal Biochemistry and Molecular Biology of the University of Saarland, Homburg) for providing the plasmid pET19b-p53wt.

FOOTNOTES

*This work was supported by funds from the Strategische Forschungsfonds of the Heinrich-Heine-University, Düsseldorf.

¹Both authors contributed equally to this study.

²Both authors share senior authorship.

³To whom correspondence should be addressed: J.J.: Institute for Pharmaceutical and Medicinal Chemistry, PharmaCampus, Westphalian Wilhelms-University, Corrensstr. 48, 48149 Münster, Germany, Tel.: +49-251-8332200, Fax: +49-25-8332210, Email: joachim.jose@uni.muenster.de; H.G.: Institute for Pharmaceutical and Medicinal Chemistry, Heinrich-Heine-University, Universitätsstrasse 1, 40225 Düsseldorf, Germany, Tel.: +49-

Peptidic inhibitors of Hsp90 dimerization

211-81-13662, Fax: +49-211-81-13847, Email: Gohlke@uni-duesseldorf.de.

⁴The abbreviations used are: Hsp90, human heat shock protein of 90 kDa; CTD, C-terminal domain; PPIs, Protein-protein interactions; MD simulations, Molecular dynamics simulations; CD, Circular dichroism; FACS, Fluorescence-activated cell sorting; MST, Microscale thermophoresis.

FIGURE LEGENDS

FIGURE 1. Peptides derived from the dimerization interface of the Hsp90 CTD. (A) Surface representation of the full length *S. cerevisiae* Hsp90 (PDB code 2CG9) showing the three protein domains (N-terminal domain: light blue, middle domain: red, C-terminal domain: wheat). (B) Homology model of the human Hsp90 CTD dimer (blue), generated as described in (29). The pair of helices from which the interface peptides investigated by MD simulations, CD spectroscopy, and FACS assay were derived are colored in wheat in the box. (C) Blow-up of the starting structures for the MD simulations: single peptides (H1 to H3, upper panel) and peptides in complex with the Hsp90 CTD monomer (H1-CTD to H3-CTD, lower panel).

FIGURE 2. Secondary structure of H1 in MD simulations and CD spectroscopy. In the upper panels, representative conformations of the peptide simulated by itself (A) or extracted from the peptide-CTD complex (B) are shown at different times during the MD simulations. In the lower panel, the secondary structure of each peptide residue (as indicated by the color scale below) is given as a function of the simulation time. The histograms on the right show the α -helix content of each peptide residue averaged over the three independent MD simulations; the standard error of the mean (SEM) is indicated by the red bars (see Experimental Procedures). (C) CD spectrum of the peptide in aqueous solution in the range 180-250 nm.

FIGURE 3. Secondary structure of H2 in MD simulations and CD spectroscopy. For further details see Figure 2.

FIGURE 4. Secondary structure of H3 in MD simulations as well as H3 and H3mut in CD spectroscopy. (A-C) Data for H3; for further details see Figure 2. (D) CD spectrum of the peptide H3mut in aqueous solution in the range 180-250.

FIGURE 5. Expression and surface display of Hsp90. SDS-PAGE (A) of the membrane protein preparation of *E. coli* BL21 (DE3) pETSH-3 Hsp90. An expected band at 137 kDa appears at Lanes 1 and 3, after inducing protein expression, respectively. Lanes 2 and 4 show membrane protein preparation of non-induced *E. coli* BL21 (DE3) pETSH-3 Hsp90 cells with and without addition of DTT. Lane 5 shows a membrane protein preparation of control cells without plasmid. (B) Western-Blot analysis of the same preparation. An additional dimeric Hsp90 band appears in lane 1 treated without DTT. Hsp90 protein is indicated by black arrows.

FIGURE 6. Schematic description of the Hsp90 dimerization assay using Autodisplay. (A) Structure of the Hsp90 fusion protein consisting of an N-terminal signal peptide for Sec-dependent translocation across the inner membrane (IM), a passenger domain, a linker domain, and the β -barrel domain. (B) Schematic view of the proposed secretion mechanism and dimerization of Hsp90. After translocation via SecYEG across the IM, the signal peptide is cleaved, and the Omp85 complex interacts with the incompletely folded β -barrel and integrates the fusion protein into the outer membrane (OM) (73). Hsp90 is released to the cell surface and dimerizes there.

FIGURE 7. Flow cytometer analysis of cells displaying Hsp90 in the dimerization assay. (A) Flow cytometric analysis showing *E. coli* BL21 (DE3) cells displaying Hsp90 (blue curves) or a control protein of similar size (red curves) after incubation of 1 μ M FITC labeled p53. A higher mean value in cellular fluorescence indicates binding of FITC labeled p53 to surface displayed Hsp90. (B) Flow cytometric analysis of the same cells after incubation of 1 μ M PF633 labeled ApoE serving as a specificity control. (C-E) Autodisplay dimerization assay with *E. coli* BL21 (DE3) cells treated like in (A) after incubation of 1 μ M FITC labeled p53 and additional 10 min preincubation of the cells with 100 μ M of the Hsp90 interface-derived peptides H1 (C), H2 (D), or H3 (E). The loss in cellular fluorescence (D and E) indicates a lower binding affinity of FITC labeled p53 to surface displayed Hsp90.

FIGURE 8. Dose dependent reduction of fluorescence by H3 and MST analysis of binding to the Hsp90 CTD. (A) Flow cytometric analysis of *E. coli* BL21 (DE3) cells displaying Hsp90 preincubated with different concentrations of the peptide H3 and then incubated with 1 μ M FITC labeled p53. The cellular fluorescence decreases in a dose dependent manner. *E. coli* BL21 (DE3) cells displaying SDH served as control. (B) Linear regression of the obtained cellular fluorescence mentioned above. The mean fluorescence of cells without addition of H3 was set to be 100 % binding. Binding [%] was plotted against the logarithm of the different H3 concentrations. (C) MST measurement of Hsp90 CTD dimer. Titration of unlabeled Hsp90 to a constant amount of NT-647 labeled Hsp90 CTD induces a change in thermophoresis. For each concentration, three independent measurements were performed and a K_{dim} value of 1.29 nM was determined using the K_D Fit formula from GraphPad Prism Software (GraphPad Prism Software, Inc. La Jolla, USA). (D) Specific binding of H3 to the CTD of Hsp90 revealed via MST analysis. Titration of the H3 peptide to a constant amount of NT-647 labeled CTD of Hsp90 induces a pronounced MST signal change. For each concentration, ten independent measurements were performed, and the mean value was determined. These values were used in the K_D Fit formula as described above and yielded an apparent K_D of 1.46 μ M.

Peptidic inhibitors of Hsp90 dimerization

TABLES

Table 1: Variants of peptides derived from the CTD of Hsp90 investigated in this study.

Variant	Peptide sequence	Helicity ^a	IC ₅₀ ^b	K _{lig} ^c	CD minima ^d
H1	PQTHANRIYRM IKLGL	7.0 ± 1.2 %	nd	nd	- ^e
H2	DKSVKDLVILLYET TAL LSSG	21.1 ± 5.6 %	nd	nd	208, 220
H3	DKSVKDLVILLYET TAL LSSGFSLEDPQTHANRIYRM IKLGLG	34.6 ± 6.0 %	8.96	3.35	208, 220
H3mut	DKSVKDLVILLYET TAL LSSGFSLEDPQTHANR AARMAKLGAG	nd	nd	nd	202

[a] Residue-wise α -helical content calculated as average from three independent MD simulations.

[b] IC₅₀ calculated with the Autodisplay competition assay; in μ M.

[c] K_{lig} calculated with the Autodisplay assay and MST measurement; in μ M.

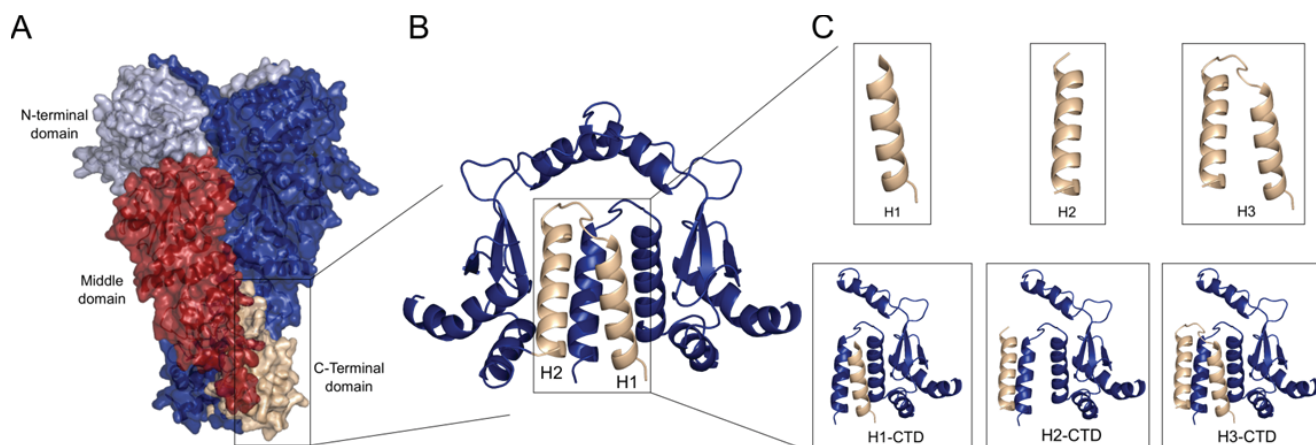
[d] Location of minima in the CD spectrum; in nm.

[e] None visible that is indicative of an α -helical structure.

nd: Not determined

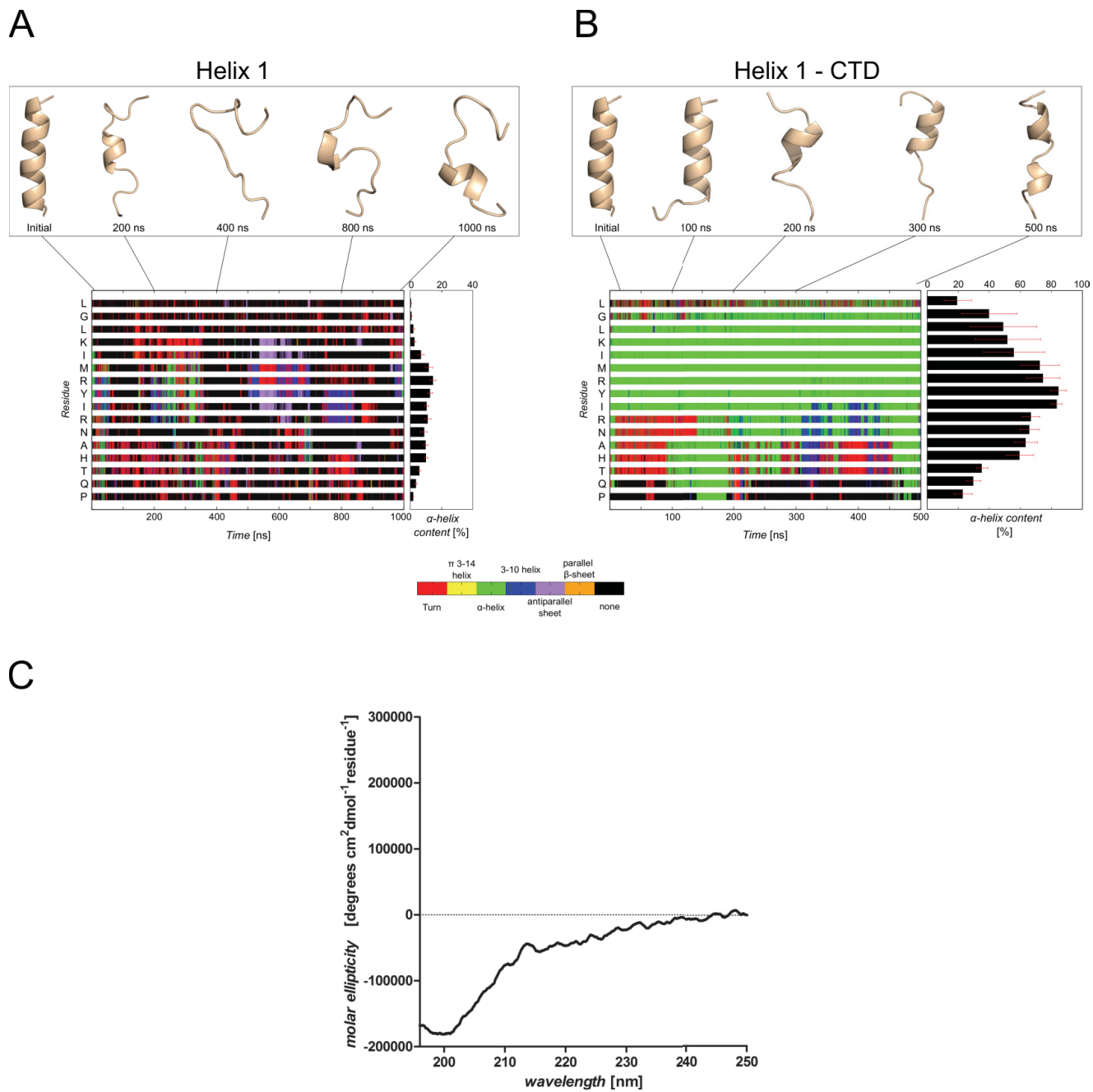
Peptidic inhibitors of Hsp90 dimerization

Figure 1



Peptidic inhibitors of Hsp90 dimerization

Figure 2



Peptidic inhibitors of Hsp90 dimerization

Figure 3

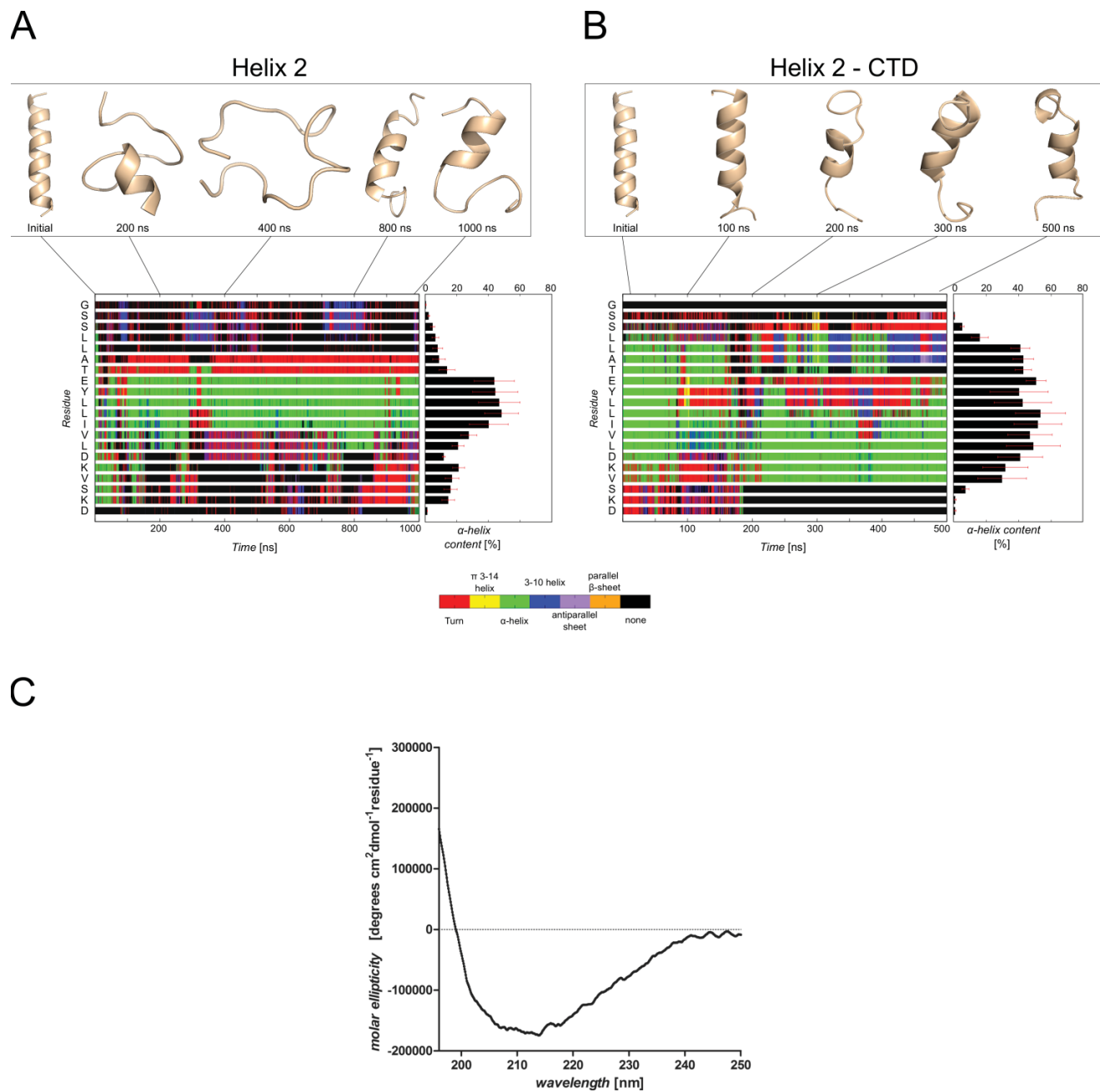
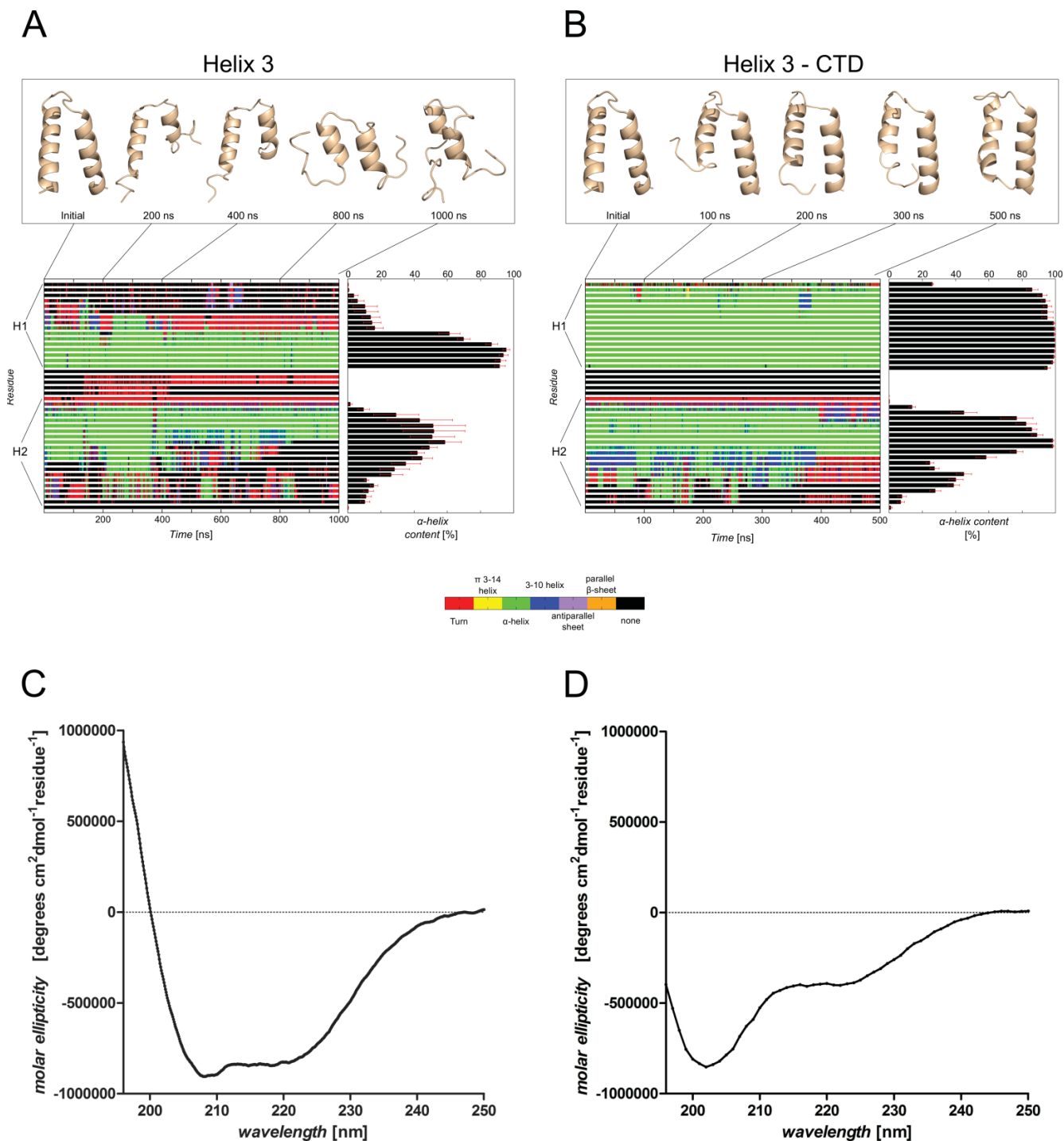
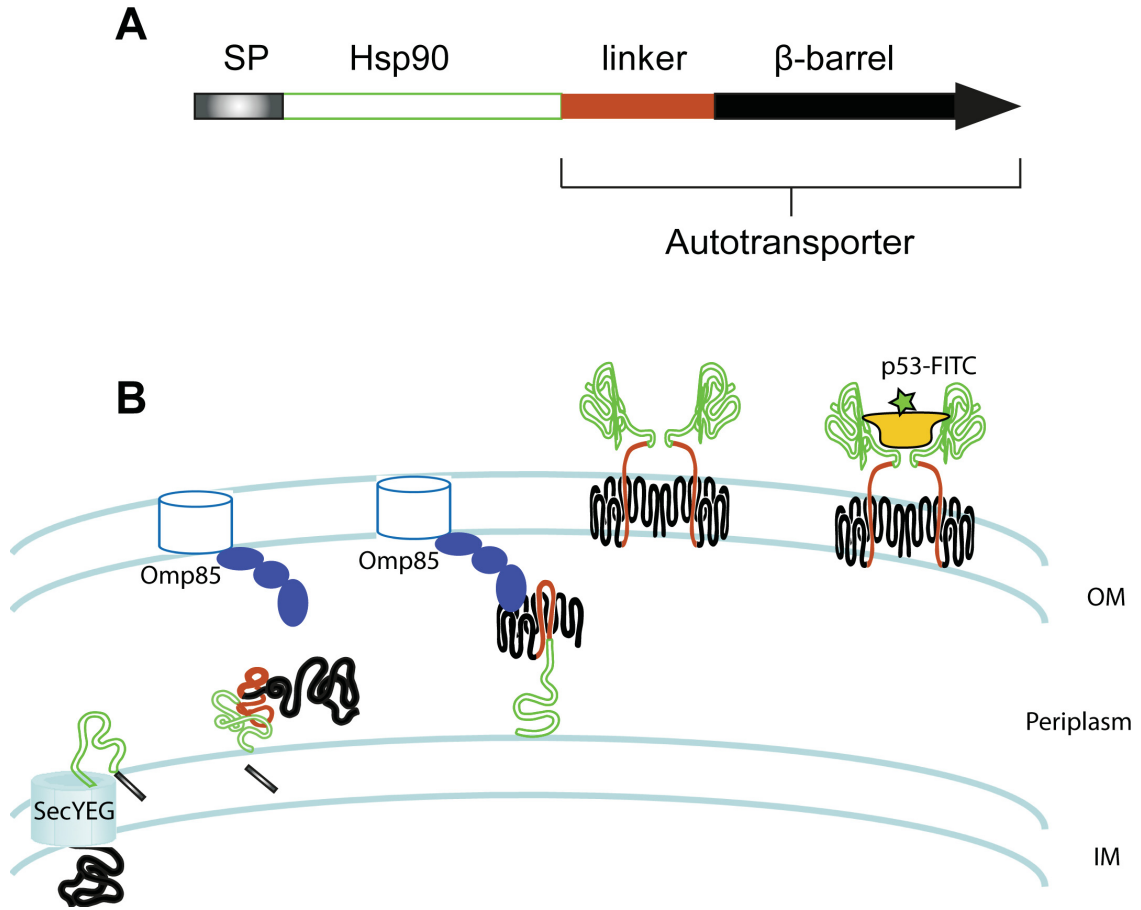


Figure 4



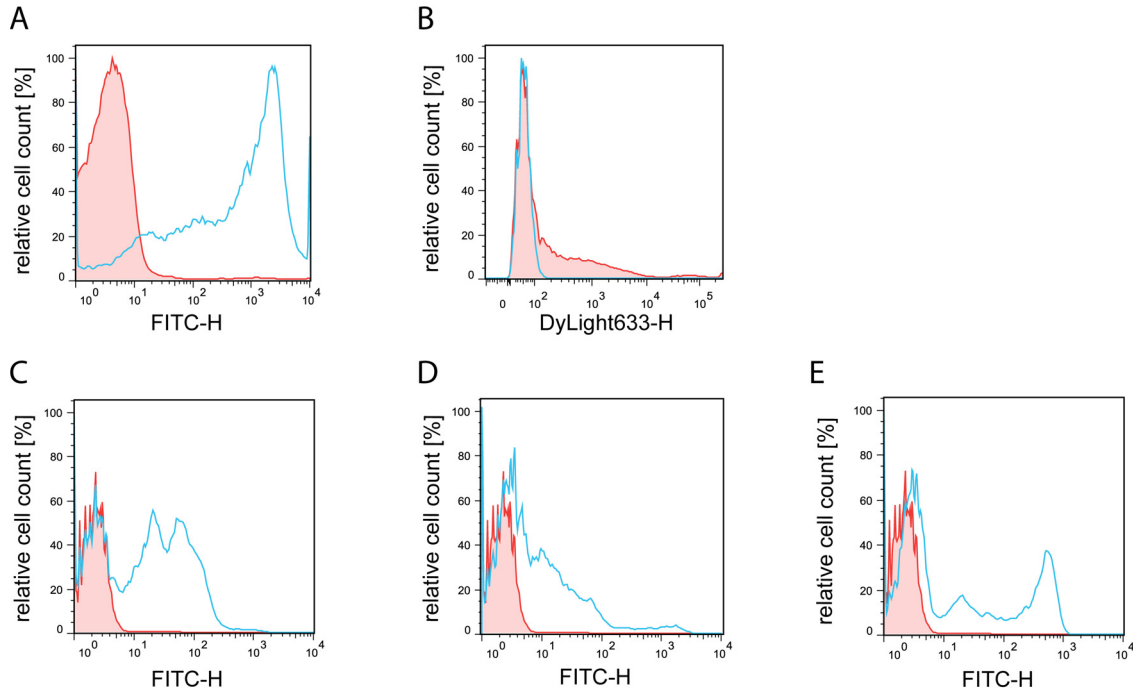
Peptidic inhibitors of Hsp90 dimerization

Figure 6



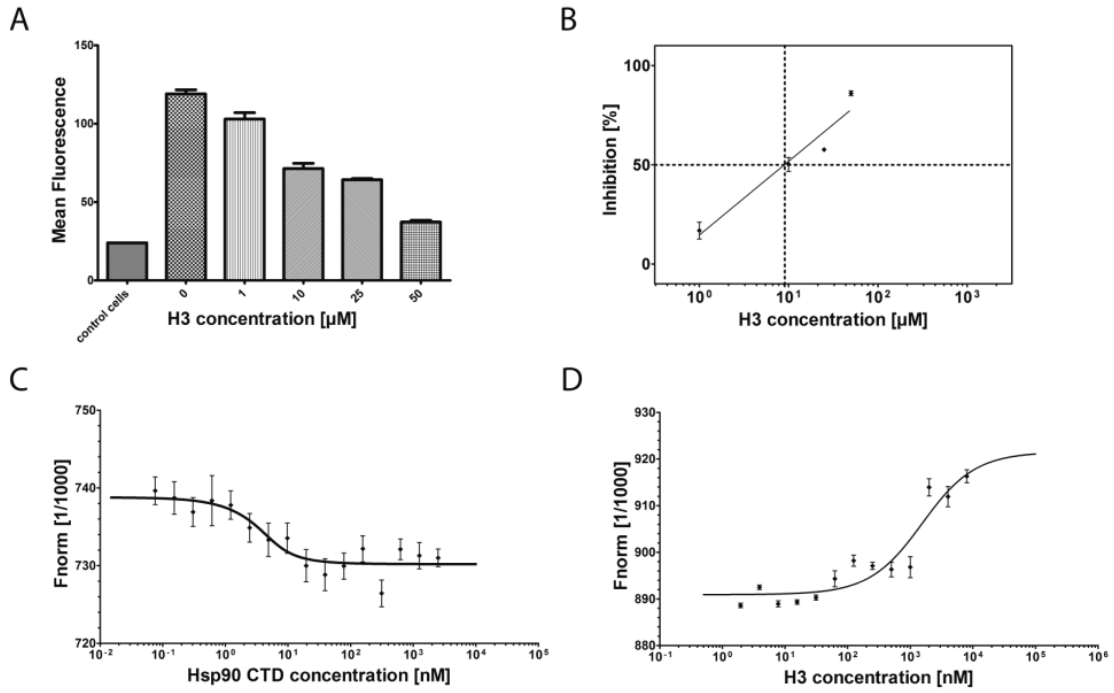
Peptidic inhibitors of Hsp90 dimerization

Figure 7



Peptidic inhibitors of Hsp90 dimerization

Figure 8



12 PUBLICATION IV

Design, Synthesis, and Conformational Analysis of Trispyrimidonamides as α -Helix Mimetics

Lukas Spanier [§], Emanuele Ciglia [§], Finn K. Hansen, Krystina Kuna, Walter Frank, Holger Gohlke, Thomas Kurz

Journal of Organic Chemistry, **2014**; 79, 1582-1593

[§] Both authors contributed equally to this work.

Design, Synthesis, and Conformational Analysis of Trispyrimidonamides as α -Helix Mimetics

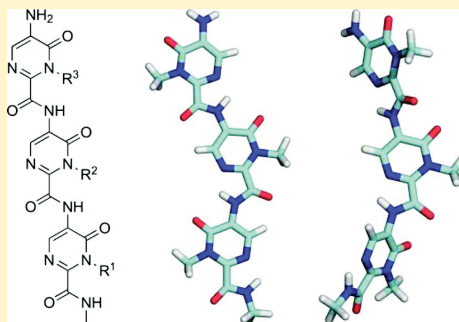
Lukas Spanier,^{†,§} Emanuele Ciglia,^{†,§} Finn K. Hansen,[†] Krystina Kuna,[†] Walter Frank,[‡] Holger Gohlke,[†] and Thomas Kurz^{*,†}

[†]Institut für Pharmazeutische und Medizinische Chemie, Heinrich-Heine-Universität Düsseldorf, Universitätsstr. 1, 40225 Düsseldorf, Germany

[‡]Institut für Anorganische Chemie und Strukturchemie, Heinrich-Heine-Universität Düsseldorf, Universitätsstr. 1, 40225 Düsseldorf, Germany

Supporting Information

ABSTRACT: The straightforward synthesis of trispyrimidonamides as a new class of α -helix mimetics is reported. Because of the versatility of our synthetic protocol, a variety of side chains including aliphatic, basic, aromatic, and heteroaromatic residues were included. A comprehensive conformational analysis revealed that in polar solvents a trimeric compound adopts conformations that can lead to $i, i + 4, i + 8$, or $i, i + 8$ patterns of side chain orientation. This suggests that trispyrimidonamides could be promising α -helix mimetics to target hot spots that are distributed over a wider angular range of an α -helix interface than in the classical $i, i + 4, i + 7$ case.

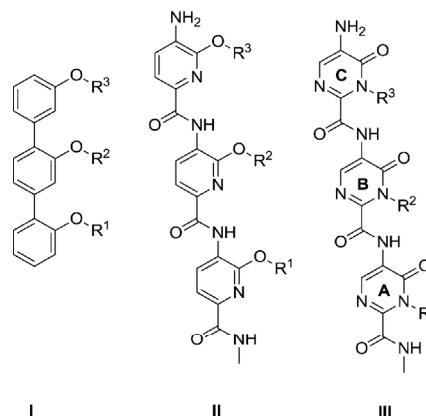


INTRODUCTION

Protein–protein interactions (PPIs) are involved in the regulation of numerous essential cellular processes^{1–7} and play a central role in disease development.^{8–10} Consequently, modulating PPIs is a promising concept to interfere with physiological and pathophysiological processes.^{1,7,11–13} Small molecule protein–protein interaction modulators (PPIMs) that efficiently and selectively affect protein–protein binding are one way of interference.^{14–18} The most frequently occurring recognition motifs in PPIs are α -helices.^{19,20} This and the fact that usually only a few key residues (so-called “hot spots”) in a protein–protein interface account for the majority of the binding affinity^{21–23} have fueled the development of small molecules mimicking α -helices (Scheme 1).^{24–32}

Such small-molecule α -helix mimetics have proven valuable as biophysical probes or modulators of protein–protein interactions.^{10,27,33} Compared to other α -helix mimetics, e.g., β -peptides, aza- and aminopeptides, γ -peptides, and peptoids, small-molecule α -helix mimetics promise to have more favorable pharmacokinetic properties.³⁴ The development of small-molecule α -helix mimetics started almost 30 years ago with the synthesis of 1,6-disubstituted indanes where the substituents mimic the i and $i + 1$ residues of an α -helix.^{35,36} A pioneering advancement was the synthesis of tris-ortho-substituted terphenyl derivatives by Hamilton and co-workers;³⁷ the substituents of this extended scaffold mimic the $i, i + 4$, and $i + 7$ residues of an α -helix. In search for small-molecule α -helix mimetics that have more hydrophilic and/or

Scheme 1. (I) Terphenyl, (II) Trispyridylamide, and (III) Trispyrimidonamide^a



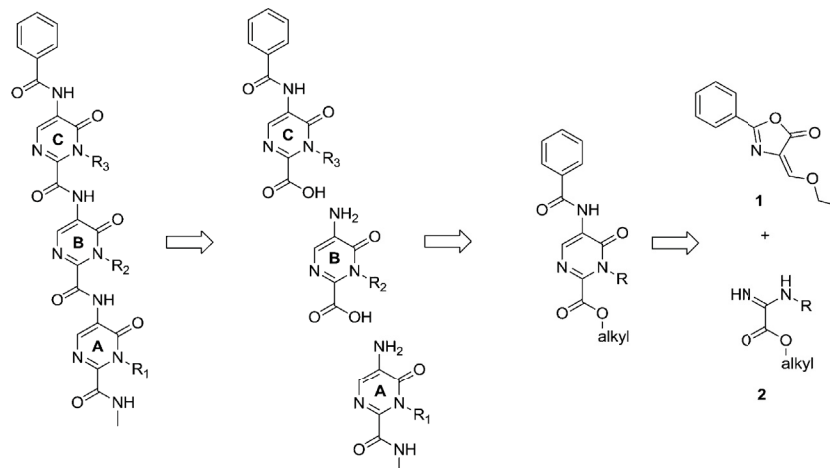
^aScaffold rings of III are labeled A, B, C.

amphiphilic scaffolds than the terphenyls, terpyridines, trisbenzamidates, terephthalamides, trispyridylamides, phenylen-aminones, pyridazine, 1,4-benzodiazine-2,5-diones, trisubstituted imidazoles, benzylidenechalcones, and trans-fused poly-

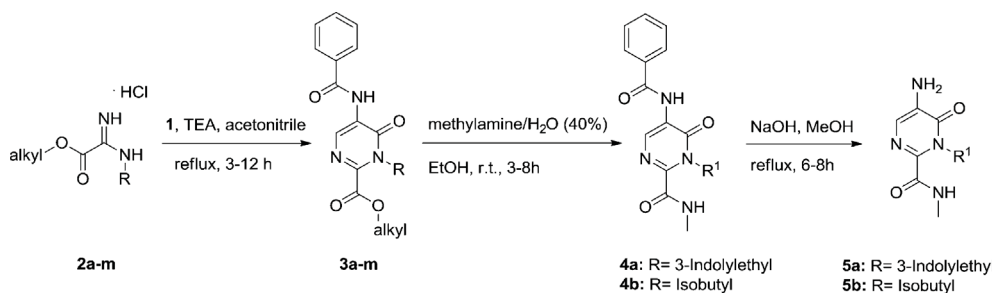
Received: October 22, 2013

Published: January 22, 2014

Scheme 2. Retrosynthesis of the Trispyrimidonamide Scaffold



Scheme 3. Synthesis of Monomers 3 and 5-Aminopyrimidones 5a,b



cyclic ethers were synthesized.^{38–49} For several of these scaffolds, only *n*-alkyl, *i*-alkyl, or arylalkyl substituents have been reported^{43,48–50} likely because of synthetic difficulties when introducing polar and/or charged substituents. As a consequence, only hydrophobic or aromatic side chains of hot spots can be mimicked. This may lead to a restricted applicability if the frequently occurring hot spots Trp, Tyr, and Arg are to be addressed.^{51,52}

This provided the incentive for us to design and synthesize previously unreported trispyrimidonamides as a new class of α -helix mimetics and investigate by 2D NMR, X-ray crystallography, and molecular modeling their conformational properties. Regarding the synthesis, our approach provides a general toolbox that allows generating trispyrimidonamides with hydrophobic and differently functionalized (aliphatic, aromatic, heteroaromatic, polar, and basic) side chains. That way, a variety of potential hot spots can be mimicked by the R-groups of our trispyrimidonamide scaffold. The 2D NMR experiments together with modeling studies suggest that trispyrimidonamide derivatives adopt conformations in polar solvents that can orient R groups in such a way that they mimic amino acid side chains at positions *i*, *i* + 4, *i* + 8 or *i*, *i* + 8 of an α -helix. The *i*, *i* + 4, *i* + 8 pattern is currently targeted by just one class of mimetics.⁵³

RESULTS AND DISCUSSION

Chemistry. We decided to pursue a monomer approach in order to develop a synthetic protocol that allows a high

structural diversity for our desired trimeric α -helix mimetics. The synthesis of polysubstituted pyrimidines is usually accomplished by (i) cyclization, (ii) ring transformation, (iii) aromatization as well as (iv) substituent modification, and various efficient preparations have been published.⁵⁴ We aimed at the synthesis of N^3 -substituted pyrimidin-4(3*H*)-ones with a protected amino group in 5-position as well as a carboxylic acid ester in 2-position as suitable monomers. Our retrosynthetic analysis (Scheme 2) led to 4-(ethoxymethylidene)-2-phenyl-1,3-oxazol-5(4*H*)-one **1**⁵⁵ and *N*-substituted amidines⁵⁶ of type **2** as starting materials.

Azlactone **1** deserves particular interest as a building block in heterocyclic chemistry because of its ambivalent behavior toward nucleophiles and has been utilized in various ring transformation reactions for the preparation of 5-benzoylamino-pyrimidin-4(3*H*)-ones.^{55,57–60} The desired 5-benzoylamino-pyrimidin-4(3*H*)-ones **3a–m** were obtained from readily available amidine hydrochloride derivatives **2a–m** and azlactone **1** by treatment with triethylamine in acetonitrile under reflux conditions (22–81% yield, Scheme 3, Table 1).

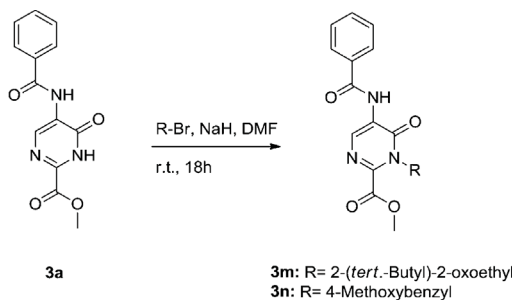
As a complementary route for the preparation of N^3 -substituted monomers of type **3**, the pyrimidone **3a** (R = H) was treated with sodium hydride and alkylating agents to provide the N^3 -substituted derivatives **3m,n** (32% and 64% yield, Scheme 4, Table 1). In all cases, the N^3 -alkylated products were obtained as the major regioisomers. An authentic sample of **3m** obtained by azlactone rearrangement was used for structural assignment. Utilizing these protocols allows the

Table 1. Monomers Synthesized

entry	alkyl	R	yield [%]
3a	Me	H	50
3b	Me	3-indolyethyl	65
3c	Et	isobutyl	31
3d	Et	sec-butyl	22
3e	Et	N-Boc-4-aminobutyl	33
3f	Et	2-propyl	30
3g	Et	4-hydroxyphenylethyl	55
3h	Et	4-methoxyphenylethyl	41
3i	Et	4-hydroxybenzyl	52
3j	Et	4-methoxybenzyl	81
3k	Et	3-(benzyloxy)-3-oxopropyl	22
3l	Me	phenylethyl	35
3m	Me	2-(<i>tert</i> -butyl)-2-oxoethyl	49, (32) ^a
3n	Me	4-methoxybenzyl	(64) ^a

^aYield from *N*-alkylation.

Scheme 4. Synthesis of Monomers 3m,n by Alkylation



preparation of a variety of monomers with a high structural diversity with regard to the nature of the *N*³-substitution. Notably, the monomers obtained are capable of mimicking aliphatic, aromatic, heteroaromatic, acidic, and basic side chains of amino acids.

After the establishment of efficient methods for preparation of the desired protected monomers 3 we studied the deprotection of both protecting groups. All attempts to deprotect the benzoyl protecting group led to the corresponding decarboxylated product. Consequently, we transformed 3b,c into the *N*-methyl carboxamide derivatives 4a,b utilizing

an excess of methylamine as nucleophile to furnish a stable C-terminus (Scheme 3). The preparation of the unprotected 5-aminopyrimidones 5a,b was achieved by saponification of the benzamide group of 4a,b through treatment with sodium hydroxide (3 equiv) in methanol under reflux conditions. The attempted conversion of the alkyl ester moiety of 3 into the free carboxylic acid resulted again in isolation of the corresponding decarboxylated product. A literature survey revealed that only few pyrimidone derivatives are known with a carboxamide moiety in 2-position. These compounds were either obtained by direct treatment of an ester with a strong nucleophile or under trimethylaluminum-mediated coupling conditions. Our efforts to obtain a dimeric compound by Me₃Al-mediated coupling of the ester 3d with the free amine 5b failed.

As a consequence, we developed a straightforward protocol for preparation of oligomeric pyrimidone compounds. The hydrolysis of 3c–f provided the corresponding lithium salts. Next, we investigated the formation of an amide bond in order to obtain dimeric pyrimidone derivatives. Several well-established coupling agents were screened using 5-aminopyrimidone 5b and the corresponding lithium salt of 3d as a model system. In all cases the progress of the reaction was monitored by HPLC (see Supporting Information for details). The results gathered from this screening were particularly interesting. The reaction was slow and we were unable to obtain a conversion of more than 50% after 24 h utilizing PyBop, HBTU, and DIC/Oxyma as coupling agents. The HATU-mediated amide coupling accomplished a conversion of 78% after 24 h, and the model dimer 6a was obtained in 55% yield after purification by flash column chromatography. Best results were achieved using COMU as a coupling agent. In this case, the reaction was essentially completed after 3 h, and we were able to isolate the desired dimeric compound 6a in 85% yield (see Supporting Information).

Having an efficient monomer synthesis and an optimized coupling reaction in hand, we turned our attention toward the preparation of dimeric and trimeric *N*³-substituted pyrimidone derivatives as α -helix mimetics. The COMU-mediated coupling reactions of 5-aminopyrimidones 5a and 5b with the corresponding lithium salts of 3c and 3d provided smoothly the benzoyl-protected dimers 6a and 6b in a batch scale (75 and 76% yield, Scheme 5, Table 2). The benzoyl-protecting groups were then cleaved by treatment of 6a and 6b with sodium hydroxide to afford the deprotected dimers 7a and 7b

Scheme 5. Synthesis of Dimers 6a,b

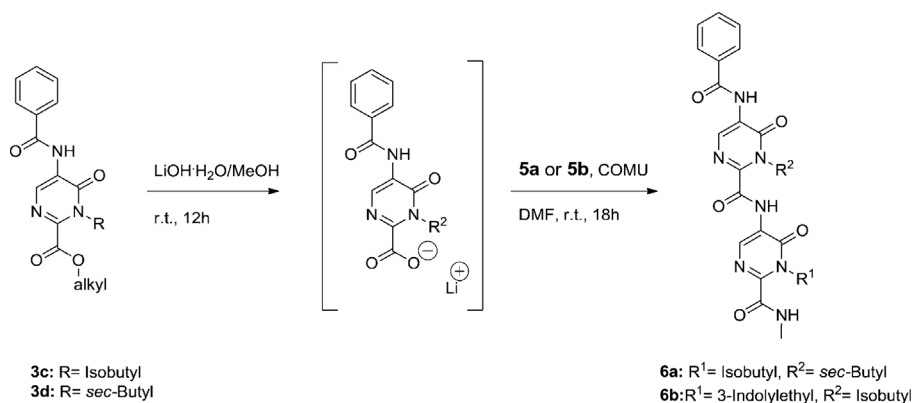
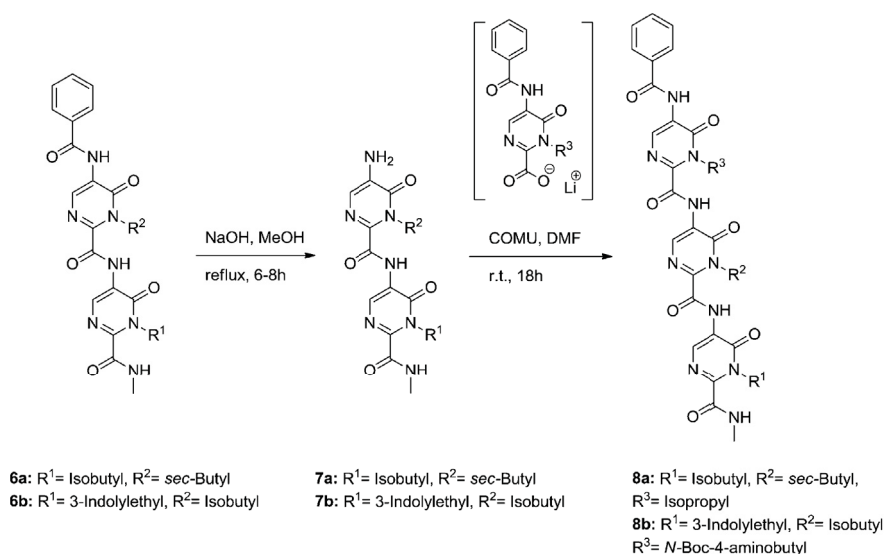


Table 2. Synthesized Di- and Trimeric Pyrimidones

entry	R ^{1a}	R ^{2a}	R ^{3a}	yield [%]
7a	Isobutyl "Leu"	sec-Butyl "Ile"	–	77
7b	3-Indolyethyl "Trp"	Isobutyl "Leu"	–	74
8a	Isobutyl "Leu"	sec-Butyl "Ile"	2-Propyl "Val"	55
8b	3-Indolyethyl "Trp"	Isobutyl "Leu"	N-Boc-4-aminobutyl "BOC-Lys"	41
8c	3-Indolyethyl "Trp"	Isobutyl "Leu"	4-Aminobutyl "Lys"	90 ^b

^aResidues corresponding to mimicked amino acids. ^bFrom 8b by TFA mediated cleavage of BOC protecting group.

Scheme 6. Synthesis of Trispyrimidonamides 8a,b



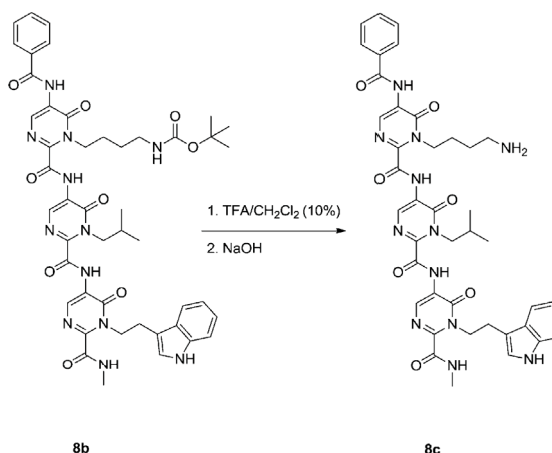
in 77 and 74% yield, respectively (Scheme 6, Table 2). Subsequently, the reaction of 7a and 7b with corresponding lithium salts of 3f and 3e in the presence of COMU led to the corresponding trispyrimidonamides 8a and 8b (55% and 41% yield, Scheme 6, Table 2).

Finally, the Boc-protecting group in 8b was removed by acidolysis to furnish trimer 8c (Scheme 7, 90% yield) with unprotected 4-aminobutyl and 3-indolyethyl side chains, thus highlighting the versatility of our synthetic protocol in regard to side chain tolerance.

The conformational properties of our synthesized trispyrimidonamides were studied by X-ray analysis of trimer 8a and 2D NMR spectroscopy (Figure 1). Diffraction quality crystals were obtained by vapor diffusion (see Supporting Information). The X-ray structure of 8a (Figure 1A) shows the trimer adopting a conformation C₁ in which only R¹ and R³ are oriented on the same side, whereas R² points in the opposite direction. In order to study the properties of 8a in solution, a ROESY experiment was performed in CDCl₃ (see Figure 1B and Figure S1, Supporting Information). All relevant signals were assigned by HSQC and HMBC spectra. Key ROE correlations are shown as arrows in Figure 1B. We observed ROE cross peaks between the pyrimidone proton of ring B with the methine and methyl protons of the isopropyl side chain. We reasoned that these ROE correlations would only be observable for a conformation C₁ (Figure 1B), which is in a good agreement with the X-ray structure of 8a (Figure 1A).

Unfortunately, 8a–c were not sufficiently soluble to perform a 2D NMR study in D₂O. However, we were able to study the

Scheme 7. Deprotection of 8b to the Corresponding Amine



conformational properties of the TFA salt of 8c in methanol-*d*₄. We observed ROE cross signals between the isobutyl side chain and the pyrimidone protons of the two terminal rings (rings A and C), which indicates the presence of a conformation C₁, analogous to the conformation observed in CDCl₃ (Figure 2 and Figures S2 and S3, Supporting Information). Interestingly, our ROESY analysis revealed an additional ROE cross peak between the methyl protons of the isobutyl side chain and the

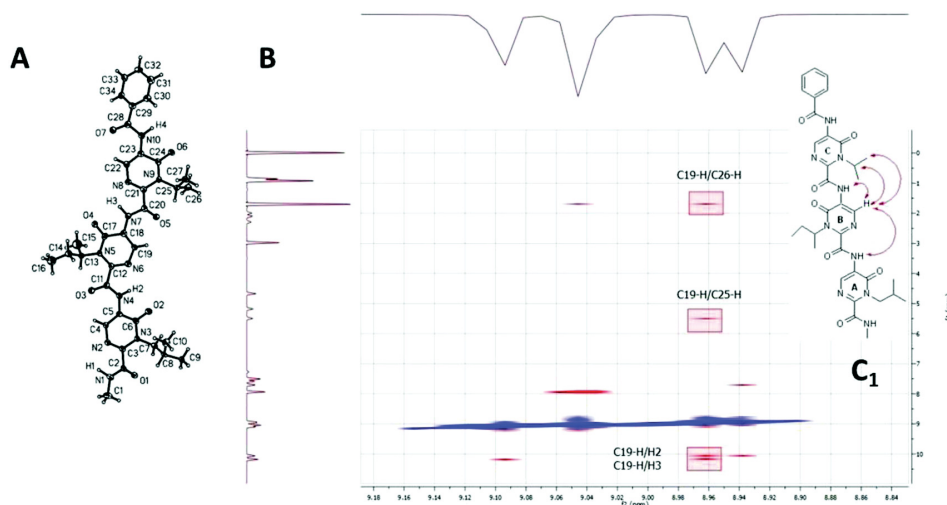


Figure 1. Structural and conformational study of compound **8a**. (A) Solid state structure. (B) ^1H - ^1H -ROESY spectra (region between 9.18 and 8.84 Hz, 600 MHz, CDCl_3) and suggested conformational structure; key ROEs are marked in red.

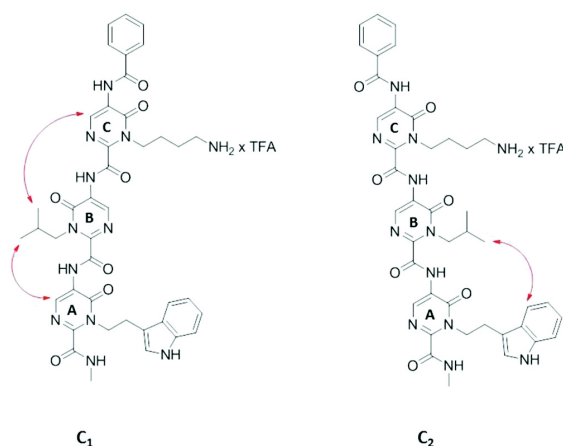


Figure 2. Conformations of **8c** (TFA salt) in $\text{MeOH-}d_4$. Key ROEs are marked in red.

aromatic C4-proton of the indolyethyl side chain. This ROE correlation can only be explained by a conformation C_2 presenting all three side chains on one side (Figure 2 and Figure S3, Supporting Information). These results suggest that in methanol- d_4 trispyrimidonamides can adopt two conformations, one in which only R^1 and R^3 are oriented on the same side and one in which all three substituents are oriented on the same side.

Modeling Studies. In order to further resolve the conformational preferences of trispyrimidonamides, we performed molecular dynamics (MD) simulations of a trimethyl-substituted trispyrimidonamide (**IV**; Figure 3A) in explicit chloroform and methanol of 1.5 μs length, respectively. Prior to this, the torsion angles ϕ and ψ (Figure S4A, Supporting Information) expected to be critical for the inter-ring orientation had been parametrized based on ab initio calculations (see Experimental Section and Figure S5, Supporting Information). The energy minima of these potentials show good agreement with ϕ and ψ values found

in the crystal structure of **8a** (Figure S4B, Supporting Information).

During the MD simulations, frequent rotations around the ϕ and ψ torsion angles are observed (data not shown), demonstrating that the sampled conformations are in equilibrium. This is also confirmed by the symmetry of the maps of the relative free energy of **IV** as a function of the orientation of the methyl substituents of rings A and B (torsion angle Ω_1 ; Figure 3A), and B and C (torsion angle Ω_2 ; Figure 3B) (Figure 3B). The relative free energy map for the simulation of **IV** in chloroform reveals a preferred conformation C_1 ($\Omega_1 \approx \pm 165^\circ$; $\Omega_2 \approx \pm 155^\circ$; Figure 3B,C). The alternative conformation C_2 ($\Omega_1 \approx \pm 55^\circ$; $\Omega_2 \approx \pm 55^\circ$) is energetically disfavored by $\Delta G \approx 2.5 \text{ kcal mol}^{-1}$ in chloroform. This relates to a ratio of 98.5/1.5 for the populations of C_1 versus C_2 in the conformational ensemble at 300 K. In contrast, the simulation of **IV** in methanol reveals C_2 as the preferred conformation (Figure 3B,D) whereas C_1 is now disfavored by $\Delta G \approx 1.0 \text{ kcal mol}^{-1}$. This relates to a ratio of 19/81 for the populations of C_1 versus C_2 in the conformational ensemble at 300 K. These results are in excellent agreement with those from the 2D-NMR studies, which identified only C_1 as the preferred conformation of **8a** in chloroform but suggested that **8c** can adopt both conformations C_1 and C_2 in methanol. In addition, the MD simulations confirm for C_1 an almost coplanar orientation of the pyrimidone rings, as found in the crystal structure of **8a**, but suggest for C_2 that neighboring rings are rotated by 55° with respect to each other. In all, these results validate our setup of the MD simulations and the quality of the force-field parameters used for the solute and solvent.

As no experimental information is available for the conformational preference of trispyrimidonamides in water, we investigated by MD simulations in explicit water the conformational preference of **IV** using the same setup as above. The MD simulations suggest that C_2 becomes even more preferred over C_1 than in methanol (Figure 3B,D), with C_1 being disfavored by $\Delta G \approx 3.0 \text{ kcal mol}^{-1}$ equivalent to a ratio of <1/99 for the populations of C_1 versus C_2 in the conformational ensemble at 300 K. This shift in the

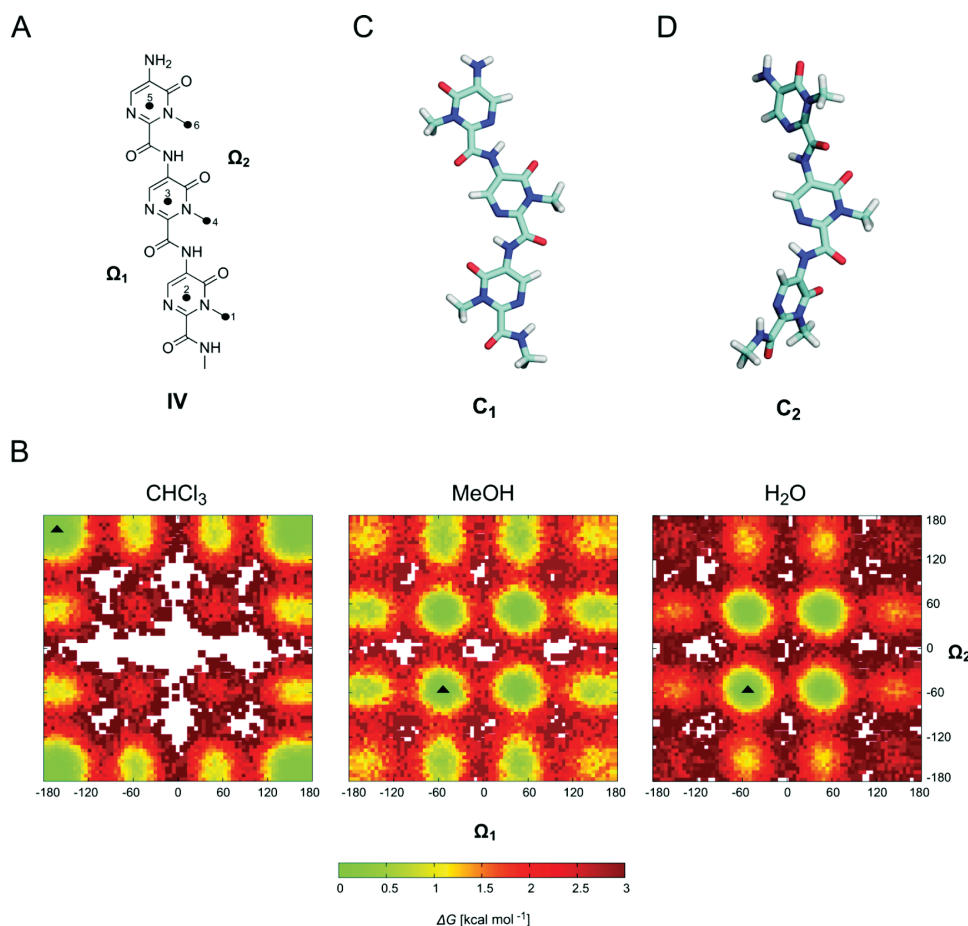


Figure 3. Relative free energy of the trimethylsubstituted trispyrimidonamide IV as a function of the orientation of the methyl substituents of rings A and B, or B and C, with respect to each other (Ω_1 and Ω_2 torsion angles as defined by the point quadruples (1, 2, 3, 4) and (4, 3, 5, 6) in the structure shown in panel A). The relative free energy of each conformation is calculated from the frequency of the conformation's occurrence during a MD simulation of 1.5 μ s length in explicit chloroform, explicit methanol, and explicit water (see respective plots in panel B) via $\Delta G = -RT \ln P_x/P_{ref}$ (where R is the gas constant, $T = 300$ K, P_x is the frequency of occurrence of conformation x , and P_{ref} is the frequency of occurrence of the most frequently represented conformation). The white spots indicate Ω_1 and Ω_2 angle combinations not found in the MD simulations. Energetically favorable conformations of IV in the different solvents are shown in panel C (chloroform; C_1) and D (methanol and water; C_2); their locations on the relative free energy maps are marked by triangles.

conformational equilibrium agrees with the solvent influence on the conformations of trispyrimidonamides observed by our 2D NMR studies in chloroform and methanol in that more polar solvents favor C_2 .

Overlaying the methyl groups of IV in the conformation C_2 favored in polar solvents with the C_β atoms of a canonical α -helix shows that the trispyrimidonamide scaffold can closely mimic the spatial arrangement of peptide side chains at positions $i, i + 4, i + 8$. When ring C is oriented toward the helix C-terminus, the root mean-square deviation (RMSD) of the coordinates of the respective atom pairs is 0.69 Å, and the average angle deviation between the respective bond vectors is $\sim 20^\circ$ (Figure 4A). These values deteriorate to 0.73 Å and $\sim 30^\circ$ if ring C is oriented toward the N-terminus (Figure 4B). To the best of our knowledge, there is only one other scaffold of α -helix mimetics that allows addressing the side chain pattern $i, i + 4, i + 8$;⁵³ this pattern becomes particularly interesting if the side chains to be mimicked lie on one side of an α -helix but are

distributed over a wider angular range than in the case of $i, i + 4, i + 7$.⁶¹ Alternatively, two of the methyl groups of conformation C_1 can overlay with C_β atoms of a canonical α -helix at positions i and $i + 8$ (when ring C is oriented toward the C(N)-terminus the RMSD = 0.2 Å (0.55 Å), and the average angle deviation between bond vectors is $\sim 10^\circ$ ($\sim 38^\circ$)) (Figure 4C,D). The $i, i + 8$ pattern would be of interest when two side chains further apart but still on the same side of an α -helix need to be mimicked. Targeting a $i, i + 4, i + 7$ side chain pattern with our trispyrimidonamides is expected to be less favorable but not excluded, as demonstrated by the increased RMSD and average angle deviations between bond vectors when overlaying the methyl groups of C_1 or C_2 with the C_β atoms of a canonical α -helix at these positions (see Supporting Information, Figure S6).

In summary, the conformational analyses by 2D NMR studies and MD simulations reveal that trispyrimidonamides adopt conformations in polar solvents that can lead to $i, i + 4,$

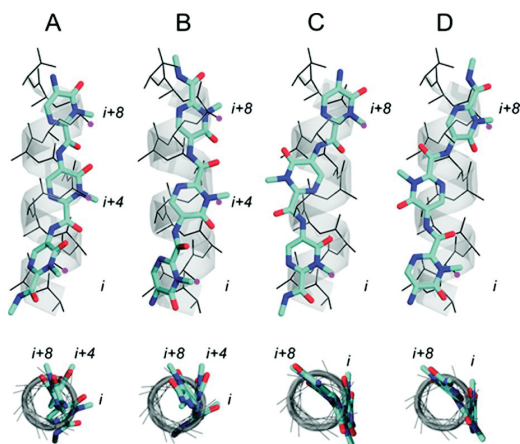


Figure 4. Overlay of C_{β} atoms of a canonical α -helix onto corresponding methyl groups of IV in conformation C_2 (A), resulting in an $i, i + 4, i + 8$ pattern, and C_1 (C), resulting in an $i, i + 8$ pattern. Ring C is oriented toward the C-terminus of the helix. (B,D) Equivalent superimpositions when IV is reversed with respect to the helix axis. The magenta dots highlight the C_{β} atoms addressed by the trispyrimidonamide's R groups. In the lower panel the overlays are rotated by 90° , with the peptide C-terminus oriented in the direction of the viewer.

$i + 8$ or $i, i + 8$ patterns of R-group orientation with respect to an α -helix.

CONCLUSIONS

In summary, we have established a straightforward preparation of 5-benzoylamino-pyrimidin-4(3H)-one monomers capable of mimicking aliphatic, aromatic, heteroaromatic, and basic side chains of amino acids. A COMU-mediated coupling procedure allowed the synthesis of trispyrimidonamide α -helix mimetics including an example with side chains that are difficult to access, such as 4-aminobutyl and 3-indolyethyl moieties. A comprehensive conformational study by X-ray, 2D NMR analysis, and MD simulations revealed a solvent dependence of the preferred conformations of the trispyrimidonamide scaffold. In polar solvents, the trispyrimidonamide scaffold adopts conformations that can lead to $i, i + 4, i + 8$ or $i, i + 8$ patterns of side chain orientation. This suggests trispyrimidonamides as promising α -helix mimetics to target hot spots that lie on one side of an α -helix but are distributed over a wider angular range than in the classical $i, i + 4, i + 7$ case.

EXPERIMENTAL SECTION

Chemistry. All solvents and chemicals were used as purchased without further purification. The progress of all reactions was monitored on silica gel plates (with fluorescence indicator UV254) using the solvent system stated. Flash column chromatography was carried out using prepacked silica cartridge. Melting points (mp) were taken in open capillaries and are uncorrected. ^1H and ^{13}C spectra were recorded at 500 (500.13 MHz for ^1H ; 125.76 MHz for ^{13}C) and 600 (600.22 MHz for ^1H ; 150.92 MHz for ^{13}C) MHz spectrometers, respectively, using $\text{DMSO-}d_6$ or CDCl_3 as solvents. Chemical shifts are given in parts million (ppm), (δ relative to residual solvent peak for ^1H and ^{13}C or to external standard tetramethylsilane). High resolution mass spectra (HRMS) were obtained on a UHR-TOF mass analyzer by electrospray ionization (ESI). Azlactone **1** was prepared as reported.⁵⁵ Amidine hydrochlorides **2a–m** are prepared following a

literature procedure⁵⁶ with the minor modification using 0.6 equiv of the corresponding amine hydrochloride.

General Procedure for the Synthesis of Alkyl 5-benzamido-6-oxo-1,6-dihydropyrimidine-2-carboxylates **3a–m.** A mixture of 4-ethoxymethylene-2-phenyl-2-oxazolin-5-one **1** (0.217 g, 1 mmol), the corresponding amidine hydrochloride **2a–m** (1 mmol) and triethylamine (0.101 g, 1 mmol) in dry acetonitrile (5 mL) was heated under a nitrogen atmosphere for 3 h (**3a,c,d,f**) or 6 h. The solvent was removed under reduced pressure, and aqueous citric acid (10 wt %, 3 mL) was added. The mixture was extracted with ethyl acetate (3×30 mL). The combined organic layers were dried over anhydrous sodium sulfate, filtered and concentrated in a vacuum. The crude products were purified by flash column chromatography (gradient: 10:90 \rightarrow 30:70 ethyl acetate:*n*-hexane) to yield the desired products **3a–m**.

Methyl 5-benzamido-6-oxo-1,6-dihydropyrimidine-2-carboxylate (3a**).** Yield 50%, 137 mg, pale white solid; $R_f = 0.42$ (ethyl acetate); mp 209°C (from ethyl acetate/methanol); ^1H NMR (500 MHz, $\text{DMSO-}d_6$) δ 13.51 (s, 1H), 9.47 (s, 1H), 8.86 (s, 1H), 7.95 (d, $J = 7.2$ Hz, 2H), 7.64 (t, $J = 7.4$ Hz, 1H), 7.56 (t, $J = 7.6$ Hz, 2H), 3.90 (s, 3H); ^{13}C NMR (126 MHz, $\text{DMSO-}d_6$) δ 165.3, 159.9, 133.1, 132.3, 128.7, 127.5, 53.2, 40.0. Anal. Calcd. for $\text{C}_{13}\text{H}_{11}\text{N}_3\text{O}_4$: C, 57.14; H, 4.06; N, 15.38. Found: C, 56.91; H, 4.02; N 15.24.

Methyl 1-(2-(1H-indol-3-yl)ethyl)-5-benzamido-6-oxo-1,6-dihydropyrimidine-2-carboxylate (3b**).** Yield 65%, 270 mg, pale yellow solid; $R_f = 0.56$ (*n*-hexane/ethyl acetate 1:1); mp 222°C (from ethyl acetate); ^1H NMR (500 MHz, $\text{DMSO-}d_6$) δ 10.92 (s, 1H), 9.62 (s, 1H), 8.79 (s, 1H), 8.00 (d, $J = 7.4$ Hz, 2H), 7.69–7.51 (m, 4H), 7.37 (d, $J = 8.1$ Hz, 1H), 7.06 (ddd, $J = 7.3, 14.8, 22.2$ Hz, 3H), 4.42 (t, $J = 7.1$ Hz, 2H), 3.46 (s, 3H), 3.12 (t, $J = 7.0$ Hz, 2H); ^{13}C NMR (126 MHz, $\text{DMSO-}d_6$) δ 165.4, 160.4, 156.7, 144.0, 136.4, 136.3, 133.1, 132.3, 128.7, 127.6, 127.5, 126.8, 123.7, 121.1, 118.4, 118.0, 111.4, 109.3, 53.0, 46.2, 23.8. Anal. Calcd. for $\text{C}_{23}\text{H}_{20}\text{N}_4\text{O}_4$: C, 66.34; H, 4.84; N, 13.45. Found: C, 66.13; H, 4.92; N 13.54.

Ethyl 5-benzamido-1-isobutyl-6-oxo-1,6-dihydropyrimidine-2-carboxylate (3c**).** Yellow solid, yield 31%, 106 mg; $R_f = 0.89$ (*n*-hexane/ethyl acetate 1:1); mp 59°C (from diethyl ether); ^1H NMR (500 MHz, CDCl_3) δ 9.18 (s, 1H), 8.96 (s, 1H), 7.93 (d, $J = 8.1$ Hz, 2H), 7.59 (t, $J = 7.8$ Hz, 1H), 7.51 (t, $J = 7.7$ Hz, 2H), 4.48 (q, $J = 7.1$ Hz, 2H), 4.25 (d, $J = 7.5$ Hz, 2H), 2.08–2.02 (m, 1H), 1.45 (t, $J = 7.2$ Hz, 3H), 0.94 (s, 3H), 0.93 (s, 3H); ^{13}C NMR (126 MHz, CDCl_3) δ 165.6, 160.9, 157.6, 143.3, 134.6, 133.4, 132.6, 128.9, 127.9, 127.3, 63.4, 51.7, 28.6, 19.9, 14.0. Anal. Calcd. for $\text{C}_{18}\text{H}_{21}\text{N}_3\text{O}_4$: C, 62.96; H, 6.16; N, 12.24. Found: C, 62.91; H, 6.30; N 12.22.

Ethyl 5-benzamido-1-(sec-butyl)-6-oxo-1,6-dihydropyrimidine-2-carboxylate (3d**).** Yield 22%, 75 mg, yellow oil; $R_f = 0.90$ (*n*-hexane/ethyl acetate 1:1); ^1H NMR (500 MHz, CDCl_3) δ 9.12 (s, 1H), 8.95 (s, 1H), 7.93 (d, $J = 7.2$ Hz, 2H), 7.58 (t, $J = 7.4$ Hz, 1H), 7.50 (t, $J = 7.6$ Hz, 2H), 4.48 (m, 2H), 4.16 (s, 1H), 2.30 (dt, $J = 7.7, 15.1$ Hz, 1H), 1.94–1.89 (m, 1H), 1.66 (d, $J = 6.8$ Hz, 3H), 1.45 (t, $J = 7.2$ Hz, 3H), 0.87 (t, $J = 7.5$ Hz, 3H); ^{13}C NMR (126 MHz, CDCl_3) δ 165.5, 161.3, 157.4, 144.9, 134.5, 133.4, 132.5, 128.9, 128.0, 127.3, 63.3, 61.4, 26.0, 17.8, 14.0, 11.3. Anal. Calcd. for $\text{C}_{18}\text{H}_{21}\text{N}_3\text{O}_4$: C, 62.96; H, 6.16; N, 12.24. Found: C, 62.69; H, 5.99; N 12.09.

Ethyl 5-benzamido-1-(4-tert-butoxycarbonylamino-butyl)-6-oxo-1,6-dihydropyrimidine-2-carboxylate (3e**).** Yield 33%, 151 mg, pale yellow solid; $R_f = 0.59$ (*n*-hexane/ethyl acetate 1:1); mp 97°C ; ^1H NMR (500 MHz, CDCl_3) δ 9.19 (s, 1H), 8.94 (s, 1H), 7.93 (d, $J = 7.3$ Hz, 2H), 7.59 (t, $J = 7.4$ Hz, 1H), 7.51 (t, $J = 7.6$ Hz, 2H), 4.70 (s, 1H), 4.48 (q, $J = 7.1$ Hz, 2H), 4.26–4.22 (m, 2H), 3.19 (d, $J = 6.1$ Hz, 2H), 1.87–1.84 (m, 2H), 1.60–1.57 (m, 2H), 1.46 (s, 9H); ^{13}C NMR (126 MHz, CDCl_3) δ 165.6, 160.7, 157.4, 155.9, 142.8, 134.7, 133.3, 132.6, 129.0, 128.0, 127.3, 79.2, 77.3, 63.5, 46.0, 39.8, 28.4, 27.2, 26.1, 14.0. Anal. Calcd. for $\text{C}_{23}\text{H}_{30}\text{N}_4\text{O}_6$: C, 60.25; H, 6.59; N, 12.22. Found: C, 60.16; H, 6.54; N 11.98.

Ethyl 5-benzamido-1-isopropyl-6-oxo-1,6-dihydropyrimidine-2-carboxylate (3f**).** Yield 30%, 98 mg, yellow solid; $R_f = 0.70$ (*n*-hexane/ethyl acetate 1:1); mp 106°C (from ethyl acetate); ^1H NMR (500 MHz, CDCl_3) δ 9.10 (s, 1H), 8.95 (s, 1H), 7.93 (d, $J = 7.2$ Hz, 1H), 7.58 (t, $J = 7.4$ Hz, 1H), 7.50 (t, $J = 7.6$ Hz, 2H), 4.52–4.46 (m, 3H), 1.82–1.57 (m, 6H), 1.45 (t, $J = 7.2$ Hz, 3H); ^{13}C NMR (126

MHz, CDCl₃) δ 165.5, 161.3, 157.5, 144.4, 134.4, 133.4, 132.5, 128.9, 128.2, 127.3, 63.3, 55.0, 19.6, 14.0. Anal. Calcd. for C₁₇H₁₉N₃O₄: C, 62.00; H, 5.81; N, 12.76. Found: C, 61.83; H, 5.73; N 12.76.

Ethyl 5-benzamido-1-(4-hydroxyphenethyl)-6-oxo-1,6-dihydropyrimidine-2-carboxylate (3g). Yield 55%, 224 mg, pale yellow solid; R_f = 0.65 (*n*-hexane/ethyl acetate 1:1); mp 191 °C (from ethyl acetate); ¹H NMR (500 MHz, DMSO-*d*₆) δ 9.57 (s, 1H), 9.30 (s, 1H), 8.79 (s, 1H), 7.98 (d, *J* = 8.4 Hz, 2H), 7.65 (t, *J* = 7.3 Hz, 1H), 7.57 (t, *J* = 7.6 Hz, 2H), 6.95 (d, *J* = 8.3 Hz, 2H), 6.70 (d, *J* = 8.4 Hz, 2H), 4.35–4.23 (m, 4H), 2.92–2.84 (m, 2H), 1.30 (t, *J* = 7.1, 3H); ¹³C NMR (126 MHz, DMSO-*d*₆) δ 165.4, 160.3, 156.6, 156.1, 144.1, 136.5, 133.1, 132.3, 129.6, 128.6, 127.6, 127.4, 127.3, 115.4, 62.9, 47.5, 32.9, 13.6. Anal. Calcd. for C₂₂H₂₁N₃O₅: C, 64.86; H, 5.20; N, 10.31. Found: C, 64.71; H, 5.22; N 10.25.

Ethyl 5-benzamido-1-(4-methoxyphenethyl)-6-oxo-1,6-dihydropyrimidine-2-carboxylate (3h). Yield 41%, 173 mg, yellow oil; R_f = 0.75 (*n*-hexane/ethyl acetate 1:1); ¹H NMR (500 MHz, CDCl₃) δ 9.20 (s, 1H), 8.98 (s, 1H), 7.94 (d, *J* = 8.6 Hz, 2H), 7.59 (t, *J* = 7.4 Hz, 1H), 7.51 (t, *J* = 6.6 Hz, 2H), 7.12 (d, *J* = 8.6 Hz, 2H), 6.85 (d, *J* = 8.6 Hz, 2H), 4.51–4.43 (m, 2H), 4.37 (q, *J* = 7.1 Hz, 2H), 3.79 (s, 3H), 3.06–3.00 (m, 2H), 1.40 (t, *J* = 7.2 Hz, 3H); ¹³C NMR (126 MHz, CDCl₃) δ 165.6, 160.6, 158.7, 157.4, 142.7, 134.7, 133.3, 132.6, 130.0, 129.2, 129.0, 128.0, 127.4, 114.2, 63.4, 55.2, 47.9, 33.9, 13.9. Anal. Calcd. for C₂₃H₂₃N₃O₅: C, 65.55; H, 5.50; N, 9.97. Found: C, 65.71; H, 5.72; N 9.70.

Ethyl 5-benzamido-1-(4-hydroxybenzyl)-6-oxo-1,6-dihydropyrimidine-2-carboxylate (3i). Pale yield 52%, 204 mg, yellow solid; R_f = 0.56 (*n*-hexane/ethyl acetate 1:1); mp 166 °C (from ethyl acetate); ¹H NMR (500 MHz, DMSO-*d*₆) δ 9.58 (s, 1H), 9.49 (s, 1H), 8.79 (s, 1H), 7.96 (d, *J* = 7.3 Hz, 2H), 7.63 (t, *J* = 7.3 Hz, 1H), 7.55 (t, *J* = 7.6 Hz, 2H), 7.04 (d, *J* = 8.5 Hz, 2H), 6.72 (d, *J* = 8.5 Hz, 2H), 5.27 (s, 2H), 4.29 (q, *J* = 7.1 Hz, 2H), 1.18 (t, *J* = 7.1 Hz, 3H); ¹³C NMR (126 MHz, DMSO-*d*₆) δ 165.4, 160.4, 157.0, 156.7, 144.7, 136.8, 133.0, 132.3, 128.9, 128.6, 127.6, 127.4, 125.6, 115.2, 62.8, 47.3, 13.5. Anal. Calcd. for C₂₁H₁₉N₃O₅: C, 64.12; H, 4.87; N, 10.68. Found: C, 63.91; H, 4.89; N 10.97.

Ethyl 5-benzamido-1-(4-methoxybenzyl)-6-oxo-1,6-dihydropyrimidine-2-carboxylate (3j). Yield 81%, 329 mg, yellow oil; R_f = 0.72 (*n*-hexane/ethyl acetate 1:1); ¹H NMR (500 MHz, CDCl₃) δ 9.19 (s, 1H), 8.96 (s, 1H), 7.92 (d, *J* = 8.6 Hz, 2H), 7.58 (t, *J* = 7.4 Hz, 1H), 7.50 (t, *J* = 7.6 Hz, 2H), 7.19 (d, *J* = 8.7 Hz, 2H), 6.85 (d, *J* = 8.7 Hz, 2H), 5.54 (s, 2H), 4.35 (q, *J* = 7.1 Hz, 2H), 3.79 (s, 3H), 1.30 (t, *J* = 7.1 Hz, 3H); ¹³C NMR (126 MHz, CDCl₃) δ 165.7, 160.9, 159.5, 157.6, 143.1, 134.8, 133.3, 132.6, 129.5, 128.9, 128.1, 127.4, 127.3, 114.2, 63.3, 55.3, 47.6, 13.9. Anal. Calcd. for C₂₂H₂₁N₃O₅: C, 64.86; H, 5.20; N, 10.31. Found: C, 64.64; H, 5.42; N 10.02.

Ethyl 5-benzamido-1-(3-(benzyloxy)-3-oxopropyl)-6-oxo-1,6-dihydropyrimidine-2-carboxylate (3k). Yield 22%, 99 mg, yellow solid; R_f = 0.73 (*n*-hexane/ethyl acetate 1:1); mp 96 °C (from ethyl acetate); ¹H NMR (600 MHz, CDCl₃) δ 9.18 (s, 1H), 8.89 (s, 1H), 7.91 (d, *J* = 7.6 Hz, 2H), 7.59 (t, *J* = 7.3 Hz, 1H), 7.51 (t, *J* = 7.6 Hz, 2H), 7.37–7.25 (m, 5H), 5.13 (s, 2H), 4.56 (t, *J* = 7.1 Hz, 2H), 4.49–4.46 (m, 2H), 2.97 (t, *J* = 7.1 Hz, 2H), 1.45 (t, *J* = 7.1 Hz, 3H); ¹³C NMR (151 MHz, CDCl₃) δ 170.6, 165.6, 160.7, 157.5, 142.9, 135.4, 134.7, 133.3, 132.6, 129.0, 128.6, 128.5, 128.4, 128.0, 127.3, 66.8, 63.5, 42.5, 32.6, 14.0. Anal. Calcd. for C₂₄H₂₃N₃O₆: C, 64.13; H, 5.16; N, 9.35. Found: C, 64.40; H, 5.16; N 9.36.

Methyl 5-benzamido-6-oxo-1-phenethyl-1,6-dihydropyrimidine-2-carboxylate (3l). Yield 35%, 132 mg, orange solid; R_f = 0.67 (*n*-hexane/ethyl acetate 1:1); mp 115 °C (from ethyl acetate); ¹H NMR (500 MHz, DMSO-*d*₆) δ 9.60 (s, 1H), 8.81 (s, 1H), 7.98 (d, *J* = 7.3 Hz, 2H), 7.65 (t, *J* = 7.3 Hz, 1H), 7.57 (t, *J* = 7.6 Hz, 2H), 7.34 (t, *J* = 7.4 Hz, 2H), 7.26 (t, *J* = 7.3 Hz, 1H), 7.20 (d, *J* = 7.2 Hz, 2H), 4.43–4.22 (m, 2H), 3.86 (s, 3H), 3.12–2.87 (m, 2H); ¹³C NMR (126 MHz, DMSO-*d*₆) δ 165.4, 160.8, 156.6, 143.8, 137.5, 136.3, 133.0, 132.3, 128.7, 128.6, 128.5, 127.7, 127.6, 126.7, 53.5, 47.4, 39.9, 39.8, 39.6, 39.4, 39.3, 33.8. Anal. Calcd. for C₂₁H₁₉N₃O₄: C, 66.83; H, 5.07; N, 11.13. Found: C, 66.65; H, 5.09; N 11.14.

Methyl 5-benzamido-1-(2-(tert-butoxy)-2-oxoethyl)-6-oxo-1,6-dihydropyrimidine-2-carboxylate (3m). Yield 49%, 189 mg, pale white

solid; R_f = 0.63 (*n*-hexane/ethyl acetate 1:1); mp 192 °C (from ethyl acetate); ¹H NMR (500 MHz, CDCl₃) δ 9.25 (s, 1H), 8.94 (s, 1H), 7.92 (d, *J* = 8.6 Hz, 2H), 7.59 (t, *J* = 7.4 Hz, 1H), 7.51 (t, *J* = 7.6 Hz, 2H), 5.21 (s, 2H), 3.98 (s, 3H), 1.50 (s, 9H); ¹³C NMR (126 MHz, CDCl₃) δ 166.3, 165.7, 161.0, 157.5, 140.7, 134.3, 133.2, 132.7, 129.0, 128.4, 127.4, 83.5, 53.9, 46.5, 28.0. Anal. Calcd. for C₁₉H₂₁N₃O₆: C, 58.91; H, 5.46; N, 10.84. Found: C, 58.71; H, 5.56; N 10.66.

General Procedure for Synthesis of Alkyl 5-benzamido-6-oxo-1,6-dihydropyrimidine-2-carboxylates 3m,n. Pyrimidone 3a (0.273 g, 1 mmol) was dissolved in absolute DMF (1 mL) under nitrogen atmosphere. Sodium hydride (40 mg, 1 mmol, 60% in mineral oil) was added, and the mixture was stirred for one hour at room temperature. The appropriate alkylating agent (1.2 mmol) was added slowly, and the resulting solution was stirred overnight. The reaction was quenched by addition of saturated sodium chloride solution (2 mL) and extracted with ethyl acetate (3 × 5 mL). The solvent was dried over sodium sulfate and evaporated under reduced pressure. The residue was purified by flash column chromatography (gradient: 10:90 → 30:70 ethyl acetate:*n*-hexane) to give monomers 3m,n.

Methyl 5-benzamido-1-(4-methoxybenzyl)-6-oxo-1,6-dihydropyrimidine-2-carboxylate (3n). Yield 64%, 251 mg, yellow solid; mp 101 °C (from ethyl acetate); R_f = 0.73 (*n*-hexane/ethyl acetate 1:1); ¹H NMR (500 MHz, CDCl₃) δ 9.18 (s, 1H), 8.98 (s, 1H), 7.92 (d, *J* = 7.4 Hz, 2H), 7.58 (t, *J* = 7.3 Hz, 1H), 7.50 (t, *J* = 7.5 Hz, 2H), 7.20 (d, *J* = 8.5 Hz, 2H), 6.85 (d, *J* = 8.5 Hz, 2H), 5.55 (s, 2H), 3.89 (s, 3H), 3.78 (s, 3H); ¹³C NMR (126 MHz, CDCl₃) δ 165.7, 161.3, 159.5, 157.6, 142.5, 134.6, 133.3, 132.6, 129.5, 128.9, 128.3, 127.4, 127.3, 114.2, 55.3, 53.7, 47.6. Anal. Calcd. for C₂₁H₁₉N₃O₅: C, 64.12; H, 4.87; N, 10.68. Found: C, 63.94; H, 4.85; N 10.67.

General Procedure for the Synthesis of 5-Benzamido-N-methyl-6-oxo-1,6-dihydropyrimidine-2-carboxamide 4a,b. An aqueous solution of methylamine (40 wt %, 2 mL) was added dropwise to a cooled mixture of the corresponding ester 3b,c (1 mmol) in ethanol (2 mL). The ice bath was removed, and the reaction was stirred at room temperature until TLC (1:1 ethyl acetate:*n*-hexane) showed complete conversion of the starting material. Water (10 mL) was added, and the crude amide was filtered off and recrystallized from an appropriate solvent to afford amides 4a,b.

1-(2-(1H-Indol-3-yl)ethyl)-5-benzamido-N-methyl-6-oxo-1,6-dihydropyrimidine-2-carboxamide (4a). Yield 90%, 373 mg, pale white solid; R_f = 0.32 (*n*-hexane/ethyl acetate 1:1); mp 270 °C (from THF); ¹H NMR (500 MHz, DMSO-*d*₆) δ 10.89 (s, 1H), 9.58 (s, 1H), 8.84 (d, *J* = 4.6, 1H), 8.78 (s, 1H), 8.00 (d, *J* = 7.4 Hz, 2H), 7.71 (d, *J* = 7.8 Hz, 1H), 7.65 (t, *J* = 7.3 Hz, 1H), 7.57 (t, *J* = 7.5 Hz, 2H), 7.36 (d, *J* = 8.0 Hz, 1H), 7.16 (s, 1H), 7.09 (t, *J* = 7.4 Hz, 1H), 7.02 (t, *J* = 7.3 Hz, 1H), 4.57–4.28 (m, 2H), 3.20–3.06 (m, 2H), 2.73 (d, *J* = 4.6 Hz, 3H); ¹³C NMR (126 MHz, DMSO-*d*₆) δ 165.4, 161.3, 157.1, 147.9, 137.2, 136.2, 133.2, 132.2, 128.6, 127.5, 126.9, 126.5, 123.1, 121.0, 118.3, 118.2, 111.4, 110.0, 46.0, 25.8, 24.5. Anal. Calcd. for C₂₃H₂₁N₅O₃: C, 66.49; H, 5.09; N, 16.86. Found: C, 66.32; H, 4.86; N 16.69.

5-Benzamido-1-isobutyl-N-methyl-6-oxo-1,6-dihydropyrimidine-2-carboxamide (4b). Yield 89%, 292 mg, white solid; R_f = 0.59 (*n*-hexane/ethyl acetate 1:1); mp 128 °C (from ethyl acetate); ¹H NMR (500 MHz, DMSO-*d*₆) δ 9.48 (s, 1H), 9.01 (d, *J* = 4.7 Hz, 1H), 8.76 (s, 1H), 7.99–7.93 (m, 2H), 7.63 (t, *J* = 7.4 Hz, 1H), 7.55 (t, *J* = 7.6 Hz, 2H), 4.18 (d, *J* = 7.4 Hz, 2H), 2.78 (d, *J* = 4.7 Hz, 3H), 2.07–1.99 (m, 1H), 0.85 (d, *J* = 6.7 Hz, 6H); ¹³C NMR (126 MHz, DMSO-*d*₆) δ 165.3, 161.6, 157.3, 147.9, 136.9, 133.2, 132.2, 128.6, 127.5, 126.4, 50.6, 27.6, 25.8, 19.6. Anal. Calcd. for C₁₇H₂₀N₄O₃: C, 62.18; H, 6.14; N, 17.06. Found: C, 62.00; H, 6.01; N 17.01.

General Procedure for the Synthesis of Monomeric 5-Amino Pyrimidonamides (5a,b). A mixture of the respective benzamide 4a,b (1 mmol) and sodium hydroxide (0.12 g, 3 mmol) in methanol (3 mL) was heated for 6 h (4b) or 8 h (4a). The solvent was removed under reduced pressure, water (5 mL) was added, and the aqueous layer was extracted with ethyl acetate (3 × 15 mL). The combined organic layers were dried over sodium sulfate, filtered and concentrated under a vacuum. The crude residues were purified by

flash column chromatography (gradient: 30:70 → 100:0 ethyl acetate:*n*-hexane) to yield the desired products **5a,b**.

1-(2-(1*H*-Indol-3-yl)ethyl)-5-amino-*N*-methyl-6-oxo-1,6-dihydropyrimidine-2-carboxamide (5a). Yield 92%, 286 mg, pale yellow solid; $R_f = 0.10$ (*n*-hexane/ethyl acetate 1:1); mp 196 °C (from ethyl acetate); $^1\text{H NMR}$ (500 MHz, DMSO- d_6) δ 10.87 (s, 1H), 8.54 (s, 1H), 7.74 (d, $J = 7.8$ Hz, 1H), 7.35 (d, $J = 8.0$ Hz, 1H), 7.23 (s, 1H), 7.14 (s, 1H), 7.08 (t, $J = 7.4$ Hz, 1H), 7.00 (t, $J = 7.4$ Hz, 1H), 5.61 (s, 2H), 4.53–4.40 (m, 2H), 3.12–3.03 (m, 2H), 2.70 (d, $J = 4.4$ Hz, 3H); $^{13}\text{C NMR}$ (126 MHz, DMSO- d_6) δ 161.9, 156.9, 139.8, 136.2, 136.1, 127.0, 122.9, 122.6, 120.9, 118.4, 118.2, 111.3, 110.6, 45.0, 25.8, 24.8. Anal. Calcd. for $\text{C}_{16}\text{H}_{17}\text{N}_5\text{O}_2$: C, 61.72; H, 5.50; N, 22.49. Found: C, 61.53; H, 5.57; N, 22.31.

5-Amino-1-isobutyl-*N*-methyl-6-oxo-1,6-dihydropyrimidine-2-carboxamide (5b). Yield 88%, 197 mg, pale white solid; $R_f = 0.21$ (*n*-hexane/ethyl acetate 1:1); mp 127 °C (from ethyl acetate); $^1\text{H NMR}$ (500 MHz, DMSO- d_6) δ 8.63 (s, 1H), 7.20 (s, 1H), 5.54 (s, 2H), 4.26 (d, $J = 7.3$ Hz, 2H), 2.71 (d, $J = 4.4$ Hz, 3H), 1.93 (s, 1H), 0.79 (s, 3H), 0.78 (s, 3H); $^{13}\text{C NMR}$ (126 MHz, DMSO- d_6) δ 162.2, 157.2, 139.7, 134.0, 122.4, 49.3, 27.8, 25.8, 19.6. Anal. Calcd. for $\text{C}_{10}\text{H}_{16}\text{N}_4\text{O}_2$: C, 53.56; H, 7.19; N, 24.98. Found: C, 53.48; H, 7.19; N, 24.95.

General Procedure for Synthesis of Dimeric Pyrimidonamides (6a,b). A mixture of the appropriate alkyl 5-benzamido-6-oxo-1,6-dihydropyrimidine-2-carboxylate (1.5 equiv) and lithium hydroxide hydrate (1.5 equiv) were dissolved in methanol and stirred for 12 h. The solvent was removed under a vacuum using an ice cooled water bath. The resulting yellow oil was treated with dry diethyl ether to crystallize. The precipitate was collected, dried under a vacuum, and transferred into a two-neck round-bottom flask containing the appropriate 5-amino pyrimidonamide **5a,b** (1 equiv) and COMU (1.8 equiv). The starting materials were dissolved in dry DMF (1 mL per mmol) and stirred for 18 h under nitrogen atmosphere. Dichloromethane (30 mL) was added, and the organic layer was washed with saturated sodium hydrogen carbonate solution (10 mL), 10% aqueous citric acid solution (10 mL) and brine (10 mL). After drying over sodium sulfate the organic layer was concentrated in a vacuum. The residue was crystallized by treatment with dry diethyl ether and recrystallized from an appropriate solvent.

5-Benzamido-1-(*sec*-butyl)-*N*-(1-isobutyl-2-methylcarbamoyl-6-oxo-1,6-dihydropyrimidin-5-yl)-6-oxo-1,6-dihydropyrimidine-2-carboxamide (6a). Yield 75%, 390 mg, pale yellow solid; $R_f = 0.68$ (*n*-hexane/ethyl acetate 1:1); mp 155 °C (from dichloromethane); $^1\text{H NMR}$ (500 MHz, DMSO- d_6) δ 10.74 (s, 1H), 9.48 (s, 1H), 8.99 (d, $J = 4.7$ Hz, 1H), 8.80 (s, 1H), 8.75 (s, 1H), 7.98 (d, $J = 7.4$ Hz, 2H), 7.64 (t, $J = 7.4$ Hz, 1H), 7.56 (t, $J = 7.6$ Hz, 2H), 4.35–4.34 (m, 1H), 4.16 (d, $J = 7.4$ Hz, 2H), 2.79 (d, $J = 4.7$ Hz, 3H), 2.20 (dt, $J = 7.5$, 14.6 Hz, 1H), 2.03 (dt, $J = 6.9$, 13.7 Hz, 1H), 1.92 (dt, $J = 7.2$, 14.0 Hz, 1H), 1.57 (d, $J = 6.7$ Hz, 3H), 0.85–0.81 (m, 9H); $^{13}\text{C NMR}$ (126 MHz, DMSO- d_6) δ 165.2, 161.5, 160.5, 157.1, 156.7, 148.6, 147.9, 137.0, 136.5, 133.1, 132.2, 128.6, 127.5, 127.1, 125.8, 59.9, 50.6, 27.6, 25.8, 25.4, 19.6, 17.1, 11.0. Anal. Calcd. for $\text{C}_{26}\text{H}_{31}\text{N}_7\text{O}_5$: C, 59.87; H, 5.99; N, 18.80. Found: C, 59.61; H, 5.97; N, 18.80.

1-(2-(1*H*-Indol-3-yl)ethyl)-5-(5-benzamido-1-isobutyl-6-oxo-1,6-dihydropyrimidine-2-carboxamido)-*N*-methyl-6-oxo-1,6-dihydropyrimidine-2-carboxamide (6b). Yield 76%, 462 mg, pale yellow solid; $R_f = 0.29$ (*n*-hexane/ethyl acetate 1:1); mp 267 °C (from ethyl acetate); $^1\text{H NMR}$ (500 MHz, DMSO- d_6) δ 10.90 (s, 1H), 10.71 (s, 1H), 9.59 (s, 1H), 8.86 (s, 1H), 8.81 (s, 1H), 8.00 (d, $J = 7.2$ Hz, 2H), 7.72–7.63 (m, 2H), 7.58 (t, $J = 7.6$ Hz, 2H), 7.36 (d, $J = 8.1$ Hz, 1H), 7.17 (d, $J = 2.1$ Hz, 1H), 7.10 (t, $J = 7.2$ Hz, 1H), 7.02 (t, $J = 7.2$ Hz, 1H), 4.47–4.36 (m, 2H), 4.28 (d, $J = 7.3$ Hz, 2H), 3.18–3.08 (m, 2H), 2.73 (d, $J = 4.7$ Hz, 3H), 2.18–2.06 (m, 1H), 0.91 (d, $J = 6.7$ Hz, 6H); $^{13}\text{C NMR}$ (126 MHz, DMSO- d_6) δ 165.4, 161.2, 159.3, 157.4, 156.6, 148.3, 145.4, 136.2, 136.1, 133.1, 132.3, 128.6, 127.6, 127.0, 126.9, 125.9, 123.2, 121.0, 118.3, 118.2, 111.4, 110.0, 50.8, 46.1, 38.1, 28.0, 25.8, 24.4, 19.8. Anal. Calcd. for $\text{C}_{32}\text{H}_{32}\text{N}_8\text{O}_5$: C, 63.15; H, 5.30; N, 18.41. Found: C, 62.92; H, 5.25; N, 18.21.

General Procedure for the Synthesis of Dimeric 5-Amino Pyrimidonamides (7a,b). A mixture of the respective benzamide **6a,b** (1 mmol) and sodium hydroxide (0.12 g, 3 mmol) in methanol

(3 mL) was heated for 6 h (**6a**) or 8 h (**6b**). The solvent was removed under reduced pressure, water (5 mL) was added, and the aqueous layer was extracted with ethyl acetate (3 × 15 mL). The combined organic layers were dried over sodium sulfate, filtered and concentrated under a vacuum. The crude residues were purified by flash column chromatography (gradient: 30:70 → 100:0 ethyl acetate:*n*-hexane) to yield the desired products **7a,b**.

5-Amino-1-(*sec*-butyl)-*N*-(1-isobutyl-2-(methylcarbamoyl)-6-oxo-1,6-dihydropyrimidin-5-yl)-6-oxo-1,6-dihydropyrimidine-2-carboxamide (7a). Yield 77%, 321 mg, yellow solid; $R_f = 0.50$ (*n*-hexane/ethyl acetate 1:1); mp 263 °C (from ethyl acetate); $^1\text{H NMR}$ (500 MHz, CDCl_3) δ 10.17 (s, 1H), 8.93 (s, 1H), 7.74 (s, 1H), 7.32 (s, 1H), 5.29 (dd, $J = 6.9$, 14.7 Hz, 1H), 4.66 (d, $J = 7.4$ Hz, 2H), 4.57 (s, 2H), 2.98 (d, $J = 5.1$ Hz, 3H), 2.31–2.29 (m, 1H), 2.10 (dt, $J = 6.9$, 13.8 Hz, 1H), 1.96–1.94 (m, 1H), 1.68 (d, $J = 6.7$ Hz, 3H), 0.90 (dd, $J = 6.6$, 19.3 Hz, 6H), 0.83 (t, $J = 7.5$ Hz, 3H); $^{13}\text{C NMR}$ (126 MHz, CDCl_3) δ 161.1, 159.4, 158.2, 158.0, 144.3, 139.3, 136.8, 133.6, 127.3, 123.0, 58.8, 51.0, 28.8, 26.6, 25.9, 19.8, 17.9, 11.4. Anal. Calcd. for $\text{C}_{19}\text{H}_{27}\text{N}_7\text{O}_4$: C, 54.66; H, 6.52; N, 23.49. Found: C, 54.38; H, 6.56; N, 23.21.

1-(2-(1*H*-Indol-3-yl)ethyl)-5-(5-amino-1-isobutyl-6-oxo-1,6-dihydropyrimidine-2-carboxamido)-*N*-methyl-6-oxo-1,6-dihydropyrimidine-2-carboxamide (7b). Yield 74%, 373 mg, yellow solid; $R_f = 0.44$ (*n*-hexane/ethyl acetate 1:1); mp 223 °C (from dichloromethane); $^1\text{H NMR}$ (500 MHz, DMSO- d_6) δ 10.92 (s, 1H), 10.39 (s, 1H), 8.78 (d, $J = 6.1$ Hz, 2H), 7.68 (d, $J = 7.8$ Hz, 1H), 7.36 (d, $J = 10.8$ Hz, 2H), 7.15 (d, $J = 1.7$ Hz, 1H), 7.09 (t, $J = 7.5$ Hz, 1H), 7.02 (t, $J = 7.4$ Hz, 1H), 6.10 (s, 2H), 4.53–4.51 (m, 2H), 4.47–4.25 (m, 2H), 3.19–2.98 (m, 2H), 2.72 (d, $J = 4.7$ Hz, 3H), 2.04 (dd, $J = 12.9$, 19.8 Hz, 1H), 0.86 (d, $J = 6.7$ Hz, 6H); $^{13}\text{C NMR}$ (126 MHz, DMSO- d_6) δ 161.7, 159.3, 157.5, 157.2, 147.5, 136.7, 135.7, 134.3, 127.4, 126.7, 123.6, 121.8, 121.5, 118.8, 118.7, 111.8, 110.5, 55.3, 49.7, 46.6, 28.8, 26.2, 24.8, 20.1. Anal. Calcd. for $\text{C}_{25}\text{H}_{29}\text{N}_8\text{O}_4$: C, 59.51; H, 5.59; N, 22.21. Found: C, 59.38; H, 5.77; N, 21.92.

General Procedure for Synthesis of Trimeric Pyrimidonamides (8a,b). A mixture of the appropriate alkyl 5-benzamido-6-oxo-1,6-dihydropyrimidine-2-carboxylate (1.5 equiv) and lithium hydroxide hydrate (1.5 equiv) were dissolved in methanol and stirred for 12 h. The solvent was removed under a vacuum using an ice cooled water bath. The resulting yellow oil was treated with dry diethyl ether to crystallize. The precipitate was collected, dried under a vacuum and was transferred into a two-neck round-bottom flask containing the appropriate 5-amino pyrimidonamide **7a,b** (1 equiv) and COMU (1.8 equiv). The starting materials were dissolved in dry DMF (1 mL per mmol) and stirred for 18 h under nitrogen atmosphere. Dichloromethane (30 mL) was added, and the organic layer was washed with saturated sodium hydrogen carbonate solution (10 mL), 10% aqueous citric acid solution (10 mL) and brine (10 mL). After drying over sodium sulfate the organic layer was concentrated in a vacuum. The residue was crystallized by treatment with dry diethyl ether and recrystallized from an appropriate solvent.

5-Benzamido-*N*-(1-(*sec*-butyl)-2-(1-isobutyl-2-(methylcarbamoyl)-6-oxo-1,6-dihydropyrimidin-5-yl)carbamoyl)-6-oxo-1,6-dihydropyrimidin-5-yl)-1-isopropyl-6-oxo-1,6-dihydropyrimidine-2-carboxamide (8a). Yield 55%, 192 mg, yellow solid; $R_f = 0.66$ (*n*-hexane/ethyl acetate 1:1); mp 257 °C (from dichloromethane); $^1\text{H NMR}$ (600 MHz, CDCl_3) δ 10.18 (s, 1H), 10.06 (s, 1H), 9.10 (s, 1H), 9.05 (s, 1H), 8.96 (s, 1H), 8.95 (s, 1H), 7.94 (d, $J = 7.3$ Hz, 2H), 7.70 (d, $J = 5.0$ Hz, 1H), 7.59 (t, $J = 7.4$ Hz, 1H), 7.51 (t, $J = 7.7$ Hz, 2H), 5.53–5.48 (m, 1H), 5.19 (dd, $J = 6.9$, 14.7 Hz, 1H), 4.68 (d, $J = 7.3$ Hz, 2H), 2.99 (d, $J = 5.1$ Hz, 3H), 2.31–2.29 (m, 1H), 2.11–2.09 (m, 1H), 2.01 (dd, $J = 7.1$, 14.1 Hz, 1H), 1.70 (t, $J = 10.0$ Hz, 9H), 0.93 (dd, $J = 1.6$, 6.7 Hz, 6H), 0.87 (t, $J = 7.4$ Hz, 3H); $^{13}\text{C NMR}$ (151 MHz, CDCl_3) δ 165.6, 160.9, 158.8, 158.3, 157.9, 157.8, 145.0, 144.8, 143.4, 134.3, 133.6, 133.4, 132.9, 132.6, 128.9, 128.8, 128.0, 127.4, 126.9, 60.2, 54.1, 51.0, 28.8, 26.6, 25.9, 19.8, 19.7, 17.9, 11.4. Anal. Calcd. for $\text{C}_{39}\text{H}_{46}\text{N}_{10}\text{O}_7$: C, 58.28; H, 5.75; N, 19.99. Found: C, 58.17; H, 5.80; N, 19.85.

***tert*-Butyl 4-(2-((1-(2-(1*H*-indol-3-yl)ethyl)-2-(methylcarbamoyl)-6-oxo-1,6-dihydropyrimidin-5-yl)carbamoyl)-1-isobutyl-6-oxo-1,6-dihydropyrimidin-5-yl)carbamoyl)-5-benzamido-6-oxopyri-**

midin-1(6H)-yl)butyl)carbamate (8b). Yield 41%, 188 mg, yellow solid; $R_f = 0.28$ (ethyl acetate); mp 243 °C (from ethyl acetate); ^1H NMR (600 MHz, DMSO- d_6) δ 10.88 (s, 1H), 10.66 (s, 1H), 10.59 (s, 1H), 9.53 (s, 1H), 8.88 (s, 1H), 8.84 (s, 1H), 8.80–8.78 (m, 2H), 7.97–7.95 (m, 2H), 7.73–7.68 (m, 1H), 7.65–7.61 (m, 1H), 7.57–7.53 (m, 2H), 7.35–7.33 (m, 1H), 7.17–7.13 (m, 1H), 7.11–7.09 (m, 1H), 7.03–6.99 (m, 1H), 6.79 (s, 1H), 4.45–4.38 (m, 2H), 4.35–4.26 (m, 4H), 3.16–3.12 (m, 2H), 2.98–2.94 (m, 2H), 2.72 (d, $J = 2.9$ Hz, 3H), 2.15–2.13 (m, 1H), 1.77–1.75 (m, 2H), 1.48–1.45 (m, 2H), 1.37 (s, 9H), 0.91 (d, $J = 5.5$ Hz, 6H); ^{13}C NMR (151 MHz, DMSO- d_6) δ 165.4, 161.2, 159.0, 158.9, 157.2, 157.0, 156.6, 155.5, 148.2, 145.5, 144.8, 144.7, 136.3, 136.0, 135.8, 134.9, 133.1, 132.4, 128.7, 127.6, 127.3, 127.0, 126.4, 125.9, 123.2, 121.1, 118.4, 118.3, 111.5, 110.0, 77.4, 50.9, 46.2, 45.3, 28.2, 26.9, 25.9, 25.8, 24.4, 19.8. Anal. Calcd. for $\text{C}_{44}\text{H}_{52}\text{N}_{12}\text{O}_9$: C, 60.25; H, 5.72; N, 18.33. Found: C, 59.98; H, 5.72; N 18.35.

Preparation of Unprotected Trimer 8c. The *tert*-butylcarbamate **8b** (0.05 g, 0.054 mmol) was suspended in dichloromethane (2 mL) and cooled with an ice bath. Trifluoroacetic acid (0.5 mL) was added slowly. After 15 min all starting material was dissolved, and the ice bath was removed. The mixture was stirred at room temperature for 3 h and evaporated under a vacuum. Toluol (2 mL) was added, and the mixture was re-evaporated.

1-(2-(1H-Indol-3-yl)ethyl)-5-(5-(1-(4-aminobutyl)-5-benzamido-6-oxo-1,6-dihydropyrimidine-2-carboxamido)-1-isobutyl-6-oxo-1,6-dihydropyrimidine-2-carboxamido)-N-methyl-6-oxo-1,6-dihydropyrimidine-2-carboxamide trifluoroacetate (8c-TFA). Yield 92%, 46 mg, yellow solid; $R_f = 0.05$ (ethyl acetate); mp 243 °C; ^1H NMR (600 MHz, DMSO- d_6) δ 10.85 (s, 1H), 10.60 (s, 1H), 10.54 (s, 1H), 9.51 (s, 1H), 8.82 (s, 1H), 8.79 (s, 1H), 8.74 (s, 2H), 7.90 (d, $J = 7.3$, 2H), 7.74 (s, 3H), 7.62 (d, $J = 7.7$, 1H), 7.57 (d, $J = 7.1$, 1H), 7.50 (d, $J = 7.2$, 2H), 7.30 (d, $J = 7.9$, 1H), 7.17 (s, 1H), 7.08 (s, 1H), 7.02 (s, 1H), 6.95 (d, $J = 7.3$, 1H), 4.32 (d, $J = 18.5$, 2H), 4.29 (s, 2H), 4.22 (s, 2H), 3.06 (s, 2H), 2.79 (s, 2H), 2.66 (d, $J = 4.2$, 3H), 2.43 (s, 2H), 2.23 (s, 1H), 2.07 (s, 1H), 1.77 (s, 2H), 1.57 (s, 2H), 0.84 (s, 3H), 0.82 (s, 3H); ^{13}C NMR (151 MHz, DMSO- d_6) δ 165.5, 161.2, 159.1, 158.9, 157.3, 157.0, 156.7, 148.3, 144.8, 136.3, 136.2, 135.0, 133.1, 132.4, 128.9, 128.7, 128.2, 127.6, 127.3, 127.0, 126.4, 125.9, 123.2, 121.1, 118.4, 118.2, 111.5, 110.0, 51.0, 46.2, 44.8, 38.5, 28.2, 25.8, 25.5, 24.4, 24.3, 19.8; HRMS (EI) m/z calcd. for $\text{C}_{41}\text{H}_{48}\text{N}_{12}\text{O}_7$ [$\text{M}]^+$ 817.35287, found 817.35302.

The residue was taken up in water (1 mL) and sodium hydroxide solution (15 wt %) was added until pH 9. The resulting suspension was extracted with ethyl acetate (3 \times 5 mL). After drying over sodium sulfate, the solvent was removed, and the residue was treated with diethyl ether to crystallize. The solid was collected and washed with ethyl acetate/hexane (1:2) to give the deprotected amine **8c**.

1-(2-(1H-Indol-3-yl)ethyl)-5-(5-(1-(4-aminobutyl)-5-benzamido-6-oxo-1,6-dihydropyrimidine-2-carboxamido)-1-isobutyl-6-oxo-1,6-dihydropyrimidine-2-carboxamido)-N-methyl-6-oxo-1,6-dihydropyrimidine-2-carboxamide (8c). Yield 90%, 44 mg, yellow solid; $R_f = 0.10$ (ethyl acetate); mp 218 °C; ^1H NMR (600 MHz, DMSO- d_6) δ 10.89 (s, 1H), 8.86 (s, 1H), 8.83 (s, 1H), 8.80 (s, 1H), 7.98 (d, $J = 7.4$ Hz, 2H), 7.69 (d, $J = 7.8$ Hz, 1H), 7.64 (d, $J = 7.4$ Hz, 1H), 7.57 (t, $J = 7.6$ Hz, 2H), 7.36 (d, $J = 8.0$ Hz, 1H), 7.16 (s, 1H), 7.09 (t, $J = 7.4$ Hz, 1H), 7.01 (t, $J = 7.4$ Hz, 1H), 4.40 (s, 2H), 4.30–4.26 (m, 4H), 3.13 (s, 2H), 2.72 (d, $J = 3.8$ Hz, 3H), 2.65 (t, $J = 7.0$ Hz, 2H), 2.13 (s, 1H), 1.80 (d, $J = 15.2$ Hz, 2H), 1.49 (s, 2H), 0.90 (d, $J = 6.6$ Hz, 6H); ^{13}C NMR (151 MHz, DMSO- d_6) δ 165.4, 161.3, 159.3, 159.2, 157.2, 157.2, 156.7, 148.2, 145.7, 145.6, 136.4, 136.3, 136.2, 135.2, 133.2, 132.4, 128.7, 127.0, 126.1, 123.2, 121.1, 118.4, 118.3, 111.5, 110.0, 50.9, 46.2, 45.3, 40.2, 40.0, 28.3, 28.1, 25.8, 25.7, 24.4, 22.6, 19.8; HRMS (EI) m/z calcd. for $\text{C}_{41}\text{H}_{48}\text{N}_{12}\text{O}_7$ [$\text{M}]^+$ 817.35287, found 817.35405.

Crystal Structure Determination. Only very thin crystals of limited quality were available in the case of compound **8a**. One was selected by means of a polarization microscope and investigated with a STOE Imaging Plate Diffraction System at 123 K using graphite monochromatized Mo $\text{K}\alpha$ radiation ($\lambda = 0.71073$ Å) applying long time exposures. Unit cell parameters were determined by least-squares

refinements on the positions of 8000 reflections. Space group type no. 14 was uniquely determined. Corrections for Lorentz and polarization effects were applied. The structure was solved by direct methods⁶² and subsequent ΔF -syntheses. In the course of structure refinement, intermolecular coupled disorder was detected with respect to the *sec*-butyl group attached to N5 and the isobutyl group attached to N3 (0.73(1):0.27(1) and 0.28(1):0.72(1)). Approximate positions of all but some of the hydrogen atoms in the disorder region were found in different stages of converging refinements by full-matrix least-squares calculations on F^2 .⁶³ Anisotropic displacement parameters were refined for all atoms heavier than hydrogen with the exception of the atoms of the disordered group including atoms C13 to C16. With idealized bond lengths and angles assumed for all the CH, CH₂, and CH₃ groups, the riding model was applied for the corresponding H atoms, and their isotropic displacement parameters were constrained to 120, 120, and 150% of the equivalent isotropic displacement parameters of the parent carbon atoms, respectively. In addition the H atoms of the CH₃ groups were allowed to rotate around the neighboring C–C bonds. Idealized bond lengths were also assumed for the NH groups; their orientation was refined, and their isotropic displacement parameters were constrained to 120% of the equivalent isotropic displacement parameters of the parent nitrogen atoms. Appropriate same distance and anisotropic displacement restraints had to be applied for atoms of the disorder region. CCDC-946095 contains the supplementary crystallographic data (excluding structure factors) for this paper. These data can be obtained free of charge from The Cambridge Crystallographic Data Centre via www.ccdc.cam.ac.uk/data_request/cif.

Modeling Studies. The torsion angles ϕ and ψ (Figure S4A, Supporting Information) are crucial for the conformational properties of the trispyrimidonamide scaffold. Thus, we parametrized the respective torsion angle potentials for use with other parameters of the molecular mechanics general AMBER force field (GAFF).⁶⁴ Conformations of a dimethyl substituted bispyrimidonamide (Figure S4A, Supporting Information) were optimized by means of Gaussian 03⁶⁵ at the MP2/6-31G* level of theory with the torsion angles ϕ and ψ constrained at intervals of 15° over a range of 360°. Similarly, the conformations were optimized (constrained to the same inter-ring torsion angles) by using the GAFF force field within Amber 11.⁶⁶ New molecular mechanics torsion angle potentials for ϕ and ψ were then derived by a fitting procedure carried out with the Amber module Paramfit.⁶⁷ Partial charges for di- and trimethyl substituted bis- and trispyrimidonamides (Figure S4A, Supporting Information, and Figure 3A (IV) in the main text, respectively) were obtained by RESP fitting to the HF/6-31G* electrostatic potentials of minimum conformations.⁶⁸ Minimization, equilibration, and MD simulations of 1.5 μs length of IV in explicit solvent were performed with the Amber11 software package using the GAFF force field together with the above derived parameters and standard procedures (TIP3P water, MeOH or CHCl₃ model, PBC, PME, SHAKE, time step of 2 fs). The distributions of torsion angles were analyzed with the Amber module *ptraj*.⁶⁹

■ ASSOCIATED CONTENT

📄 Supporting Information

Detailed description of amide coupling optimization, ^1H NMR and ^{13}C NMR spectra for compounds 3–8, X-ray crystallographic data for **8c** (CIF), parametrization of the inter-ring torsion angles ψ and ϕ , and overlay of C $_{\beta}$ atoms of a canonical α -helix at positions i , $i + 4$, and $i + 7$ onto corresponding methyl groups of IV. This material is available free of charge via the Internet at <http://pubs.acs.org>.

■ AUTHOR INFORMATION

Corresponding Author

*Fax: (+) 49 211 81 13847. E-mail: thomas.kurz@uni-duesseldorf.de.

Author Contributions

[§]L. Spanier and E. Ciglia share the first authorship.

Notes

The authors declare no competing financial interest.

ACKNOWLEDGMENTS

This work was supported by funds from the Strategischer Forschungsfonds of the Heinrich-Heine-University, Düsseldorf. H.G. is grateful to the Zentrum für Informations und Medientechnologie of the Heinrich-Heine-University, Düsseldorf, for computational support. W.F. is grateful to E. Hammes and G. J. Reiß for technical support. The Deutsche Forschungsgemeinschaft (DFG) is acknowledged for funds used to purchase the UHR-TOF maXis 4G, Bruker Daltonics, Bremen HRMS instrument used in this research.

REFERENCES

- Archakov, A. I.; Govorun, V. M.; Dubanov, A. V.; Ivanov, Y. D.; Veselovsky, A. V.; Lewi, P.; Janssen, P. *Proteomics* **2003**, *3*, 380.
- Beuming, T.; Skrabanek, L.; Niv, M. Y.; Mukherjee, P.; Weinstein, H. *Bioinformatics* **2005**, *21*, 827.
- Cory, S.; Adams, J. M. *Nat. Rev. Cancer* **2002**, *2*, 647.
- Fischer, P. M. *Drug Des. Rev.—Online* **2005**, *2*, 179.
- Pagel, P.; Kovac, S.; Oesterheld, M.; Brauner, B.; Dunger-Kaltenbach, L.; Frishman, G.; Montrone, C.; Mark, P.; Stumpfen, V.; Mewes, H. W.; Ruepp, A.; Frishman, D. *Bioinformatics* **2005**, *21*, 832.
- Villunger, A.; Scott, C.; Bouillet, P.; Strasser, A. *Blood* **2003**, *101*, 2393.
- Xenarios, I.; Eisenberg, D. *Curr. Opin. Biotechnol.* **2001**, *12*, 334.
- Blazer, L. L.; Neubig, R. R. *Neuropsychopharmacology* **2009**, *34*, 126.
- Ryan, D. P.; Matthews, J. M. *Curr. Opin. Struct. Biol.* **2005**, *15*, 441.
- Wells, J. A.; McClendon, C. L. *Nature* **2007**, *450*, 1001.
- Chene, P. *ChemMedChem* **2006**, *1*, 400.
- Gerrard, J. A.; Hutton, C. A.; Perugini, M. A. *Mini-Rev. Med. Chem.* **2007**, *7*, 151.
- Zinzalla, G.; Thurston, D. E. *Future Med. Chem.* **2009**, *1*, 65.
- Azzarito, V.; Long, K.; Murphy, N. S.; Wilson, A. J. *Nat. Chem.* **2013**, *5*, 161.
- Berg, T. *Angew. Chem., Int. Ed. Engl.* **2003**, *42*, 2462.
- Bienstock, R. J. *Curr. Pharm. Des.* **2012**, *18*, 1240.
- Metz, A.; Ciglia, E.; Gohlke, H. *Curr. Pharm. Des.* **2012**, *18*, 4630.
- Wilson, A. J. *Chem. Soc. Rev.* **2009**, *38*, 3289.
- Bullock, B. N.; Jochim, A. L.; Arora, P. S. *J. Am. Chem. Soc.* **2011**, *133*, 14220.
- Jochim, A. L.; Arora, P. S. *Mol. Biosyst.* **2009**, *5*, 924.
- Bogan, A. A.; Thorn, K. S. *J. Mol. Biol.* **1998**, *280*, 1.
- Clackson, T.; Wells, J. A. *Science* **1995**, *267*, 383.
- Metz, A.; Pfeiffer, C.; Kopitz, H.; Pfeiffer-Marek, S.; Baringhaus, K. H.; Gohlke, H. *J. Chem. Inf. Model.* **2012**, *52*, 120.
- Albert, J. S.; Goodman, M. S.; Hamilton, A. D. *J. Am. Chem. Soc.* **1995**, *117*, 1143.
- Albert, J. S.; Pecuh, M. W.; Hamilton, A. D. *Bioorg. Med. Chem.* **1997**, *5*, 1455.
- Cummings, C. G.; Hamilton, A. D. *Curr. Opin. Chem. Biol.* **2010**, *14*, 341.
- Davis, J. M.; Tsou, L. K.; Hamilton, A. D. *Chem. Soc. Rev.* **2007**, *36*, 326.
- Gomes, C. P.; Metz, A.; Bats, J. W.; Gohlke, H.; Gobel, M. W. *Eur. J. Org. Chem.* **2012**, 3270.
- Ko, E.; Liu, J.; Burgess, K. *Chem. Soc. Rev.* **2011**, *40*, 4411.
- Ko, E.; Liu, J.; Perez, L. M.; Lu, G.; Schaefer, A.; Burgess, K. *J. Am. Chem. Soc.* **2011**, *133*, 462.
- Pecuh, M. W.; Hamilton, A. D. *Chem. Rev.* **2000**, *100*, 2479.
- Yin, H.; Hamilton, A. D. *Angew. Chem., Int. Ed. Engl.* **2005**, *44*, 4130.
- Arkin, M. R.; Randal, M.; DeLano, W. L.; Hyde, J.; Luong, T. N.; Oslob, J. D.; Raphael, D. R.; Taylor, L.; Wang, J.; McDowell, R. S.; Wells, J. A.; Braisted, A. C. *Proc. Natl. Acad. Sci. U. S. A.* **2003**, *100*, 1603.
- Martinek, T. A.; Fulop, F. *Chem. Soc. Rev.* **2012**, *41*, 687.
- Horwell, D. C.; Howson, W.; Nolan, W. P.; Ratcliffe, G. S.; Rees, D. C.; Willems, H. M. G. *Tetrahedron* **1995**, *51*, 203.
- Nolan, W. P.; Ratcliffe, G. S.; Rees, D. C. *Tetrahedron Lett.* **1992**, *33*, 6879.
- Orner, B. P.; Ernst, J. T.; Hamilton, A. D. *J. Am. Chem. Soc.* **2001**, *123*, 5382.
- Adler, M. J.; Scott, R. T. W.; Hamilton, A. D. *Chem.—Eur. J.* **2012**, *18*, 12974.
- Ahn, J. M.; Han, S. Y. *Tetrahedron Lett.* **2007**, *48*, 3543.
- Antuch, W.; Menon, S.; Chen, Q. Z.; Lu, Y. C.; Sakamuri, S.; Beck, B.; Schauer-Vukasinovic, V.; Agarwal, S.; Hess, S.; Domling, A. *Bioorg. Med. Chem. Lett.* **2006**, *16*, 1740.
- Biros, S. M.; Moisan, L.; Mann, E.; Carella, A.; Zhai, D.; Reed, J. C.; Rebek, J. *Bioorg. Med. Chem. Lett.* **2007**, *17*, 4641.
- Cummings, M. D.; Schubert, C.; Parks, D. J.; Calvo, R. R.; LaFrance, L. V.; Lattanze, J.; Milkiewicz, K. L.; Lu, T. B. *Chem. Biol. Drug Des.* **2006**, *67*, 201.
- Davis, J. M.; Truong, A.; Hamilton, A. D. *Org. Lett.* **2005**, *7*, 5405.
- Ernst, J. T.; Becerril, J.; Park, H. S.; Yin, H.; Hamilton, A. D. *Angew. Chem., Int. Ed. Engl.* **2003**, *42*, 535.
- Oguri, H.; Tanabe, S.; Oomura, A.; Umetsu, M.; Hiram, M. *Tetrahedron Lett.* **2006**, *47*, 5801.
- Shaginian, A.; Whitby, L. R.; Hong, S.; Hwang, I.; Farooqi, B.; Searcey, M.; Chen, J. C.; Vogt, P. K.; Boger, D. L. *J. Am. Chem. Soc.* **2009**, *131*, 5564.
- Stoll, R.; Renner, C.; Hansen, S.; Palme, S.; Klein, C.; Belling, A.; Zeslawski, W.; Kamionka, M.; Rehm, T.; Muhlhahn, P.; Schumacher, R.; Hesse, F.; Kaluza, B.; Voelter, W.; Eng, R. A.; Holak, T. A. *Biochemistry* **2001**, *40*, 336.
- Yin, H.; Lee, G. I.; Sedey, K. A.; Kutzki, O.; Park, H. S.; Orner, B. P.; Ernst, J. T.; Wang, H. G.; Sebt, S. M.; Hamilton, A. D. *J. Am. Chem. Soc.* **2005**, *127*, 10191.
- Yin, H.; Lee, G. I.; Sedey, K. A.; Rodriguez, J. M.; Wang, H. G.; Sebt, S. M.; Hamilton, A. D. *J. Am. Chem. Soc.* **2005**, *127*, 5463.
- Kim, I. C.; Hamilton, A. D. *Org. Lett.* **2006**, *8*, 1751.
- Hu, Z.; Ma, B.; Wolfson, H.; Nussinov, R. *Proteins* **2000**, *39*, 331.
- Moreira, I. S.; Fernandes, P. A.; Ramos, M. J. *Proteins* **2007**, *68*, 803.
- Restorp, P.; Rebek, J., Jr. *Bioorg. Med. Chem. Lett.* **2008**, *18*, 5909.
- Von Angerer, S. In *Science of Synthesis*; Thieme: Stuttgart, 2004; Vol. 16.
- Matos, M. R. P. N.; Gois, P. M. P.; Mata, M. L. E. N.; Cabrita, E. J.; Afonso, C. A. M. *Synth. Commun.* **2003**, *33*, 1285.
- Martin, T.; Dailey, W. P. *J. Org. Chem.* **2004**, *69*, 7359.
- Hansen, F. K.; Geffken, D. *Synthesis* **2010**, 2583.
- Pozgan, F.; Polanc, S.; Kocevcar, M. *Heterocycles* **2001**, *54*, 1011.
- Takahashi, D.; Honda, Y.; Izawa, K. *Heterocycles* **2012**, *85*, 1089.
- Wetzel, B.; Woitun, E.; Reuter, W.; Maier, R.; Lechner, U. *Arzneim.-Forsch./Drug Res.* **1985**, *35*, 343.
- Jochim, A. L.; Arora, P. S. *ACS Chem. Biol.* **2010**, *5*, 919.
- Sheldrick, G. M. *SHELXL97: Program for the Refinement of Crystal Structures*; University of Göttingen: Göttingen, Germany, 1997.
- Sheldrick, G. M. *SHELXS86: Program for the Solution of Crystal Structures*; University of Göttingen: Göttingen, Germany, 1985.
- Wang, J. M.; Wolf, R. M.; Caldwell, J. W.; Kollman, P. A.; Case, D. A. *J. Comput. Chem.* **2004**, *25*, 1157.
- Frisch, M. J.; Trucks, G. W.; Schlegel, H. B.; Scuseria, G. E.; Robb, M. A.; Cheeseman, J. R.; Montgomery, J. J. A.; Vreven, T.; Kudin, K. N.; Burant, J. C.; Millam, J. M.; Iyengar, S. S.; Tomasi, J.;

Barone, V.; Mennucci, B.; Cossi, M.; Scalmani, G.; Rega, N.; Petersson, G. A.; Nakatsuji, H.; Hada, M.; Ehara, M.; Toyota, K.; Fukuda, R.; Hasegawa, J.; Ishida, M.; Nakajima, T.; Honda, Y.; Kitao, O.; Nakai, H.; Klene, M.; Li, X.; Knox, J. E.; Hratchian, H. P.; Cross, J. B.; Bakken, V.; Adamo, C.; Jaramillo, J.; Gomperts, R.; Stratmann, R. E.; Yazyev, O.; Austin, A. J.; Cammi, R.; Pomelli, C.; Ochterski, J. W.; Ayala, P. Y.; Morokuma, K.; Voth, G. A.; Salvador, P.; Dannenberg, J. J.; Zakrzewski, V. G.; Dapprich, S.; Daniels, A. D.; Strain, M. C.; Farkas, O.; Malick, D. K.; Rabuck, A. D.; Raghavachari, K.; Foresman, J. B.; Ortiz, J. V.; Cui, Q.; Baboul, A. G.; Clifford, S.; Cioslowski, J.; Stefanov, B. B.; Liu, G.; Liashenko, A.; Piskorz, P.; Komaromi, I.; Martin, R. L.; Fox, D. J.; Keith, T.; Al-Laham, M. A.; Peng, C. Y.; Nanayakkara, A.; Challacombe, M.; Gill, P. M. W.; Johnson, B.; Chen, W.; Wong, M. W.; Gonzalez, C.; Pople, J. A. *Gaussian 03*; Gaussian, Inc.: Wallingford, CT, 2004.

(66) Case, D. A.; Darden, T. A.; Cheatham, T. E. I.; Simmerling, C. L.; Wang, J.; Duke, R. E.; Luo, R.; Walker, R. C.; Zhang, W.; Merz, K. M.; Roberts, B.; Wang, B.; Hayik, S.; Roitberg, A.; Seabra, G.; Kolossváry, L.; Wong, K. F.; Paesani, F.; Vanicek, J.; Liu, J.; Wu, X.; Brozell, S. R.; Steinbrecher, T.; Gohlke, H.; Cai, Q.; Ye, X.; Wang, J.; Hsieh, M.-J.; Cui, G.; Roe, D. R.; Mathews, D. H.; Seetin, M. G.; Sagui, C.; Babin, V.; Luchko, T.; Gusarov, S.; Kovalenko, A.; Kollman, P. A. *AMBER 11*; University of California: San Francisco, 2010.

(67) Case, D. A.; Darden, T. A.; Cheatham, T. E. I.; Simmerling, C. L.; Wang, J.; Duke, R. E.; Luo, R.; Walker, R. C.; Zhang, W.; Merz, K. M.; Roberts, B.; Hayik, S.; Roitberg, A.; Seabra, G.; Swails, J.; Goetz, A. W.; Kolossváry, L.; Wong, K. F.; Paesani, F.; Vanicek, J.; Wolf, R. M.; Liu, J.; Wu, X.; Brozell, S. R.; Steinbrecher, T.; Gohlke, H.; Cai, Q.; Ye, X.; Wang, J.; Hsieh, M.-J.; Cui, G.; Roe, D. R.; Mathews, D. H.; Seetin, M. G.; Salomon-Ferrer, R.; Sagui, C.; Babin, V.; Luchko, T.; Gusarov, S.; Kovalenko, A.; Kollman, P. A. *AMBER 12*; University of California: San Francisco, 2012.

(68) Cieplak, P.; Cornell, W. D.; Bayly, C.; Kollman, P. A. *J. Comput. Chem.* 1995, 16, 1357.

(69) Roe, D. R.; Cheatham, T. E. *J. Chem. Theory Comput.* 2013, 9, 3084.

12.1 PUBLICATION IV – Supporting Information

Supporting Information

Design, Synthesis and Conformational Analysis of Trispyrimidonamides as α -Helix Mimetics

*Lukas Spanier,^{‡[a]} Emanuele Ciglia,^{‡[a]} Finn K. Hansen,^[a] Krystina Kuna,^[a] Walter Frank,^[b]
Holger Gohlke,^[a] and Thomas Kurz^{*[a]}*

[a] Institut für Pharmazeutische und Medizinische Chemie, Heinrich-Heine-Universität
Düsseldorf, Universitätsstr. 1, 40225 Düsseldorf (Germany)

[b] Institut fuer Anorganische Chemie und Strukturchemie, Heinrich-Heine-Universität
Düsseldorf, Universitätsstr. 1, 40225 Düsseldorf (Germany)

TABLE OF CONTENTS:

1. OPTIMIZATION OF AMIDE COUPLING.....	S2
2. 1D AND 2D NMR SPECTRA.....	S4
3. BISPYRIMIDONAMIDE USED FOR THE PARAMETERIZATION PROCEDURE AND POTENTIALS OF THE INTER-RING TORSION ANGLES ϕ and ψ	S46
4. FORCE FIELD PARAMETERS DERIVED FOR THE ϕ and ψ INTER-RING TORSION ANGLES.....	S48
5. SUPERIMPOSITION OF A TRISPYRIMIDONAMIDE AND C β ATOMS OF A CANONICAL α -HELIX AT POSITIONS i , $i+4$, AND $i+7$	S49

1. OPTIMIZATION OF AMIDE COUPLING

For optimization of the amide coupling five experiments using each time another coupling reagent and a fixed combination of starting materials were carried out. HATU, HBTU, COMU, PyBop and DIC/Oxyma were chosen as coupling agents (see Table S1).

The reaction was carried out as follows: compound **5b** (0.046 g, 0.20 mmol), the corresponding lithium salt of compound **3d** (0.1 g, 0.31 mmol) and the appropriate coupling reagent (0.37 mmol) were dissolved in dimethylformamide (1 mL) and stirred for 24 hours under nitrogen atmosphere. After 1, 3, 6, 8 and 24 hours 5 μ L of the reaction mixture were diluted with 995 μ L of methanol (HPLC grade) and analysed by HPLC. A gradient elution (60:40 \rightarrow 0:100

acetate buffer (5 mmol%): acetonitrile, flow rate: 1mL/min) and a reverse phase column (C18) were chosen to analyse the reaction mixture.

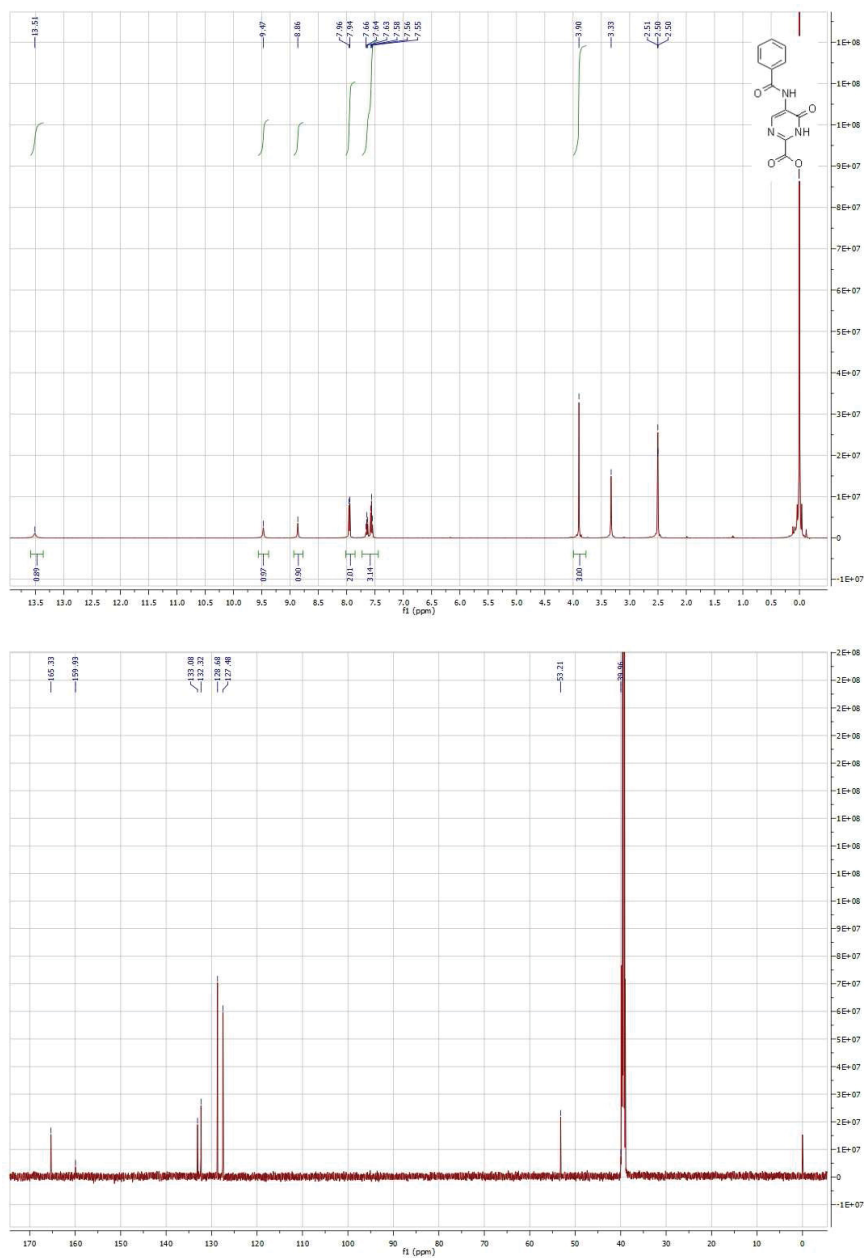
Table S1. Screening of coupling conditions.

Entry	Coupling reagent	Time ^[a]	Conversion ^[b]
1	COMU	1	92
2	COMU	3	95
3	HATU	1	74
4	HATU	24	78
5	PyBop	1	35
6	PyBop	24	44
7	HBTU	1	26
8	HBTU	24	37
9	DIC/Oxyma	1	11
10	DIC/Oxyma	24	18

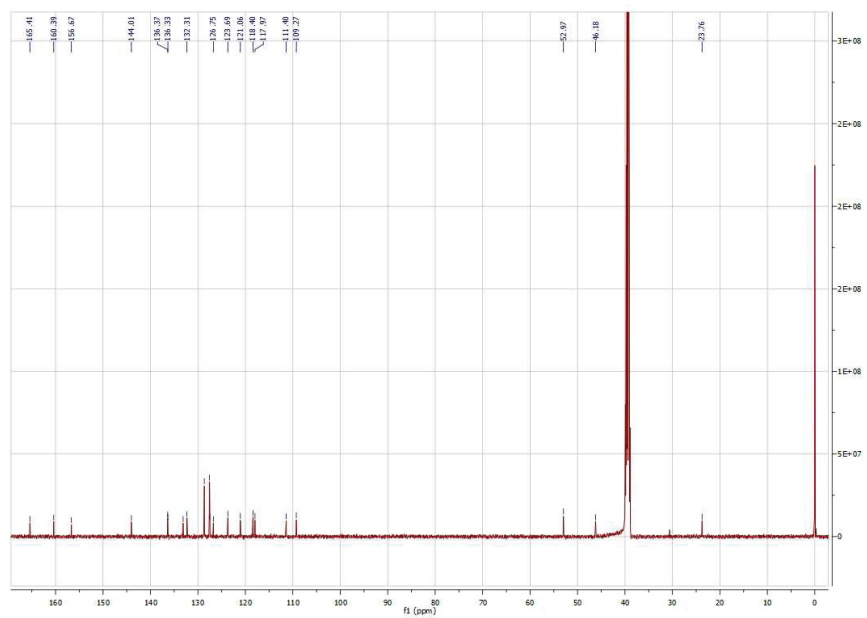
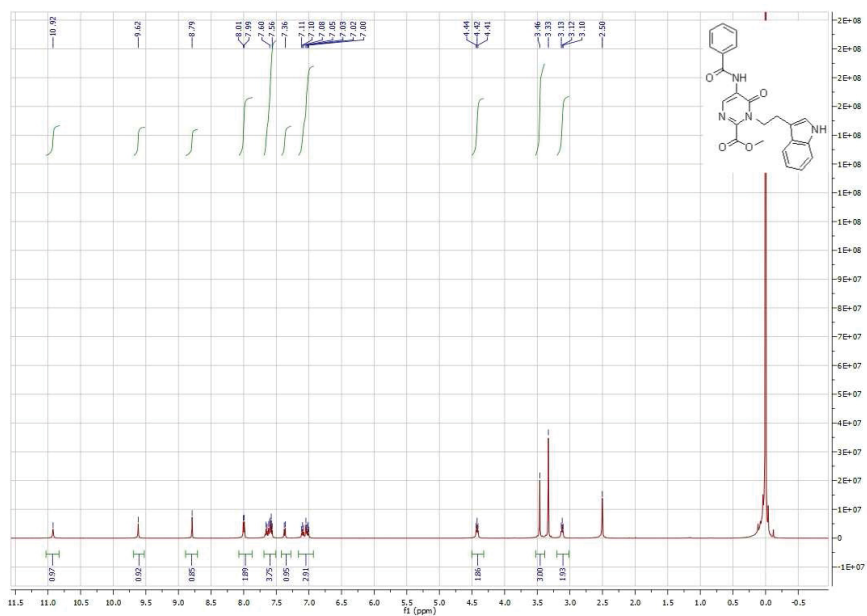
[a] Time (h) after which HPLC analysis was performed, [b] Conversion (%) was calculated as follows $[\text{Area\% [product]} / (\text{Area\% [starting material]} + \text{Area\% [product]}) * 100]$.

2. 1D AND 2D NMR-DATA

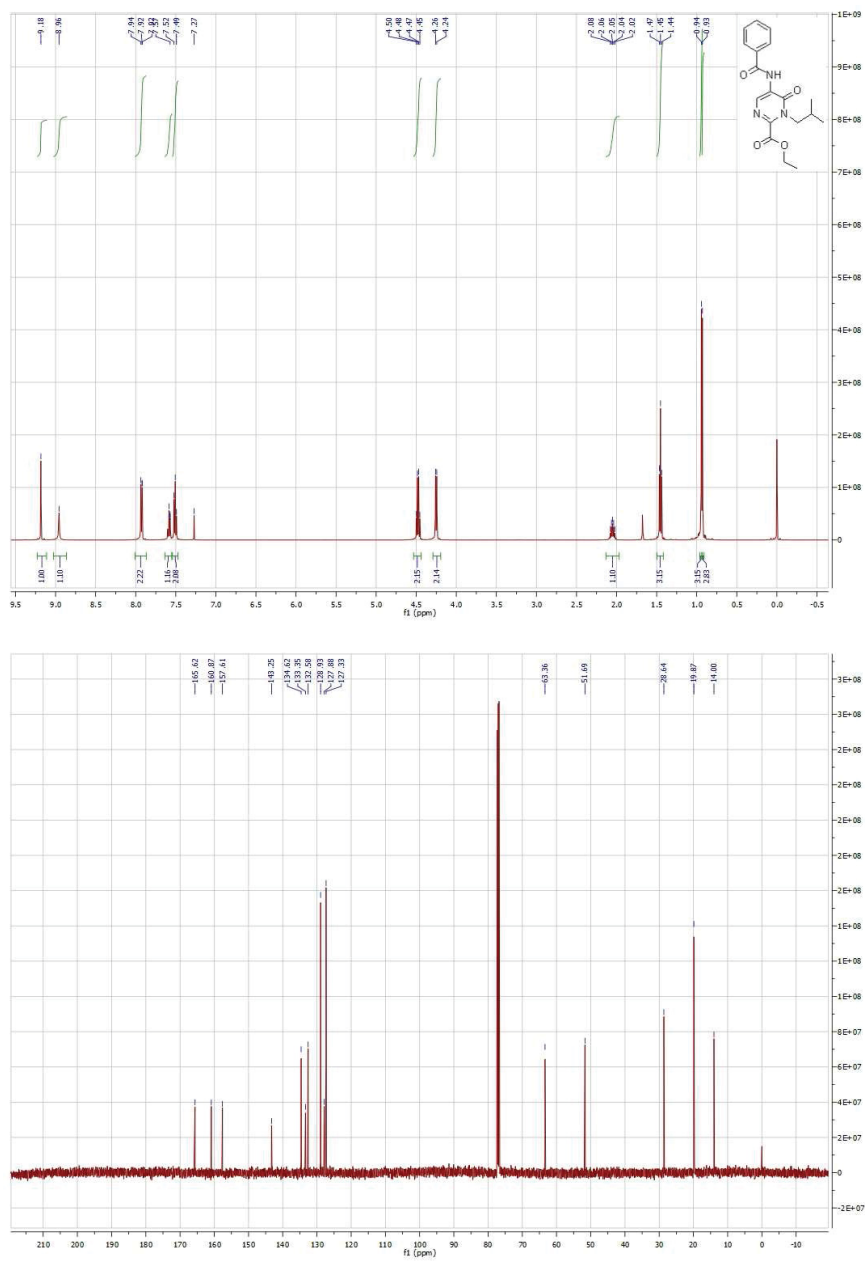
^1H -NMR and ^{13}C -NMR of Compound **3a**:



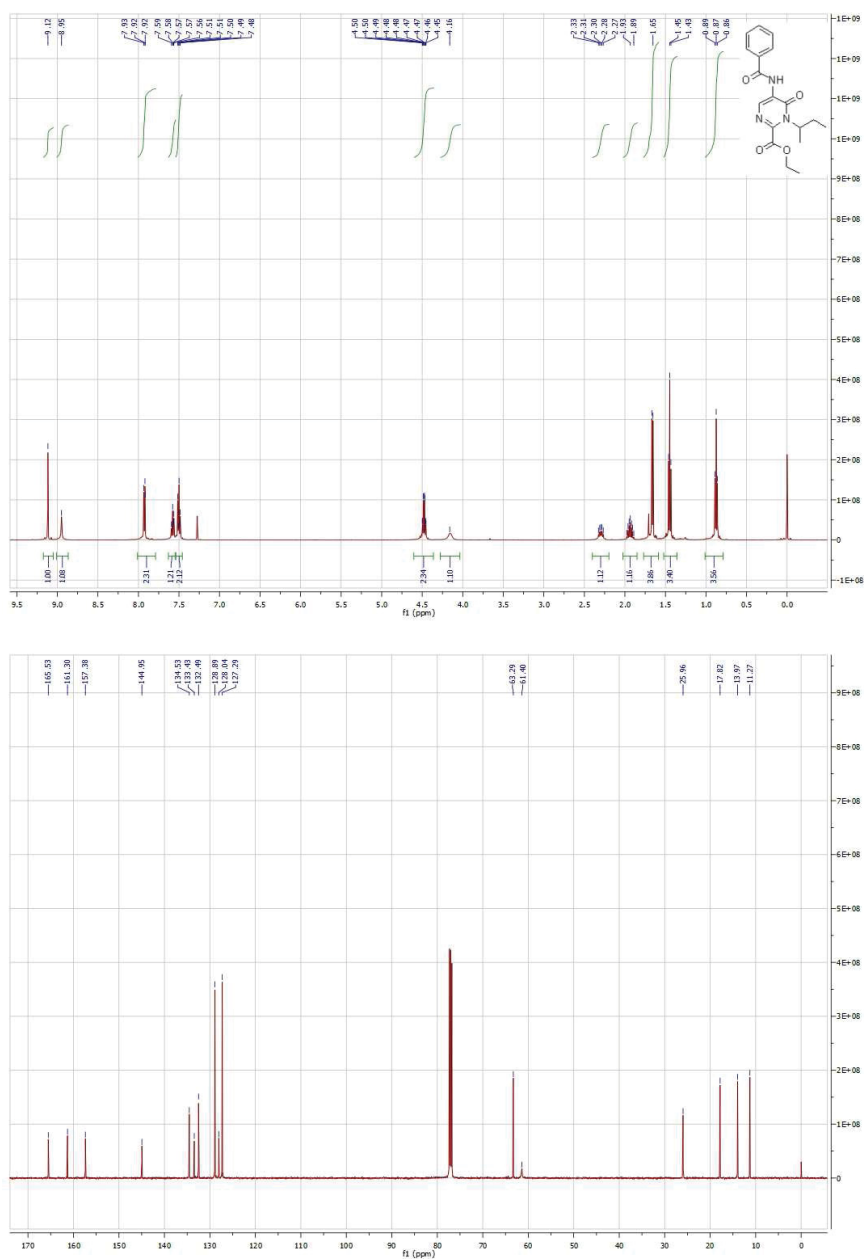
$^1\text{H-NMR}$ and $^{13}\text{C-NMR}$ of Compound **3b**:



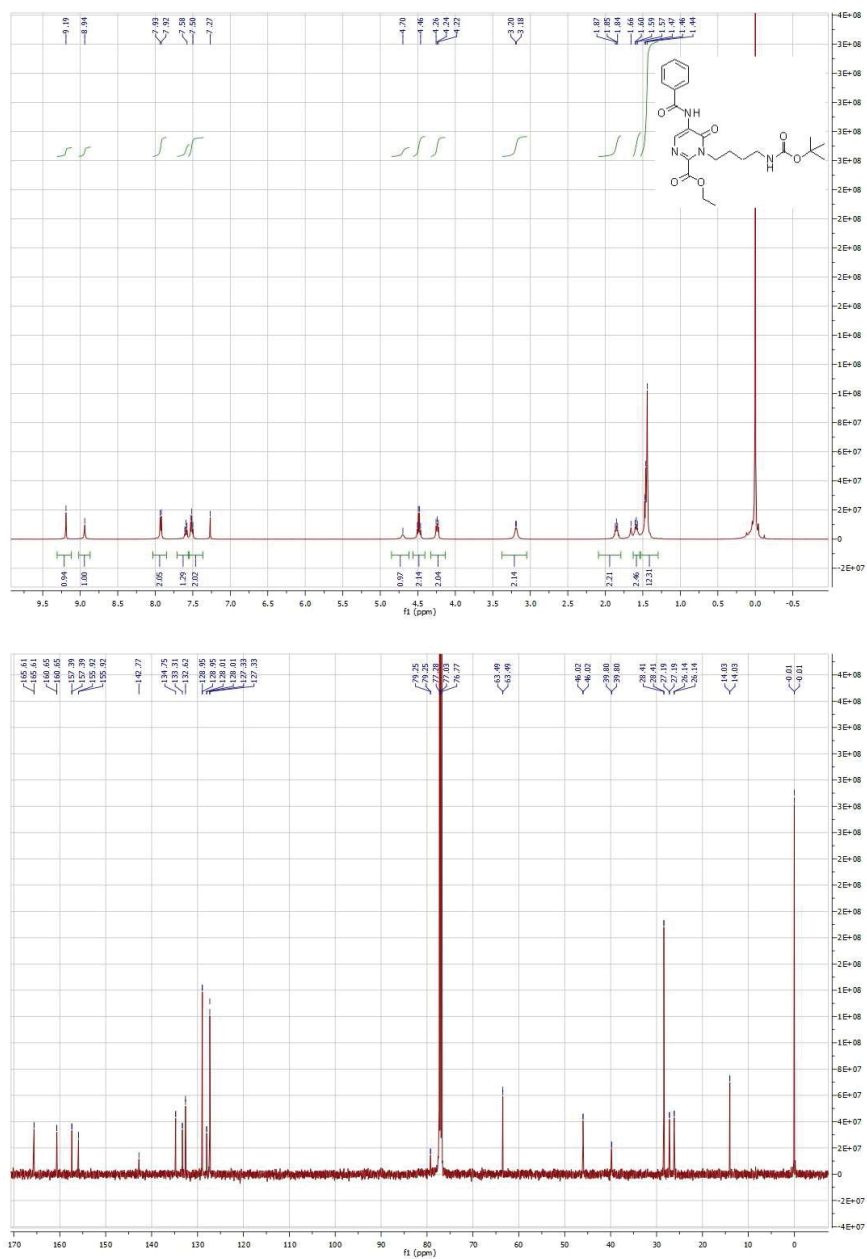
$^1\text{H-NMR}$ and $^{13}\text{C-NMR}$ of Compound **3c**:



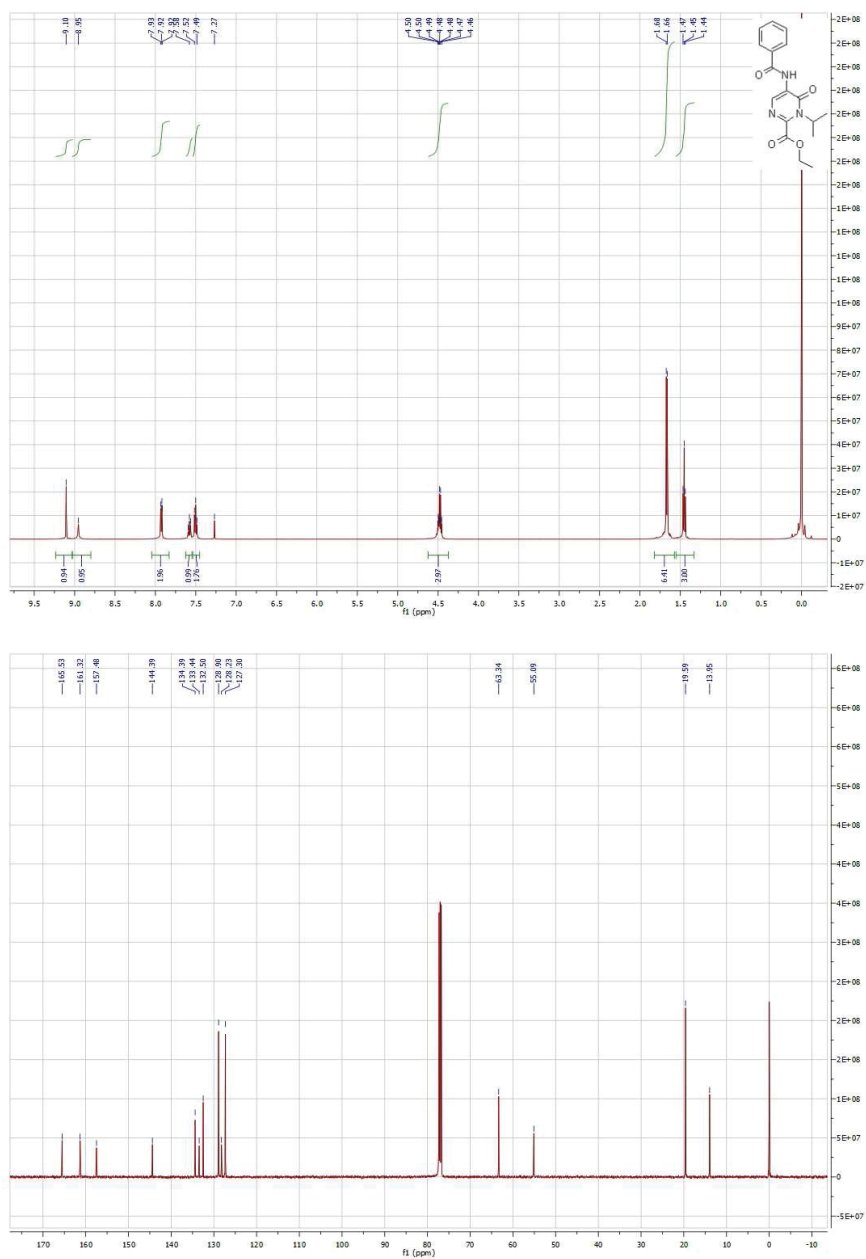
$^1\text{H-NMR}$ and $^{13}\text{C-NMR}$ of Compound **3d**:



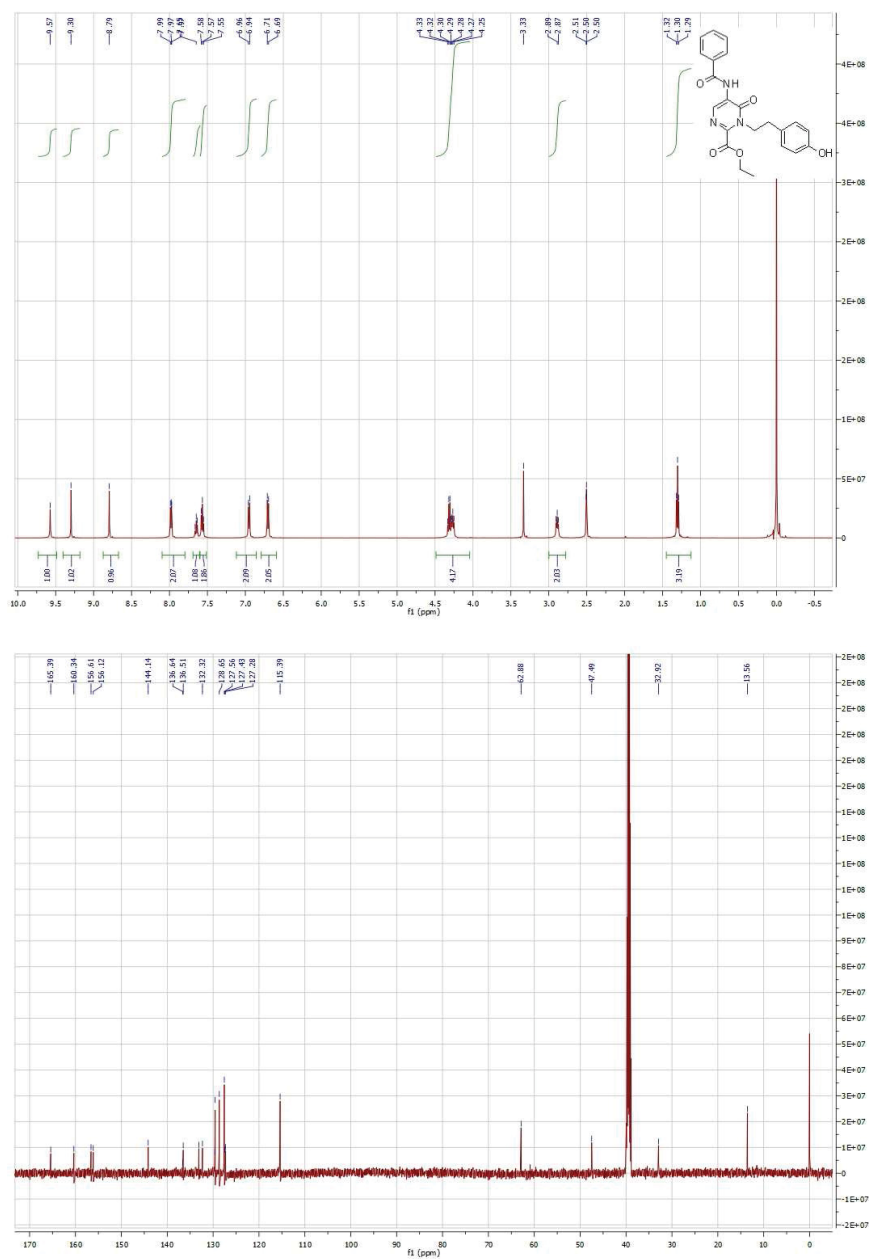
$^1\text{H-NMR}$ and $^{13}\text{C-NMR}$ of Compound **3e**:



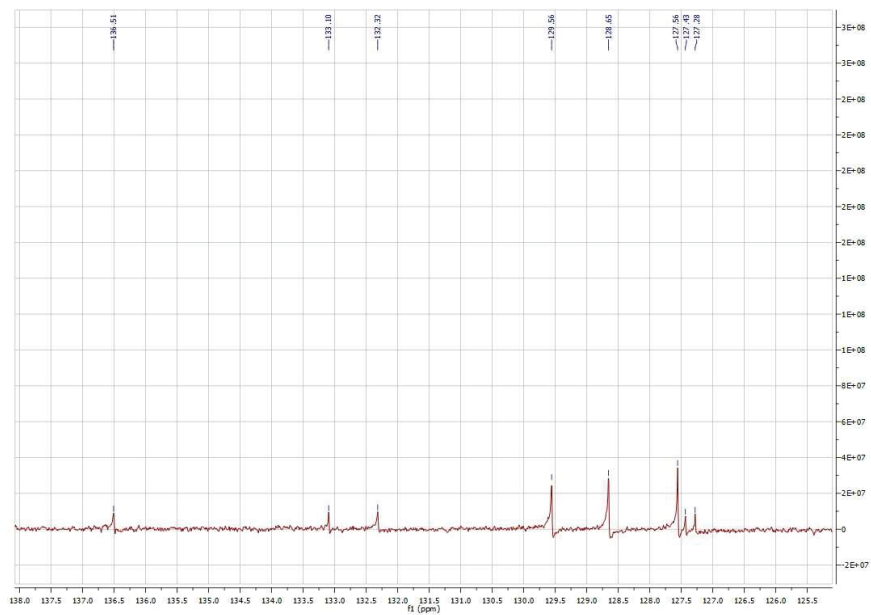
$^1\text{H-NMR}$ and $^{13}\text{C-NMR}$ of Compound **3f**:



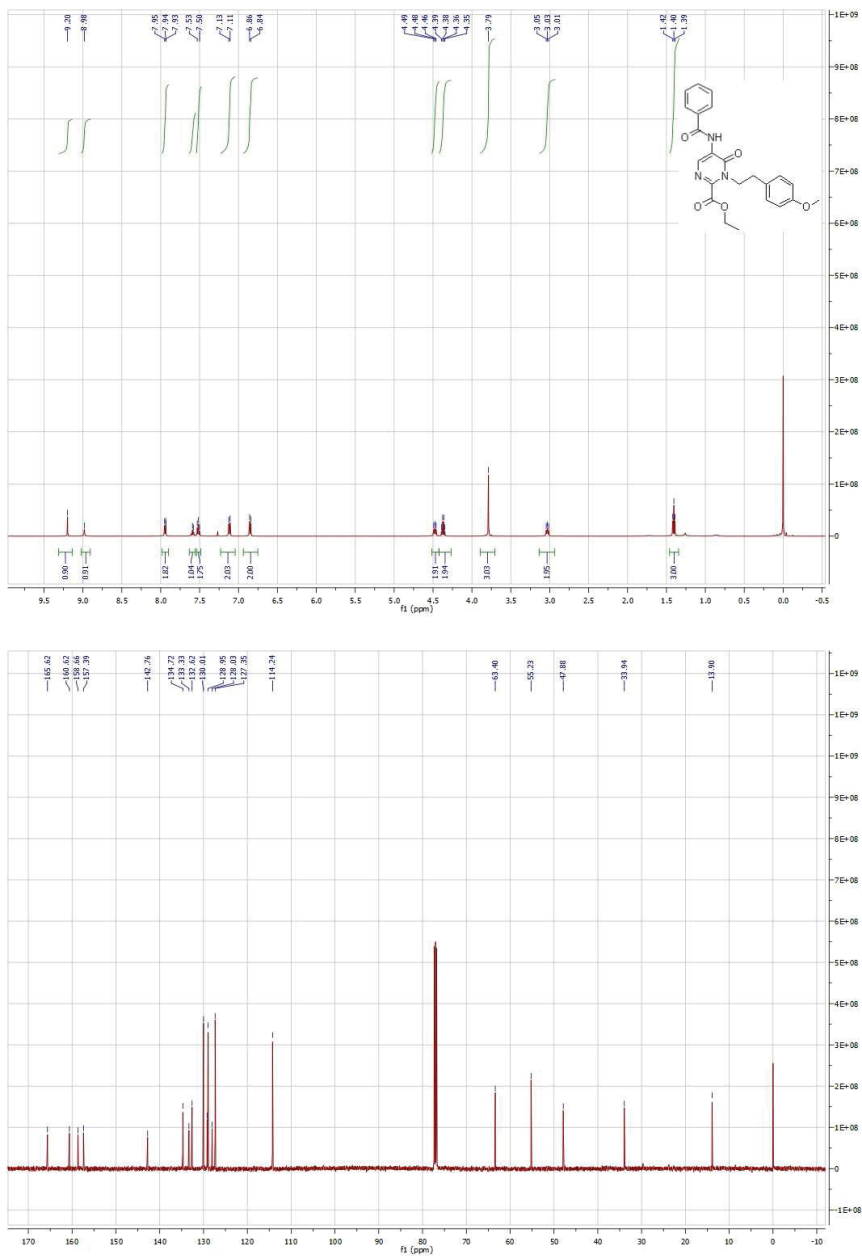
$^1\text{H-NMR}$ and $^{13}\text{C-NMR}$ of Compound **3g**:



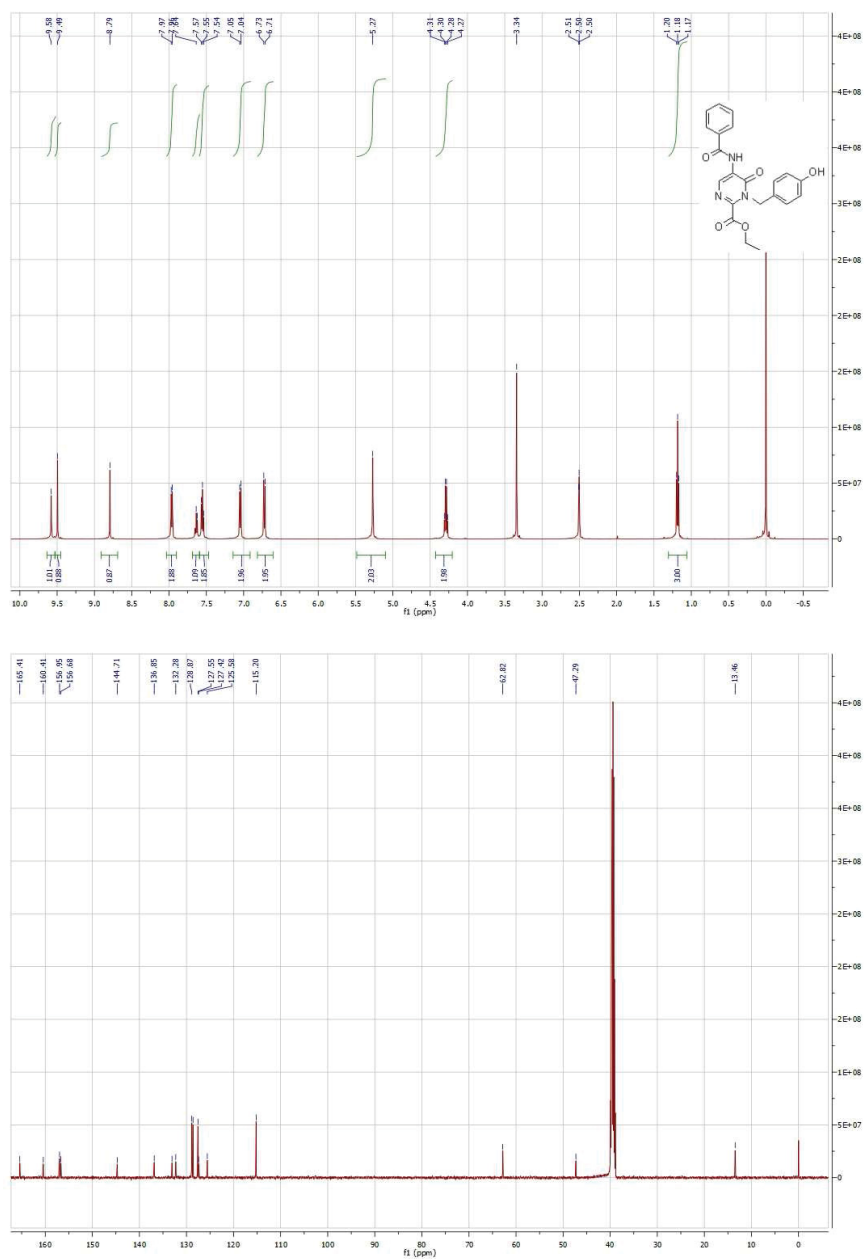
Expansion of the ^{13}C NMR spectrum of **3g**



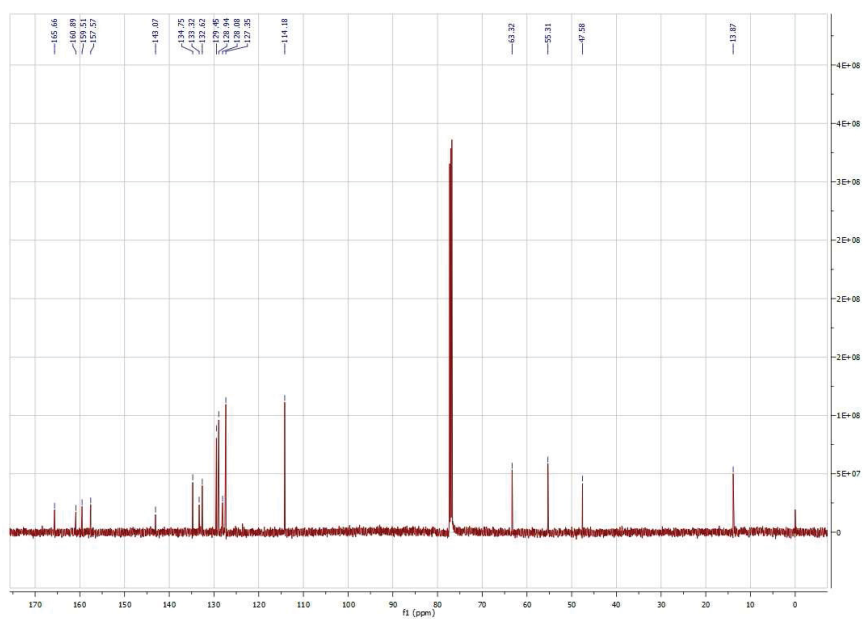
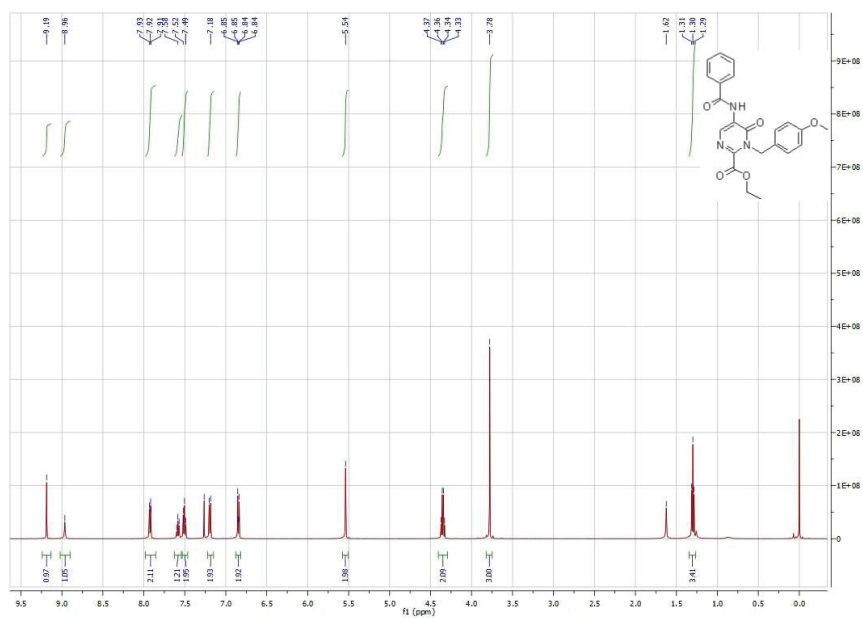
$^1\text{H-NMR}$ and $^{13}\text{C-NMR}$ of Compound **3h**:



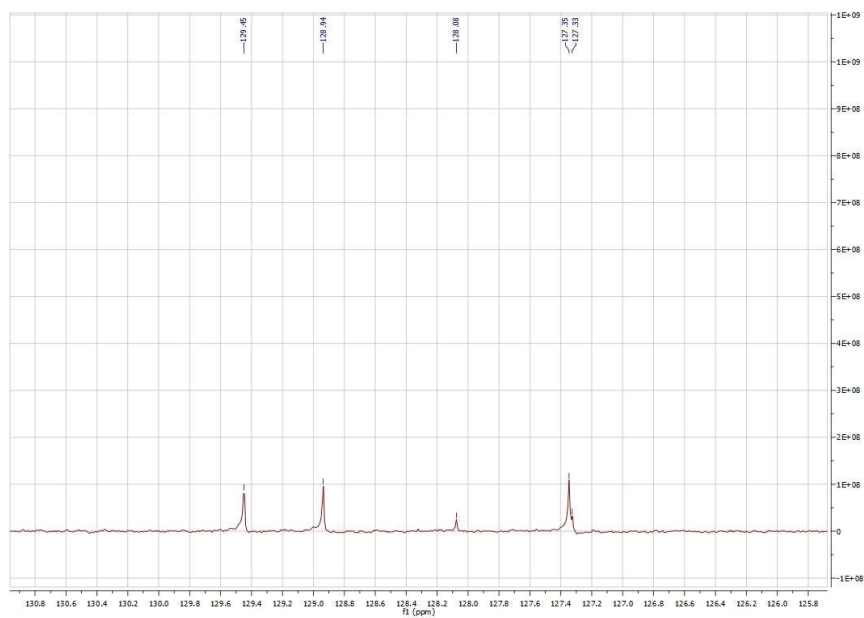
$^1\text{H-NMR}$ and $^{13}\text{C-NMR}$ of Compound **3i**:



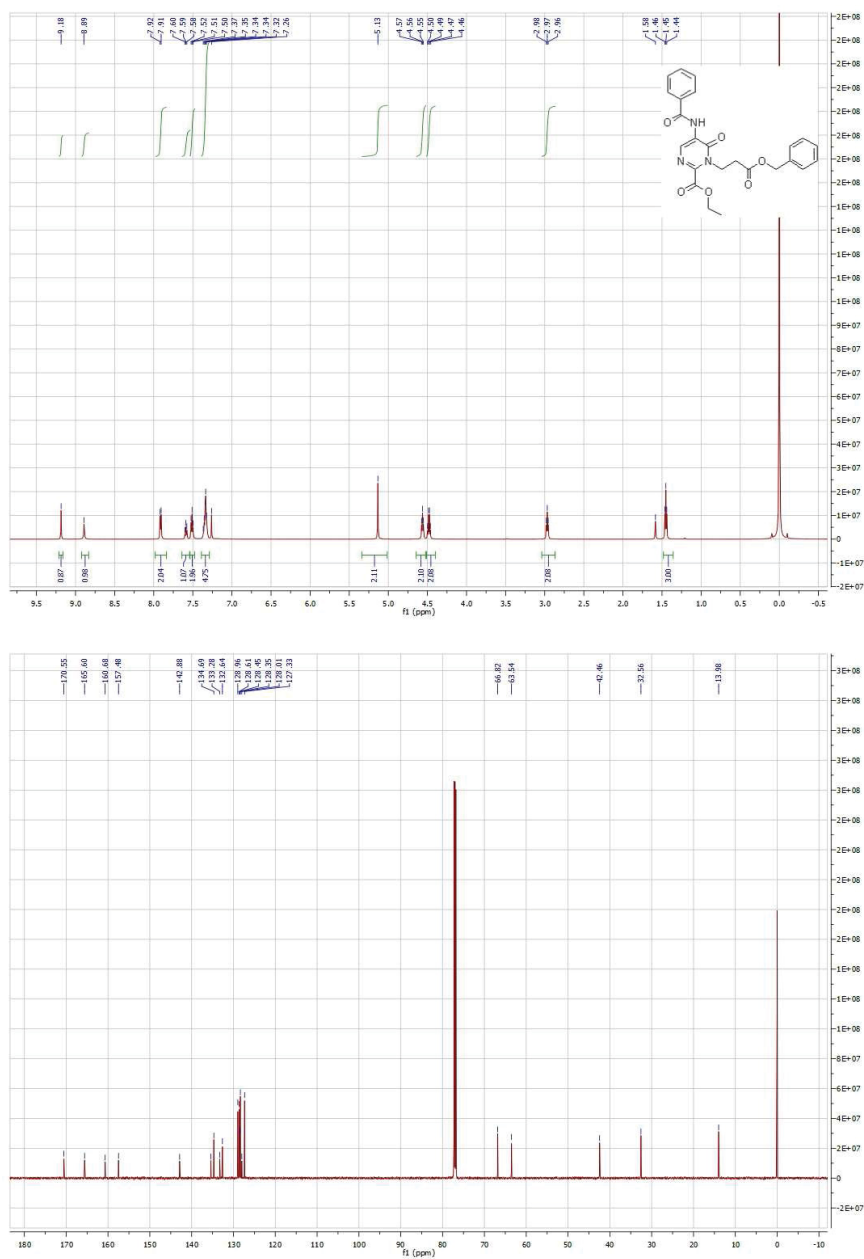
$^1\text{H-NMR}$ and $^{13}\text{C-NMR}$ of Compound **3j**:



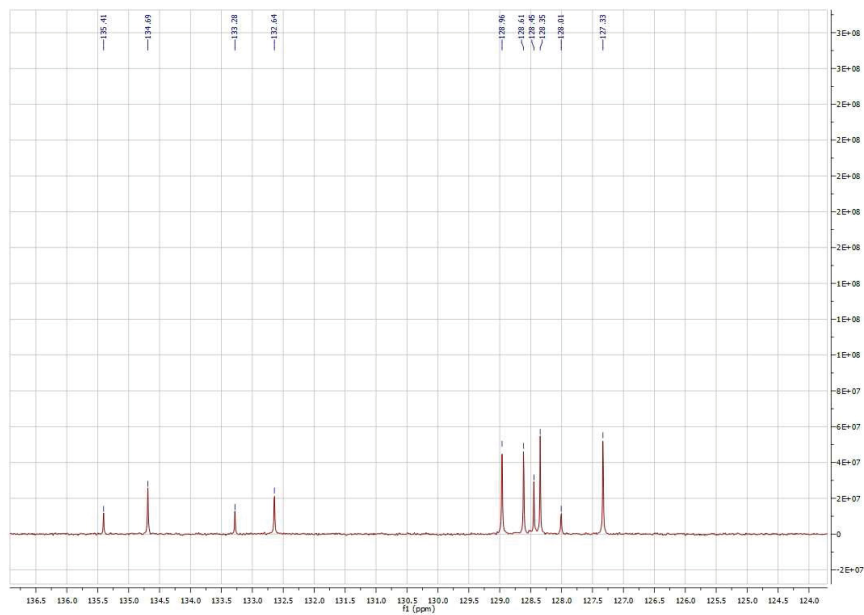
Expansion of the ^{13}C NMR spectrum of **3j**



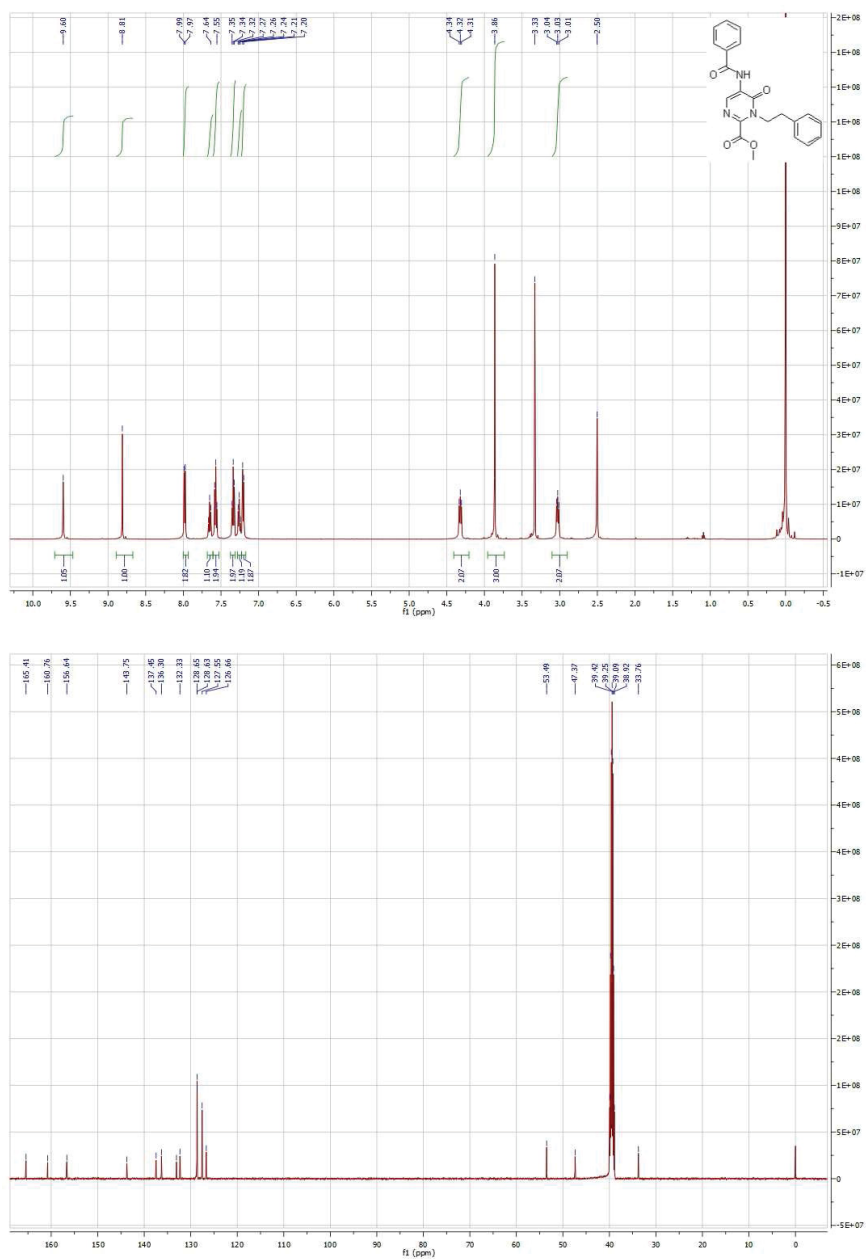
$^1\text{H-NMR}$ and $^{13}\text{C-NMR}$ of Compound **3k**:



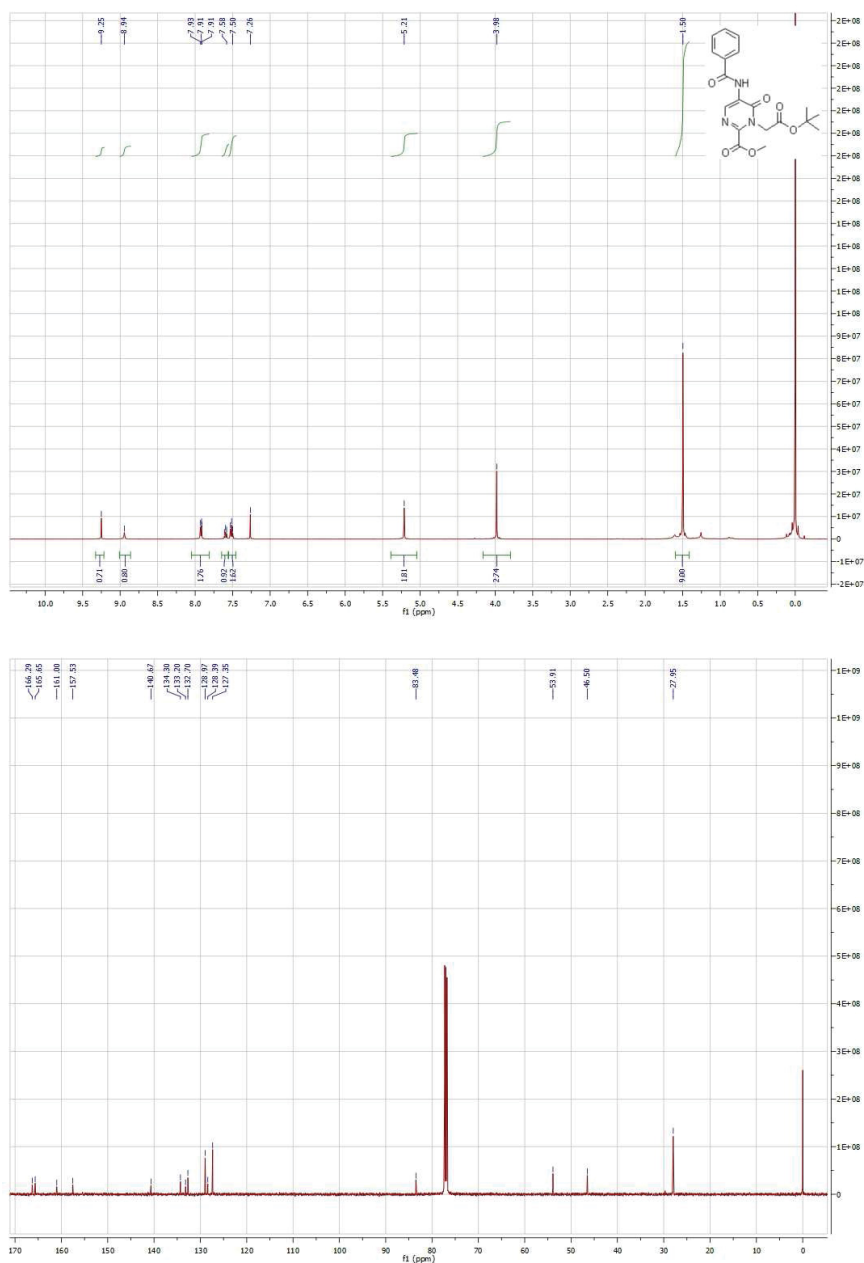
Expansion of the ^{13}C NMR spectrum of **3k**



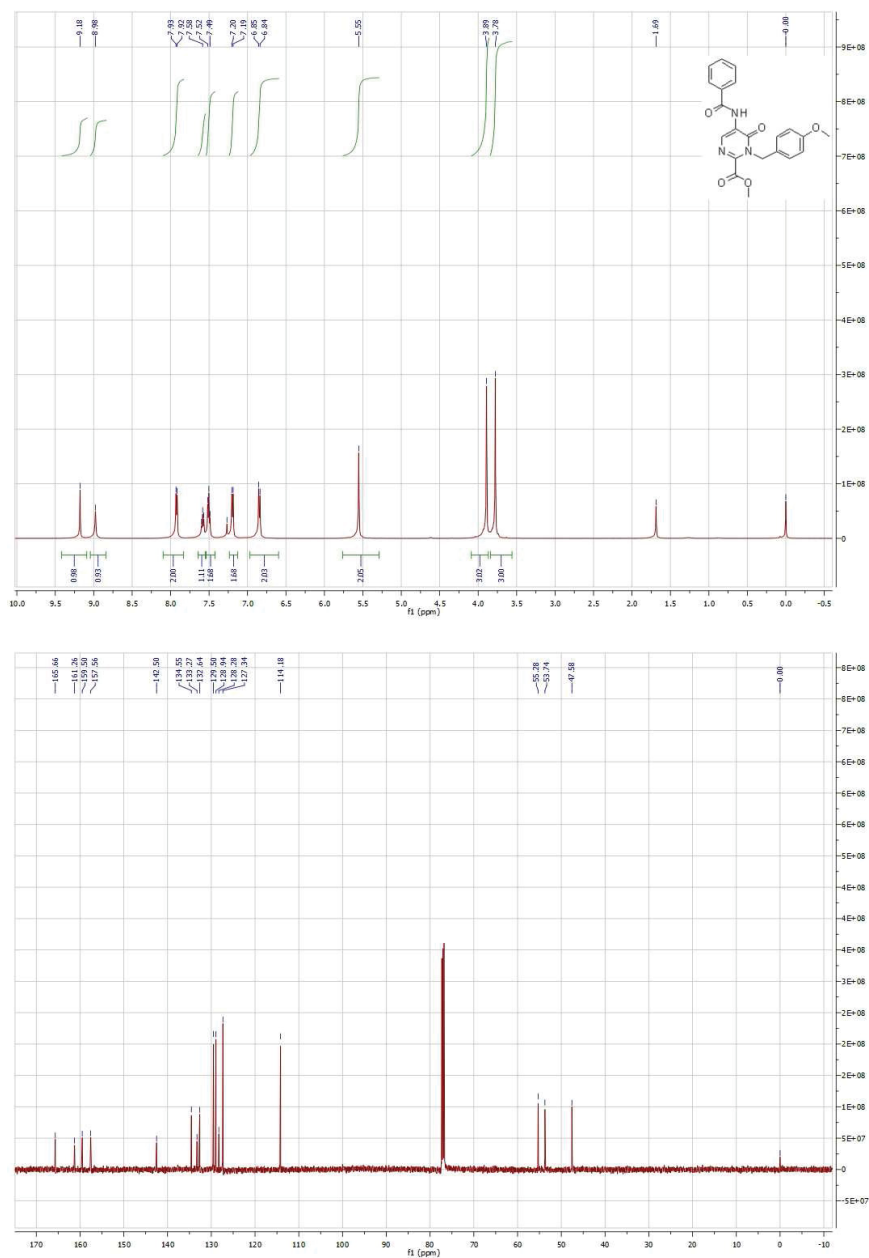
$^1\text{H-NMR}$ and $^{13}\text{C-NMR}$ of Compound **31**:



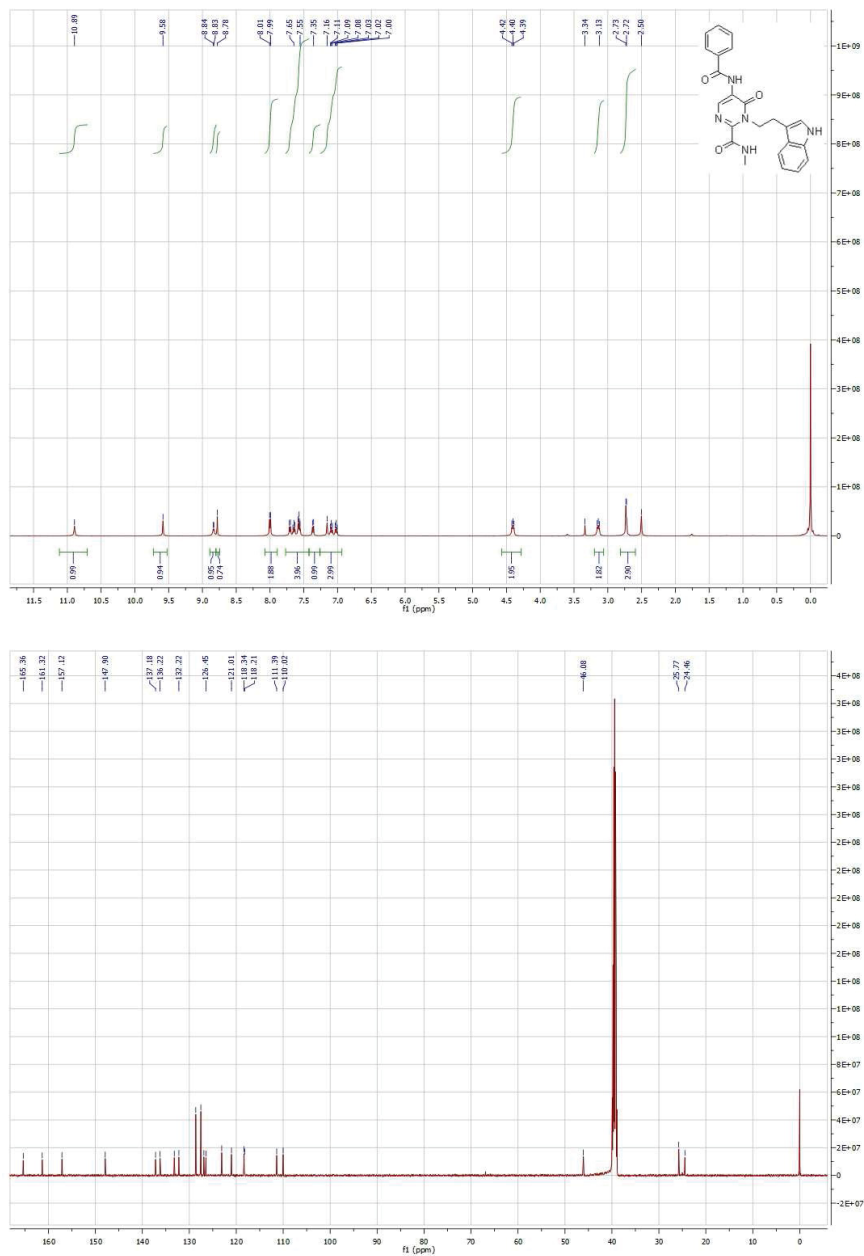
$^1\text{H-NMR}$ and $^{13}\text{C-NMR}$ of Compound **3m**:



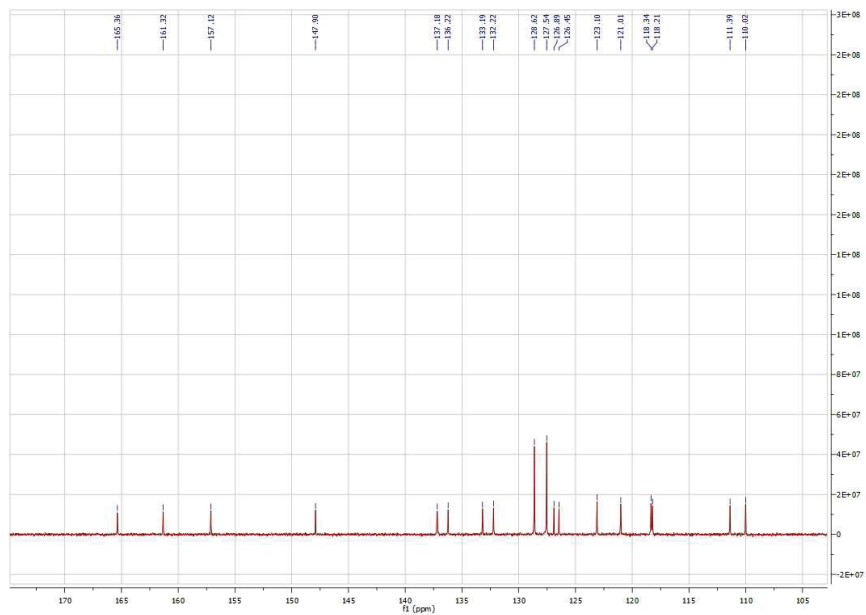
$^1\text{H-NMR}$ and $^{13}\text{C-NMR}$ of Compound **3n**:



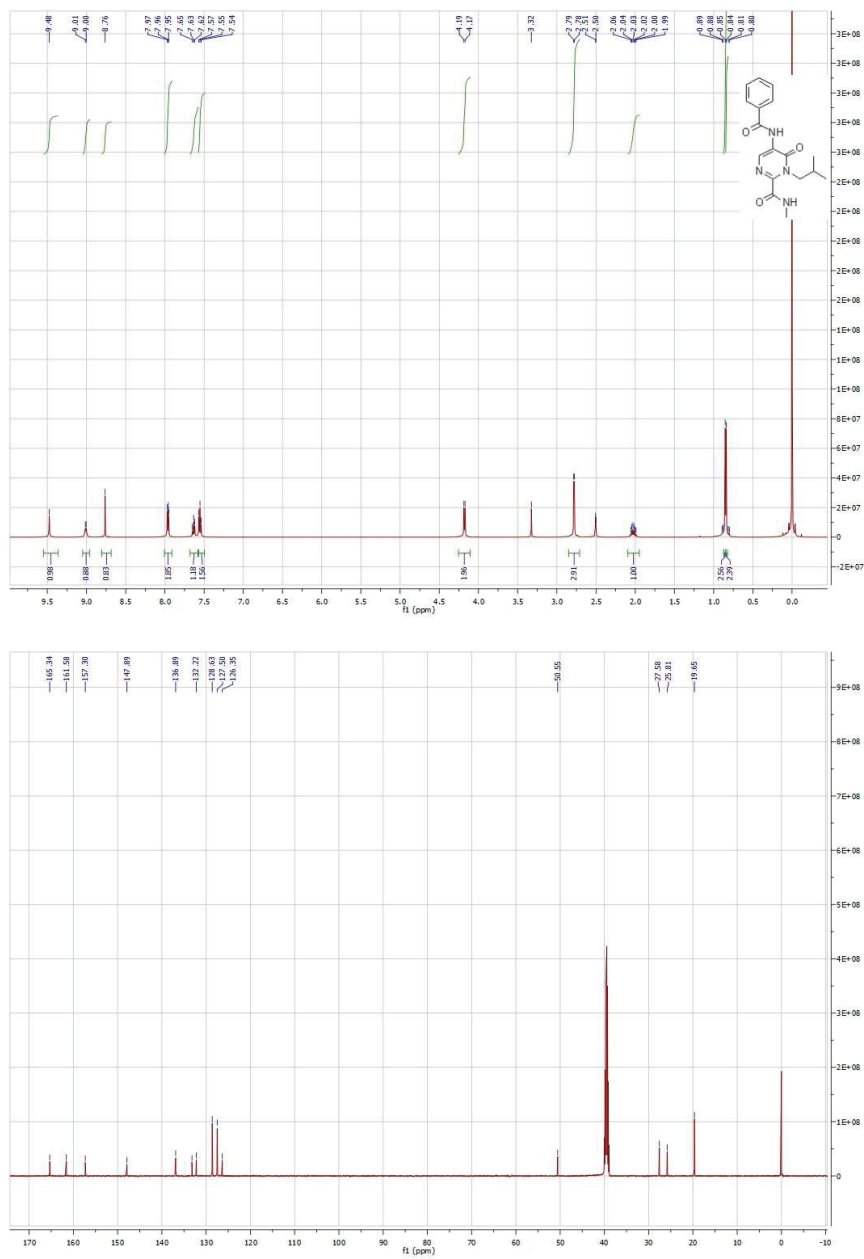
$^1\text{H-NMR}$ and $^{13}\text{C-NMR}$ of Compound 4a:



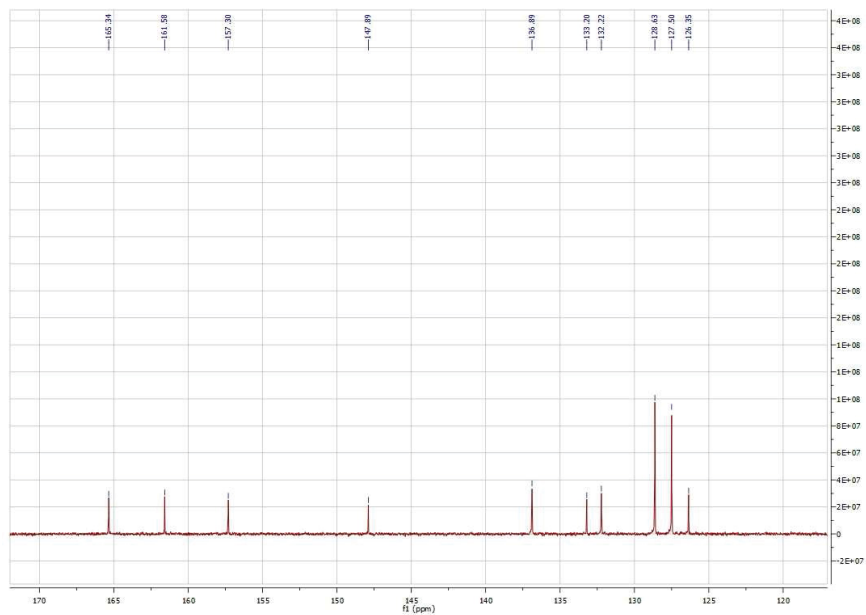
Expansion of the ^{13}C NMR spectrum of **4a**



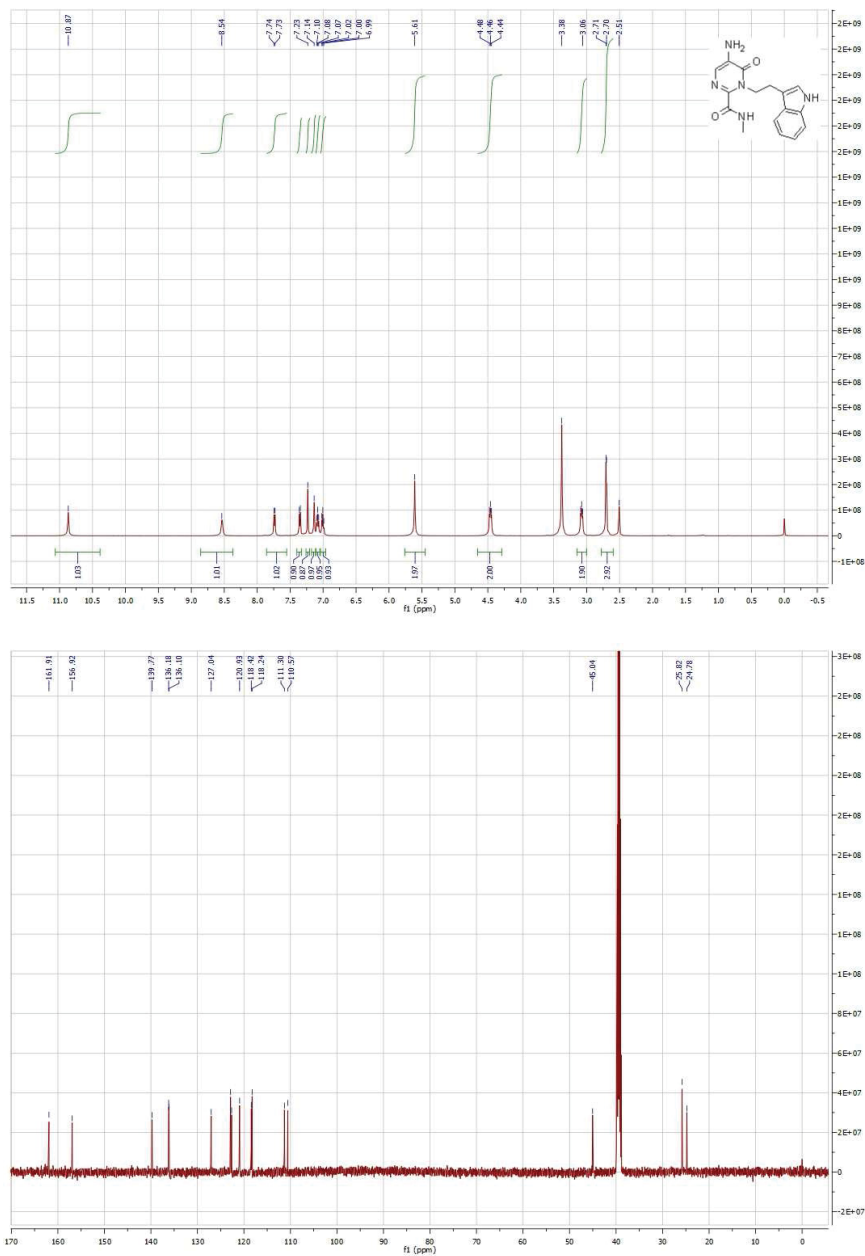
$^1\text{H-NMR}$ and $^{13}\text{C-NMR}$ of Compound **4b**:



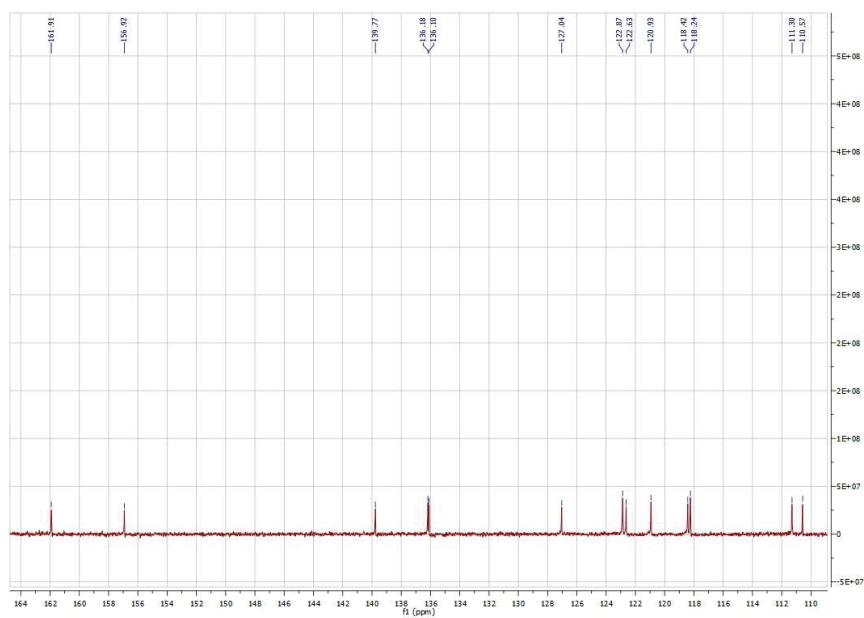
Expansion of the ^{13}C NMR spectrum of **4b**



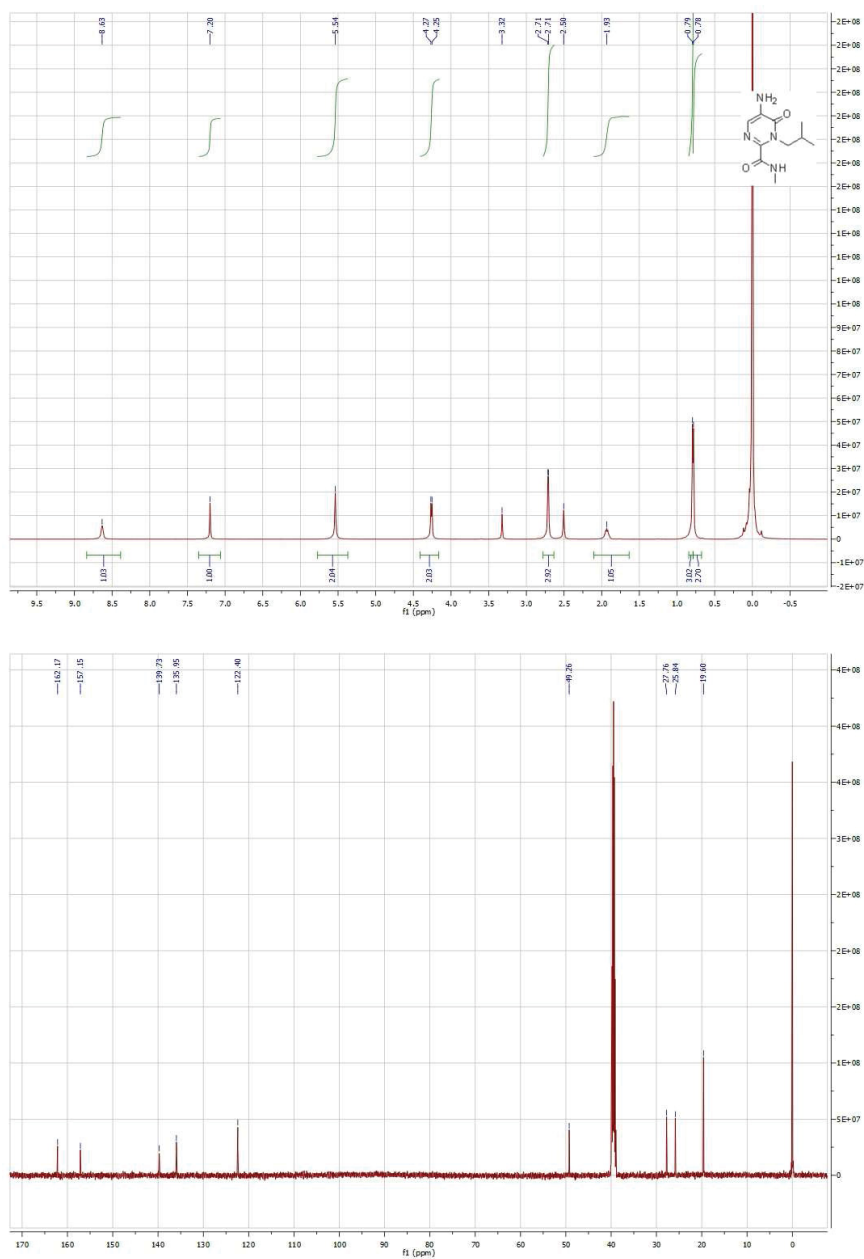
$^1\text{H-NMR}$ and $^{13}\text{C-NMR}$ of Compound 5a:



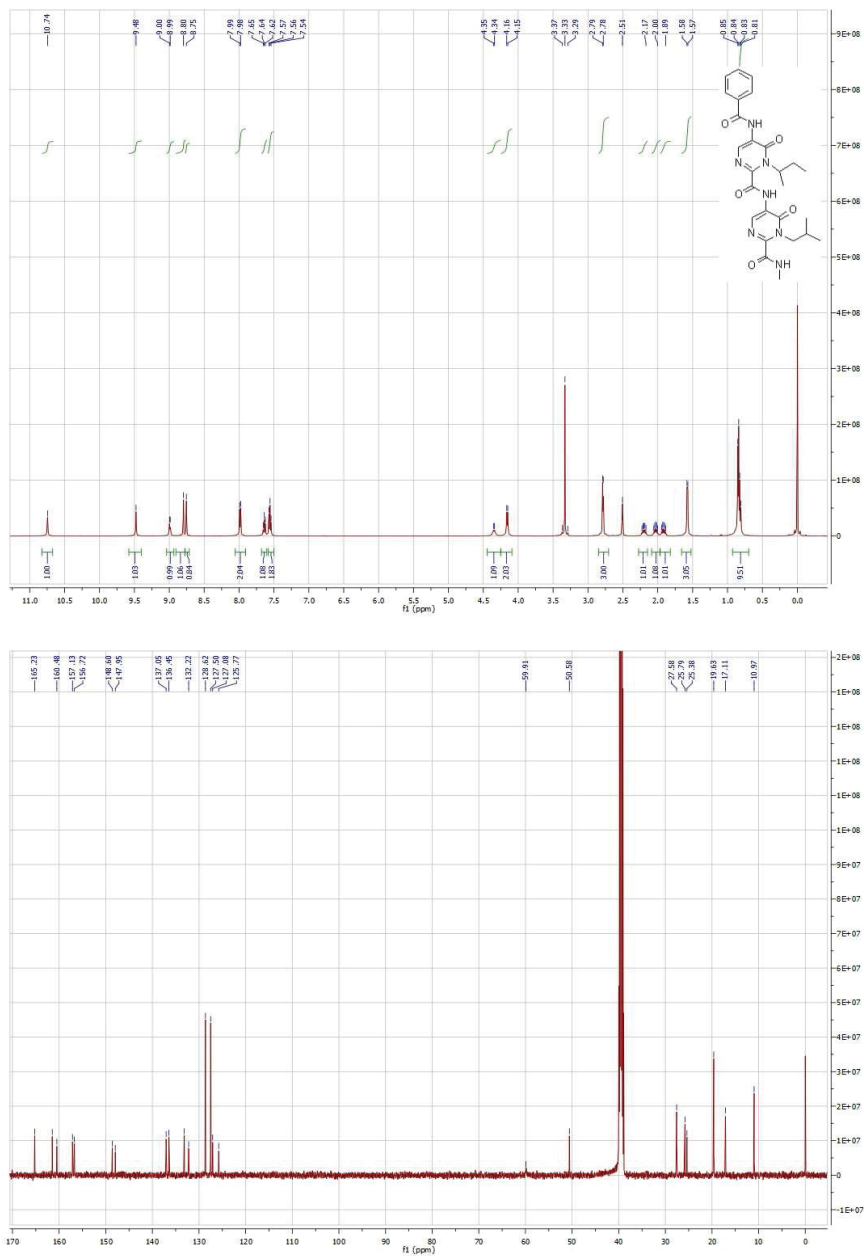
Expansion of the ^{13}C NMR spectrum of **5a**



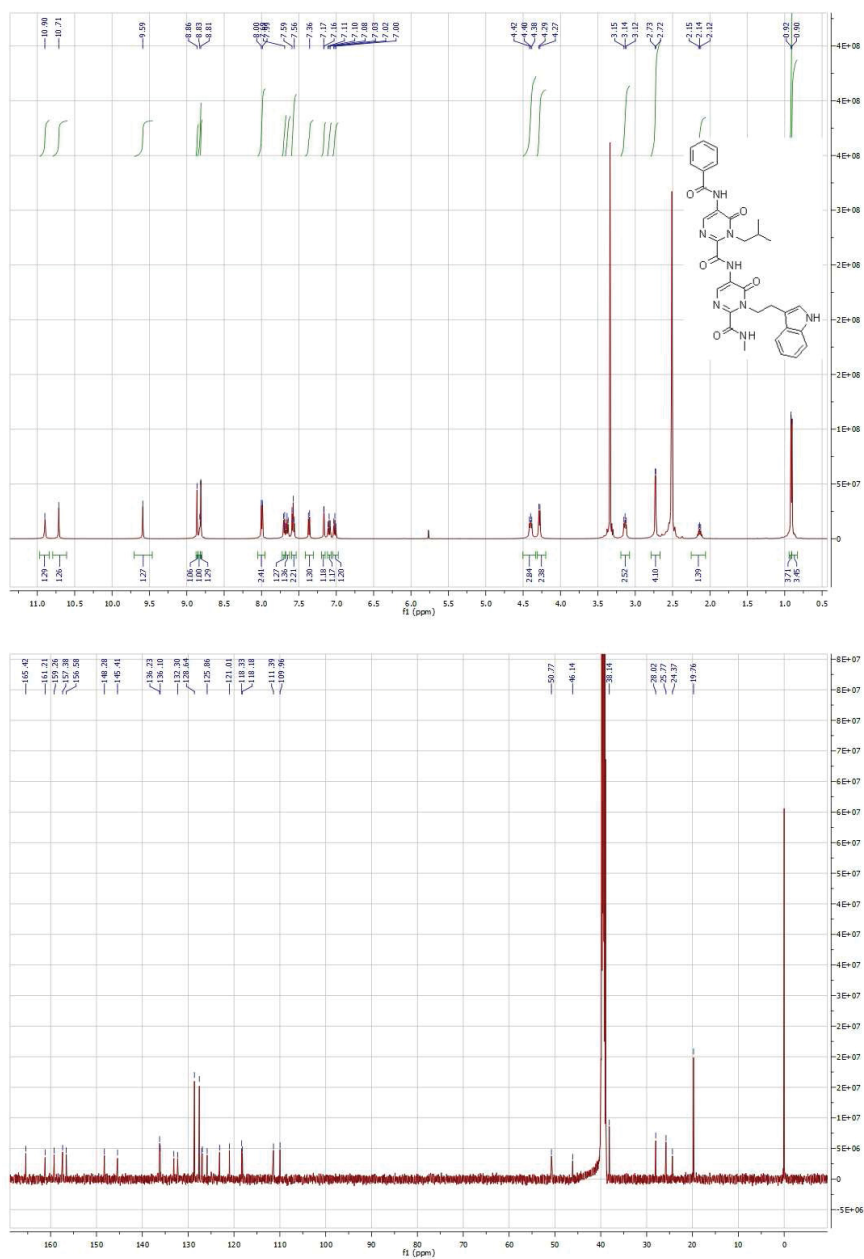
$^1\text{H-NMR}$ and $^{13}\text{C-NMR}$ of Compound **5b**:



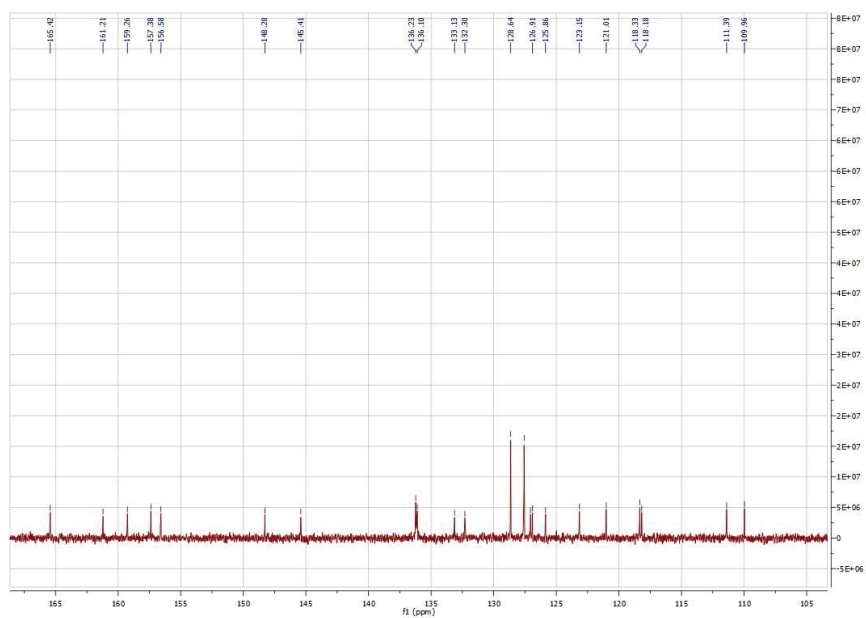
$^1\text{H-NMR}$ and $^{13}\text{C-NMR}$ of Compound **6a**:



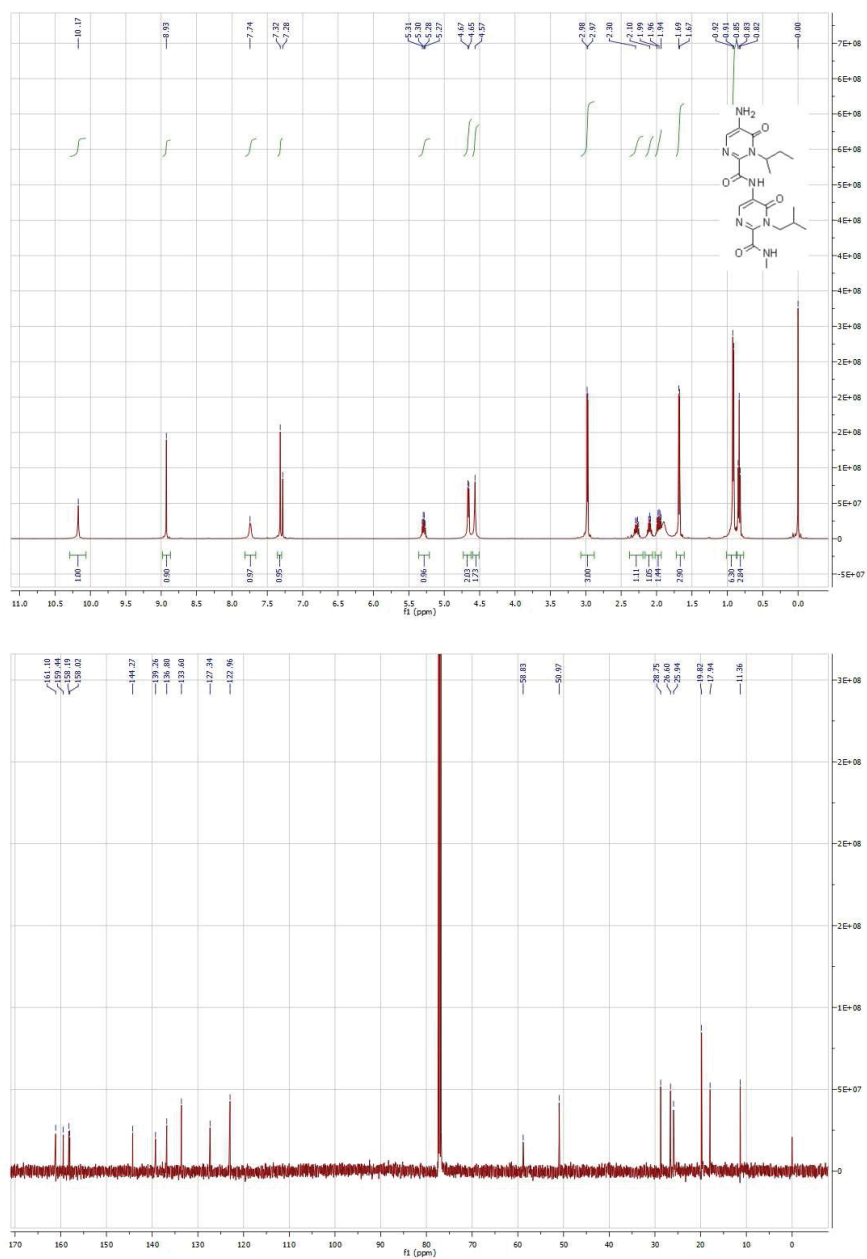
$^1\text{H-NMR}$ and $^{13}\text{C-NMR}$ of Compound **6b**:



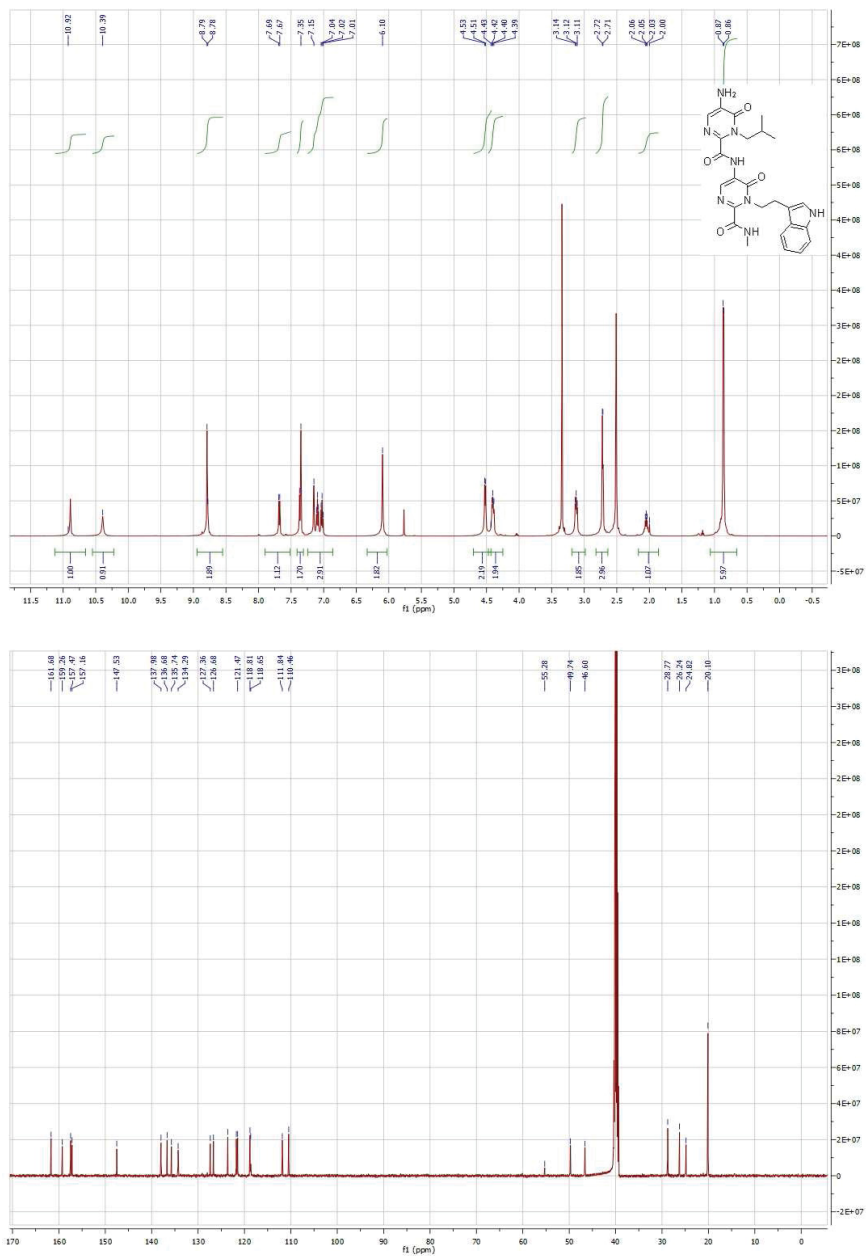
Expansion of the ^{13}C NMR spectrum of **6b**



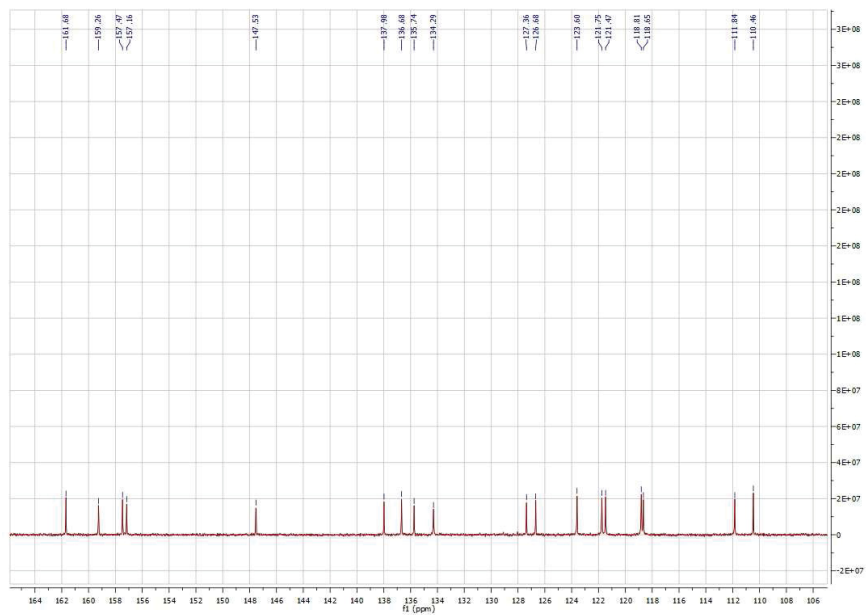
$^1\text{H-NMR}$ and $^{13}\text{C-NMR}$ of Compound 7a:



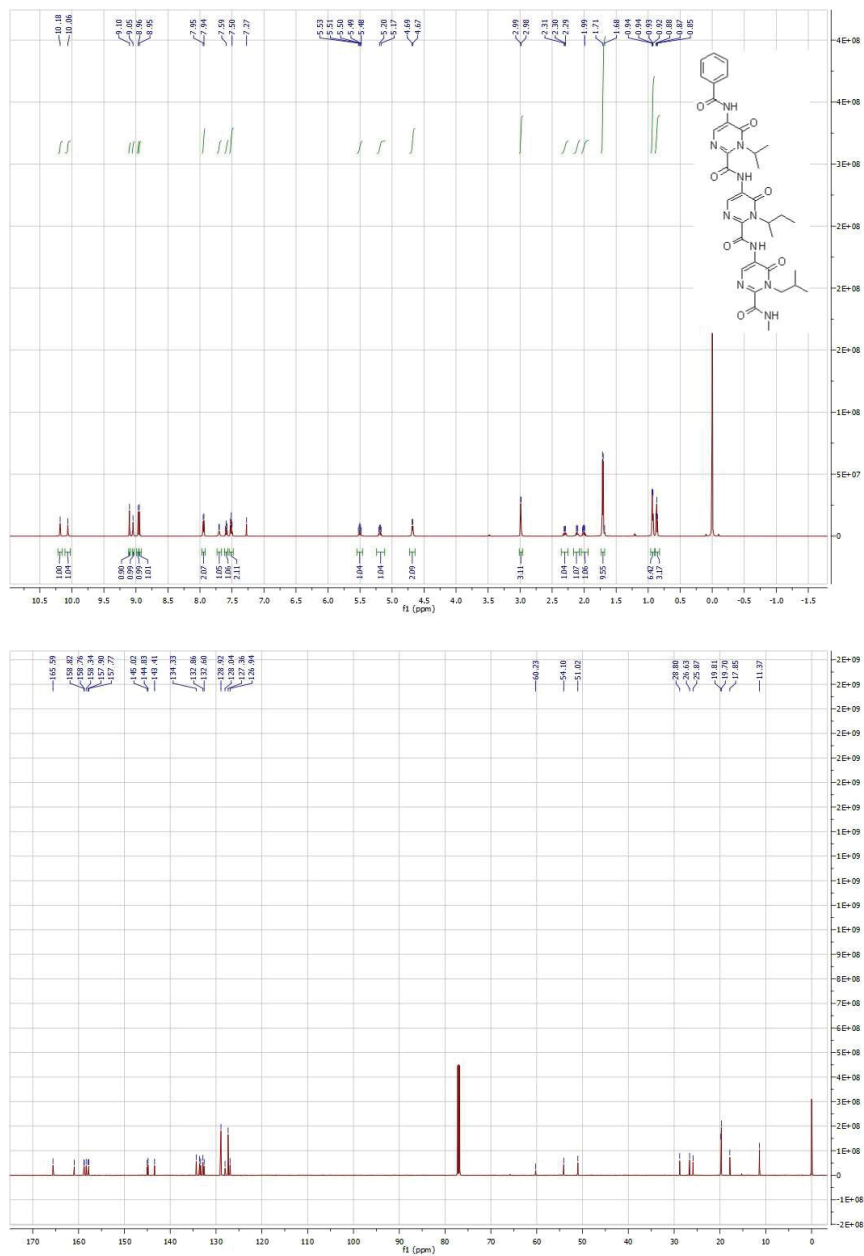
$^1\text{H-NMR}$ and $^{13}\text{C-NMR}$ of Compound **7b**:



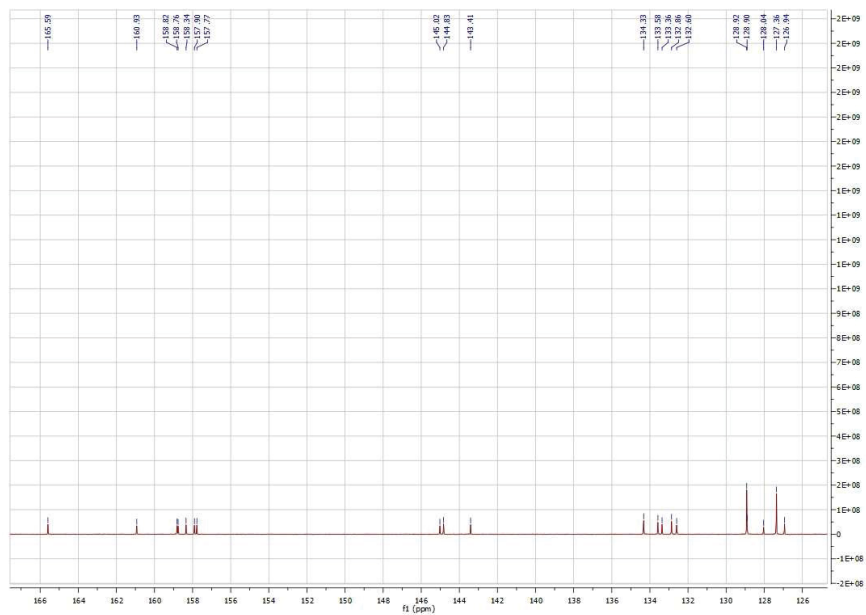
Expansion of the ^{13}C NMR spectrum of **7b**



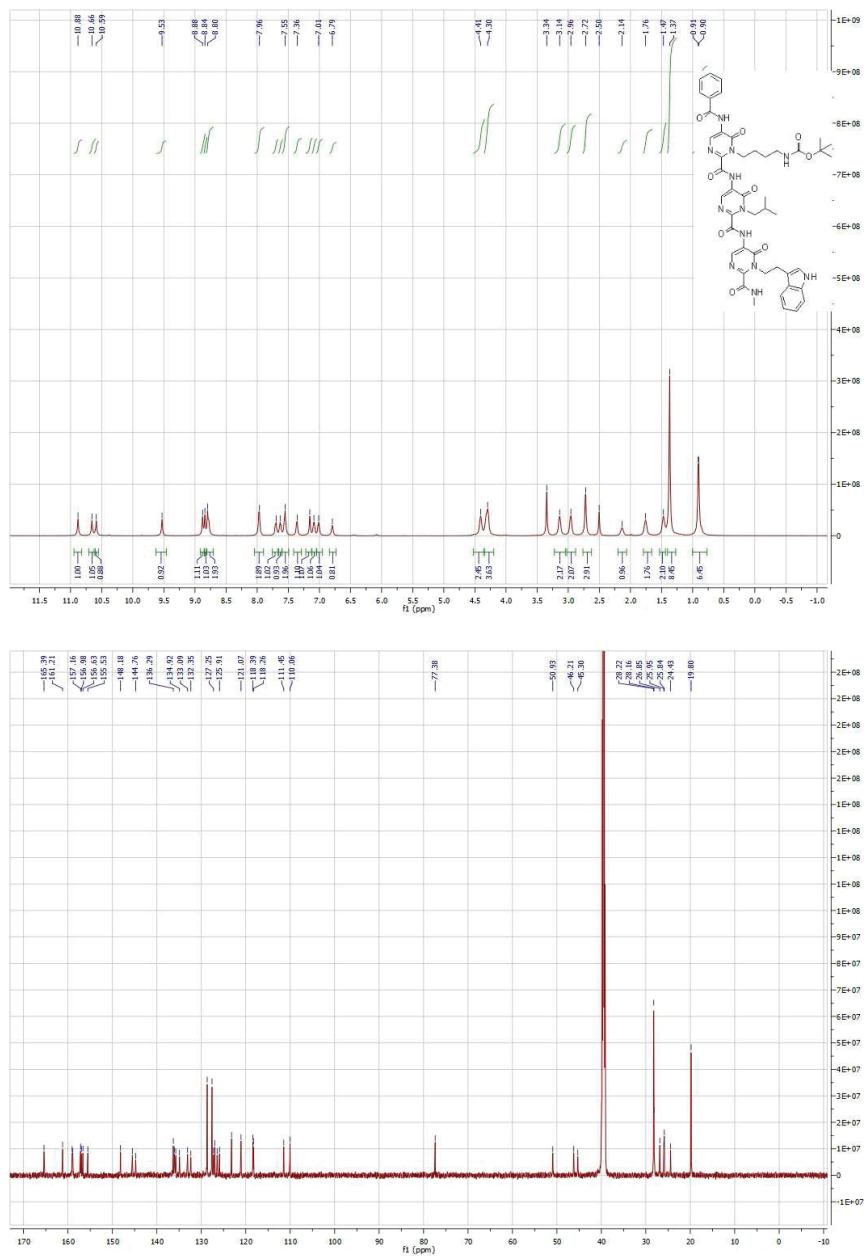
$^1\text{H-NMR}$ and $^{13}\text{C-NMR}$ of Compound **8a**:



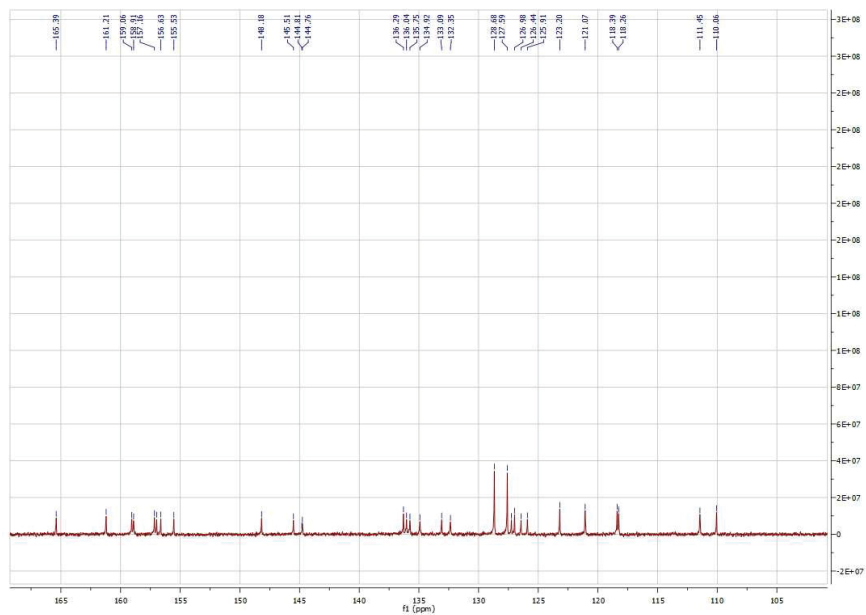
Expansion of the ^{13}C NMR spectrum of **8a**



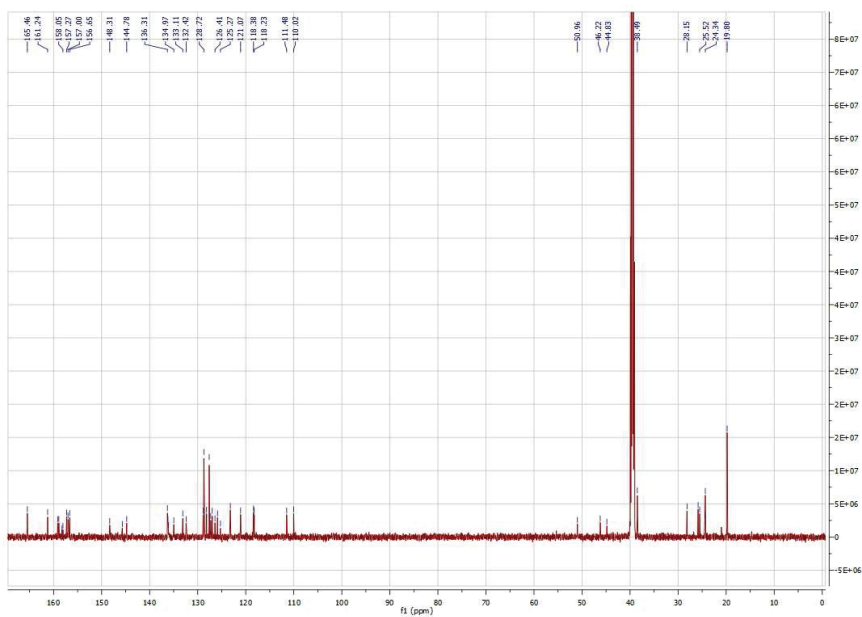
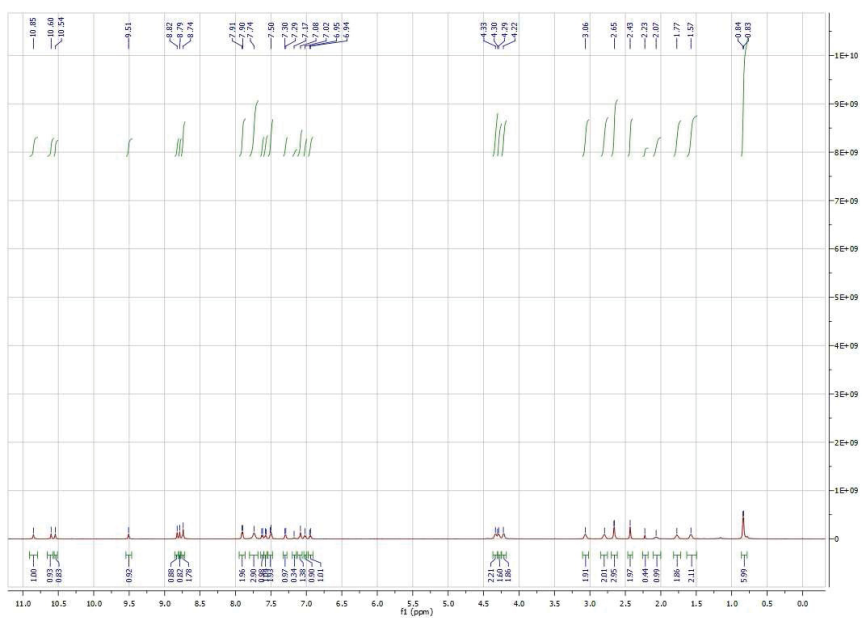
$^1\text{H-NMR}$ and $^{13}\text{C-NMR}$ of Compound **8b**:



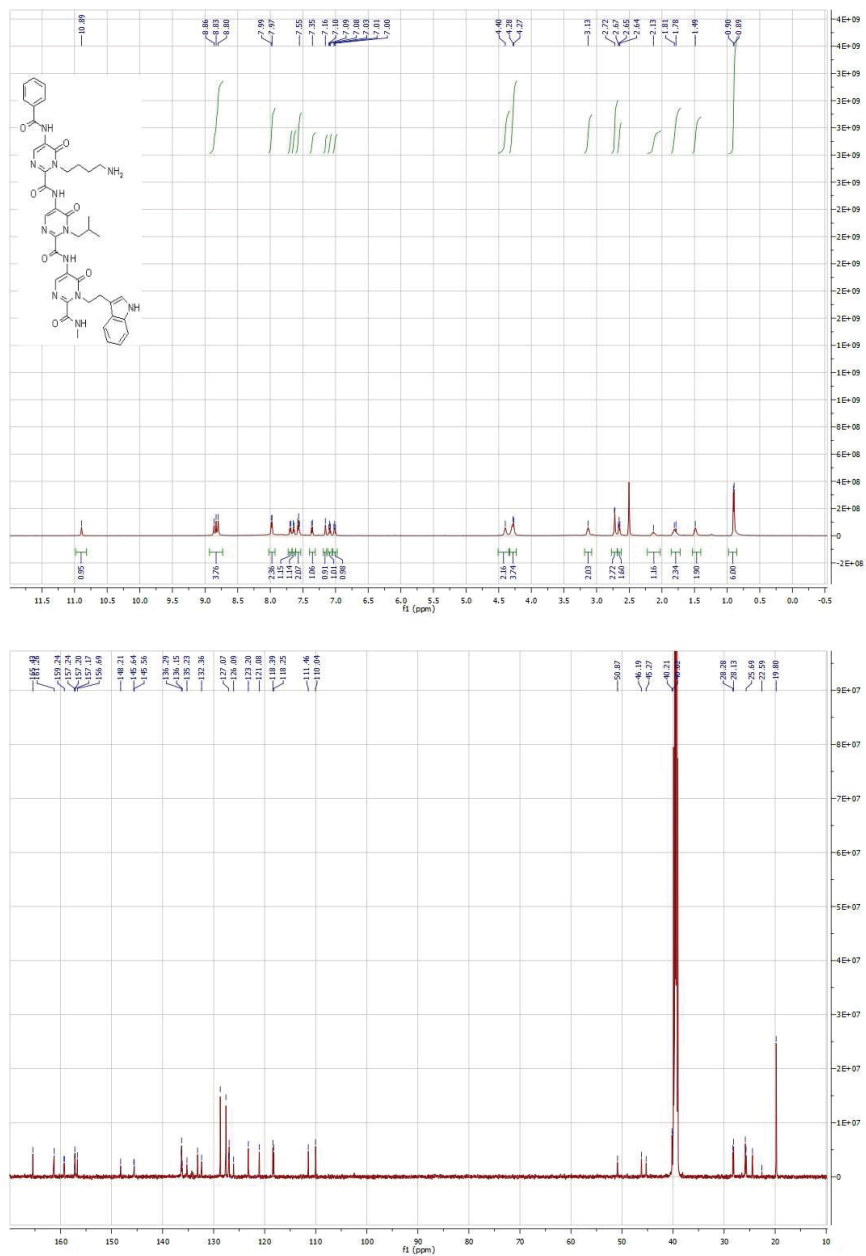
Expansion of the ^{13}C NMR spectrum of **8b**



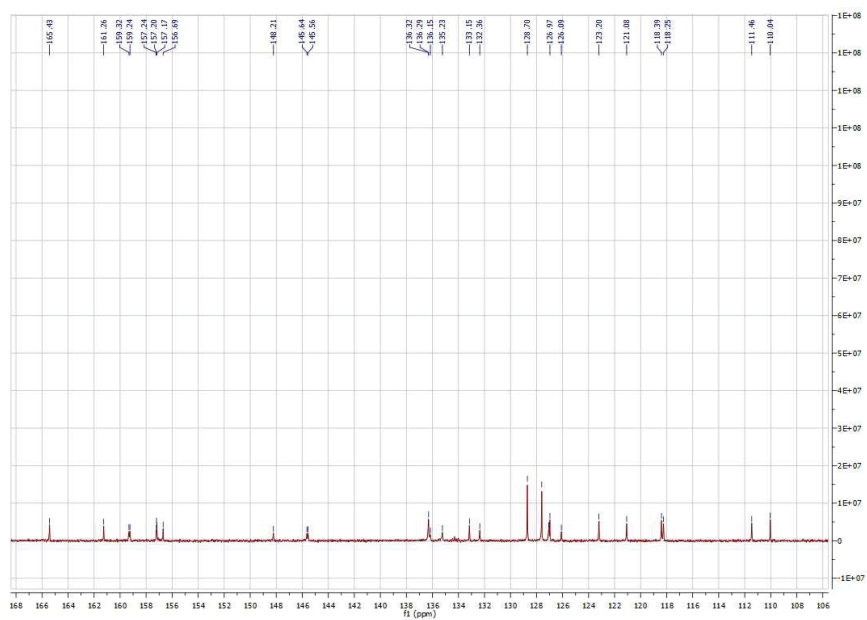
$^1\text{H-NMR}$ and $^{13}\text{C-NMR}$ of Compound **8c** ·TFA:



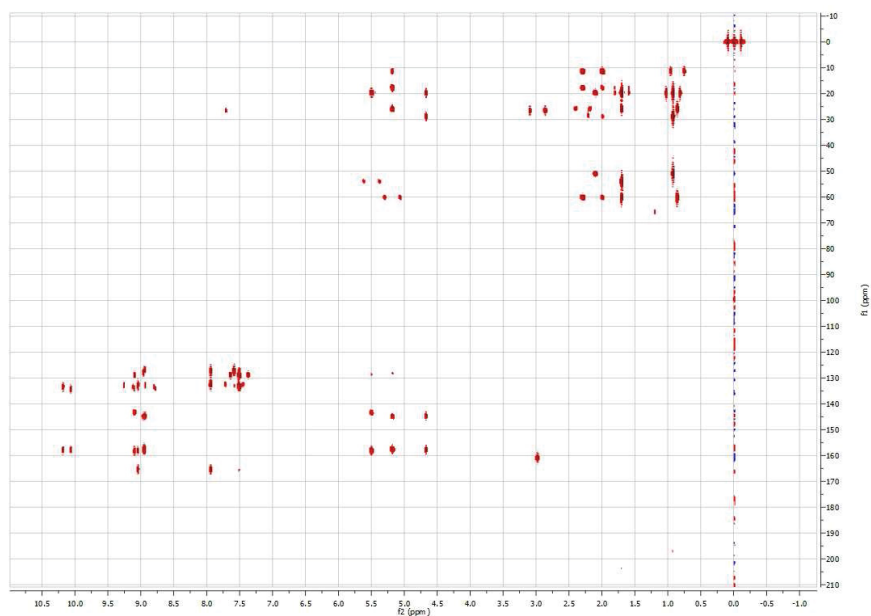
$^1\text{H-NMR}$ and $^{13}\text{C-NMR}$ of Compound **8c**:



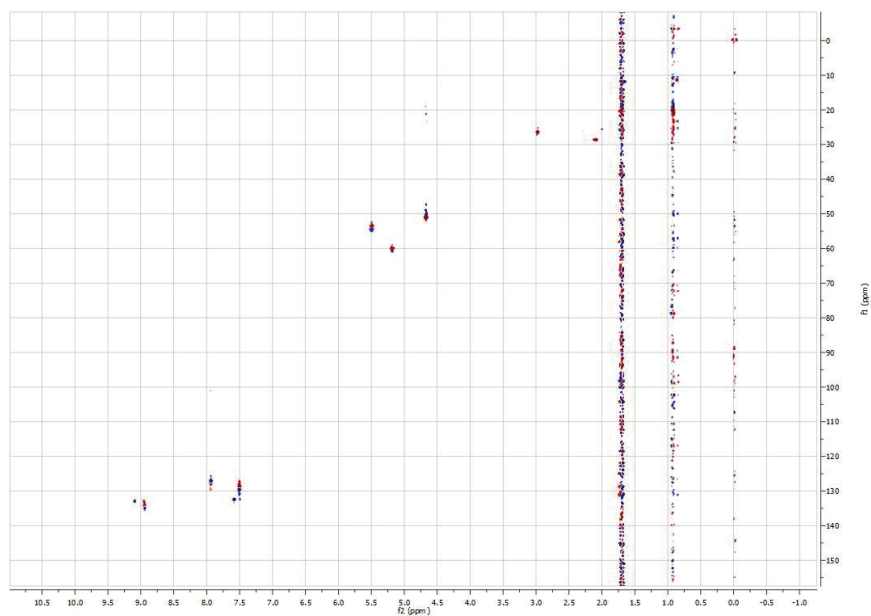
Expansion of the ^{13}C NMR spectrum of **8c**



HMBC spectrum of compound **8a** (600 MHz, CDCl₃, 20 mM):



HSQC spectrum of compound **8a** (600 MHz, CDCl₃, 20 mM):



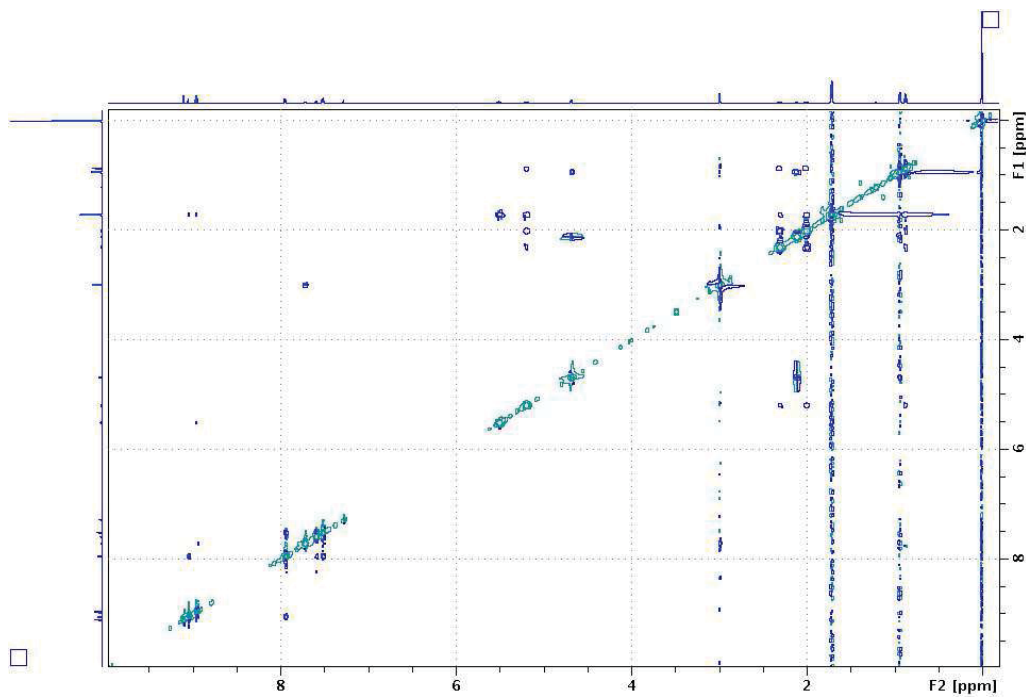


Figure S1. ROESY spectrum of compound **8a** (600 MHz, CDCl₃, 20 mM, 298K):

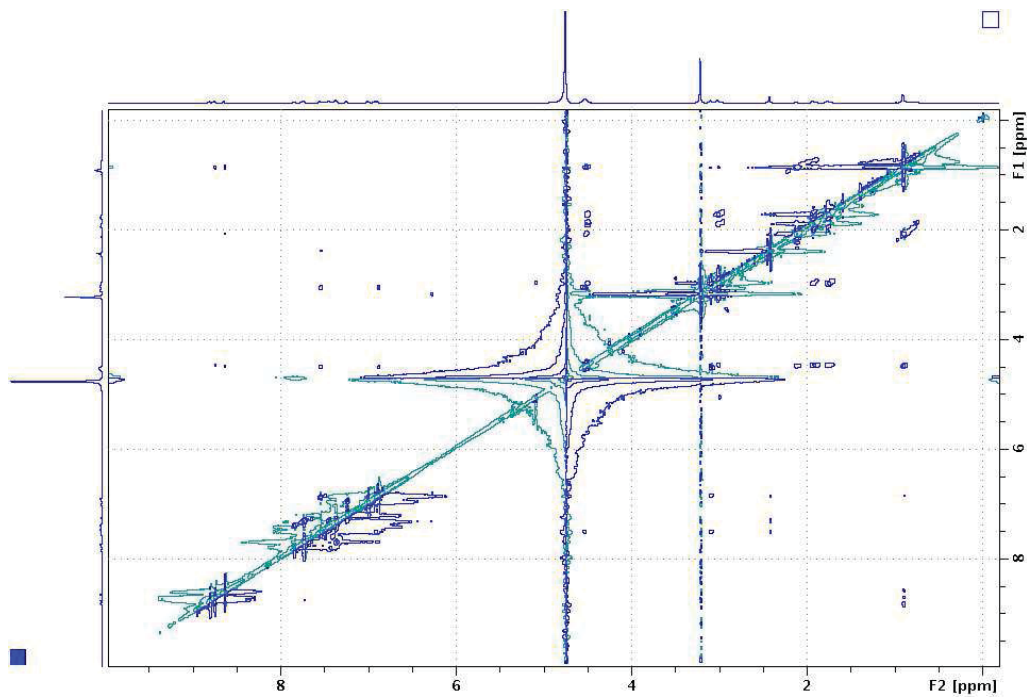


Figure S2. ROESY spectrum of compound **8c** TFA (600 MHz, methanol- d_4 , 10 mM, 298K):

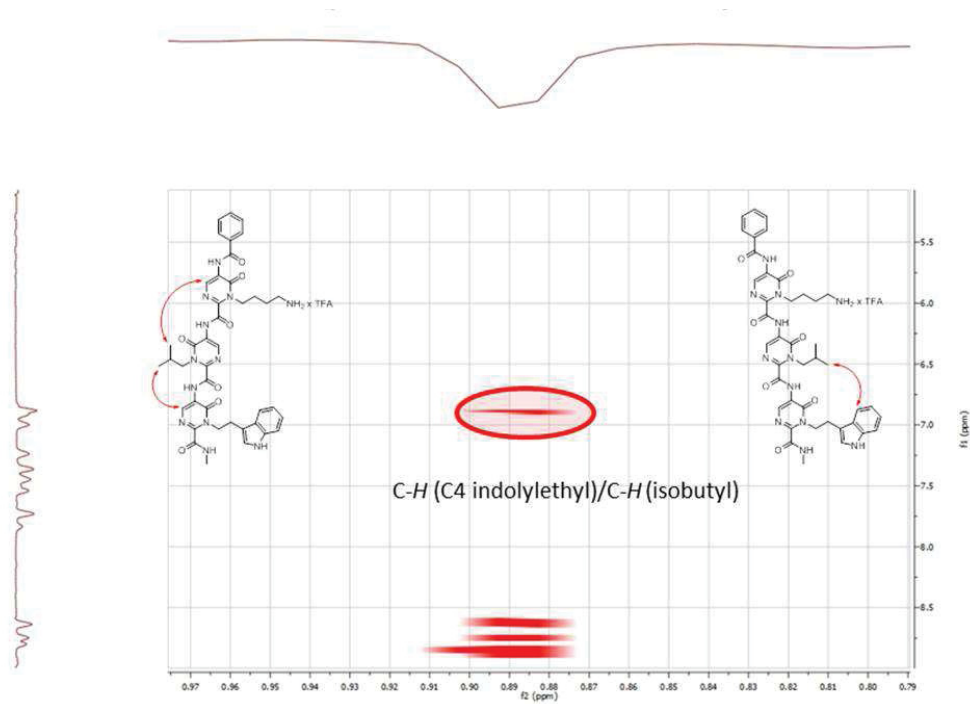
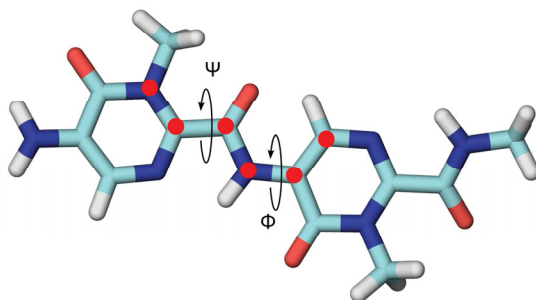


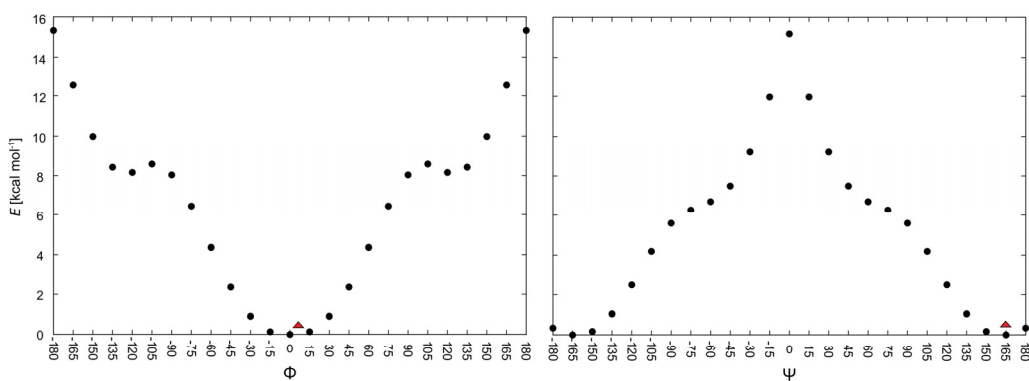
Figure S3. Expansion of the ROESY spectrum of **8c** TFA shown in Figure S2; key ROEs are marked in red.

3. BISPYRIMIDONAMIDE USED FOR THE PARAMETERIZATION PROCEDURE
AND POTENTIALS OF THE INTER-RING TORSION ANGLES ϕ and ψ

A



B



C

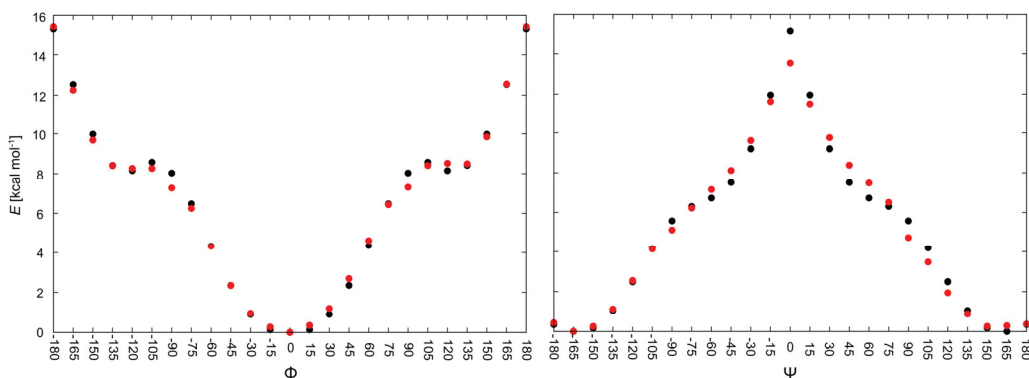


Figure S4. (A) Dimethyl substituted bispyrimidonamide used for the *ab initio*-based parameterization of the ϕ and ψ inter-ring torsion angles defined by the atoms indicated with red dots (see also Experimental Section in the main text). (B) Relative MP2/6-31G* energy of the dimethyl substituted bispyrimidonamide calculated for constrained ϕ and ψ angles in the range $[180^\circ, -180^\circ]$ at intervals of 15° (see Experimental Section in the main text). The red triangles indicate average values of ϕ and ψ angles found in the crystal structure of **8a** (7.4° and 165.4° , respectively), which correspond to energy minima in the torsion potentials. (C) Same *ab initio* potentials (black points) together with the relative molecular mechanics energy (red points) calculated for constrained ϕ and ψ angles in the range $[180^\circ, -180^\circ]$ at intervals of 15° utilizing the newly derived force field parameters in combination with the general AMBER force field (GAFF). The fitting procedure for ϕ and ψ angles provided correlation coefficients (R^2) between the *ab initio* and molecular mechanics energies of 0.99 and 0.98, respectively.

4. FORCE FIELD PARAMETERS DERIVED FOR THE φ and ψ INTER-RING

TORSION ANGLES

MASS

BOND

ANGLE

c -cc-nh	67.880	115.220	same as c -ce-nh
----------	--------	---------	------------------

DIHE

c -cc-n -hn	1	0.5421	180.000	1
cd -cc-n -hn	1	0.4792	180.000	0
n -cc-c -o	1	1.1733	180.000	1
c -n -cc-c	1	3.1865	180.000	-2
n -cc-c -n	1	1.2770	180.000	1
nd -cc-c -n	1	0.3141	180.000	0
nd -cc-c -o	1	2.3661	180.000	2
c -n -cc-cd	1	1.1077	180.000	1

IMPR

c -n -cc-nd	1.1	180.0	2.0	Using default value
cc-h4-cd-nd	1.1	180.0	2.0	Using default value
c -cd-cc-nh	1.1	180.0	2.0	Using default value
cc-n -c -o	10.5	180.0	2.0	General improper torsional angle (2 general atom types)
cc-hn-nh-hn	1.1	180.0	2.0	Using default value
c -cc-n -hn	1.1	180.0	2.0	General improper torsional angle (2 general atom types)
c -cd-cc-n	1.1	180.0	2.0	Using default value
c -c3-n -cc	1.1	180.0	2.0	Using default value

NONBON

Figure S5. Force field modification file for the AMBER package of molecular simulation programs containing the dihedral parameters derived for the φ and ψ torsion angles of the bispyrimidonamide scaffold. In the GAFF force field, the dihedral term of the total energy function is calculated according to the equation:

$$E_{dihedral}(\theta) = \sum_{n=1}^3 V_n (1 + \cos(n\theta - \gamma_n))$$

where V_n is the dihedral force constant (amplitude); n is the dihedral periodicity; γ is the phase of the dihedral angle θ (see ref. 64 in the main text).

5. SUPERIMPOSITION OF A TRISPYRIMIDONAMIDE AND C_β ATOMS OF A CANONICAL α -HELIX AT POSITIONS i , $i + 4$, AND $i + 7$

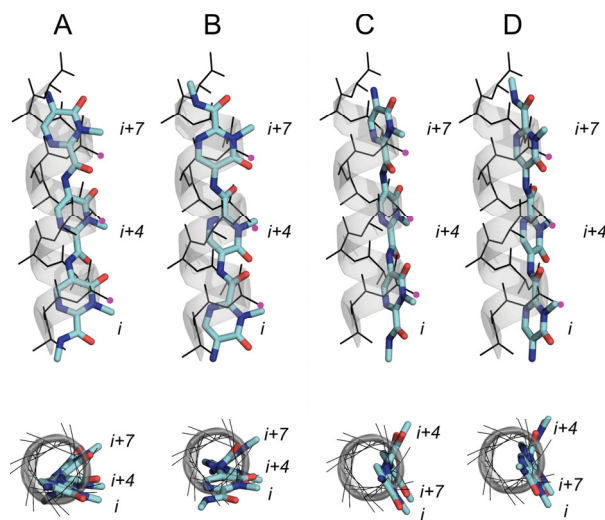


Figure S6. Overlay of C_β atoms of a canonical α -helix at positions i , $i + 4$, and $i + 7$ onto the methyl groups of **IV** in conformation **C**₂ (RMSD = 1.1 Å, average angle deviation between bond vectors = 22°) (A) and **C**₁ (RMSD = 1.2 Å, average angle deviation between bond vectors = 54°) (C). Ring C is oriented towards the C-terminus of the helix. (B), (D): Equivalent superimpositions when **IV** is reversed with respect to the helix axis (RMSD = 1.5 Å and 1.7 Å, average angle deviation between bond vectors = 39° and 70°, respectively). The magenta dots highlight the C_β atoms addressed by the trispyrimidonamide's R groups. In the lower panel the overlays are rotated by 90°, with the peptide C-terminus oriented in the direction of the viewer.

13 CURRICULUM VITAE

Personal Information

Name: Emanuele Ciglia
Date of birth: 16/11/1984 in Pescara (Italy)

Education

- 01/2011-05/2015** *PhD student and research assistant*
Group of Computational Pharmaceutical Chemistry and Molecular Bioinformatics at the Heinrich-Heine University, Düsseldorf
Supervisor: Prof. Dr. H. Gohlke
- 10/2003-10/2009** *Diploma in Pharmaceutical Chemistry and Technology*
G. D'Annunzio University, Chieti-Pescara (Italy)
Thesis defended in March 2010; Final grade: 108/110
Professional qualification: Pharmacist
- 02/2006-07/2006** *Erasmus fellow*
Faculty of Pharmacy at the University of Barcelona (Spain)
- 09/1998-06/2003** *High school degree*
Liceo Classico G. D'Annunzio, Pescara (Italy). Final grade: 94/100

Work experience and internships

- 04/2009-10/2009** *Trainee*
Drug formulation laboratory and over the counter sales
Pharmacy Dr. Zenobii, Pescara (Italy)
- 02/2009** *Visiting Student*
Research within the Diploma thesis project
Drug Design Unit at Siena Biotech spa, Siena (Italy). Supervisor: Dr. A. Padova
- 03/2008** *Visiting student*
Overview of an analytical laboratory
Chemical and microbiological analysis laboratory L.A.C.I. srl, S. Giovanni Teatino (Italy)

Teaching experience

- 04/2011-05/2015** *Teaching assistant*
Teaching and supervising Pharmacy students within the “Drug analysis” practical course
Heinrich-Heine University, Düsseldorf (Germany)
- 09/2007-09/2009** *Faculty Tutor*
Teaching and supervising Pharmacy students for the preparation of Physics and Mathematics exams
G. D’Annunzio University Chieti-Pescara (Italy)

Additional skills

Computer skills Operating systems: Linux, Microsoft Windows, Mac OS

Molecular modeling: Amber molecular simulations package, Schrodinger Maestro, Openeye scientific software, Modeller, Gaussian, VMD, Pymol, ChemDraw, Shell scripting, basic knowledge of Python and Pipeline Pilot

Others: Microsoft Office package, Openoffice, Gimp, Inkscape, Gnuplot, Endnote.

Languages

Italian: native speaker
English: fluent in spoken and written
German: upper intermediate
Spanish: upper intermediate

Advanced training

Interdisciplinary Graduate and Research Academy (iGRAD), Düsseldorf

- Good scientific practice for doctoral researchers
- Presenting science I – comprehensive, competent and convincing
- Fundamentals of project management for doctoral researchers
- Career planning in Business – How to shape up your future

Publications

Papers

Metz, A., Ciglia, E., Gohlke, H. “Modulating protein-protein interactions: From structural determinants of binding to druggability prediction to application” *Curr. Pharm. Des.* **2012**, 18, 4630-4647

Spanier, L., Ciglia, E., Hansen, F. K., Kuna, K., Frank, W., Gohlke, H., Kurz, T. “Design, synthesis, and conformational analysis of trispyrimidonamides as α -helix mimetics” *J. Org. Chem.* **2014**, 79, 1582-1593.

Ciglia, E., Vergin, J., Reimann, S., Smits, S.H.J., Schmitt, L., Groth, G., Gohlke, H. “Resolving hot spots in the C-terminal dimerization domain that determine the stability of the molecular chaperone Hsp90” *PLOS ONE* **2014**, 9(4): e96031.

Metz, A., Ciglia, E., Kröger, T., Gohlke, H. “Protein-Protein-Interaktionen nachgeahmt: Strukturbasierte Identifizierung niedermolekularer Inhibitoren“. *GIT - Labor-Fachzeitschrift* **2014**, 8, 33-35.

Poster presentations

“Determinants of HSP90 dimerization and design of peptidic and non-peptidic dimerization inhibitors”

3rd Indo-German Conference on Modeling Chemical and Biological (Re)activity, Chandigarh (India), February 2013.

“Inhibiting protein-protein interactions in HSP90 dimerization as a novel approach for targeting cancer”

26th Molecular Modelling Workshop, Erlangen (Germany), March 2012.

14 REFERENCES

1. Hughes, J. P., Rees, S., Kalindjian, S. B., and Philpott, K. L. (2011) Principles of early drug discovery. *Br J Pharmacol* **162**, 1239-1249
2. Rawlins, M. D. (2004) Cutting the cost of drug development? *Nat Rev Drug Discovery* **3**, 360-364
3. DiMasi, J. A., Hansen, R. W., and Grabowski, H. G. (2003) The price of innovation: new estimates of drug development costs. *J Health Econ* **22**, 151-185
4. Kaitin, K. I., and DiMasi, J. A. (2011) Pharmaceutical innovation in the 21st century: new drug approvals in the first decade, 2000-2009. *Clin Pharmacol Ther* **89**, 183-188
5. Kaitin, K. I. (2010) Deconstructing the drug development process: the new face of innovation. *Clin Pharmacol Ther* **87**, 356-361
6. Paul, S. M., Mytelka, D. S., Dunwiddie, C. T., Persinger, C. C., Munos, B. H., Lindborg, S. R., and Schacht, A. L. (2010) How to improve R&D productivity: the pharmaceutical industry's grand challenge. *Nature Rev Drug Discovery* **9**, 203-214
7. Cuatrecasas, P. (2006) Drug discovery in jeopardy. *J Clin Invest* **116**, 2837-2842
8. Bolten, B. M., and DeGregorio, T. (2002) Trends in development cycles. *Nat Rev Drug Discovery* **1**, 335-336
9. Overington, J. P., Al-Lazikani, B., and Hopkins, A. L. (2006) Opinion - How many drug targets are there? *Nat Rev Drug Discovery* **5**, 993-996
10. Rask-Andersen, M., Masuram, S., and Schioth, H. B. (2014) The druggable genome: Evaluation of drug targets in clinical trials suggests major shifts in molecular class and indication. *Annu Rev Pharmacol Toxicol* **54**, 9-26
11. Hopkins, A. L., and Groom, C. R. (2002) The druggable genome. *Nat Rev Drug Discovery* **1**, 727-730
12. Russ, A. P., and Lampel, S. (2005) The druggable genome: an update. *Drug Discovery Today* **10**, 1607-1610
13. Imming, P., Sinning, C., and Meyer, A. (2006) Opinion - Drugs, their targets and the nature and number of drug targets. *Nat Rev Drug Discovery* **5**, 821-834
14. Rask-Andersen, M., Almen, M. S., and Schioth, H. B. (2011) Trends in the exploitation of novel drug targets. *Nat Rev Drug Discovery* **10**, 579-590
15. Bonetta, L. (2010) Protein-protein interactions: Interactome under construction. *Nature* **468**, 851-854
16. Stumpf, M. P., Thorne, T., de Silva, E., Stewart, R., An, H. J., Lappe, M., and Wiuf, C. (2008) Estimating the size of the human interactome. *Proc Natl Acad Sci U S A* **105**, 6959-6964
17. Zhang, Q. C., Petrey, D., Deng, L., Qiang, L., Shi, Y., Thu, C. A., Bisikirska, B., Lefebvre, C., Accili, D., Hunter, T., Maniatis, T., Califano, A., and Honig, B. (2012) Structure-based prediction of protein-protein interactions on a genome-wide scale. *Nature* **490**, 556-560
18. Garner, A. L., and Janda, K. D. (2011) Protein-Protein Interactions and Cancer: Targeting the Central Dogma. *Curr Top Med Chem* **11**, 258-280
19. Hanahan, D., and Weinberg, R. A. (2011) Hallmarks of Cancer: The Next Generation. *Cell* **144**, 646-674
20. Ivanov, A. A., Khuri, F. R., and Fu, H. A. (2013) Targeting protein-protein interactions as an anticancer strategy. *Trends Pharmacol Sci* **34**, 393-400
21. Blazer, L. L., and Neubig, R. R. (2009) Small molecule protein-protein interaction inhibitors as CNS therapeutic agents: current progress and future hurdles. *Neuropsychopharmacology* **34**, 126-141

22. Ryan, D. P., and Matthews, J. M. (2005) Protein-protein interactions in human disease. *Curr Opin Struct Biol* **15**, 441-446
23. Wells, J. A., and McClendon, C. L. (2007) Reaching for high-hanging fruit in drug discovery at protein-protein interfaces. *Nature* **450**, 1001-1009
24. Fischer, P. M. (2005) Protein-protein Interactions in Drug Discovery. *Drug Des Rev -- Online* **2**, 179-207
25. Gerrard, J. A., Hutton, C. A., and Perugini, M. A. (2007) Inhibiting protein-protein interactions as an emerging paradigm for drug discovery. *Mini-Rev Med Chem* **7**, 151-157
26. Fuller, J. C., Burgoyne, N. J., and Jackson, R. M. (2009) Predicting druggable binding sites at the protein-protein interface. *Drug Discovery Today* **14**, 155-161
27. Surade, S., and Blundell, T. L. (2012) Structural biology and drug discovery of difficult targets: the limits of ligandability. *Chem Biol* **19**, 42-50
28. Fry, D. C. (2012) Small-Molecule Inhibitors of Protein-Protein Interactions: How to Mimic a Protein Partner. *Curr Pharm Des* **18**, 4679-4684
29. Azzarito, V., Long, K., Murphy, N. S., and Wilson, A. J. (2013) Inhibition of alpha-helix-mediated protein-protein interactions using designed molecules. *Nat Chem* **5**, 161-173
30. Villoutreix, B. O., Kuenemann, M. A., Poyet, J. L., Bruzzoni-Giovanelli, H., Labbe, C., Lagorce, D., Sperandio, O., and Miteva, M. A. (2014) Drug-Like Protein-Protein Interaction Modulators: Challenges and Opportunities for Drug Discovery and Chemical Biology. *Mol Inf* **33**, 414-437
31. Metz, A., Ciglia, E., and Gohlke, H. (2012) Modulating Protein-Protein Interactions: From Structural Determinants of Binding to Druggability Prediction to Application. *Curr Pharm Des* **18**, 4630-4647
32. Ciglia, E., Vergin, J., Reimann, S., Smits, S. H. J., Schmitt, L., Groth, G., and Gohlke, H. (2014) Resolving Hot Spots in the C-Terminal Dimerization Domain that Determine the Stability of the Molecular Chaperone Hsp90. *PLOS ONE* **9**
33. Spanier, L., Ciglia, E., Hansen, F. K., Kuna, K., Frank, W., Gohlke, H., and Kurz, T. (2014) Design, Synthesis, and Conformational Analysis of Trispyrimidonamides as alpha-Helix Mimetics. *J Org Chem* **79**, 1582-1593
34. Zinzalla, G., and Thurston, D. E. (2009) Targeting protein-protein interactions for therapeutic intervention: a challenge for the future. *Future Med Chem* **1**, 65-93
35. Mullard, A. (2012) Protein-protein interaction inhibitors get into the groove. *Nat Rev Drug Discovery* **11**, 173-175
36. Archakov, A. I., Govorun, V. M., Dubanov, A. V., Ivanov, Y. D., Veselovsky, A. V., Lewi, P., and Janssen, P. (2003) Protein-protein interactions as a target for drugs in proteomics. *Proteomics* **3**, 380-391
37. Beuming, T., Skrabanek, L., Niv, M. Y., Mukherjee, P., and Weinstein, H. (2005) PDZBase: a protein-protein interaction database for PDZ-domains. *Bioinformatics* **21**, 827-828
38. Pagel, P., Kovac, S., Oesterheld, M., Brauner, B., Dunger-Kaltenbach, I., Frishman, G., Montrone, C., Mark, P., Stumpflen, V., Mewes, H. W., Ruepp, A., and Frishman, D. (2005) The MIPS mammalian protein-protein interaction database. *Bioinformatics* **21**, 832-834
39. Xenarios, I., and Eisenberg, D. (2001) Protein interaction databases. *Curr Opin Biotechnol* **12**, 334-339
40. Cory, S., and Adams, J. M. (2002) The Bcl2 family: regulators of the cellular life-or-death switch. *Nat Rev Cancer* **2**, 647-656
41. Villunger, A., Scott, C., Bouillet, P., and Strasser, A. (2003) Essential role for the BH3-only protein Bim but redundant roles for Bax, Bcl-2, and Bcl-w in the control of granulocyte survival. *Blood* **101**, 2393-2400

42. Chene, P. (2006) Drugs targeting protein-protein interactions. *ChemMedChem* **1**, 400-411
43. Arkin, M. R., and Whitty, A. (2009) The road less traveled: modulating signal transduction enzymes by inhibiting their protein-protein interactions. *Curr Opin Chem Biol* **13**, 284-290
44. Fischer, E. (1894) Einfluss der Configuration auf die Wirkung der Enzyme. *Ber Dtsch Chem Ges*, 2985
45. Gohlke, H., and Klebe, G. (2002) Approaches to the description and prediction of the binding affinity of small-molecule ligands to macromolecular receptors. *Angew Chem Int Ed* **41**, 2645-2676
46. Bon, R. S., and Waldmann, H. (2010) Bioactivity-Guided Navigation of Chemical Space. *Acc Chem Res* **43**, 1103-1114
47. Doppelt-Azeroual, O., Delfaud, F., Moriaud, F., and de Brevern, A. G. (2010) Fast and automated functional classification with MED-SuMo: An application on purine-binding proteins. *Protein Sci* **19**, 847-867
48. Leung, C. H., Chan, D. S. H., Kwan, M. H. T., Cheng, Z., Wong, C. Y., Zhu, G. Y., Fong, W. F., and Ma, D. L. (2011) Structure-Based Repurposing of FDA-Approved Drugs as TNF-alpha Inhibitors. *ChemMedChem* **6**, 765-768
49. Moriaud, F., Richard, S. B., Adcock, S. A., Chanas-Martin, L., Surgand, J. S., Ben Jelloul, M., and Delfaud, F. (2011) Identify drug repurposing candidates by mining the Protein Data Bank. *Briefings Bioinf* **12**, 336-340
50. Scheck, M., Koch, M. A., and Waldmann, H. (2008) Synthesis of a dysidiolide-inspired compound library and discovery of acetylcholinesterase inhibitors based on protein structure similarity clustering (PSSC). *Tetrahedron* **64**, 4792-4802
51. Cheng, A. C., Coleman, R. G., Smyth, K. T., Cao, Q., Soulard, P., Caffrey, D. R., Salzberg, A. C., and Huang, E. S. (2007) Structure-based maximal affinity model predicts small-molecule druggability. *Nat Biotechnol* **25**, 71-75
52. Smith, R. D., Hu, L., Falkner, J. A., Benson, M. L., Nerothin, J. P., and Carlson, H. A. (2006) Exploring protein-ligand recognition with Binding MOAD. *J Mol Graphics Modell* **24**, 414-425
53. Chakrabarti, P., and Janin, J. (2002) Dissecting protein-protein recognition sites. *Proteins* **47**, 334-343
54. Jones, S., and Thornton, J. M. (1996) Principles of protein-protein interactions. *Proc Natl Acad Sci U S A* **93**, 13-20
55. Lo Conte, L., Chothia, C., and Janin, J. (1999) The atomic structure of protein-protein recognition sites. *J Mol Biol* **285**, 2177-2198
56. Arkin, M. R., and Wells, J. A. (2004) Small-molecule inhibitors of protein-protein interactions: progressing towards the dream. *Nat Rev Drug Discovery* **3**, 301-317
57. DeLano, W. L., Ultsch, M. H., de Vos, A. M., and Wells, J. A. (2000) Convergent solutions to binding at a protein-protein interface. *Science* **287**, 1279-1283
58. Deeds, E. J., Ashenberg, O., Gerardin, J., and Shakhnovich, E. I. (2007) Robust protein-protein interactions in crowded cellular environments. *Proc Natl Acad Sci U S A* **104**, 14952-14957
59. Keskin, O., Gursoy, A., Ma, B., and Nussinov, R. (2008) Principles of protein-protein interactions: what are the preferred ways for proteins to interact? *Chem Rev* **108**, 1225-1244
60. Nooren, I. M., and Thornton, J. M. (2003) Diversity of protein-protein interactions. *EMBO J* **22**, 3486-3492
61. Taverna, D. M., and Goldstein, R. A. (2002) Why are proteins marginally stable? *Proteins* **46**, 105-109

62. Eyrisch, S., and Helms, V. (2007) Transient pockets on protein surfaces involved in protein-protein interaction. *J Med Chem* **50**, 3457-3464
63. Metz, A., Pflieger, C., Kopitz, H., Pfeiffer-Marek, S., Baringhaus, K. H., and Gohlke, H. (2012) Hot Spots and Transient Pockets: Predicting the Determinants of Small-Molecule Binding to a Protein-Protein Interface. *J Chem Inf Model* **52**, 120-133
64. Perot, S., Sperandio, O., Miteva, M. A., Camproux, A. C., and Villoutreix, B. O. (2010) Druggable pockets and binding site centric chemical space: a paradigm shift in drug discovery. *Drug Discovery Today* **15**, 656-667
65. Dong, Y. D., and Boyd, B. J. (2011) Applications of X-ray scattering in pharmaceutical science. *Int J Pharm* **417**, 101-111
66. Svergun, D. I., and Koch, M. H. J. (2003) Small-angle scattering studies of biological macromolecules in solution. *Rep Prog Phys* **66**, 1735-1782
67. Acoca, S., Cui, Q., Shore, G. C., and Purisima, E. O. (2011) Molecular dynamics study of small molecule inhibitors of the Bcl-2 family. *Proteins* **79**, 2624-2636
68. Brown, S. P., and Hajduk, P. J. (2006) Effects of conformational dynamics on predicted protein druggability. *ChemMedChem* **1**, 70-72
69. Cozzini, P., Kellogg, G. E., Spyraakis, F., Abraham, D. J., Costantino, G., Emerson, A., Fanelli, F., Gohlke, H., Kuhn, L. A., Morris, G. M., Orozco, M., Pertinhez, T. A., Rizzi, M., and Sotriffer, C. A. (2008) Target flexibility: an emerging consideration in drug discovery and design. *J Med Chem* **51**, 6237-6255
70. Eyrisch, S., and Helms, V. (2009) What induces pocket openings on protein surface patches involved in protein-protein interactions? *J Comput-Aided Mol Des* **23**, 73-86
71. Shaw, D. E., Maragakis, P., Lindorff-Larsen, K., Piana, S., Dror, R. O., Eastwood, M. P., Bank, J. A., Jumper, J. M., Salmon, J. K., Shan, Y., and Wriggers, W. (2010) Atomic-level characterization of the structural dynamics of proteins. *Science* **330**, 341-346
72. Yang, C. Y., and Wang, S. (2011) Hydrophobic Binding Hot Spots of Bcl-xL Protein-Protein Interfaces by Cosolvent Molecular Dynamics Simulation. *ACS Med Chem Lett* **2**, 280-284
73. Ahmed, A., Kazemi, S., and Gohlke, H. (2007) Protein Flexibility and Mobility in Structure-Based Drug Design. *Front Drug Des Discovery* **3**, 455-476
74. Isvoran, A., Badel, A., Craescu, C. T., Miron, S., and Miteva, M. A. (2011) Exploring NMR ensembles of calcium binding proteins: perspectives to design inhibitors of protein-protein interactions. *BMC Struct Biol* **11**, 24
75. Li, X., Keskin, O., Ma, B., Nussinov, R., and Liang, J. (2004) Protein-protein interactions: hot spots and structurally conserved residues often locate in complemented pockets that pre-organized in the unbound states: implications for docking. *J Mol Biol* **344**, 781-795
76. Ma, B., Elkayam, T., Wolfson, H., and Nussinov, R. (2003) Protein-protein interactions: structurally conserved residues distinguish between binding sites and exposed protein surfaces. *Proc Natl Acad Sci U S A* **100**, 5772-5777
77. Ahmad, S., Keskin, O., Mizuguchi, K., Sarai, A., and Nussinov, R. (2010) CCRXP: exploring clusters of conserved residues in protein structures. *Nucleic Acids Res* **38**, W398-W401
78. Moreira, I. S., Fernandes, P. A., and Ramos, M. J. (2007) Hot spots--a review of the protein-protein interface determinant amino-acid residues. *Proteins* **68**, 803-812
79. Bogan, A. A., and Thorn, K. S. (1998) Anatomy of hot spots in protein interfaces. *J Mol Biol* **280**, 1-9
80. Bradshaw, R. T., Patel, B. H., Tate, E. W., Leatherbarrow, R. J., and Gould, I. R. (2011) Comparing experimental and computational alanine scanning techniques for probing a prototypical protein-protein interaction. *Protein Eng Des Sel* **24**, 197-207

81. Clackson, T., and Wells, J. A. (1995) A Hot-Spot of Binding-Energy in a Hormone-Receptor Interface. *Science* **267**, 383-386
82. Tuncbag, N., GURSOY, A., GUNAY, E., NUSSINOV, R., and KESKIN, O. (2008) Architectures and functional coverage of protein-protein interfaces. *J Mol Biol* **381**, 785-802
83. Keskin, O., Ma, B., and Nussinov, R. (2005) Hot regions in protein-protein interactions: the organization and contribution of structurally conserved hot spot residues. *J Mol Biol* **345**, 1281-1294
84. Cukuroglu, E., GURSOY, A., and KESKIN, O. (2010) Analysis of hot region organization in hub proteins. *Ann Biomed Eng* **38**, 2068-2078
85. Thorn, K. S., and Bogan, A. A. (2001) ASEdb: a database of alanine mutations and their effects on the free energy of binding in protein interactions. *Bioinformatics* **17**, 284-285
86. Rajamani, D., Thiel, S., Vajda, S., and Camacho, C. J. (2004) Anchor residues in protein-protein interactions. *Proc Natl Acad Sci U S A* **101**, 11287-11292
87. Yogurtcu, O. N., Erdemli, S. B., Nussinov, R., Turkay, M., and Keskin, O. (2008) Restricted mobility of conserved residues in protein-protein interfaces in molecular simulations. *Biophys J* **94**, 3475-3485
88. Keskin, O., Ma, B., Rogale, K., Gunasekaran, K., and Nussinov, R. (2005) Protein-protein interactions: organization, cooperativity and mapping in a bottom-up Systems Biology approach. *Phys Biol* **2**, S24-35
89. Reichmann, D., Cohen, M., Abramovich, R., Dym, O., Lim, D., Strynadka, N. C., and Schreiber, G. (2007) Binding hot spots in the TEM1-BLIP interface in light of its modular architecture. *J Mol Biol* **365**, 663-679
90. Reichmann, D., Rahat, O., Albeck, S., Meged, R., Dym, O., and Schreiber, G. (2005) The modular architecture of protein-protein binding interfaces. *Proc Natl Acad Sci U S A* **102**, 57-62
91. Schreiber, G., and Fersht, A. R. (1995) Energetics of protein-protein interactions: analysis of the barnase-barstar interface by single mutations and double mutant cycles. *J Mol Biol* **248**, 478-486
92. Shulman-Peleg, A., Shatsky, M., Nussinov, R., and Wolfson, H. J. (2007) Spatial chemical conservation of hot spot interactions in protein-protein complexes. *BMC Biol* **5**, 43
93. Fromer, M., and Linial, M. (2010) Exposing the co-adaptive potential of protein-protein interfaces through computational sequence design. *Bioinformatics* **26**, 2266-2272
94. Cunningham, B. C., and Wells, J. A. (1993) Comparison of a structural and a functional epitope. *J Mol Biol* **234**, 554-563
95. Lawrence, M. C., and Colman, P. M. (1993) Shape complementarity at protein/protein interfaces. *J Mol Biol* **234**, 946-950
96. Raschke, T. M. (2006) Water structure and interactions with protein surfaces. *Curr Opin Struct Biol* **16**, 152-159
97. Rodier, F., Bahadur, R. P., Chakrabarti, P., and Janin, J. (2005) Hydration of protein-protein interfaces. *Proteins* **60**, 36-45
98. Tsai, C. J., Lin, S. L., Wolfson, H. J., and Nussinov, R. (1997) Studies of protein-protein interfaces: a statistical analysis of the hydrophobic effect. *Protein Sci* **6**, 53-64
99. Tsai, C. J., Xu, D., and Nussinov, R. (1997) Structural motifs at protein-protein interfaces: protein cores versus two-state and three-state model complexes. *Protein Sci* **6**, 1793-1805
100. Young, L., Jernigan, R. L., and Covell, D. G. (1994) A role for surface hydrophobicity in protein-protein recognition. *Protein Sci* **3**, 717-729
101. Fuentes, E. J., Gilmore, S. A., Mauldin, R. V., and Lee, A. L. (2006) Evaluation of energetic and dynamic coupling networks in a PDZ domain protein. *J Mol Biol* **364**, 337-351

102. James, L. C., Roversi, P., and Tawfik, D. S. (2003) Antibody multispecificity mediated by conformational diversity. *Science* **299**, 1362-1367
103. Lindner, A. B., Eshhar, Z., and Tawfik, D. S. (1999) Conformational changes affect binding and catalysis by ester-hydrolysing antibodies. *J Mol Biol* **285**, 421-430
104. Ma, B., Kumar, S., Tsai, C. J., and Nussinov, R. (1999) Folding funnels and binding mechanisms. *Protein Eng* **12**, 713-720
105. Norel, R., Sheinerman, F., Petrey, D., and Honig, B. (2001) Electrostatic contributions to protein-protein interactions: fast energetic filters for docking and their physical basis. *Protein Sci* **10**, 2147-2161
106. Sheinerman, F. B., and Honig, B. (2002) On the role of electrostatic interactions in the design of protein-protein interfaces. *J Mol Biol* **318**, 161-177
107. Sheinerman, F. B., Norel, R., and Honig, B. (2000) Electrostatic aspects of protein-protein interactions. *Curr Opin Struct Biol* **10**, 153-159
108. Xu, D., Lin, S. L., and Nussinov, R. (1997) Protein binding versus protein folding: the role of hydrophilic bridges in protein associations. *J Mol Biol* **265**, 68-84
109. Lichtarge, O., Bourne, H. R., and Cohen, F. E. (1996) An evolutionary trace method defines binding surfaces common to protein families. *J Mol Biol* **257**, 342-358
110. Kuritzkes, D., Kar, S., and Kirkpatrick, P. (2008) Fresh from the pipeline - Maraviroc. *Nat Rev Drug Discovery* **7**, 15-16
111. Liu, G. (2001) Small molecule antagonists of the LFA-1/ICAM-1 interaction as potential therapeutic agents. *Expert Opin Ther Pat* **11**, 1383-1393
112. Owellen, R. J., Hartke, C. A., Dickerson, R. M., and Hains, F. O. (1976) Inhibition of tubulin-microtubule polymerization by drugs of the Vinca alkaloid class. *Cancer Res* **36**, 1499-1502
113. Sillerud, L. O., and Larson, R. S. (2005) Design and structure of peptide and peptidomimetic antagonists of protein-protein interaction. *Curr Protein Pept Sci* **6**, 151-169
114. Cheng, G. (2011) Eltrombopag for the treatment of immune thrombocytopenia. *Expert Rev Hematol* **4**, 261-269
115. Cheng, G., Saleh, M. N., Marcher, C., Vasey, S., Mayer, B., Aivado, M., Arning, M., Stone, N. L., and Bussel, J. B. (2011) Eltrombopag for management of chronic immune thrombocytopenia (RAISE): a 6-month, randomised, phase 3 study. *Lancet* **377**, 393-402
116. Domling, A. (2008) Small molecular weight protein-protein interaction antagonists - an insurmountable challenge? *Curr Opin Chem Biol* **12**, 281-291
117. Popowicz, G. M., Domling, A., and Holak, T. A. (2011) The Structure-Based Design of Mdm2/Mdmx-p53 Inhibitors Gets Serious. *Angew Chem Int Edit* **50**, 2680-2688
118. Smith, J., Stewart, B. J., Glaysher, S., Peregrin, K., Knight, L. A., Weber, D. J., and Cree, I. A. (2010) The effect of pentamidine on melanoma ex vivo. *Anti-Cancer Drugs* **21**, 181-185
119. Tse, C., Shoemaker, A. R., Adickes, J., Anderson, M. G., Chen, J., Jin, S., Johnson, E. F., Marsh, K. C., Mitten, M. J., Nimmer, P., Roberts, L., Tahir, S. K., Mao, Y., Yang, X. F., Zhang, H. C., Fesik, S., Rosenberg, S. H., and Elmore, S. W. (2008) ABT-263: A potent and orally bioavailable Bcl-2 family inhibitor. *Cancer Res* **68**, 3421-3428
120. Higuero, A. P., Jubb, H., and Blundell, T. L. (2013) Protein-protein interactions as druggable targets: recent technological advances. *Curr Opin Pharmacol* **13**, 791-796
121. Wass, M. N., David, A., and Sternberg, M. J. (2011) Challenges for the prediction of macromolecular interactions. *Curr Opin Struct Biol* **21**, 382-390
122. Tuncbag, N., Kar, G., Keskin, O., Gursoy, A., and Nussinov, R. (2009) A survey of available tools and web servers for analysis of protein-protein interactions and interfaces. *Briefings Bioinf* **10**, 217-232

123. de Vries, S. J., and Bonvin, A. M. J. J. (2008) How proteins get in touch: Interface prediction in the study of biomolecular complexes. *Curr Protein Pept Sci* **9**, 394-406
124. Ezkurdia, L., Bartoli, L., Fariselli, P., Casadio, R., Valencia, A., and Tress, M. L. (2009) Progress and challenges in predicting protein-protein interaction sites. *Briefings Bioinf* **10**, 233-246
125. Fernandez-Recio, J. (2011) Prediction of protein binding sites and hot spots. *Wires Comput Mol Sci* **1**, 680-698
126. Leis, S., Schneider, S., and Zacharias, M. (2010) In Silico Prediction of Binding Sites on Proteins. *Curr Med Chem* **17**, 1550-1562
127. Ofran, Y., and Rost, B. (2007) Protein-protein interaction hotspots carved into sequences. *PLoS Comput Biol* **3**, 1169-1176
128. Egner, U., and Hillig, R. C. (2008) A structural biology view of target drugability. *Expert Opin Drug Discovery* **3**, 391-401
129. Bullock, B. N., Jochim, A. L., and Arora, P. S. (2011) Assessing helical protein interfaces for inhibitor design. *J Am Chem Soc* **133**, 14220-14223
130. Fauman, E. B., Rai, B. K., and Huang, E. S. (2011) Structure-based druggability assessment--identifying suitable targets for small molecule therapeutics. *Curr Opin Chem Biol* **15**, 463-468
131. Hajduk, P. J., Huth, J. R., and Tse, C. (2005) Predicting protein druggability. *Drug Discovery Today* **10**, 1675-1682
132. Jochim, A. L., and Arora, P. S. (2009) Assessment of helical interfaces in protein-protein interactions. *Mol Biosyst* **5**, 924-926
133. Hajduk, P. J., Huth, J. R., and Fesik, S. W. (2005) Druggability indices for protein targets derived from NMR-based screening data. *J Med Chem* **48**, 2518-2525
134. Gonzalez-Ruiz, D., and Gohlke, H. (2006) Targeting protein-protein interactions with small molecules: challenges and perspectives for computational binding epitope detection and ligand finding. *Curr Med Chem* **13**, 2607-2625
135. Nisius, B., Sha, F., and Gohlke, H. (2012) Structure-based computational analysis of protein binding sites for function and druggability prediction. *J Biotechnol* **159**, 123-134
136. Jochim, A. L., and Arora, P. S. (2010) Systematic analysis of helical protein interfaces reveals targets for synthetic inhibitors. *ACS Chem Biol* **5**, 919-923
137. Jones, S., and Thornton, J. M. (1995) Protein-Protein Interactions - a Review of Protein Dimer Structures. *Prog Biophys Mol Biol* **63**, 31-&
138. Berman, H. M., Westbrook, J., Feng, Z., Gilliland, G., Bhat, T. N., Weissig, H., Shindyalov, I. N., and Bourne, P. E. (2000) The Protein Data Bank. *Nucleic Acids Res* **28**, 235-242
139. Kussie, P. H., Gorina, S., Marechal, V., Elenbaas, B., Moreau, J., Levine, A. J., and Pavletich, N. P. (1996) Structure of the MDM2 oncoprotein bound to the p53 tumor suppressor transactivation domain. *Science* **274**, 948-953
140. DeLano, W. L. (2002) Unraveling hot spots in binding interfaces: progress and challenges. *Curr Opin Struct Biol* **12**, 14-20
141. Weiss, G. A., Watanabe, C. K., Zhong, A., Goddard, A., and Sidhu, S. S. (2000) Rapid mapping of protein functional epitopes by combinatorial alanine scanning. *Proc Natl Acad Sci U S A* **97**, 8950-8954
142. Sidhu, S. S., Fairbrother, W. J., and Deshayes, K. (2003) Exploring protein-protein interactions with phage display. *ChemBioChem* **4**, 14-25
143. Katz, C., Levy-Beladev, L., Rotem-Bamberger, S., Rito, T., Rudiger, S. G., and Friedler, A. (2011) Studying protein-protein interactions using peptide arrays. *Chem Soc Rev* **40**, 2131-2145

144. Erlanson, D. A., Wells, J. A., and Braisted, A. C. (2004) Tethering: fragment-based drug discovery. *Annu Rev Biophys Biomol Struct* **33**, 199-223
145. Erlanson, D. A., and Hansen, S. K. (2004) Making drugs on proteins: site-directed ligand discovery for fragment-based lead assembly. *Curr Opin Chem Biol* **8**, 399-406
146. Toth, G., Mukhyala, K., and Wells, J. A. (2007) Computational approach to site-directed ligand discovery. *Proteins* **68**, 551-560
147. Erlanson, D. A., Braisted, A. C., Raphael, D. R., Randal, M., Stroud, R. M., Gordon, E. M., and Wells, J. A. (2000) Site-directed ligand discovery. *Proc Natl Acad Sci U S A* **97**, 9367-9372
148. Davies, D. R., Begley, D. W., Hartley, R. C., Staker, B. L., and Stewart, L. J. (2011) Predicting the success of fragment screening by X-ray crystallography. *Methods Enzymol* **493**, 91-114
149. Shuker, S. B., Hajduk, P. J., Meadows, R. P., and Fesik, S. W. (1996) Discovering high-affinity ligands for proteins: SAR by NMR. *Science* **274**, 1531-1534
150. Oltersdorf, T., Elmore, S. W., Shoemaker, A. R., Armstrong, R. C., Augeri, D. J., Belli, B. A., Bruncko, M., Deckwerth, T. L., Dinges, J., Hajduk, P. J., Joseph, M. K., Kitada, S., Korsmeyer, S. J., Kunzer, A. R., Letai, A., Li, C., Mitten, M. J., Nettesheim, D. G., Ng, S., Nimmer, P. M., O'Connor, J. M., Oleksijew, A., Petros, A. M., Reed, J. C., Shen, W., Tahir, S. K., Thompson, C. B., Tomaselli, K. J., Wang, B., Wendt, M. D., Zhang, H., Fesik, S. W., and Rosenberg, S. H. (2005) An inhibitor of Bcl-2 family proteins induces regression of solid tumours. *Nature* **435**, 677-681
151. Hajduk, P. J., Mack, J. C., Olejniczak, E. T., Park, C., Dandliker, P. J., and Beutel, B. A. (2004) SOS-NMR: a saturation transfer NMR-based method for determining the structures of protein-ligand complexes. *J Am Chem Soc* **126**, 2390-2398
152. Hajduk, P. J., and Greer, J. (2007) A decade of fragment-based drug design: strategic advances and lessons learned. *Nat Rev Drug discovery* **6**, 211-219
153. Buhrman, G., O'Connor, C., Zerbe, B., Kearney, B. M., Napoleon, R., Kovrigina, E. A., Vajda, S., Kozakov, D., Kovrigin, E. L., and Mattos, C. (2011) Analysis of binding site hot spots on the surface of Ras GTPase. *J Mol Biol* **413**, 773-789
154. Bernini, A., Venditti, V., Spiga, O., and Niccolai, N. (2009) Probing protein surface accessibility with solvent and paramagnetic molecules. *Prog Nucl Magn Reson Spectrosc* **54**, 278-289
155. Weigelt, J., van Dongen, M., Uppenberg, J., Schultz, J., and Wikstrom, M. (2002) Site-selective screening by NMR spectroscopy with labeled amino acid pairs. *J Am Chem Soc* **124**, 2446-2447
156. Grimme D., G.-R. D., Gohlke H. (2012) Computational Strategies and Challenges for Targeting Protein-Protein Interactions with Small Molecules. in *Physico-chemical and Computational Approaches to Drug Discovery* (Luque FJ, B. X. ed.), RSC Drug Discovery Series, London. pp 319-359
157. Berg, T. (2004) Use of "tethering" for the identification of a small molecule that binds to a dynamic hot spot on the interleukin-2 surface. *ChemBioChem* **5**, 1051-1053
158. Bickerton, G. R., Higuieruelo, A. P., and Blundell, T. L. (2011) Comprehensive, atomic-level characterization of structurally characterized protein-protein interactions: the PICCOLO database. *BMC Bioinf* **12**, 313
159. Fischer, T. B., Arunachalam, K. V., Bailey, D., Mangual, V., Bakhru, S., Russo, R., Huang, D., Paczkowski, M., Lalchandani, V., Ramachandra, C., Ellison, B., Galer, S., Shapley, J., Fuentes, E., and Tsai, J. (2003) The binding interface database (BID): a compilation of amino acid hot spots in protein interfaces. *Bioinformatics* **19**, 1453-1454

160. Rohl, C., Price, Y., Fischer, T. B., Paczkowski, M., Zettel, M. F., and Tsai, J. (2006) Cataloging the relationships between proteins: a review of interaction databases. *Mol Biotechnol* **34**, 69-93
161. Guney, E., Tuncbag, N., Keskin, O., and Gursoy, A. (2008) HotSprint: database of computational hot spots in protein interfaces. *Nucleic Acids Res* **36**, D662-D666
162. Shoemaker, B. A., and Panchenko, A. R. (2007) Deciphering protein-protein interactions. Part I. Experimental techniques and databases. *PLOS Comput Biol* **3**, e42
163. Morrow, J. K., and Zhang, S. (2012) Computational prediction of protein hot spot residues. *Curr Pharm Des* **18**, 1255-1265
164. Massova, I., and Kollman, P. A. (1999) Computational alanine scanning to probe protein-protein interactions: A novel approach to evaluate binding free energies. *J Am Chem Soc* **121**, 8133-8143
165. Gohlke, H., Hendlich, M., and Klebe, G. (2000) Knowledge-based scoring function to predict protein-ligand interactions. *J Mol Biol* **295**, 337-356
166. Kruger, D. M., and Gohlke, H. (2010) DrugScore(PPI) webserver: fast and accurate in silico alanine scanning for scoring protein-protein interactions. *Nucleic Acids Res* **38**, W480-W486
167. Schymkowitz, J., Borg, J., Stricher, F., Nys, R., Rousseau, F., and Serrano, L. (2005) The FoldX web server: an online force field. *Nucleic Acids Res* **33**, W382-W388
168. Kim, D. E., Chivian, D., and Baker, D. (2004) Protein structure prediction and analysis using the Robetta server. *Nucleic Acids Res* **32**, W526-531
169. Kortemme, T., and Baker, D. (2002) A simple physical model for binding energy hot spots in protein-protein complexes. *Proc Natl Acad Sci U S A* **99**, 14116-14121
170. Kortemme, T., Kim, D. E., and Baker, D. (2004) Computational alanine scanning of protein-protein interfaces. *Sci Signal* **2004**, pl2
171. Benedix, A., Becker, C. M., de Groot, B. L., Caflisch, A., and Bockmann, R. A. (2009) Predicting free energy changes using structural ensembles. *Nat Methods* **6**, 3-4
172. Gohlke, H., and Case, D. A. (2004) Converging free energy estimates: MM-PB(GB)SA studies on the protein-protein complex Ras-Raf. *J Comput Chem* **25**, 238-250
173. Gohlke, H., Kiel, C., and Case, D. A. (2003) Insights into protein-protein binding by binding free energy calculation and free energy decomposition for the Ras-Raf and Ras-RaIGDS complexes. *J Mol Biol* **330**, 891-913
174. Homeyer, N., and Gohlke, H. (2012) Free Energy Calculations by the Molecular Mechanics Poisson-Boltzmann Surface Area Method. *Mol Inf* **31**, 114-122
175. Huo, S., Massova, I., and Kollman, P. A. (2002) Computational alanine scanning of the 1:1 human growth hormone-receptor complex. *J Comput Chem* **23**, 15-27
176. Moreira, I. S., Fernandes, P. A., and Ramos, M. J. (2007) Computational alanine scanning mutagenesis--an improved methodological approach. *J Comput Chem* **28**, 644-654
177. Bourgeas, R., Basse, M. J., Morelli, X., and Roche, P. (2010) Atomic analysis of protein-protein interfaces with known inhibitors: the 2P2I database. *PLOS ONE* **5**, e9598
178. Higuero, A. P., Schreyer, A., Bickerton, G. R., Pitt, W. R., Groom, C. R., and Blundell, T. L. (2009) Atomic interactions and profile of small molecules disrupting protein-protein interfaces: the TIMBAL database. *Chem Biol Drug Des* **74**, 457-467
179. Oldham, R. K., and Dillman, R. O. (2008) Monoclonal antibodies in cancer therapy: 25 years of progress. *J Clin Oncol* **26**, 1774-1777
180. Stockwin, L. H., and Holmes, S. (2003) Antibodies as therapeutic agents: vive la renaissance! *Expert Opin Biol Ther* **3**, 1133-1152
181. Vogel, C., Cobleigh, M. A., Tripathy, D., Gutheil, J. C., Harris, L. N., Fehrenbacher, L., Slamon, D. J., Murphy, M., Novotny, W. F., Burchmore, M., Shak, S., and Stewart, S. J.

- (2001) First-line, single-agent Herceptin(R) (trastuzumab) in metastatic breast cancer. a preliminary report. *Eur J Cancer* **37 Suppl 1**, 25-29
182. Lafont, V., Schaefer, M., Stote, R. H., Altschuh, D., and Dejaegere, A. (2007) Protein-protein recognition and interaction hot spots in an antigen-antibody complex: free energy decomposition identifies "efficient amino acids". *Proteins* **67**, 418-434
183. Griffin, L., and Lawson, A. (2011) Antibody fragments as tools in crystallography. *Clin Exp Immunol* **165**, 285-291
184. Imai, K., and Takaoka, A. (2006) Comparing antibody and small-molecule therapies for cancer. *Nat Rev Cancer* **6**, 714-727
185. Berg, T. (2008) Small-molecule inhibitors of protein-protein interactions. *Curr Opin Drug Discovery Dev* **11**, 666-674
186. Zhong, S. J., Macias, A. T., and MacKerell, A. D. (2007) Computational identification of inhibitors of protein-protein interactions. *Curr Top Med Chem* **7**, 63-82
187. Buchwald, P. (2010) Small-molecule protein-protein interaction inhibitors: therapeutic potential in light of molecular size, chemical space, and ligand binding efficiency considerations. *IUBMB Life* **62**, 724-731
188. Sperandio, O., Reynes, C. H., Camproux, A. C., and Villoutreix, B. O. (2010) Rationalizing the chemical space of protein-protein interaction inhibitors. *Drug Discovery Today* **15**, 220-229
189. Vogler, M., Dinsdale, D., Dyer, M. J., and Cohen, G. M. (2009) Bcl-2 inhibitors: small molecules with a big impact on cancer therapy. *Cell Death Differ* **16**, 360-367
190. Vogelstein, B., Lane, D., and Levine, A. J. (2000) Surfing the p53 network. *Nature* **408**, 307-310
191. Suzuki, K., and Matsubara, H. (2011) Recent advances in p53 research and cancer treatment. *J Biomed Biotechnol* **2011**, 978312
192. Lane, D. P., Cheok, C. F., and Lain, S. (2010) p53-based cancer therapy. *Cold Spring Harbor Perspect Biol* **2**, a001222
193. Picksley, S. M., Vojtesek, B., Sparks, A., and Lane, D. P. (1994) Immunochemical analysis of the interaction of p53 with MDM2;--fine mapping of the MDM2 binding site on p53 using synthetic peptides. *Oncogene* **9**, 2523-2529
194. Vassilev, L. T., Vu, B. T., Graves, B., Carvajal, D., Podlaski, F., Filipovic, Z., Kong, N., Kammlott, U., Lukacs, C., Klein, C., Fotouhi, N., and Liu, E. A. (2004) In vivo activation of the p53 pathway by small-molecule antagonists of MDM2. *Science* **303**, 844-848
195. Grasberger, B. L., Lu, T., Schubert, C., Parks, D. J., Carver, T. E., Koblisch, H. K., Cummings, M. D., LaFrance, L. V., Milkiewicz, K. L., Calvo, R. R., Maguire, D., Lattanze, J., Franks, C. F., Zhao, S., Ramachandren, K., Bylebyl, G. R., Zhang, M., Manthey, C. L., Petrella, E. C., Pantoliano, M. W., Deckman, I. C., Spurlino, J. C., Maroney, A. C., Tomczuk, B. E., Molloy, C. J., and Bone, R. F. (2005) Discovery and cocrystal structure of benzodiazepinedione HDM2 antagonists that activate p53 in cells. *J Med Chem* **48**, 909-912
196. Khoury, K., Popowicz, G. M., Holak, T. A., and Domling, A. (2011) The p53-MDM2/MDMX axis - A chemotype perspective. *MedChemComm* **2**, 246-260
197. Galatin, P. S., and Abraham, D. J. (2004) A nonpeptidic sulfonamide inhibits the p53-mdm2 interaction and activates p53-dependent transcription in mdm2-overexpressing cells. *J Med Chem* **47**, 4163-4165
198. Hardcastle, I. R., Ahmed, S. U., Atkins, H., Calvert, A. H., Curtin, N. J., Farnie, G., Golding, B. T., Griffin, R. J., Guyenne, S., Hutton, C., Kallblad, P., Kemp, S. J., Kitching, M. S., Newell, D. R., Norbedo, S., Northen, J. S., Reid, R. J., Saravanan, K., Willems, H. M., and Lunec, J. (2005) Isoindolinone-based inhibitors of the MDM2-p53 protein-protein interaction. *Bioorg Med Chem Lett* **15**, 1515-1520

199. Zhuang, C., Miao, Z., Zhu, L., Zhang, Y., Guo, Z., Yao, J., Dong, G., Wang, S., Liu, Y., Chen, H., Sheng, C., and Zhang, W. (2011) Synthesis and biological evaluation of thio-benzodiazepines as novel small molecule inhibitors of the p53-MDM2 protein-protein interaction. *Eur J Med Chem* **46**, 5654-5661
200. Hu, C., Li, X., Wang, W., Zhang, L., Tao, L., Dong, X., Sheng, R., Yang, B., and Hu, Y. (2011) Design, synthesis, and biological evaluation of imidazoline derivatives as p53-MDM2 binding inhibitors. *Bioorg Med Chem* **19**, 5454-5461
201. Ding, K., Lu, Y., Nikolovska-Coleska, Z., Wang, G., Qiu, S., Shangary, S., Gao, W., Qin, D., Stuckey, J., Krajewski, K., Roller, P. P., and Wang, S. (2006) Structure-based design of spiro-oxindoles as potent, specific small-molecule inhibitors of the MDM2-p53 interaction. *J Med Chem* **49**, 3432-3435
202. Galatin, P. S., and Abraham, D. J. (2001) QSAR: hydrophobic analysis of inhibitors of the p53-mdm2 interaction. *Proteins* **45**, 169-175
203. Agrafiotis, D. K. (1997) Stochastic algorithms for maximizing molecular diversity. *J Chem Inf Comput Sci* **37**, 841-851
204. Kalinski, C., Umkehrer, M., Weber, L., Kolb, J., Burdack, C., and Ross, G. (2010) On the industrial applications of MCRs: molecular diversity in drug discovery and generic drug synthesis. *Mol Diversity* **14**, 513-522
205. Ding, K., Lu, Y., Nikolovska-Coleska, Z., Qiu, S., Ding, Y., Gao, W., Stuckey, J., Krajewski, K., Roller, P. P., Tomita, Y., Parrish, D. A., Deschamps, J. R., and Wang, S. (2005) Structure-based design of potent non-peptide MDM2 inhibitors. *J Am Chem Soc* **127**, 10130-10131
206. Shangary, S., Qin, D., McEachern, D., Liu, M., Miller, R. S., Qiu, S., Nikolovska-Coleska, Z., Ding, K., Wang, G., Chen, J., Bernard, D., Zhang, J., Lu, Y., Gu, Q., Shah, R. B., Pienta, K. J., Ling, X., Kang, S., Guo, M., Sun, Y., Yang, D., and Wang, S. (2008) Temporal activation of p53 by a specific MDM2 inhibitor is selectively toxic to tumors and leads to complete tumor growth inhibition. *Proc Natl Acad Sci U S A* **105**, 3933-3938
207. Rothweiler, U., Czarna, A., Krajewski, M., Ciombor, J., Kalinski, C., Khazak, V., Ross, G., Skobeleva, N., Weber, L., and Holak, T. A. (2008) Isoquinolin-1-one inhibitors of the MDM2-p53 interaction. *ChemMedChem* **3**, 1118-1128
208. Bowman, A. L., Nikolovska-Coleska, Z., Zhong, H., Wang, S., and Carlson, H. A. (2007) Small molecule inhibitors of the MDM2-p53 interaction discovered by ensemble-based receptor models. *J Am Chem Soc* **129**, 12809-12814
209. Malek, T. R. (2008) The biology of interleukin-2. *Annu Rev Immunol* **26**, 453-479
210. Braisted, A. C., Oslob, J. D., Delano, W. L., Hyde, J., McDowell, R. S., Waal, N., Yu, C., Arkin, M. R., and Raimundo, B. C. (2003) Discovery of a potent small molecule IL-2 inhibitor through fragment assembly. *J Am Chem Soc* **125**, 3714-3715
211. Craig, I. R., Pflieger, C., Gohlke, H., Essex, J. W., and Spiegel, K. (2011) Pocket-space maps to identify novel binding-site conformations in proteins. *J Chem Inf Model* **51**, 2666-2679
212. Langabeer, S. E., Walker, H., Rogers, J. R., Burnett, A. K., Wheatley, K., Swirsky, D., Goldstone, A. H., and Linch, D. C. (1997) Incidence of AML1/ETO fusion transcripts in patients entered into the MRC AML trials. MRC Adult Leukaemia Working Party. *Br J Haematol* **99**, 925-928
213. Wichmann, C., Becker, Y., Chen-Wichmann, L., Vogel, V., Vojtkova, A., Herglotz, J., Moore, S., Koch, J., Lausen, J., Mantele, W., Gohlke, H., and Grez, M. (2010) Dimer-tetramer transition controls RUNX1/ETO leukemogenic activity. *Blood* **116**, 603-613
214. Metz, A., Schanda, J., Grez, M., Wichmann, C., and Gohlke, H. (2013) From Determinants of RUNX1/ETO Tetramerization to Small-Molecule Protein-Protein Interaction Inhibitors Targeting Acute Myeloid Leukemia. *J Chem Inf Model* **53**, 2197-2202
215. Irwin, J. J., and Shoichet, B. K. (2005) ZINC--a free database of commercially available compounds for virtual screening. *J Chem Inf Model* **45**, 177-182

216. Topol, E. J., Byzova, T. V., and Plow, E. F. (1999) Platelet GPIIb-IIIa blockers. *Lancet* **353**, 227-231
217. Morelli, X., Bourgeas, R., and Roche, P. (2011) Chemical and structural lessons from recent successes in protein-protein interaction inhibition (2P2I). *Curr Opin Chem Biol* **15**, 475-481
218. Villoutreix, B. O., Labbe, C. M., Lagorce, D., Laconde, G., and Sperandio, O. (2012) A leap into the chemical space of protein-protein interaction inhibitors. *Curr Pharm Des* **18**, 4648-4667
219. Faller, B., Ottaviani, G., Ertl, P., Berellini, G., and Collis, A. (2011) Evolution of the physicochemical properties of marketed drugs: can history foretell the future? *Drug Discovery Today* **16**, 976-984
220. Berg, T. (2003) Modulation of protein-protein interactions with small organic molecules. *Angew Chem* **42**, 2462-2481
221. Fry, D. C. (2006) Protein-protein interactions as targets for small molecule drug discovery. *Biopolymers* **84**, 535-552
222. Wilson, A. J. (2009) Inhibition of protein-protein interactions using designed molecules. *Chem Soc Rev* **38**, 3289-3300
223. Lipinski, C. A., Lombardo, F., Dominy, B. W., and Feeney, P. J. (2001) Experimental and computational approaches to estimate solubility and permeability in drug discovery and development settings. *Adv Drug Delivery Rev* **46**, 3-26
224. Reynes, C., Host, H., Camproux, A. C., Laconde, G., Leroux, F., Mazars, A., Deprez, B., Fahraeus, R., Villoutreix, B. O., and Sperandio, O. (2010) Designing Focused Chemical Libraries Enriched in Protein-Protein Interaction Inhibitors using Machine-Learning Methods. *PLoS Comput Biol* **6**
225. Metz, A. (2014) Predicting and Exploiting the Determinants of Protein/Protein Interactions to Identify Low-Molecular Inhibitors of RUNX1-ETO Tetramerization. *PhD Thesis, Heinrich Heine Universität, Düsseldorf*
226. Zhao, H. (2011) Lead optimization in the nondrug-like space. *Drug Discovery Today* **16**, 158-163
227. Allen, T. M., and Cullis, P. R. (2004) Drug delivery systems: entering the mainstream. *Science* **303**, 1818-1822
228. Makley, L. N., and Gestwicki, J. E. (2013) Expanding the number of 'druggable' targets: non-enzymes and protein-protein interactions. *Chem Biol Drug Des* **81**, 22-32
229. Taipale, M., Jarosz, D. F., and Lindquist, S. (2010) HSP90 at the hub of protein homeostasis: emerging mechanistic insights. *Nat Rev Mol Cell Biol* **11**, 515-528
230. Mayer, M. P., Prodromou, C., and Frydman, J. (2009) The Hsp90 mosaic: a picture emerges. *Nat Struct Mol Biol* **16**, 2-6
231. Young, J. C., Agashe, V. R., Siegers, K., and Hartl, F. U. (2004) Pathways of chaperone-mediated protein folding in the cytosol. *Nat Rev Mol Cell Biol* **5**, 781-791
232. Wiech, H., Buchner, J., Zimmermann, R., and Jakob, U. (1992) Hsp90 chaperones protein folding in vitro. *Nature* **358**, 169-170
233. Pearl, L. H., and Prodromou, C. (2006) Structure and mechanism of the Hsp90 molecular chaperone machinery. *Annu Rev Biochem* **75**, 271-294
234. Wandinger, S. K., Richter, K., and Buchner, J. (2008) The Hsp90 chaperone machinery. *J Biol Chem* **283**, 18473-18477
235. Whitesell, L., and Lindquist, S. L. (2005) HSP90 and the chaperoning of cancer. *Nat Rev Cancer* **5**, 761-772
236. Barrott, J. J., and Haystead, T. A. J. (2013) Hsp90, an unlikely ally in the war on cancer. *FEBS J* **280**, 1381-1396

-
237. Chiosis, G., Dickey, C. A., and Johnson, J. L. (2013) A global view of Hsp90 functions. *Nat Struct Mol Biol* **20**, 1-4
238. Johnson, J. L. (2012) Evolution and function of diverse Hsp90 homologs and cochaperone proteins. *Biochim Biophys Acta, Mol Cell Res* **1823**, 607-613
239. Erlejman, A. G., Lagadari, M., Toneatto, J., Piwien-Pilipuk, G., and Galigniana, M. D. (2014) Regulatory role of the 90-kDa-heat-shock protein (Hsp90) and associated factors on gene expression. *Biochim Biophys Acta, Gene Regul Mech* **1839**, 71-87
240. Prodromou, C. (2012) The 'active life' of Hsp90 complexes. *Biochim Biophys Acta* **1823**, 614-623
241. Pratt, W. B. (1998) The hsp90-based chaperone system: Involvement in signal transduction from a variety of hormone and growth factor receptors. *Proc Soc Exp Biol Med* **217**, 420-434
242. Workman, P., and de Billy, E. (2007) Putting the heat on cancer. *Nat Med* **13**, 1415-1417
243. Sreedhar, A. S., Kalmar, E., Csermely, P., and Shen, Y. F. (2004) Hsp90 isoforms: functions, expression and clinical importance. *FEBS Lett* **562**, 11-15
244. Neckers, L., and Workman, P. (2012) Hsp90 molecular chaperone inhibitors: are we there yet? *Clin Cancer Res* **18**, 64-76
245. Bagatell, R., and Whitesell, L. (2004) Altered Hsp90 function in cancer: a unique therapeutic opportunity. *Mol Cancer Ther* **3**, 1021-1030
246. Workman, P., Burrows, F., Neckers, L., and Rosen, N. (2007) Drugging the cancer chaperone HSP90 combinatorial therapeutic exploitation of oncogene addiction and tumor stress. *Ann N Y Acad Sci* **1113**, 202-216
247. Eustace, B. K., Sakurai, T., Stewart, J. K., Yimlamai, D., Unger, C., Zehetmeier, C., Lain, B., Torella, C., Henning, S. W., Beste, G., Scroggins, B. T., Neckers, L., Ilag, L. L., and Jay, D. G. (2004) Functional proteomic screens reveal an essential extracellular role for hsp90 alpha in cancer cell invasiveness. *Nat Cell Biol* **6**, 507-514
248. Nemoto, T. K., Ono, T., and Tanaka, K. (2001) Substrate-binding characteristics of proteins in the 90 kDa heat shock protein family. *Biochem J* **354**, 663-670
249. Moullintraffort, L., Bruneaux, M., Nazabal, A., Allegro, D., Giudice, E., Zal, F., Peyrot, V., Barbier, P., Thomas, D., and Garnier, C. (2010) Biochemical and biophysical characterization of the Mg²⁺-induced 90-kDa heat shock protein oligomers. *J Biol Chem* **285**, 15100-15110
250. Krishna, P., Reddy, R. K., Sacco, M., Frappier, J. R., and Felsheim, R. F. (1997) Analysis of the native forms of the 90 kDa heat shock protein (hsp90) in plant cytosolic extracts. *Plant Mol Biol* **33**, 457-466
251. Lee, C. C., Lin, T. W., Ko, T. P., and Wang, A. H. J. (2011) The Hexameric Structures of Human Heat Shock Protein 90. *PLOS ONE* **6**
252. Prodromou, C., Roe, S. M., O'Brien, R., Ladbury, J. E., Piper, P. W., and Pearl, L. H. (1997) Identification and structural characterization of the ATP/ADP-binding site in the Hsp90 molecular chaperone. *Cell* **90**, 65-75
253. Young, J. C., Moarefi, I., and Hartl, F. U. (2001) Hsp90: a specialized but essential protein-folding tool. *J Cell Biol* **154**, 267-273
254. Panaretou, B., Prodromou, C., Roe, S. M., O'Brien, R., Ladbury, J. E., Piper, P. W., and Pearl, L. H. (1998) ATP binding and hydrolysis are essential to the function of the Hsp90 molecular chaperone in vivo. *EMBO J* **17**, 4829-4836
255. Obermann, W. M., Sondermann, H., Russo, A. A., Pavletich, N. P., and Hartl, F. U. (1998) In vivo function of Hsp90 is dependent on ATP binding and ATP hydrolysis. *J Cell Biol* **143**, 901-910
256. Powers, M. V., and Workman, P. (2007) Inhibitors of the heat shock response: Biology and pharmacology. *FEBS Lett* **581**, 3758-3769

257. Sharp, S., and Workman, P. (2006) Inhibitors of the HSP90 molecular chaperone: Current status. *Adv Cancer Res* **95**, 323-348
258. Sgobba, M., and Rastelli, G. (2009) Structure-based and in silico design of Hsp90 inhibitors. *ChemMedChem* **4**, 1399-1409
259. Minami, Y., Kimura, Y., Kawasaki, H., Suzuki, K., and Yahara, I. (1994) The carboxy-terminal region of mammalian HSP90 is required for its dimerization and function in vivo. *Mol Cell Biol* **14**, 1459-1464
260. Marcu, M. G., Chadli, A., Bouhouche, I., Catelli, M., and Neckers, L. M. (2000) The heat shock protein 90 antagonist novobiocin interacts with a previously unrecognized ATP-binding domain in the carboxyl terminus of the chaperone. *J Biol Chem* **275**, 37181-37186
261. Garnier, C., Lafitte, D., Tsvetkov, P. O., Barbier, P., Leclerc-Devin, J., Millot, J. M., Briand, C., Makarov, A. A., Catelli, M. G., and Peyrot, V. (2002) Binding of ATP to heat shock protein 90: evidence for an ATP-binding site in the C-terminal domain. *J Biol Chem* **277**, 12208-12214
262. Donnelly, A., and Blagg, B. S. (2008) Novobiocin and additional inhibitors of the Hsp90 C-terminal nucleotide-binding pocket. *Curr Med Chem* **15**, 2702-2717
263. Marcu, M. G., Schulte, T. W., and Neckers, L. (2000) Novobiocin and related coumarins and depletion of heat shock protein 90-dependent signaling proteins. *J Natl Cancer Inst* **92**, 242-248
264. Matts, R. L., Dixit, A., Peterson, L. B., Sun, L., Voruganti, S., Kalyanaraman, P., Hartson, S. D., Verkhivker, G. M., and Blagg, B. S. (2011) Elucidation of the Hsp90 C-terminal inhibitor binding site. *ACS Chem Biol* **6**, 800-807
265. Harris, S. F., Shiau, A. K., and Agard, D. A. (2004) The crystal structure of the carboxy-terminal dimerization domain of htpG, the Escherichia coli Hsp90, reveals a potential substrate binding site. *Structure* **12**, 1087-1097
266. Rohl, A., Rohrberg, J., and Buchner, J. (2013) The chaperone Hsp90: changing partners for demanding clients. *Trends Biochem Sci* **38**, 253-262
267. Shiau, A. K., Harris, S. F., Southworth, D. R., and Agard, D. A. (2006) Structural Analysis of E. coli hsp90 reveals dramatic nucleotide-dependent conformational rearrangements. *Cell* **127**, 329-340
268. Ali, M. M., Roe, S. M., Vaughan, C. K., Meyer, P., Panaretou, B., Piper, P. W., Prodromou, C., and Pearl, L. H. (2006) Crystal structure of an Hsp90-nucleotide-p23/Sba1 closed chaperone complex. *Nature* **440**, 1013-1017
269. Pearl, L. H., Prodromou, C., and Workman, P. (2008) The Hsp90 molecular chaperone: an open and shut case for treatment. *Biochemical J* **410**, 439-453
270. Ratzke, C., Mickler, M., Hellenkamp, B., Buchner, J., and Hugel, T. (2010) Dynamics of heat shock protein 90 C-terminal dimerization is an important part of its conformational cycle. *Proc Natl Acad Sci U S A* **107**, 16101-16106
271. Krukenberg, K. A., Forster, F., Rice, L. M., Sali, A., and Agard, D. A. (2008) Multiple conformations of E. coli Hsp90 in solution: insights into the conformational dynamics of Hsp90. *Structure* **16**, 755-765
272. Southworth, D. R., and Agard, D. A. (2008) Species-dependent ensembles of conserved conformational states define the Hsp90 chaperone ATPase cycle. *Mol Cell* **32**, 631-640
273. Street, T. O., Lavery, L. A., and Agard, D. A. (2011) Substrate binding drives large-scale conformational changes in the Hsp90 molecular chaperone. *Mol Cell* **42**, 96-105
274. Richter, K., Muschler, P., Hainzl, O., and Buchner, J. (2001) Coordinated ATP hydrolysis by the Hsp90 dimer. *J Biol Chem* **276**, 33689-33696

275. Morra, G., Verkhivker, G., and Colombo, G. (2009) Modeling signal propagation mechanisms and ligand-based conformational dynamics of the Hsp90 molecular chaperone full-length dimer. *PLOS Comput Biol* **5**, e1000323
276. Capdeville, R., Buchdunger, E., Zimmermann, J., and Matter, A. (2002) Glivec (STI571, imatinib), a rationally developed, targeted anticancer drug. *Nat Rev Drug Discovery* **1**, 493-502
277. Melnikova, I., and Golden, J. (2004) Targeting protein kinases. *Nat Rev Drug Discovery* **3**, 993-994
278. Fishman, M. C., and Porter, J. A. (2005) Pharmaceuticals: a new grammar for drug discovery. *Nature* **437**, 491-493
279. Li, J., Sun, L., Xu, C., Yu, F., Zhou, H., Zhao, Y., Zhang, J., Cai, J., Mao, C., Tang, L., Xu, Y., and He, J. (2012) Structure insights into mechanisms of ATP hydrolysis and the activation of human heat-shock protein 90. *Acta Biochim Biophys Sin* **44**, 300-306
280. Stebbins, C. E., Russo, A. A., Schneider, C., Rosen, N., Hartl, F. U., and Pavletich, N. P. (1997) Crystal structure of an Hsp90-geldanamycin complex: targeting of a protein chaperone by an antitumor agent. *Cell* **89**, 239-250
281. Mahalingam, D., Swords, R., Carew, J. S., Nawrocki, S. T., Bhalla, K., and Giles, F. J. (2009) Targeting HSP90 for cancer therapy. *Br J Cancer* **100**, 1523-1529
282. Pearl, L. H., and Prodromou, C. (2000) Structure and in vivo function of Hsp90. *Curr Opin Struct Biol* **10**, 46-51
283. Whitesell, L., Mimnaugh, E. G., Decosta, B., Myers, C. E., and Neckers, L. M. (1994) Inhibition of Heat-Shock Protein Hsp90-Pp60(V-Src) Heteroprotein Complex-Formation by Benzoquinone Ansamycins - Essential Role for Stress Proteins in Oncogenic Transformation. *Proc Natl Acad Sci U S A* **91**, 8324-8328
284. Sharma, S. V., Agatsuma, T., and Nakano, H. (1998) Targeting of the protein chaperone, HSP90, by the transformation suppressing agent, radicicol. *Oncogene* **16**, 2639-2645
285. Kim, Y. S., Alarcon, S. V., Lee, S., Lee, M. J., Giaccone, G., Neckers, L., and Trepel, J. B. (2009) Update on Hsp90 inhibitors in clinical trial. *Curr Top Med Chem* **9**, 1479-1492
286. Garcia-Carbonero, R., Carnero, A., and Paz-Ares, L. (2013) Inhibition of HSP90 molecular chaperones: moving into the clinic. *Lancet Oncol* **14**, e358-369
287. Hong, D. S., Banerji, U., Tavana, B., George, G. C., Aaron, J., and Kurzrock, R. (2013) Targeting the molecular chaperone heat shock protein 90 (HSP90): lessons learned and future directions. *Cancer Treat Rev* **39**, 375-387
288. Jhaveri, K., Taldone, T., Modi, S., and Chiosis, G. (2012) Advances in the clinical development of heat shock protein 90 (Hsp90) inhibitors in cancers. *Biochim Biophys Acta* **1823**, 742-755
289. Kamal, A., Thao, L., Sensintaffar, J., Zhang, L., Boehm, M. F., Fritz, L. C., and Burrows, F. J. (2003) A high-affinity conformation of Hsp90 confers tumour selectivity on Hsp90 inhibitors. *Nature* **425**, 407-410
290. Zerbe, B. S., Hall, D. R., Vajda, S., Whitty, A., and Kozakov, D. (2012) Relationship between Hot Spot Residues and Ligand Binding Hot Spots in Protein-Protein Interfaces. *J Chem Inf Model* **52**, 2236-2244
291. Jakobi, S., Nguyen, T. X., Debaene, F., Metz, A., Sanglier-Cianferani, S., Reuter, K., and Klebe, G. (2014) Hot-spot analysis to dissect the functional protein-protein interface of a tRNA-modifying enzyme. *Proteins* **82**, 2713-2732
292. Sali, A., and Blundell, T. L. (1993) Comparative Protein Modeling by Satisfaction of Spatial Restraints. *J Mol Biol* **234**, 779-815

293. Laskowski, R. A., Macarthur, M. W., Moss, D. S., and Thornton, J. M. (1993) Procheck - a Program to Check the Stereochemical Quality of Protein Structures. *J Appl Crystallogr* **26**, 283-291
294. Case, D. A., Darden, T. A., Cheatham, T. E. I., Simmerling, C. L., Wang, J., Duke, R. E., Luo, R., Walker, R. C., Zhang, W., Merz, K. M., Roberts, B., Wang, B., Hayik, S., Roitberg, A., Seabra, G., Kolossváry, I., Wong, K. F., Paesani, F., Vanicek, J., Liu, J., Wu, X., Brozell, S. R., Steinbrecher, T., Gohlke, H., Cai, Q., Ye, X., Wang, J., Hsieh, M.-J., Cui, G., Roe, D. R., Mathews, D. H., Seetin, M. G., Sagui, C., Babin, V., Luchko, T., Gusarov, S., Kovalenko, A., and Kollman, P. A. (2010) *AMBER 11*. University of California, San Francisco
295. Kruger, D. M., and Gohlke, H. (2011) Protein-protein interactions, web-based analysis. *Nachr Chem* **59**, 44-45
296. Massova, I., and Kollman, P. A. (2000) Combined molecular mechanical and continuum solvent approach (MM-PBSA/GBSA) to predict ligand binding. *Perspect Drug Discovery Des* **18**, 113-135
297. Gohlke, H., and Klebe, G. (2002) Approaches to the description and prediction of the binding affinity of small-molecule ligands to macromolecular receptors. *Angew Chem* **41**, 2644-2676
298. Pantoliano, M. W., Petrella, E. C., Kwasnoski, J. D., Lobanov, V. S., Myslik, J., Graf, E., Carver, T., Asel, E., Springer, B. A., Lane, P., and Salemme, F. R. (2001) High-density miniaturized thermal shift assays as a general strategy for drug discovery. *J Biomol Screening* **6**, 429-440
299. Gavenonis, J., Jonas, N. E., and Kritzer, J. A. (2014) Potential C-terminal-domain inhibitors of heat shock protein 90 derived from a C-terminal peptide helix. *Bioorg Med Chem* **22**, 3989-3993
300. Li, Y., Liu, X., Dong, X., Zhang, L., and Sun, Y. (2014) Biomimetic design of affinity peptide ligand for capsomere of virus-like particle. *Langmuir* **30**, 8500-8508
301. Milroy, L. G., and Brunsveld, L. (2013) Pharmaceutical implications of helix length control in helix-mediated protein-protein interactions. *Future Med Chem* **5**, 2175-2183
302. Cardinale, D., Guaitoli, G., Tondi, D., Luciani, R., Henrich, S., Salo-Ahen, O. M., Ferrari, S., Marverti, G., Guerrieri, D., Ligabue, A., Frassinetti, C., Pozzi, C., Mangani, S., Fessas, D., Guerrini, R., Ponterini, G., Wade, R. C., and Costi, M. P. (2011) Protein-protein interface-binding peptides inhibit the cancer therapy target human thymidylate synthase. *Proc Natl Acad Sci U S A* **108**, E542-549
303. London, N., Raveh, B., Movshovitz-Attias, D., and Schueler-Furman, O. (2010) Can self-inhibitory peptides be derived from the interfaces of globular protein-protein interactions? *Proteins* **78**, 3140-3149
304. Mukherjee, P., Desai, P., Zhou, Y. D., and Avery, M. (2010) Targeting the BH3 domain mediated protein-protein interaction of Bcl-xL through virtual screening. *J Chem Inf Model* **50**, 906-923
305. De Sancho, D., and Best, R. B. (2011) What is the time scale for alpha-helix nucleation? *J Am Chem Soc* **133**, 6809-6816
306. Gnanakaran, S., Nymeyer, H., Portman, J., Sanbonmatsu, K. Y., and Garcia, A. E. (2003) Peptide folding simulations. *Curr Opin Struct Biol* **13**, 168-174
307. Lin, M. M., Mohammed, O. F., Jas, G. S., and Zewail, A. H. (2011) Speed limit of protein folding evidenced in secondary structure dynamics. *Proc Natl Acad Sci U S A* **108**, 16622-16627
308. Spomer, L., Gertzen, C. G., Schmitz, B., Haussinger, D., Gohlke, H., and Keitel, V. (2014) A membrane-proximal, C-terminal alpha-helix is required for plasma membrane localization and function of the G Protein-coupled receptor (GPCR) TGR5. *J Biol Chem* **289**, 3689-3702
309. Cummings, C. G., and Hamilton, A. D. (2010) Disrupting protein-protein interactions with non-peptidic, small molecule alpha-helix mimetics. *Curr Opin Chem Biol* **14**, 341-346

-
310. Gomes, C. P., Metz, A., Bats, J. W., Gohlke, H., and Gobel, M. W. (2012) Modular Solid-Phase Synthesis of Teroxazoles as a Class of α -Helix Mimetics. *Eur J Org Chem*, 3270-3277
311. Lanning, M., and Fletcher, S. (2013) Recapitulating the alpha-helix: nonpeptidic, low-molecular-weight ligands for the modulation of helix-mediated protein-protein interactions. *Future Med Chem* **5**, 2157-2174
312. Horwell, D. C., Howson, W., Ratcliffe, G. S., and Willems, H. M. (1996) The design of dipeptide helical mimetics: the synthesis, tachykinin receptor affinity and conformational analysis of 1,1,6-trisubstituted indanes. *Bioorg Med Chem* **4**, 33-42
313. Davis, J. M., Tsou, L. K., and Hamilton, A. D. (2007) Synthetic non-peptide mimetics of alpha-helices. *Chem Soc Rev* **36**, 326-334
314. Arkin, M. R., Randal, M., DeLano, W. L., Hyde, J., Luong, T. N., Oslob, J. D., Raphael, D. R., Taylor, L., Wang, J., McDowell, R. S., Wells, J. A., and Braisted, A. C. (2003) Binding of small molecules to an adaptive protein-protein interface. *Proc Natl Acad Sci U S A* **100**, 1603-1608
315. Yin, H., Lee, G. I., Sedey, K. A., Rodriguez, J. M., Wang, H. G., Sebt, S. M., and Hamilton, A. D. (2005) Terephthalamide derivatives as mimetics of helical peptides: disruption of the Bcl-x(L)/Bak interaction. *J Am Chem Soc* **127**, 5463-5468
316. Yin, H., Lee, G. I., Sedey, K. A., Kutzki, O., Park, H. S., Orner, B. P., Ernst, J. T., Wang, H. G., Sebt, S. M., and Hamilton, A. D. (2005) Terphenyl-Based Bak BH3 α -helical proteomimetics as low-molecular-weight antagonists of Bcl-xL. *J Am Chem Soc* **127**, 10191-10196
317. Restorp, P., and Rebek, J., Jr. (2008) Synthesis of alpha-helix mimetics with four side-chains. *Bioorg Med Chem Lett* **18**, 5909-5911

15 APPENDIX – References of Figure 4

1. Fujii, N., Haresco, J. J., Novak, K. A. P., Gage, R. M., Pedemonte, N., Stokoe, D., Kuntz, I. D., and Guy, R. K. (2007) Rational design of a nonpeptide general chemical scaffold for reversible inhibition of PDZ domain interactions. *Bioorg Med Chem Lett* **17**, 549-552.
2. Hammond, M. C., Harris, B. Z., Lim, W. A., and Bartlett, P. A. (2006) Beta strand peptidomimetics as potent PDZ domain ligands. *Chem Biol* **13**, 1247-1251.
3. Shan, J. F., Shi, D. L., Wang, J. M., and Zheng, J. (2005) Identification of a specific inhibitor of the dishevelled PDZ domain. *Biochemistry* **44**, 15495-14503.
4. Lee, H. J., Wang, N. X., Shi, D. L., and Zheng, J. J. (2009) Sulindac inhibits canonical Wnt signaling by blocking the PDZ domain of the protein dishevelled. *Angew Chem Int Edit* **48**, 6448-6652.
5. Herrmann, C., Block, C., Geisen, C., Haas, K., Weber, C., Winde, G., Möröy, T., and Müller, O. (1998) Sulindac sulfide inhibits Ras signaling. *Oncogene* **17**, 1769-1776.
- 6a. Kato-Stankiewicz, J., Hakimi, I., Zhi, G., Zhang, J., Serebriiskii, I., Guo, L., Edamatsu, H., Koide, H., Menon, S., Eckl, R., Sakamuri, S., Lu, Y., Chen, Q. Z., Agarwal, S., Baumbach, W. R., Golemis, E. A., Tamanoi, F., and Khazak, V. (2002) Inhibitors of Ras/Raf-1 interaction identified by two-hybrid screening revert Ras-dependent transformation phenotypes in human cancer cells. *Proc Natl Acad Sci USA* **99**, 14398-14403.
- 6b. Lu, Y. C., Sakamuri, S., Chen, Q. Z., Keng, Y. F., Khazak, V., Illgen, K., Schabbert, S., Weber, L., and Menon, S. R. (2004) Solution phase parallel synthesis and evaluation of MAPK inhibitory activities of close structural analogues of a Ras pathway modulator. *Bioorg Med Chem Lett* **14**, 3957-3962.
7. Stebbins, J. L., De, S. K., Machleidt, T., Becattini, B., Vazquez, J., Kuntzen, C., Chen, L. H., Cellitti, J., Riel-Mehan, M., Emdadi, A., Solinas, G., Karin, M., and Pellacchia, M. (2008) Identification of a new JNK inhibitor targeting the JNK-JIP interaction site. *Proc Natl Acad Sci USA* **105**, 16809-16813.
8. Chen, T., Kablaoui, N., Little, J., Timofeevski, S., Tschantz, W. R., Chen, P., Feng, J., Charlton, M., Stanton, R., and Bauer, P. (2009) Identification of small-molecule inhibitors of the JIP-JNK interaction. *Biochem J* **420**, 283-294.
9. Dorr, P., Westby, M., Dobbs, S., Griffin, P., Irvine, B., Macartney, M., Mori, J., Rickett, G., Smith-Burchnell, C., Napier, C., Webster, R., Armour, D., Price, D., Stammen, B., Wood, A., and Perros, M. (2005) Maraviroc (UK-427,857), a potent, orally bioavailable, and selective small-molecule inhibitor of chemokine receptor CCR5 with broad-spectrum anti-human immunodeficiency virus type 1 activity. *Antimicrob Agents Chemother* **49**, 4721-4732.
10. Erickson-Miller, C. L., Delorme, E., Tian, S. S., Hopson, C. B., Landis, A. J., Valoret, E. I., Sellers, T. S., Rosen, J., Miller, S. G., Luengo, J. I., Duffy, K. J., and Jenkins, J. M. (2009) Preclinical activity of Eltrombopag (SB-497115), an oral, nonpeptide thrombopoietin receptor agonist. *Stem Cells* **27**, 424-30.
11. Jackson, D. Y., Quan, C., Artis, D. R., Rawson, T., Blackburn, B., Struble, M., Fitzgerald, G., Chan, K., Mullis, S., Burnier, J. P., Fairbrother, W. J., Clark, K., Berisini, M., Chui, H., Renz, M., Jones, S., and Fong, S. (1997) Potent alpha 4 beta 1 peptide antagonists as potential anti-inflammatory agents. *J Med Chem* **40**, 3359-3368.
12. Sillerud, L. O., and Larson, R. S. (2005) Design and structure of peptide and peptidomimetic antagonists of protein-protein interaction. *Curr Protein Pept Sci* **6**, 151-169.
13. Carron, C. P., Meyer, D. M., Pegg, J. A., Engleman, V. W., Nickols, M. A., Settle, S. L., Westlin, W. F., Ruminski P. G., and Nickols G. A. (1998) A peptidomimetic antagonist of the integrin alpha(v)beta3 inhibits Leydig cell tumor growth and the development of hypercalcemia of malignancy. *Cancer Res* **58**, 1930-1935.

14. Viaud, J., Zeghouf, M., Barelli, H., Zeeh, J. C., Padilla, A., Guibert, B., Chardin, P., Royer, C. A., Cherfils, J., and Chavanieu, A. (2007) Structure-based discovery of an inhibitor of Arf activation by Sec7 domains through targeting of protein-protein complexes. *Proc Natl Acad Sci USA* **104**, 10370-10375.
15. Corradi, V., Mancini, M., Santucci, M. A., Carlomagno, T., Sanfelice, D., Mori, M., Vignaroli, G., Falchi, F., Manetti, F., Radi, M., and Botta, M. (2011) Computational techniques are valuable tools for the discovery of protein-protein interaction inhibitors: The 14-3-3 sigma case. *Bioorg Med Chem Lett* **21**, 6867-6871.
16. Oost, T. K., Sun, C. H., Armstrong, R. C., Al-Assaad, A. S., Betz, S. F., Deckwerth, T. L., Ding, H., Elmore, S. W., Meadows, R. P., Olejniczak, E. T., Oleksijew, A., Oltersdorf, T., Rosenberg, S. H., Shoemaker, A. R., Tomaselli, K. J., Zour, H., and Fesik, S. (2004) Discovery of potent antagonists of the antiapoptotic protein XIAP for the treatment of cancer. *J Med Chem* **47**, 4417-4426.
17. Sun, H. Y., Nikolovska-Coleska, Z., Lu, J. F., Meagher, J. L., Yang, C. Y., Qiu, S., Tomita, Y., Ueda, Y., Jiang, S., Krajewski, K., Roller, P. R., Stuckey, J. A., and Wang, S. (2007) Design, synthesis, and characterization of a potent, nonpeptide, cell-permeable, bivalent smac mimetic that concurrently targets both the BIR2 and BIR3 domains in XIAP. *J Am Chem Soc* **129**, 15279-15294.
18. Peng, Y., Sun, H., Nikolovska-Coleska, Z., Qiu, S., Yang, C. Y., Lu, J., Cai, Q., Yi, H., Kang, S., Yang, D., and Wang, S. (2008) Potent, orally bioavailable diazabicyclic small-molecule mimetics of second mitochondria-derived activator of caspases. *J Med Chem* **51**, 8158-8162.
19. Cai, Q., Sun, H. Y., Peng, Y., Lu, J., Nikolovska-Coleska, Z., McEachern, D., Liu, L., Qiu, S., Yang, C. Y., Miller, R., Yi, H., Zhang, T., Sun, D., Kang, S., Guo, M., Leopold, L., Yang, D., and Wang, S. (2011) A potent and orally active antagonist (SM-406/AT-406) of multiple inhibitor of apoptosis proteins (IAPs) in clinical development for cancer treatment. *J Med Chem* **54**, 2714-2726.
20. Zhang, B., Corbel, C., Gueritte, F., Couturier, C., Bach, S., and Tan V. B. C. (2011) An in silico approach for the discovery of CDK5/p25 interaction inhibitors. *Biotechnol J* **6**, 871-881.
21. Wang, H. B., Hammoudeh, D. I., Follis, A. V., Reese, B. E., Lazo, J. S., Metallo, S. J., and Prochownik E. V. (2007) Improved low molecular weight Myc-Max inhibitors. *Mol Cancer Ther* **6**, 2399-2408.
22. Christ, F., Voet, A., Marchand, A., Nicolet, S., Desimmie, B. A., Marchand, D., Bardiot, D., Van der Veken, N. J., Van Remoortel, B., Strelkov, S. V., De Maeyer, M., Chaltin, P., and Debyser, Z. (2010) Rational design of small molecule inhibitors of the LEDGF/p75-integrase interaction and HIV replication. *Nat Chem Biol* **6**, 442-448.
23. Wang, T., Zhang, Z. X., Wallace, O. B., Deshpande, M., Fang, H., Yang, Z., Zadjura, L. M., Tweedie, D. L., Huang, S., Zhao, F., Ranadive, S., Robinson, B. S., Gong, Y. F., Ricarrdi, K., Spicer, T. P., Deminie, C., Rose, R., Wang, H. G. H., Blair, W. S., Shi, P. Y., Lin, P. F., Colonna, R. J., and Meanwell, N. A. (2003) Discovery of 4-benzoyl-1-[(4-methoxy-1H-pyrrolo[2,3-b]pyridin-3-yl)oxoacetyl]-2-(R)-methylpiperazine (BMS-378806): A novel HIV-1 attachment inhibitor that interferes with CD4-gp120 interactions. *J Med Chem* **46**, 4236-4239.
24. Bonacci, T. M., Mathews, J. L., Yuan, C., Lehmann, D. M., Malik, S., Wu, D., Font, J. L., Bidlack, J. M., and Smrcka, A. V. (2006) Differential targeting of G beta gamma-subunit signaling with small molecules. *Science* **312**, 443-446.
- 25a. Yap, J. L., Worlikar, S., MacKerell, A. D., Shapiro, P., and Fletcher, S. (2011) Small-molecule inhibitors of the ERK signaling pathway: Towards novel anticancer therapeutics. *ChemMedChem* **6**, 38-48.
- 25b. Chen, F., Hancock, C. N., Macias, A. T., Joh, J., Still, K., Zhong, S., MacKerell A. D., and Shapiro, P. (2006) Characterization of ATP-independent ERK inhibitors identified through *in silico* analysis of the active ERK2 structure. *Bioorg Med Chem Lett* **16**, 6281-6287.

26. Yoakim, C., Ogilvie, W. W., Goudreau, N., Naud, J., Hacé, B., O'Meara, J. A., Cordingley, M. G., Archambault, J., and White P. W. (2003) Discovery of the first series of inhibitors of human papillomavirus type 11: Inhibition of the assembly of the E1-E2-origin DNA complex. *Bioorg Med Chem Lett* **13**, 2539-2541.
27. White, P. W., Titolo, S., Brault, K., Thauvette, L., Pelletier, A., Welchner, E., Bourgon, L., Doyon, L., Ogilvie, W. W., Yoakim, C., Cordingley, M. G., and Archambault, J. (2003) Inhibition of human papillomavirus DNA replication by small molecule antagonists of the E1-E2 protein interaction. *J Biol Chem* **278**, 26765-26772.
28. Cerchietti, L. C., Ghetu, A. F., Zhu, X., Da Silva, G. F., Zhong, S., Matthews, M., Bunting, K. L., Polo, J. M., Farès, C., Arrowsmith, C. H., Yang, S. N., Garcia, M., Coop, A., MacKerell A. D., Privé G. G., and Melnick, A. (2010) A small-molecule inhibitor of BCL6 kills DLBCL cells *in vitro* and *in vivo*. *Cancer Cell* **17**, 400-411.
29. Rush, T. S., Grant, J. A., Mosyak, L., and Nicholls, A. (2005) A shape-based 3-D scaffold hopping method and its application to a bacterial protein-protein interaction. *J Med Chem* **48**, 1489-1495.
30. Huang, N., Nagarsekar, A., Xia, G. J., Hayashi, J., and MacKerell, A. D. (2004) Identification of non-phosphate-containing small molecular weight inhibitors of the tyrosine kinase p56 Lck SH2 domain via *in silico* screening against the pY+3 binding site. *J Med Chem* **47**, 3502-3511.
31. Capps, K. J., Humiston, J., Dominique, R., Hwang, I., and Boger, D. L. (2005) Discovery of AICAR Tfase inhibitors that disrupt requisite enzyme dimerization. *Bioorg Med Chem Lett* **15**, 2840-2844.
32. He, M. M., Smith, A. S., Oslob, J. D., Flanagan, W. M., Braisted, A. C., Whitty, A., Cancilla, M. T., Wang, J., Lugovskoy, A. A., Yoburn, J. C., Fung, A. D., Farrington, G., Eldredge, J. K., Day, E. S., Cruz, L. A., Cachero, T. G., Miller, S. K., Friedman, J. E., Choong I. C., and Cunningham, B. C. (2005) Small-molecule inhibition of TNF-alpha. *Science* **310**, 1022-1025.
33. Paige, J. S., and Jaffrey, S. R. (2007) Pharmacologic manipulation of nitric oxide signaling: Targeting NOS dimerization and protein-protein interactions. *Curr Top Med Chem* **7**, 97-114.
34. Gorczynski, M. J., Grembecka, J., Zhou, Y. P., Kong, Y., Roudaia, L., Douvas, M. G., Newman, M., Bielnicka, I., Baber, G., Corpora, T., Shi, J., Sridharan, M., Lilien, R., Donald, B. R., Speck, N. A., Brown, M. L., and Bushweller, J. H. (2007) Allosteric inhibition of the protein-protein interaction between the leukemia-associated proteins Runx1 and CBF beta. *Chem Biol* **14**, 1186-1197.
35. Reindl, W. G., Yuan, J. P., Krämer, A., Strebhardt, K., and Berg, T. (2008) Inhibition of polo-like kinase 1 by blocking Polo-box domain-dependent protein-protein interactions. *Chem Biol* **15**, 459-466.
36. Shangary, S., Qin, D. G., McEachern, D., Liu, M., Miller, R. S., Qiu, S., Nikolovska-Coleska, Z., Ding, K., Wang, G., Chen, J., Bernard, D., Zhang, J., Lu, Y., Gu, Q., Shah, R. B., Pienta, K. J., Ling, X., Kang, S., Guo, M., Sun, Y., Yang, D., and Wang, S. (2008) Temporal activation of p53 by a specific MDM2 inhibitor is selectively toxic to tumors and leads to complete tumor growth inhibition. *Proc Natl Acad Sci USA* **105**, 3933-3938.
37. Grasberger, B. L., Lu, T. B., Schubert, C., Parks, D. J., Carver, T. E., Koblisch, H. K., Cummings, M. D., LaFrance, L. V., Milkiewicz, K. L., Calvo, R. R., Maguire, D., Lattanze, J., Franks, C. F., Zhao, S., Ramachandren, K., Bylebyl, G. R., Zhang, M., Mantley, C. L., Petrella, E. C., Pantoliano, M. W., Deckman, I. C., Spurlino, J. C., Maroney, A. C., Tomczuk, B. E., Molloy, C. J., and Bone, R. F. (2005) Discovery and cocrystal structure of benzodiazepinedione HDM2 antagonists that activate p53 in cells. *J Med Chem* **48**, 909-912.
38. Popowicz, G. M., Czarna, A., Wolf, S., Wang, K., Wang, W., Dömling, A., and Holak, T. A. (2010) Structures of low molecular weight inhibitors bound to MDMX and MDM2 reveal new approaches for p53-MDMX/MDM2 antagonist drug discovery. *Cell Cycle* **9**, 1104-1111.

39. Shaginian, A., Whitby, L. R., Hong, S., Hwang, I., Farooqi, B., Searcey, M., Chen, J., Vogt, P. K., and Boger, D. L. (2009) Design, synthesis, and evaluation of an alpha-helix mimetic library targeting protein-protein interactions. *J Am Chem Soc* **131**, 5564-5572.
40. Markowitz, J., Chen, J., Gitti, R., Baldisseri, D. M., Pan, Y., Udan, R., Carrier, F., MacKerell, A. D., and Weber, D. J. (2004) Identification and characterization of small molecule inhibitors of the calcium-dependent S100B-p53 tumor suppressor interaction. *J Med Chem* **47**, 5085-5093.
41. Wilder, P. T., Charpentier, T. H., Liriano, M. A., Gianni, K., Varney, K. M., Pozharski, E., Coop, A., Toth, E. A., MacKerell, A. D. and Weber, D. J. (2010) *In vitro* screening and structural characterization of inhibitors of the S100B-p53 interaction. *Int J High Throughput Screening* **2010**, 109-126.
42. Yin, H., Lee, G. I., Sedey, K. A., Kutzki, O., Park, H. S., Orner, B. P., Ernst, J. T., Wang, H. G., Sebti, S. M., and Hamilton, A. D. (2005) Terphenyl-based bak BH3 alphahelical proteomimetics as low-molecular-weight antagonists of Bcl-xL. *J Am Chem Soc* **127**, 10191-10196.
43. Rodriguez, J. M., and Hamilton, A. D. (2007) Benzoylurea oligomers: Synthetic foldamers that mimic extended alpha helices. *Angew Chem Int Ed* **46**, 8614-8617.
44. Tse, C., Shoemaker, A. R., Adickes, J., Anderson, M. G., Chen, J., Jin, S., Johnson, E. F., Marsh, K. C., Mitten, M. J., Nimmer, P., Roberts, L., Tahir, S. K., Xiao, Y., Yang, X., Zhang, H., Fesik, S., Rosenberg, S. H., and Elmore, S. W. (2008) ABT-263: A potent and orally bioavailable Bcl-2 family inhibitor. *Cancer Res* **68**, 3421-3428.
45. Oltersdorf, T., Elmore, S. W., Shoemaker, A. R., Armstrong, R. C., Augeri, D. J., Belli, B. A., Bruncko, M., Deckwerth, T. L., Dinges, J., Hajduk, P. J., Joseph M. K., Kitada, S., Korsmeyer, S. J., Kunzer, A. R., Letai, A., Li, C., Mitten, M. J., Nettesheim, D. G., Ng, S., Nimmer, P. M., O'Connor, J. M., Oleksijew, A., Petros, A. M., Reed, J. C., Shen, W., Tahir S. K., Thompson, C. B., Tomaselli, K. J., Wang, B., Wendt, M. D., Zhang, H., Fesik, S. W., and Rosenberg, S. H. (2005) An inhibitor of Bcl-2 family proteins induces regression of solid tumours. *Nature* **435**, 677-681.
46. Zhai, D., Jin, C., Satterthwait, A. C., and Reed, J. C. (2006) Comparison of chemical inhibitors of antiapoptotic Bcl-2-family proteins. *Cell Death Differ* **13**: 1419-1421.
47. Tang, G. Z., Yang, C. Y., Nikolovska-Coleska, Z., Guo, J., Qiu, S., Wang, R., Gao, W., Wang, G., Stuckey, J., Krajewski, K., Jiang, S., Roller, P. P., and Wang, S. (2007) Pyrogallol-based molecules as potent inhibitors of the antiapoptotic Bcl-2 proteins. *J Med Chem* **50**, 1723-1726.
48. Wang, G., Nikolovska-Coleska, Z., Yang, C. Y., Wang, R., Tang, G., Guo, J., Shangary, S., Qiu, S., Gao, W., Yang, D., Meagher, J., Stuckey, J., Krajewski, K., Jiang, S., Roller, P. P., Abaan, H. O., Tomita, Y., and Wang S. (2006) Structure-based design of potent small-molecule inhibitors of anti-apoptotic Bcl-2 proteins. *J Med Chem* **49**, 6139-6142.
49. Degterev, A., Lugovskoy, A., Cardone, M., Mulley, B., Wagner, G., Mitchison, T., and Yuan, J. (2001) Identification of small-molecule inhibitors of interaction between the BH3 domain and Bcl-xL. *Nat Cell Biol* **3**, 173-182.
50. Chan, S. L., Lee, M. C., Tan, K. O., Yang, L. K., Lee, A. S., Flotow, H., Fu, N. Y., Butler, M. S., Soejarto, D. D., Buss, A. D., and Yu, V. C. (2003) Identification of chelerythrine as an inhibitor of BclXL function. *J Biol Chem* **278**, 20453-20456.
51. Kitada, S., Leone, M., Sareth, S., Zhai, D., Reed, J. C., and Pellecchia, M. (2003) Discovery, characterization, and structure-activity relationships studies of proapoptotic polyphenols targeting B-cell lymphocyte/leukemia-2 proteins. *J Med Chem* **46**, 4259-4264.
52. Becattini, B., Kitada, S., Leone, M., Monosov, E., Chandler, S., Zhai, D., Kipps, T. J., Reed, J. C., and Pellecchia, M. (2004) Rational design and real time, in-cell detection of the proapoptotic activity of a novel compound targeting Bcl-XL. *Chem Biol* **11**, 389-395.

53. Arkin, M. R., Randal, M., DeLano, W. L., Hyde, J., Luong, T. N., Oslob, J. D., Raphael, D. R., Taylor, L., Wang, J., McDowell, R. S., Wells, J. A., and Braisted, A. C. (2003) Binding of small molecules to an adaptive protein-protein interface. *Proc Natl Acad Sci USA* **100**, 1603-1608.
54. Raimundo, B. C., Oslob, J. D., Braisted, A. C., Hyde, J., McDowell, R. S., Randal, M., Waal, N. D., Wilkinson, J., Yu, C. H., and Arkin, M. R. (2004) Integrating fragment assembly and biophysical methods in the chemical advancement of small-molecule antagonists of IL-2: An approach for inhibiting protein-protein interactions. *J Med Chem* **47**, 3111-3130.
55. Braisted, A. C., Oslob, J. D., Delano, W. L., Hyde, J., McDowell, R. S., Waal, N., Yu, C., Arkin, M. R., and Raimundo, B. C. (2003) Discovery of a potent small molecule IL-2 inhibitor through fragment assembly. *J Am Chem Soc* **125**, 3714-3715.
56. Thanos, C. D., DeLano, W. L., and Wells, J. A. (2006) Hot-spot mimicry of a cytokine receptor by a small molecule. *Proc Natl Acad Sci USA* **103**, 15422-15427.